Final Report

Project Title: Next Generation Wind Turbine

Covering Period: September 3, 2010 – September 1, 2012
Date of Report: September 1, 2012

Recipient: Western New England University
Award Number: DE-EE0003276

Working Partners:

Prime Recipient: Western New England University
Dr. S. Hossein Cheraghi (Principal Investigator)
Telephone: (413) 796-2302
Email: cheraghi@wne.edu

Western New England University
Matthew VanHeynigen (Programmatic Support)
Telephone: 413-782-1373
Email: mvanheynigen@wne.edu

Sub-Recipient: FloDesign Wind Turbine Corp.
Frank Madden (Program Manager)
Telephone: 781-609-4743
Email: fmadden@fdwt.com

Cost-Sharing Partners: FloDesign Wind Turbine Corp.
Contacts: Frank Madden
Telephone: 781-609-4743
Email: fmadden@fdwt.com

DOE Project Team: DOE HQ Program Manager – Jacques Beaudry-Losique
DOE Field Contract Officer – Pam Brodie
DOE Field Contract Specialist – Fania Gordon
DOE Field Project Officer – Gary Nowakowski
DOE/NAVARRO Project Monitor – Tyler Beins

Acknowledgment: "This material is based upon work supported by the Department of Energy under Award Number DE-EE0003276."

TABLE OF CONTENTS

1.0 EXECUTIVE SUMMARY ____ *6*

2.0 GOALS AND OBJECTIVES ____ *7*

2.1 MEWT Prototype Analysis and Testing ____ **7**

2.2 Small Scale MEWT Model Test Programs ____ **8**

2.3 Small Wind Turbine Feasibility Study ____ **8**

3.0 TECHNICAL BACKGROUND ____ *9*

3.1 Mixer Ejector Wind Turbine Concept and Potential ____ **9**

3.1a MEWT Key Components: ____ 11

Feature 1: Tandem High-Camber, Ring-Wing Shrouds: ____ 11

Feature 2: Shrouded Rotor Turbine: ____ 12

Feature 3: Mixer/Ejector Pump: ____ 12

3.1b MEWT Cycle Efficiency: ____ 13

4.0 SUMMARY OF TECHNICAL ACHIEVEMENT ____ *15*

4.1 Briza Testing and Analysis ____ **16**

4.1a Briza Demonstrator ____ 16

4.1b Briza Test Site - High Wind Speed Location ____ 21

4.1c Briza Data Acquisition System ____ 23

4.1d Briza Power Control ____ 26

4.1e Briza Measurement Procedures ____ 27

4.1f Briza Power Results ____ 28

4.1g Yaw Control & Off-axis Gust ____ 30

4.1h Briza Alternate Component Tests ____ 31

4.1i Acoustic Testing ____ 35

4.1j Dynamic FEA Analyses ____ 40

4.1k Briza Load Tests: ____ 42

4.1l Downstream Wake Modeling: ____ 44

4.1m Briza Summary: ____ 45

4.2 Small Scale MEWT Model Test Programs ____ **46**

4.2a Wind Tunnel Characterization: ____ 53

4.2b MEWT Component Testing and Evaluation ____ 60

4.2c Drag Reduction Testing ____ 75

4.3 Small Wind Turbine Feasibility Study ____ **78**

4.3a. MEWT Benefits for Distributive Wind ____ 79

4.3b. Research Wind Classifications: ____ 80

4.3c Market Research study of competitor landscape: ____ 84

4.3d Annual Energy Production (AEP): ____ 87

4.3e. Identify optimal target size: ____ 89

4.3f FloDesign Mustang (FDM) Concept Design: ____ 89

4.3g. Feasibility Cost Estimate: ____ 92

4.3h. Summarize all Findings and Incorporate Feasibility Study into course Curriculum for WNU: ____ 93

4.3i Feasibility Study Summary ____ 98

5.0 REFERENCES ____ *99*

6.0 APPENDICES: ***105***

Appendix A: Design of an Ethernet based Data Collection System for Modern Wind Turbines 105

Appendix B: Measurement and Analysis of Shrouded and Unshrouded Wind Turbine Noise 132

Appendix C: Load Analysis of Horizontal Axis and Mixer-Ejector Wind Turbine Towers 191

Appendix D: Dynamic Fatigue Analysis of Turbine Mount Using Dynamic FEA Analysis 206

Appendix E: Small Wind Turbine Report 235

LIST OF TABLES

Table 1: Demonstration turbine configuration. 18
Table 2: Equipment Specifications 36
Table 3: General Wind 81
Table 4: Turbine Classes 81
Table 5: Available C_p Estimates for Small Wind Turbines 85
Table 6: AEP and Energy Cost Comparison 88
Table 7: Small Wind Turbine Specs 89

LIST OF FIGURES

Figure 1: MEWT Turbine 9
Figure 2: HAWT Wind Turbines 10
Figure 3: Ring-Wing Shroud 11
Figure 4: Shrouded Rotor 12
Figure 5: Mixer/Ejector Pump 12
Figure 6: Mixer/Ejector 13
Figure 7: Shrouded Wind 13
Figure 8: Newly Developed Theory Changes Wind Turbine Cycle 14
Figure 9: HAWT And MEWT Cycle Analysis Comparison 15
Figure 10: Briza Concept 16
Figure 11: Photograph of the Briza Model 17
Figure 12: Briza Dimensions 17
Figure 13: Briza Major Components 18
Figure 14: Composite Shroud Fabrication 19
Figure 15: Wilbraham Test Site 19
Figure 16: Interns & FDWT Engineers 19
Figure 17: Tower Failure 20
Figure 18: Shroud Repair Process 20
Figure 19: View of Demonstration Turbine 22
Figure 20: Plot Plan of the Test Site. 23
Figure 21: Data Acquisition System Modules for Analog to Digital Conversion 24
Figure 22: Graphical User Interface for Data Collection System 24
Figure 24: Briza DAS, Located on Tower Base Trailer 25

Figure 23: Bergey XL1 HAWT outside of 25
Figure 25: Schematic of DAS Inputs and Current Flow from Turbine 26
Figure 26: Bergey Power Controller use in Testing. 26
Figure 27: Measured and Predicted Power Curve for the 1kW Briza 29
Figure 28: Histogram of Power Curve Wind Speed Bins. 29
Figure 29: Yaw Design 30
Figure 30: Coefficient of Performance vs. Off Axis Wind Direction 30
Figure 31: Tracking Ability of Briza. 31
Figure 32: Composite Rotor Blades 32
Figure 33: Composite Rotor Blade Performance 32
Figure 34: Stator Flaps 33
Figure 35: Stator Flap for Aerodynamic Braking 33
Figure 36: Fabric Shroud Construction 34
Figure 37: Fabric Shroud Dimensions 34
Figure 38: Google Sky Screenshot of Rutland Test Site with Pertinent Distances and Heights 35
Figure 39: 86 ft and 0^{o} Test Location-Rutland, Ma. 36
Figure 40: Acoustic Measurement Setup 37
Figure 41: View from the Roof of Sleith Hall of the Bergey 1 kW Wind Turbine 38
Figure 42: Briza Quieter Than Bergey 38
Figure 43: Tonal Analysis 39
Figure 44: 1/3 Octave Band Analysis 39
Figure 45: Briza Prototype in Rutland 40
Figure 46: Load Beam Instrumented with Strain Gages 41
Figure 47: Von Mises Stress Contour Plot 42
Figure 48: Load Cell Measurements 43
Figure 49: Briza Cd Comparison With UMD Wind Tunnel Results 44
Figure 50: Sample Wake Measurements on Briza 45
Figure 51: Dual Flow Wind Tunnel Test Setup 47
Figure 52: Core Flow Wind Tunnel configuration 47
Figure 53: Open Jet Wind Tunnel Configuration 48
Figure 54: Automated Traverse System 49
Figure 55: Pitot-static Probe Measures Both Static and Total Pressure 49
Figure 56: Load Balance and Yaw Measurement System 50
Figure 57: Mixer-Ejector Test Setup 51
Figure 58: Manometer used During MEWT Testing 52
Figure 59: Laptop with Windflow Traverse Program 52
Figure 60: Open Jet Outlet Duct Exit Plane 54
Figure 61: Open Jet Traverse of X-Direction 55
Figure 62: Open Jet Traverse of Y-Direction 55
Figure 63: Average Flow Velocity versus Motor Frequency 57
Figure 64: Core Flow Outlet Duct Exit Plane 58
Figure 65: Core Flow Traverse of X-Direction 59
Figure 66: Core Flow Traverse of Y-Direction 59
Figure 67: Mixing of Primary and Secondary Flows 60
Figure 68: Diagram of a Straight Ejector 61
Figure 69: Diagram of a Diffused Shroud 61

Figure 70: Diagram of a Cambered Shroud 62
Figure 71: Mixer/Ejector System with Cambered Shroud 62
Figure 72: Diagram of Traverse Data Collection 64
Figure 73: L2 Inverted Mixer/ejector Pumping Results 66
Figure 74: C144 L2 Scalloped Mixer/ejector Pumping Results 67
Figure 75: C144 L2 Mixer/Ejector Pumping Results 68
Figure 76: C120 L4 ALMEC Mixer/Ejector Pumping Results 69
Figure 77: C120 L3 ALMEC Mixer/Ejector Pumping Results 70
Figure 78: C120 L2 ALMEC Mixer/Ejector Pumping Results 71
Figure 79: C120 L1 ALMEC Mixer/Ejector Pumping Results 71
Figure 80: Ejector Pumping results and comparison to ideal 72
Figure 81: Ejector Pumping vs. Ideal Results 73
Figure 82: Velocity Profile for C144 L2 using an L/D = 0.50 74
Figure 83: Velocity Profile for C144 L2 Scalloped using an L/D = 0.50 74
Figure 84: Velocity Profile for L2 Inverted using an L/D = 0.50 75
Figure 85: Scale model of the L15s C481 Turbine Shroud 76
Figure 87: FDWT Ejector Facility, Shown in Open-Jet Configuration 77
Figure 86: Model Mount with Force Balance. New Yawing Force Balance on Right 77
Figure 88: MEWT Drag versus Yaw Angle 78
Figure 89: Acoustic Comparison 79
Figure 90: Wind Power Classification Key for the Following Maps 82
Figure 91: Wind Map of Massachusetts Showing Annual Average Wind Speeds at 50 m High. 82
Figure 92: Wind Map of Connecticut Showing Annual Average Wind 83
Figure 93: Wind Map of Maine Showing Annual Average Wind 83
Figure 94: Annual Average Wind Speed at 80m [reference 26] 84
Figure 95: Comparison of All 1kw Turbines Found Regarding Price, Mass, and Diameter 85
Figure 96: U.S. Small Wind Turbine Market Growth 86
Figure 97: USA year 2000 Wind Power Capacity 87
Figure 98: USA year 2009 Wind Power Capacity 87
Figure 99: US Tax Incentives [reference 23] 87
Figure 100: AEP calcuator 88
Figure 101: Students Final FDM 89
Figure 102: T-Slot Connection of Mixer to Leading Edge 90
Figure 103: Shroud with 90
Figure 104: Student Interns Exploded 3D Model of FDM 91
Figure 105: Tubular Stand 91
Figure 106: Four-legged Stand 91
Figure 107: Tension Fabric Shroud ..... **Error! Bookmark not defined.**
Figure 108: Bill of Materials and Cost Estimate for FDM Prototype 92
Figure 109: Bill of Materials and Cost Estimate to Manufacture the FDM 93
Figure 110: Homework Assignment Given to Class (ME415) 94
Figure 111: Weibull Wind Speed Distribution and AEP Calculator 95
Figure 112: Weibull Wind Speed Distribution Example 96
Figure 113: Power Curve Example 96
Figure 114: AEP Prediction Plot Example 97

1.0 EXECUTIVE SUMMARY

The goal of this collaborative effort between Western New England (WNE) University's College of Engineering and FloDesign Wind Turbine (FDWT) Corporation to work on a novel aerodynamic concept that could potentially lead to the next generation of wind turbines. Analytical studies and early scale model tests of FDWT's Mixer/Ejector Wind Turbine (MEWT) concept, which exploits jet-age advanced fluid dynamics, indicate that the concept has the potential to significantly reduce the cost of electricity over conventional Horizontal Axis Wind Turbines (HAWT's) while reducing land usage. This project involved the design, fabrication, and wind tunnel testing of components of Mixer/Ejector Wind Turbines (MEWT) to provide the research and engineering data necessary to validate the design iterations and optimize system performance. Based on these tests, a scale model prototype called Briza was designed, fabricated, installed and tested on a portable tower to investigate and improve the system design in real world conditions. The results of these scale prototype efforts were very promising and have contributed significantly to FDWT's ongoing development of a product scale wind turbine for deployment in multiple locations around the United States. This research was mutually beneficial to WNE University, FDWT, and the Department of Energy (DOE) by utilizing over 30 student Interns and multiple number of faculty in all efforts. It brought real-world wind turbine experience into the classroom to further enhance the Green Engineering Program at WNE University. It also simultaneously provided on the job training to many students helping to improve their future employment opportunities while providing valuable information to further advance FDWT's mixer-ejector wind turbine technology creating opportunities for future innovation and job creation. This report contains detailed descriptions of different phases of the project including goals and achievements in each phase.

2.0 GOALS AND OBJECTIVES

The MEWT technology employs a unique aerodynamic structure that permits the turbine to extract energy from a flow of air that is greater than the swept area of the turbine blades. An innovative mixer/ejector system uses some of the oncoming wind energy to pump more flow through the wind turbine rotor. This benefit allows a MEWT system to generate a given power output with a rotor diameter that is roughly half that required with a traditional horizontal axis wind turbine (HAWT).

The overall goal of this project was to advance FDWT's novel MEWT wind turbine concept, and to enhance WNE University's Green Energy Program by providing real-world wind turbine technology and experience in the classroom. It simultaneously provided on the job training to many students helping to improve their future employment opportunities while providing valuable information to further advance FDWT's mixer-ejector wind turbine technology creating opportunities for future innovation and job creation.

Over the time period from June 2010 to September 2012, a multitude of tasks were performed across all aspects of the MEWT in an effort to improve the system efficiency and identify areas of importance as the concept transitions into a product. The focal points of these studies were based on three main tasks with the following technical objectives;

a. MEWT Prototype Analysis and Testing
b. Small Scale MEWT Model Test Programs
c. Small Wind Turbine Feasibility Study

The MEWT prototype was installed on a tower and was used to demonstrate the potential of the concept in real wind conditions. The Small Scale MEWT Model Tests allowed sub scale model tests to be used to quickly evaluate many new concepts and changes with minimal costs. The Small Wind Turbine Feasibility Study provided an evaluation of the MEWT concept for the home and small community market. Thus, Students and Faculty at Western New England University were involved with actual wind turbine performance, development efforts using a wind tunnel, and new product market and evaluation studies. The following sections describe each of these main tasks in more detail.

2.1 MEWT Prototype Analysis and Testing

The prototype MEWT, referred to as Briza, consists of a rotor that is roughly five feet in diameter producing up to 1kW of power limited by its generator size. This turbine was installed onto a telescoping tower located upon a mobile trailer allowing for it to be deployed and stowed quickly at various locations in order to investigate multiple aspects of the system performance. This program utilized many students and faculty to perform various field tests with the following objectives defined;

- Briza Power curve measurement
- Off-axis gust performance Investigation
- Acoustic measurement and analysis

- Structural analysis of turbine system
- Downstream wake modeling
- Design of data collection system
- Yaw control
- Off-grid field testing
- Performance studies with alternate aerodynamic components

Each of the efforts performed provided valuable information in the process of developing a concept into a product scale MEWT, and provided on site engineering work experience for numerous Western New England (WNE) University Professors and Student Interns. It also brought real-world wind turbine experience into the classroom further enhancing the Green Engineering Program at WNE University

2.2 Small Scale MEWT Model Test Programs

The optimal MEWT configuration is one where the performance of energy extraction is at a maximum while the materials required to form the aerodynamic structure and components is at a minimum, thereby producing the maximum power at the lowest cost per kilowatt. In addition to optimizing the performance of the MEWT, the loading conditions resulting from aerodynamic drag must also be understood in order to meet building specifications.

The process of optimizing this MEWT system begins with the aerodynamic design of various shroud geometries, fabricating small scale models, testing their performance using a wind tunnel test setup, and comparing their results to determine which features to modify for the next design iteration. As part of this optimization process, students were trained in the use of a small scale wind tunnel located at FDWT and performed numerous tests with the following objectives:

- Wind tunnel characterization
- MEWT Scale Model Ejector Pumping and Performance Evaluation Testing
- Wake Traverse testing
- MEWT Scale Model Drag Reduction Testing

This process allowed numerous versions of the MEWT geometry to be tested quickly. The wind tunnel scale model test results provided valuable drag and load estimates for the trade studies.

2.3 Small Wind Turbine Feasibility Study

Although the focus of FDWT has been to design, manufacture, and market large wind turbines for the distributed wind market, the high efficiencies recorded throughout the small scale and Briza testing provided a unique value proposition for the home and small community market as well. The possibility of such a product initiated a research project on these small wind turbines where the following objectives were defined:

- MEWT benefits for Small Wind Turbines

- Research wind classifications
- Market research study of competitor landscape
- Annual Energy Production (AEP) power analysis based on Briza data
- Identify target size of product concept components
- Perform preliminary design of product concept
- Estimate Cost of prototype concept design
- Summarize all findings and incorporate design process into course curriculum for WNU

This research project gave students the unique opportunity to incorporate design data from many aspects of the MEWT into a product concept study to determine the feasibility of a home or small community product offering. This design process also provided multiple course curriculum opportunities and will be used for years to come in the Green Engineering Program at WNE University.

3.0 TECHNICAL BACKGROUND

Each of the tasks performed for this program are related to optimizing the performance and efficiency of FDWT's new and novel Mixer-Ejector Wind Turbine (MEWT). It is important to have a basic understanding of the MEWT technology and its components in order to understand the tasks performed within this program. The following section provides a basic technical background of the MEWT technology as a reference for the subsequent sections summarizing the technical achievements.

3.1 Mixer Ejector Wind Turbine Concept and Potential

FloDesign Wind Turbine Corp. has developed the Mixer Ejector Wind Turbine (MEWT): a new, shrouded, axial-flow wind turbine capable of delivering significantly more energy per unit swept area with greatly reduced rotor loading as compared to existing horizontal axis wind turbines (HAWT). The lower loads, smaller rotor and shrouded concept provide significant potential for mass production and other cost reduction manufacturing techniques. As a result, the new, patent pending MEWT design has the potential to be the next generation wind turbine by providing significantly lower first and life costs compared to traditional horizontal axis wind turbines. The patented concept (see References 1 & 2), as shown in Figure 1, incorporates three major interacting components: high camber multiple shrouds, a shrouded turbine rotor and a mixer/ejector pump augmenter. The high camber shrouds enhance flow pumping and increases the velocity at the rotor station for higher available energy extraction levels. The shrouded turbine could be either a shrouded rotor, or a stator/rotor cascade design similar to jet engines. The mixer/ejector system pumps more flow through the rotor while using

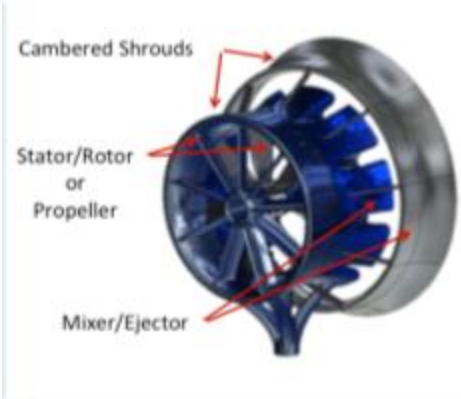

Figure 1: MEWT Turbine

the bypass flow to energize the turbine exit flow allowing more turbine power extraction without wake stall. It provides energy transfer from the bypass flow to the rotor wake flow thus changing the wind turbine cycle and allowing more energy generation for a given system size. These breakthroughs, coupled with advanced propulsion aerodynamics, have been used to design a tightly integrated turbine system capable of initially delivering three to four times more power per unit swept area than a bare turbine while shifting the majority of the axial loading off the rotating and onto the static structures. While these power enhancements have already been demonstrated, there is still significant potential for future enhancements of aerodynamic efficiencies with further development. Four or more times the power per unit swept area of a traditional HAWT (as shown in Figure 2) may be possible as the key component technology is developed. This new MEWT wind turbine concept was made possible by the development, of a first-principles based generalization of the Betz power extraction analysis of shrouded wind turbines with ejector augmenters. Optimization studies based on this analysis demonstrated the feasibility of increasing the ideal power generation by a factor of 3 to 4 times the Betz level while shifting a significant portion of the loading from the rotating components to the static structure of the machine. CFD studies and wind tunnel model tests conducted by FloDesign Wind have further verified this performance potential. This performance gain can be used to reduce the size of wind turbine system. As a result, a MEWT system can produce the same power as a conventional HAWT system with approximately one quarter or less of the swept area with significantly lower axial and vibrational loads. This results in a number of MEWT benefits over existing HAWT systems which include the following:

Figure 2: HAWT Wind Turbines

- Smaller and shrouded design allows mass production of major components for lower costs.
- Lower life costs due to reduced maintenance.
- Lower transportation and installation costs due to size reduction and modularization.
- Safer designs due to the shroud shielding the rotating blade.
- Significantly reduced thrust loading on the blades, shaft and gear box.
- Significantly reduced fluctuating blade loading.
- Environmentally friendly design due to visibility of the stator/rotor system to wildlife. Shielding by the shroud and smaller rotor hold potential for significantly lower bird and bat strikes.
- More productive turbine arrays due to faster mix-out of the wake velocity deficits and lower levels of wake flow swirl impacting downwind turbines.
- Reduction of low-frequency, long wave sound propagation due to frequency shifting at the rotor/stator and sound absorption or shielding by the shrouds.

- More durable design due to both smaller rotors and rotor shroud shielding.
- Shorter tower requirements.
- Reduced radar cross section.
- Elimination of ice slinging
- Self aligning capability
- Potential to integrate the generator in the shroud contour.
- Ability to gather more energy from off axis wind and gusts
- Lower cut in wind velocities, with lower vulnerability to gusts and high wind speeds
- Reduced acoustic signature

Some of the MEWT benefits allow the usage of wind turbines in locations previously not feasible due to safety and noise issues. The shrouded MEWT system eliminates these constraints and provides a direct path to community wind applications. Many of these potential benefits will be discussed further in the remainder of this report. Again, it should be mentioned that even higher performance gains (i.e. 4 or 5 times the Betz limit or more) for such MEWT systems cannot be ruled out at this time, and may be possible in future designs.

3.1a MEWT Key Components:

MEWTs benefit from three critical, tightly coupled features that differentiate these systems from all competing technologies and deliver the highest possible wind energy conversion efficiency possible.

Feature 1: Tandem High-Camber, Ring-Wing Shrouds:

As depicted in Figure 3, the mixer-ejector turbine systems employ two tandem, high camber ring wing shrouds, the turbine shroud and the ejector shroud. These are designed to act together to accelerate flow over the respective surfaces based on the same principles as the cambered wing depicted in the inset of Figure 3. Applied to a ring-wing configuration, this assures the collection of a large amount of the free stream flow because, as indicated, the effective capture area is increased. This well-known and well-documented phenomenon is very different from other diffuser-augmented ducts and/or Venturi tubes—both of which attempt to collect/capture more flow but do not employ the critical influence of camber and are thus generally longer than their ring-wing counterparts. The resulting tandem high-cambered, ring-wing shrouds provide the following differentiating benefits:

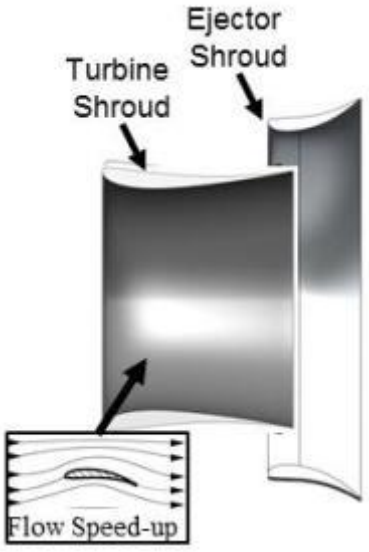

Figure 3: Ring-Wing Shroud

- Speed up of the incoming flow at the rotor station to two or more times the current velocity, leading to earlier start-up of the turbine plus delivering more flow energy to the rotor for extraction/harvesting.

- High energy bypass flow entering the ejector inlet, lowering the turbine back pressure and energizing the ejector shroud inner wall boundary layer similar to airplane trailing edge wing-slots

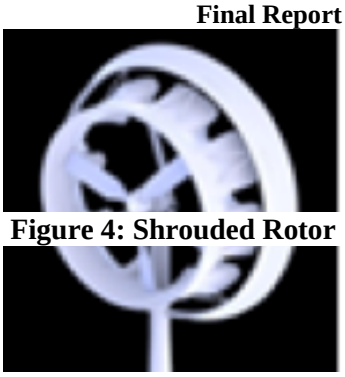

Figure 4: Shrouded Rotor

Feature 2: Shrouded Rotor Turbine:

As depicted in Figure 4, the MEWTs employ a shrouded stator/rotor, or shrouded rotor configuration located at the throat of the turbine shroud. This approach provides the shifting of a significant portion of the axial loads off the rotating turbine onto the stationary shrouds due to well understood and long standing propulsion aerodynamic principles. The same shrouded rotor provides the following differentiating benefits:

- Reduced blade tip losses for higher performance,
- Shielding for lower acoustic and radar signature,
- Significant reduction of bird and bat impacts.

Feature 3: Mixer/Ejector Pump:

As depicted in Figures 1, 4 and 5, the use of a mixer-ejector pump in wind is unique to the MEWT system. It is, by far, the most important feature of the system because, as shown by Werle and Presz in their breakthrough papers (References 6 & 8), it allows one to extract more power from the stream than any other system by avoiding/suppressing flow stall or recirculating in the wake. The high performance levels are a result of the efficient energy transfer in the mixer/ejector system which changes the ideal cycle of a wind turbine. Werle and Presz, inventors of the MEWT have been doing frontier research in this arena for over 30 years (see References. 9-20 for example) and applying the results to numerous applications as discussed below. As indicated in Figure 5, the original mixer-ejector pump was patented by Presz et al in 1989.

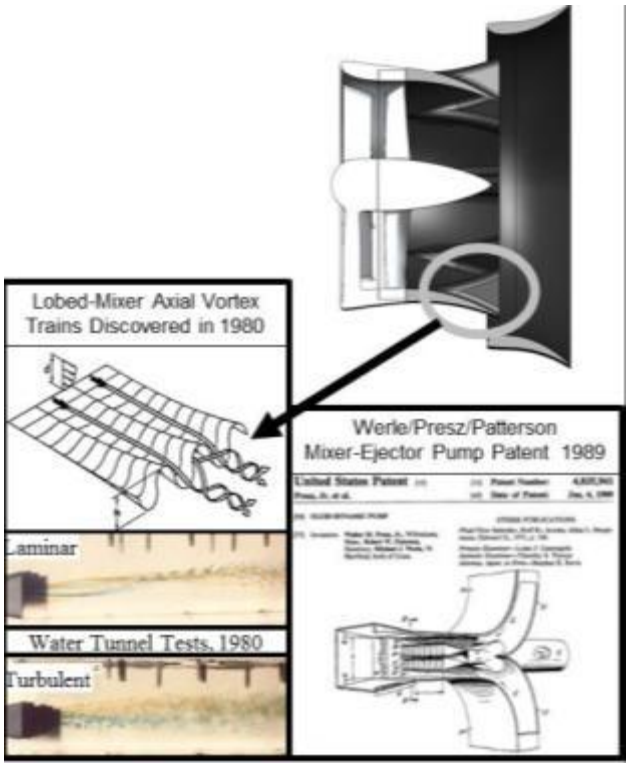

Figure 5: Mixer/Ejector Pump

When this concept is incorporated in the MEWT, its role is to employ the counter-rotating axial stirring vortices depicted in Figure 5 from Reference 20 to mix the high energy flow entering through the ejector inlet into the low energy flow that gave up power to the turbine—thereby energizing the flow in the wake just enough to avoid/suppress wake recirculation and its attendant efficiency losses. The mixer-ejector pump employed in MEWT provides the following differentiating benefits:

- Large scale, rapid vortex energy transfer between the turbine and ejector streams leading to more compact and efficient turbine systems.

- Much smaller rotor size for a given desired power output.
- Re-energized turbine exit flow allowing higher power extraction.
- Reduced wake swirl leading to higher efficiency.
- Quieter/calmer wake disturbance and visibility
- Self alignment with oncoming wind flow direction.

3.1b MEWT Cycle Efficiency:

As mentioned above, mixer-ejector systems represent the combination of over 30 years of aerospace/defense propulsion technology plus a theoretical breakthrough in 2007 leading to over 3 years of application to wind turbines and MEWTs. In the aerospace/defense sector, FloDesign has been involved for the past 25 years with the design and deployment of several flight-worthy mixer/ejector exhaust systems for jet engines. Optimally designed lobed mixers in a mixer/ejector generate axial vortices which provide a vigorous but low-loss energy transfer in the ejector to dramatically improve performance. FloDesign has used its proprietary mixer technology to design very efficient, effective and compact light-weight mixer/ejector noise reduction kits for jet aircraft as shown in Figures 6 (a) and (b), and engine exhaust temperature reduction systems for the Comanche helicopter and V22 as shown in Figures 6 (c) and (d) and as discussed further in References 9-15. These mixer/ejectors are found to be very effective and provide compact systems for rapidly energizing and pumping a low energy stream, by using the kinetic energy of an adjacent higher energy stream.

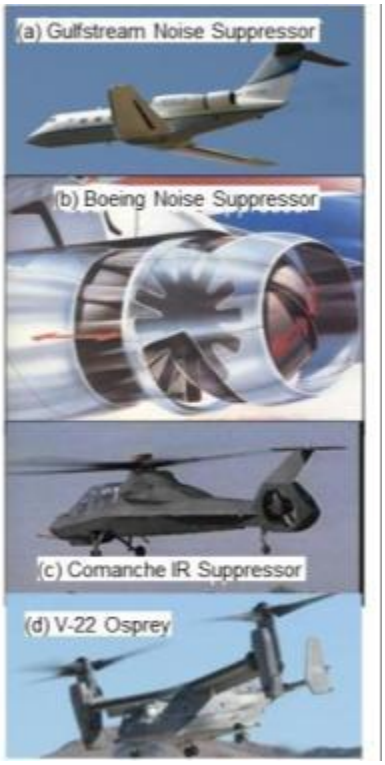

Figure 6: Mixer/Ejector Experience

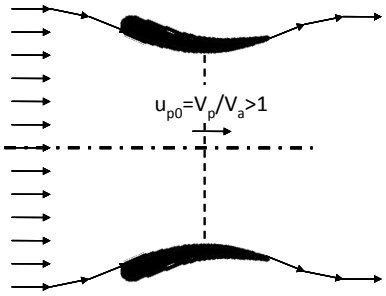

Figure 7: Shrouded Wind Turbine Simulation

FloDesign's expertise and experience described above was recently augmented by its two theoretical breakthroughs related to mixer-ejector power and propulsion systems. These two breakthroughs, vetted in the open literature (References 6 and 8), led directly to the successful science-based design of the MEWT system depicted in Figures 4 and 5 and provide a sound scientific basis. The first breakthrough by Werle and Presz, provided the long sought after first-principles based generalization of the Betz power extraction analysis for unshrouded turbines to shrouded turbines. This new theory was critically reviewed by the propulsion and power fluid dynamic community in Reference 8 and were independently verified by Jamieson in Reference 7. This new theory provides, for the first time, a straightforward means of analytically representing the close coupling of the flow inside and outside a shroud with the power extracted by a rotor system, such as depicted in Figure 7.

It also shows how a wind turbine shroud system can capture more of the free stream flow and thereby generate more power, and it verifies the earlier empirical successes for shrouded wind turbines of Igar (Reference 3), Hansen (Reference 4) and others. A major contribution of the Werle-Presz model is that it provides a simple path for optimizing the system through a decoupling of the shroud's design from that of the full coupled system. In particular, it was shown that the extractable power is directly proportional to the velocity ratio at the turbine station when no turbine is present, i.e., u_{p0} in Figure 7. This theoretical breakthrough allows one to design the shroud system to maximize u_{p0} prior to, and independent of the turbine design. Once completed, the turbine blade geometries can be designed to achieve the predicted maximum power at each annulus in exactly the same fashion employed for bare turbines and as discussed in Reference 5 for example.
The second breakthrough by Werle and Presz (References 6 and 8) was a generalization of the

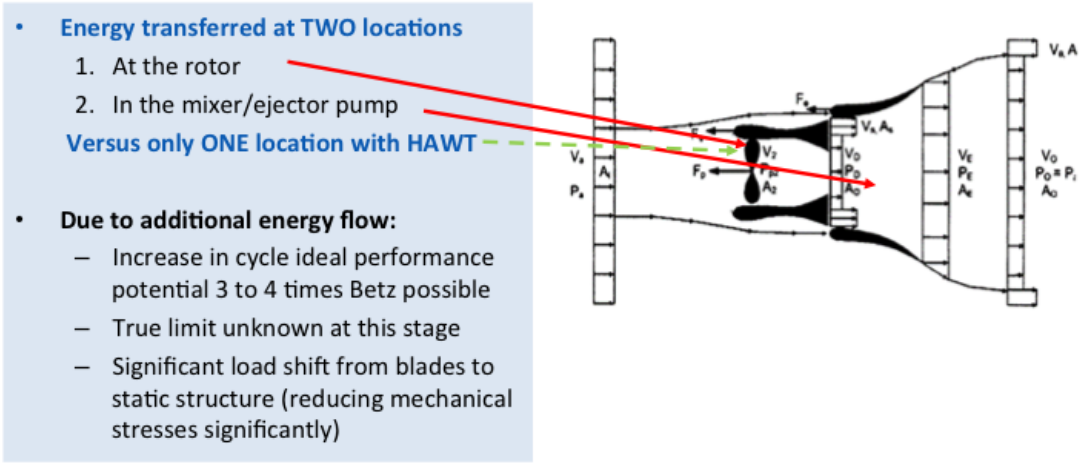

Figure 8: Newly Developed Theory Changes Wind Turbine Cycle

shrouded turbine analysis of Reference 6 to include a mixer/ejector pump system aft of the turbine duct, as depicted in Figure 8. Such an ejector augmentation system pumps more flow through the rotor while using the bypass flow to energize the turbine rotor exit flow which allows more turbine power extraction by the rotor. FloDesign's Mixer Ejector Wind Turbine (MEWT) changes the wind turbine cycle by providing energy transfer at two locations: energy extraction at the rotor, and energy transfer in the mixer/ejector from the bypass flow to the rotor flow. This energy transfer continues downstream of the ejector exit in the rapid wake diffusion set in place by the tandem shroud circulation. The downstream diffusion and energy transfer has a significant impact on the possible MEWT power extraction. Figure 9 presents the control volume results for the optimum performance of the MEWT cycle as compared to a HAWT system. The HAWT analysis generates a maximum power extraction, or power coefficient of 0.593 which is the Betz limit. The MEWT system uses some of the wind energy to both: pump more flow through the rotor, and to energize the rotor wake flow. The pumping in the mixer/ejector reduces the pressure below ambient at the rotor shroud exit and allows the system to extract power levels well above the free stream kinetic energy of the air flow passing through the rotor. The MEWT optimum

performance presented in the graph of Figure 9 varies with the ejector characteristics and the shroud camber. A value of 1 on the vertical axis represents the Betz limit of 59.3% of the free stream kinetic energy. The horizontal axis represents the MEWT load coefficient. The three curved prediction lines represent performance potential for different shroud circulation values. The u_{po} labels reflect different shroud aerodynamic circulation values. The shrouds are ringed airfoils where the airfoil circulation is used to increase velocity levels at the rotor station. An u_{po}value of 2 represents a rotor station velocity that is 2 times the free stream value. The u_{po}value of 2 is not an upper limit. Rather, it is a value that seems achievable with minimal development efforts based on conventional airfoil theory. u_{po}values larger than 2 should be possible as

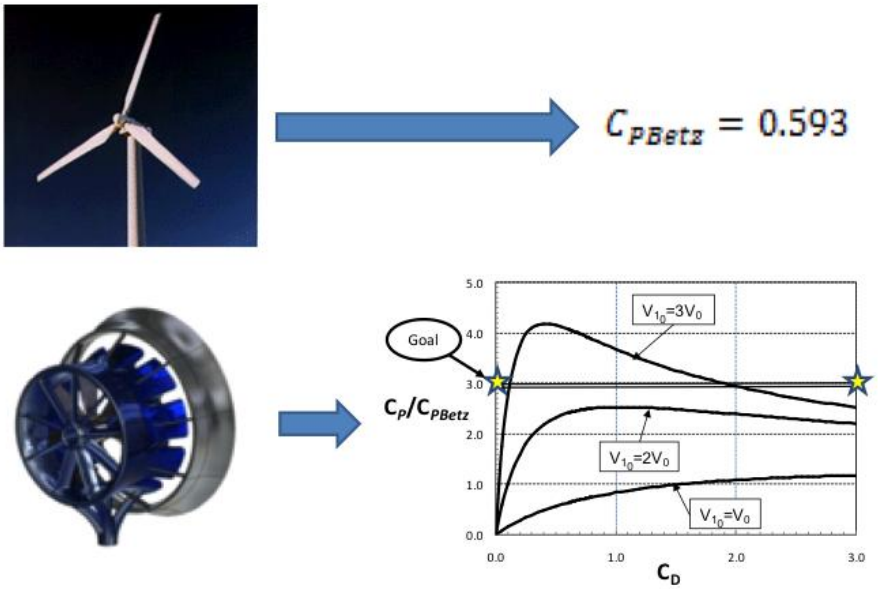

Figure 9: HAWT And MEWT Cycle Analysis Comparison

new and novel ringed airfoils are developed for MEWT application. The starred point in Figure 9 represents an operating point for the MEWT that is consistent with previous successful mixer/ejector and ringed airfoil applications. As indicated by the starred point in Figure 9, MEWT predicted power levels more than three times that of a traditional HAWT are achievable with ejectors whose exit areas are two or more times that of turbine swept area, allowing one to generate the same power with significantly reduced rotor size.

4.0 SUMMARY OF TECHNICAL ACHIEVEMENT

The overall goal of this project was to advance FDWT's novel MEWT wind turbine concept, and to enhance WNE University's Green Energy Program. It simultaneously provided

- on the job training to many students helping to improve their future employment opportunities and,
- valuable information to further advance FDWT's mixer-ejector wind turbine technology creating opportunities for future innovation and job creation.

Over the time period from the summer of 2010 to the summer of 2012, a multitude of technical efforts were performed across all aspects of the MEWT in an effort to improve the system efficiency and to demonstrate MEWT capabilities. The focal points of these studies were based in three main areas with the following technical objectives;

a. MEWT Prototype Testing and Analysis
b. Small Scale MEWT Model Test Programs
c. Small Wind Turbine Feasibility Study

The following sections describe each area in more detail.

4.1 MEWT Prototype Testing and Analysis

The majority of the technical effort involved the fabrication, testing and analysis of FloDesign Wind Turbine's prototype MEWT concept. The MEWT prototype, known as Briza, has a rotor diameter of approximately five feet and produces 1kW of power, which is limited by its generator. Figure 10 presents a schematic of the Briza MEWT prototype. This turbine prototype was installed on a tower which is located atop a mobile trailer so it can be moved and tested in various locations. The testing was done by both Western New England University Interns and Faculty, as well as Engineers and Technicians from FDWT and FloDesign Inc. The testing was focused on accomplishing the goals stated in section 2.0, as well as below:

- Power curve measurement
- Investigation of off-axis gust performance
- Acoustic measurement and analysis
- Structural analysis of turbine system
- Downstream wake modeling
- Design of data collection system
- Yaw control
- Off-grid field testing
- Performance studies with alternate components

Figure 10: Briza Concept

4.1a Briza Demonstrator

The demonstration turbine is a 1kW Mixer Ejector Wind Turbine (MEWT) with 12 stator blades, and a10 bladed rotor utilizing the Bergey XL.1, Permanent Magnet (PM) generator. Figure 11 presents a photograph of the Briza Model. Figure 12 presents the key dimensions associated with Briza. The turbine shroud maximum diameter is 62.8 inches. The system is 66.68 inches long with a maximum diameter at the exit of 91.94 inches. The rotor diameter is 52.59 inches. Table 1 lists the configuration of the FDWT Briza 1-kW that was tested. Figure 13 is a schematic showing the various key Briza components The Bergey generator shown in Figure 13 is identical to the generator in the 1 kW Bergey wind turbine installed at Western New England University. This allows direct comparison of a HAWT and MEWT system. A stator/rotor system was used to

minimize swirl losses at the smaller, 1 kW size. Figure 13 shows the latest design with 9 stators and 7 rotor blades. Both the leading edge of the turbine shroud and the ejector shroud were machined to assure good aerodynamic contours. The remainder of the shrouds were made of composite by Boston Boatworks.

Figure 11: Photograph of the Briza Model

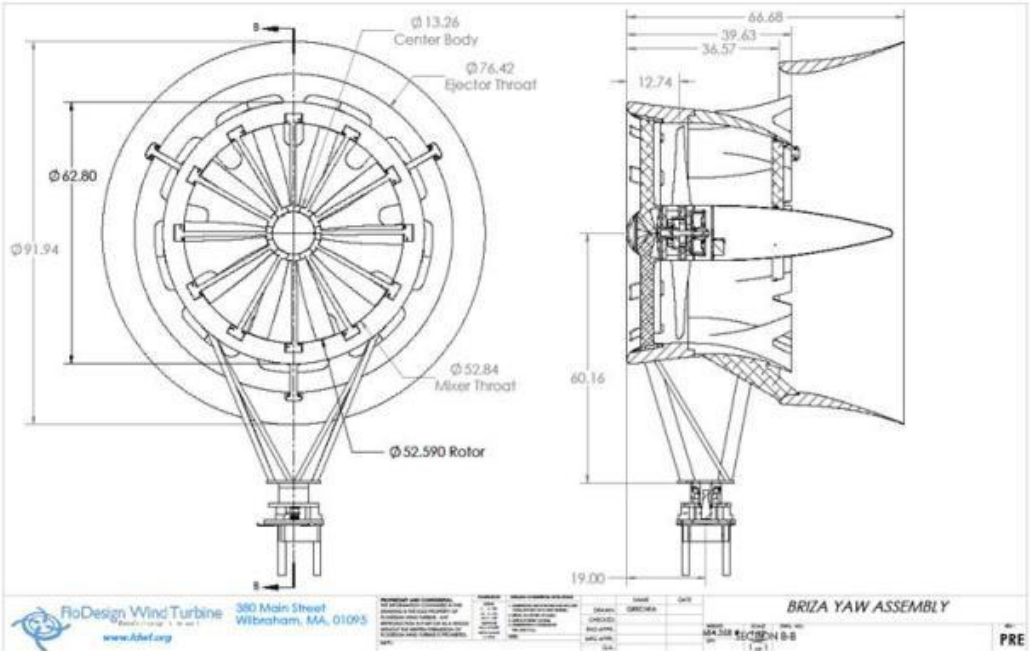

Figure 12: Briza Dimensions

Table 1: Demonstration turbine configuration.

Turbine make, model, serial number, production year	FDWT Briza 1-kW, MEWT C144, 2009
Rotor diameter (in)	52.6
Hub height (ft)	86
Overall Shroud Diameter (in)	92
Tower type	Truss, guyed, (Tower Solutions PTM-100)
Rated electrical power (kW)	1
Rated wind speed (m/s)	11
Rotor speed range (rpm)	90–700
Fixed or variable pitch	Fixed blade, (stator flaps installed Sept. 2010)
Number of blades	10 (7 bladed rotor installed Sept. 2010
Stator Flap pitch angle (deg)	60
Blade make, type, serial number	Solid Aluminum (Carbon fiber, Sept. 2010)
Control system (device and software version)	Bergey PowerCenter

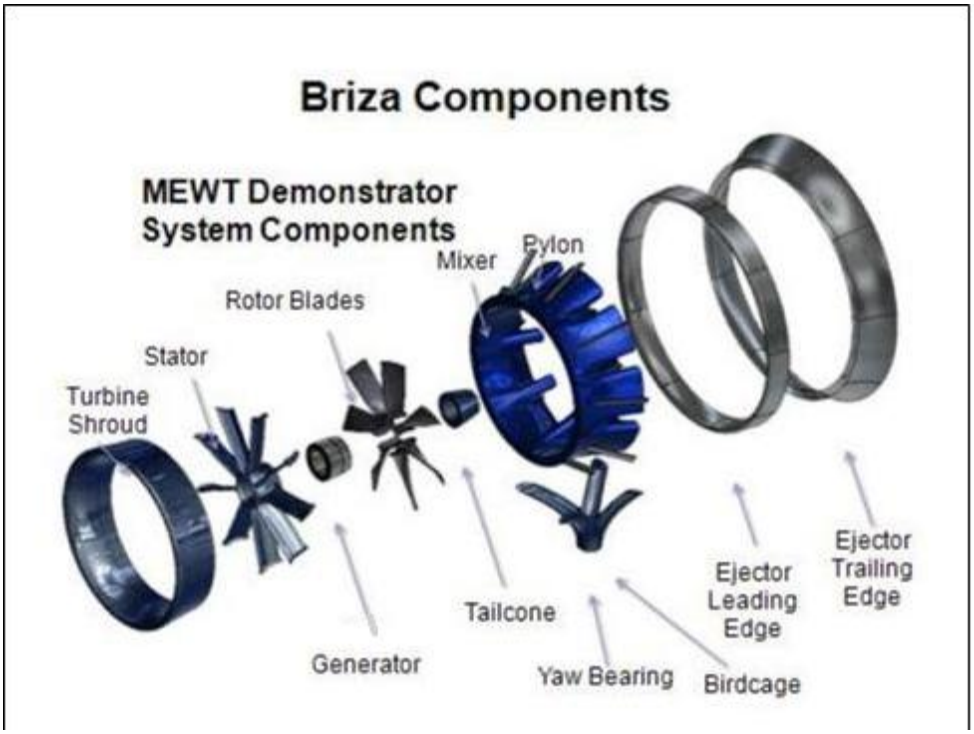

Figure 13: Briza Major Components

Figure 14: Composite Shroud Fabrication

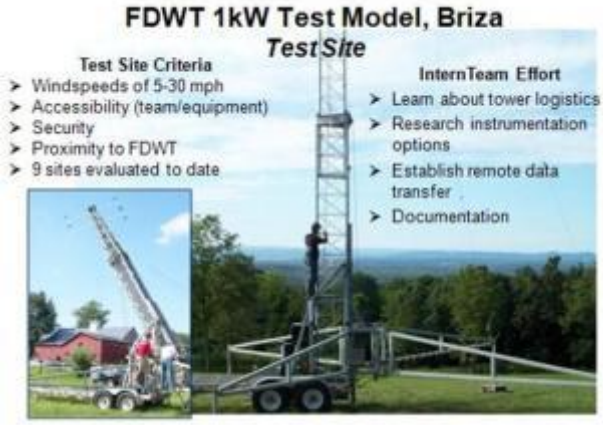

Figure 15: Wilbraham Test Site

Figure 16: Interns & FDWT Engineers

Figure 14 shows a schematic of the composite fabrication process. Initial testing was conducted at a local, low wind speed site near FDWT's office. Figures 15 and 16 presents photographs of the site and the initial, expandable tower used for the testing. The MEWT prototype testing was conducted in collaboration with Western New England College. This expandable tower failed a few months before the start of this program. Figure 17 presents photographs of the damage caused by the tower failure. As part of the cost share for this program, FDWT designed and fabricated Briza repair, modifications and new components based on available technology and research. Figure 18 is a photograph of the shroud repair process.

The Briza design was based on three year old technology, since this is when the fabrication was initiated. New technology and developments have allowed significant performance potential over the Briza design. Therefore, the tests were not designed to generate maximum performance, rather they were designed to compare performance to predicted values, and to demonstrate feasibility while introducing WNE University Students and Faculty to real wind turbine testing and evaluation.

Figure 17: Tower Failure

Figure 18: Shroud Repair Process

The tests were conducted in accordance/guidance with the following International Electrotechnical Commission (IEC) and American Wind Energy Association standards:
AWEA Small Wind Turbine Performance and Safety Standard (AWEA 9.1 – 2009)

- IEC 61400 Part 12-1: Wind turbines – Power performance measurements of electricity producing wind turbines (2005)
- IEC 61400-11: Wind turbine generator systems – Part 11: Acoustic noise measurement techniques

Because the Briza 1kW is a small turbine according to the IEC definition (less than 200 m^2 rotor swept area), FDWT also followed Annex H of IEC 61400-12.1, which applies to small wind turbines. Experimentation consisted of the measurement of meteorological conditions, turbine electrical characteristics, turbine/support mechanical loads, and site specific turbulence

measurements. Specific measurements were made of electrical power, turbine thrust, and turbine rotor speed as well as the non-dimensionalized values of coefficient of power and coefficient of thrust. In these tests, power is normalized to sea-level air density. Please note that these tests are not an accredited power performance analyses because parts of the test do not follow IEC standards. However, the standards are used as guidelines and major deviations are noted. The purpose of the tests were to demonstrate FDWT's novel MEWT wind turbine operating on a tower. The objective of the effort was to investigate the performance of the FloDesign Wind Turbine (FDWT) 1kW Briza demonstration turbine under real world conditions and compare the results with the previously calculated performance (based on pilot plant wind tunnel testing and engineering theory). Furthermore, conducting these efforts in conjunction with Western New England University's Faculty and Students enhanced WNU's Green Energy Program by providing real-world wind turbine technology and experience in the classroom. It simultaneously provided on the job training to many students helping to improve their future employment opportunities while providing valuable information to further advance FDWT's mixer-ejector wind turbine technology creating opportunities for future innovation and job creation

4.1b Briza Test Site - High Wind Speed Location

The anemometry analysis for wind resource assessment was conducted at the former Rutland Heights State Hospital site in Rutland, Massachusetts. Preliminary results were presented as part of a Feasibility Study (FS) report completed by Boreal Renewable Energy Development (Boreal) in June of 2008. The FS report presented results based on a total of 2,168 hours of data logged between November 2007 and January 2008. An additional 5,589 hours of data were successfully measured and recorded, so there was a total of 7,757 hours of wind data that was recorded by the Second Wind Nomad 2 data logger from anemometers and wind vanes mounted on the site's 50m meteorological tower. An addendum to the initial FS report was added in June 2009 to include this additional data. Wind speed measurements were taken at 50m, 40m, and 30m. The prevailing wind direction and power density were found to be from 290 degrees. The wind speed data was correlated to the Worcester Regional airport. The long term 50m height wind speed estimate is 5.96 m/s which is one of the best inland test sites in Massachusetts. Therefore, the Briza was relocated to the former Rutland Heights State Hospital site in Rutland, MA, which is 10 miles Northwest of Worcester, MA. The terrain consists of an open field with a slight slope towards the west and sloping off towards the east. The field is open except for a few deciduous trees, two evergreens, and thick forest on the perimeter. The trees are generally 60 ft tall. The site has prevailing winds bearing 290 degrees relative to true north. For measurements for which it is important to accurately measure wind speed, FDWT uses data obtained when the wind direction is from all directions except between 20 and 160 degrees true. In this measurement sector, the influence of terrain and obstructions on the anemometer is significant. Figure 19 and Figure 20 show the turbine and meteorological tower locations as well as nearby obstructions and topographical features of the site. Figure 20 also shows the location of a 6kW test wind turbine installed in February, 2011.

The Rutland Heights test site has a low air density (approximately 1.1 kg/m3). This parameter affects the test results. For example, low air density will result in lower power output compared to output at sea level sites. The International standard for power performance measurements, IEC

61400-12.1, provides a method to correct for this effect (see section 6.3.1). The IEC standard uses the expression "measurement sector" to define wind directions that can be used for power performance measurements. The first step in defining the measurement sector is to consider historical wind data, if available. Data at the Rutland site has shown that the prevailing wind direction is 290° for winds above 4 m/s. These winds usually come during the "wind season," which normally lasts from November to April. Next we analyze the site to estimate the wakes from obstructions. The preliminary measurement sector should avoid wake effects on the turbine and the meteorological instruments. This includes the potential for the turbine wake to affect the anemometers on the meteorological tower. Based on the effects of the obstructions and position of the anemometer, the preliminary measurement sector is 160° to 20° true.

To conduct a power performance test without a site calibration, the terrain surrounding the demonstration turbine must meet all the criteria listed in Section A.1 of the IEC standard. The site passed all criteria. Because the turbine is placed on a relatively high tower with respect to the rotor diameter, the influence on the power performance is negligible. In this case, FDWT chose to forgo the site calibration.

Figure 19: View of Demonstration Turbine Toward the Prevailing West Wind.

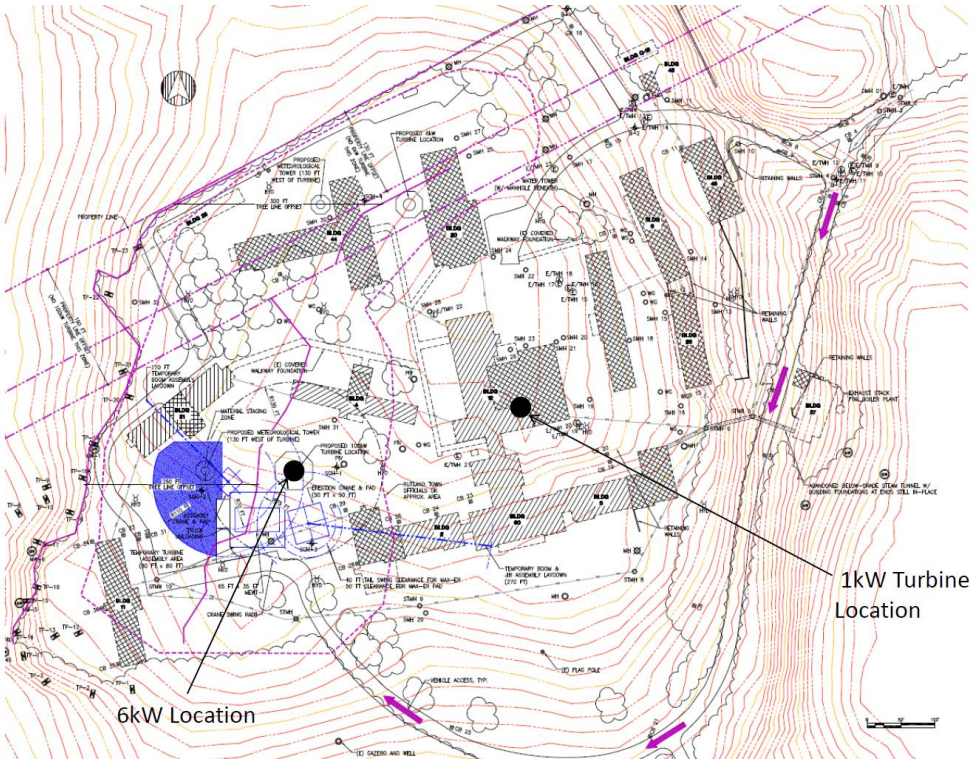

Figure 20: Plot Plan of the Test Site.

4.1c Briza Data Acquisition System

FDWT conducted power test using procedures in the Standards as guidance. The sampling rate was more than 4 Hz while the 1 Hz data was recorded. The averaging time was 1 minute for the mean values. FDWT also collected standard deviation, minimum, and maximum values for each averaging period. Data recording is accomplished by the DAS taking samples four times a second and displaying that data. The data is saved once a second for further review and post processing analysis later allows for one minute or ten minute averages to be found. This data is then stored in a relational database called MYSQL which is resident on one of the FDWT's servers. All data is protected and secured by being on this server and only those with access rights can view the proprietary information.

The data acquisition system is an ethernet based collection system that converts analog signals from the test instruments to digital which are recorded at a remote server as an SQL database. Figure 21 presents a photograph of the modules. These analog to digital converters are ADAM modules. The data is continually transmitted by a Verizon CDMA wireless modem. The data is then post processed and presented on a user interface developed in Visual Basic. Figure 22 shows a screenshot of the user interface. The system collects all the data from all the analogue sensors and converts it through the ADAM modules into digital signals that are then transferred to the PC for display. The ADAM 6017 module can accept up to eight separate analogue inputs and output two separate digital outputs. This module is the backbone of the data collection system.

Figure 21: Data Acquisition System Modules for Analog to Digital Conversion

Power generated by the turbine is 3 phase AC which must then be transformed into DC power by a rectifier circuit. The rectifier circuit removes the power spikes and delivers a constant DC waveform of 24 volts DC. This current is then passed through the power sensor, Bergey PowerCenter controller, and on to the battery charge controller.

As part of this program, a similar acquisition system was developed for the Bergey XL.1 wind turbine which was installed outside of Sleith Engineering Hall at Western New England University. Figure 23 is a photograph of the wind turbine installation. The addition of two photovoltaic arrays, two solar collectors, and the Bergey Wind Turbine were accompanied by subsequent senior projects aimed at aiding future students in WNEC's Green Engineering Program. The data collection system development effort of the Bergey XL1 wind turbine is presented in detail as Appendix A.

Figure 22: Graphical User Interface for Data Collection System

Figure 23: Bergey XL1 HAWT outside of Sleith Engineering Building

The goal was to construct a data collection system that mirrored the one designed, built and used on the Briza prototype, located at the test site in Rutland, MA. This system is shown in Figure 24 below.

Figure 24: Briza DAS, Located on Tower Base Trailer

The power generated by the Bergey turbine at Western New England University is 3 phase AC which must then be transformed into DC power by a rectifier circuit, similar to Briza. The rectifier circuit, shown in Figure 25, removes the power spikes and delivers a constant DC waveform of 24 volts DC. This current is then passed through the power sensor, Hall Effect sensor, and on to the inverter. Once the power generated by the turbine is sent to the inverter it is then transformed back in to AC current so as to be used by the lights in the mechanical engineering laboratory. This is shown in schematic form in Figure 25, which also displays the various sensors which send data to the Data Acquisition System (DAS).

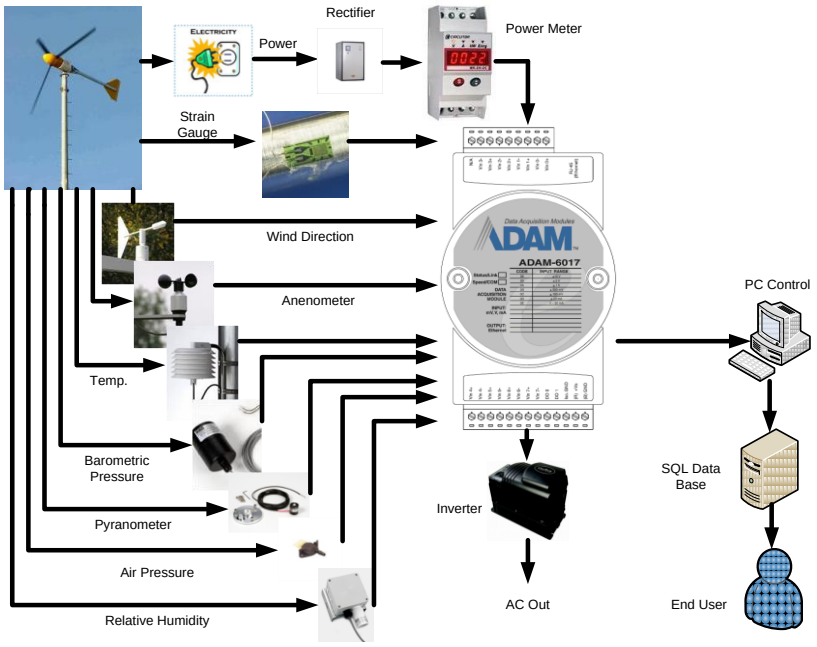

Figure 25: Schematic of DAS Inputs and Current Flow from Turbine

4.1d Briza Power Control

Initially the DC output from the Briza turbine was connected directly to a 1 ohm resistor. In accordance with IEC 61400-12.1 Annex H section C, the wind turbine was connected to an electrical load that is representative of the load for which the turbine is designed. In the case of battery charging applications, the load consists of a battery bank, a voltage regulator, and a means to dissipate the power that passes through the voltage regulator. In the ideal test set-up, the battery bank does not store energy produced by the turbine. Rather all turbine output is routed through the voltage regulator. Therefore, the battery bank may be smaller than typically recommended for the turbine as long as voltage at the connection of the turbine to the load can be maintained at 25.2 VDC. Therefore the DC output of the turbine was changed and connected to the Bergey PowerCenter (voltage regulator) and then to a battery bank and a

Figure 26: Bergey Power Controller use in Testing.

custom pulse width modulated load controller. The load controller kept the voltage constant at 25.2 VDC by controlling power flow to a dumpload, which prevented the turbine from shutting down due to high voltage caused by full batteries. Figure 26 presents a photograph of Bergey power controller used in testing.

4.1e Briza Measurement Procedures

The anemometer is mounted at hub height and 137 inches to the west of the turbine on a boom attached to the turbine tower. This corresponds to 2.6 times the rotor diameter (or 1.5 times the overall shroud diameter). The anemometer meets the IEC 61400-12.1 section 6.2 class standard. The requirements given in IEC 61400-12.1 Annex G and Annex H section g, with respect to mounting are used. Temperature and humidity were measured within 1.5 times the rotor diameter below hub height. This fulfills requirements given in IEC 61400-12.1 Annex H section j. The net electric power of the wind turbine was measured using a power measurement device (e.g. power transducer) and was based on measurements of current and voltage on each phase. The class of the current transformers met the requirements of IEC 61400-12.1 section 6.1. The power transducer was calibrated to traceable standards. The power measurement device was mounted between the wind turbine and the electrical load. This test uses an Ohio Semitronics power transducer that meets these requirements. The data was collected using IEC 61400-12.1 Annex H sections m-n. The database was considered complete when it met the following criteria:

1) each wind speed bin between 3 m/s and 14 m/s shall contain a minimum of 10 min of sampled data,

2) the total database contains at least 60 hours of data with the small wind turbine within the wind speed range,

Selected data sets are based on 1-min periods derived from contiguous measured data.
After data normalization the selected data sets were sorted using the "method of bins" procedure. The selected data sets covered a wind speed range extending from 3 m/s to 14 m/s. The wind speed range was divided into 0.5 m/s contiguous bins centered on multiples of 0.5 m/s. To ensure that only data obtained during normal operation of the turbine are used in the analysis, and to ensure data are not corrupted, data sets were excluded from the database under the following circumstances:

– external conditions other than wind speed are out of the operating range of the wind turbine;
– turbine cannot operate because of a turbine fault condition;
– turbine is manually shut down or in a test or maintenance operating mode;
– failure or degradation (e.g. due to icing) of test equipment;
– wind direction outside the measurement sector(s);
– wind directions outside valid (complete) site calibration sectors.

The selected data sets were normalized to two reference air densities. One was the sea level air density, referring to ISO standard atmosphere (1,225 kg/m3). The other was the average of the measured air density data at the test site during periods of valid data

collection, rounded to the nearest 0.05 kg/m3. No air density normalization to actual average air density is needed when the actual average air density is within 1,225 ± 0.05 kg/m3. The air density, power, and wind speed were determined from measured air temperature and air pressure according to the equation found in IEC 61400-12.1 Section 8.1.

The measured power curve was determined by applying the "method of bins" for the normalized data sets, using 0.5 m/s bins and by calculation of the mean values of the normalized wind speed and normalized power output for each wind speed bin according to the equations found in IEC 61400-12.1 Section 8.2. The power coefficient, C_p, of the wind turbine was added to the test results. C_p was determined from the measured power curve according to IEC 61400 standards.

4.1f Briza Power Results

The 1kW Briza turbine has operated at the Rutland, MA site since May 20, 2010, having previously been operated starting in November 2009 in Wilbraham, MA. Operational and performance data has been collected and recorded according to the requirements set in the IEC 61400-12.1 Power curve testing standard. Besides brief period for maintenance, the turbine has operated continually. Over 12,000 operational hours have been logged. This includes low wind speed and off-axis wind. Figure 27 presents the measured power in watts versus wind speed. This power reading is after frictional losses, transmission losses and generator losses. The Bergey generator was tested separately and was found to have a very poor efficiency. Data measurements, Briza predicted power, and a polynomial curve fit for the data are all presented in Figure 27. The Briza predicted power curve was obtained by using the methods of section 3.1b of this report. The ideal performance from this section was corrected for frictional losses, transmission losses and the Bergey generator losses. Even with these corrections the predicted Briza power curve is well above the Betz limit (i.e. C_p =0.593). The measured power data points are seen to scatter around the prediction. These results indicate a C_p for the Briza between 0.5 and 0.75 after losses, over the entire range of operation. This is well above the Betz limit of .593 and demonstrates that the Briza can operate on a tower in real wind conditions, and produce power potential of a HAWT with the same rotor swept area. This is a very important result! It verifies the potential of FDWT's MEWT concept. The Briza is an early version of the MEWT, and significant performance improvements have been made on shroud design and rotor design since the Briza lines were frozen for fabrication and testing. The data scatter seen in Figure 27 is consistent with standard wind turbine measurements. This scatter can be caused by turbulence, wind gusts, wind mis-alignment, wind shear and inertial effects. The overall trends are consistent and agree very well with the predicted curve. Figure 28 presents the histogram of the power curve wind speed bins. All the bins are full according to the IEC standard. These full bins indicate a complete power curve test effort for small wind turbine tests.

For the test, normalization to sea level air density is made by multiplying power by the ratio of sea level air density to site air density. These results are based on data sampled once per second and "pre-averaged" into 1-minute data points. The binning process sorts the data points into 0.5 m/s wind bins and then averages the power data within each wind bin. Table 3 gives the results in tabular format for sea-level conditions. In addition, table 3 shows the number of data points in each bin (10 is the minimum to consider the bin filled).

Figure 28 gives the binned power curve for the predicted, actual 1 minute data points, and the averaged data normalized to sea level air density (1.225 kg/m3). The predicted and measured power curve correlates very well. The predicted power curve is based on aerodynamic theory, computational fluid dynamics (CFD), and wind tunnel testing results. This accurate correlation increases our confidence in predicting performance on larger wind turbines from CFD and wind tunnel testing. All bins are full according to the IEC standard. These full bins indicate a complete power curve test effor for small wind turbine tests.

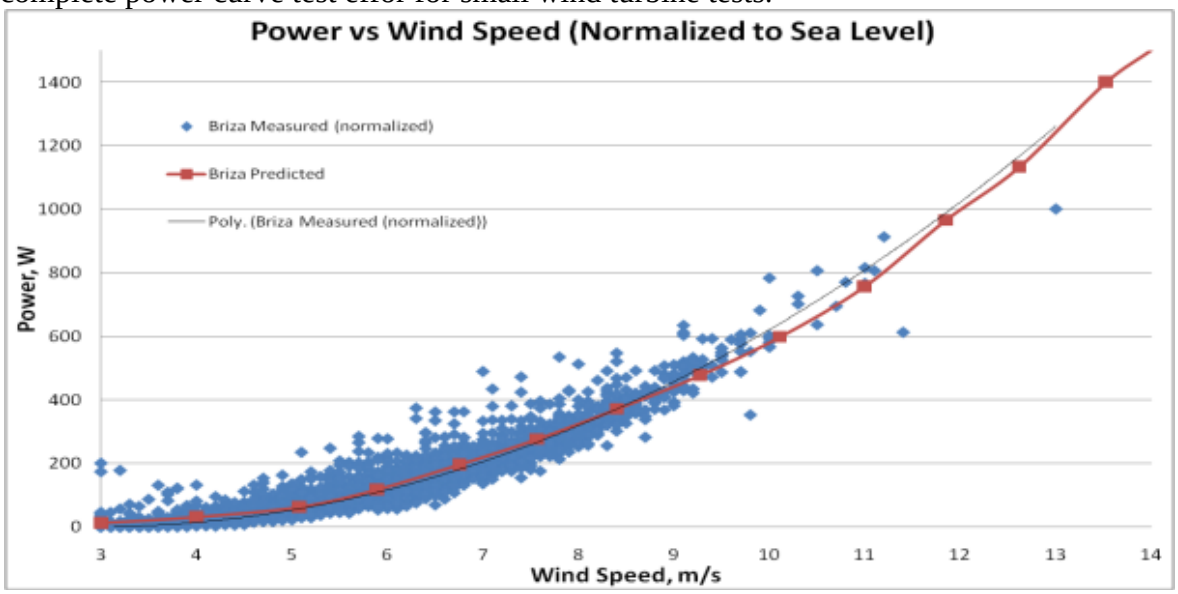

Figure 27: Measured and Predicted Power Curve for the 1kW Briza

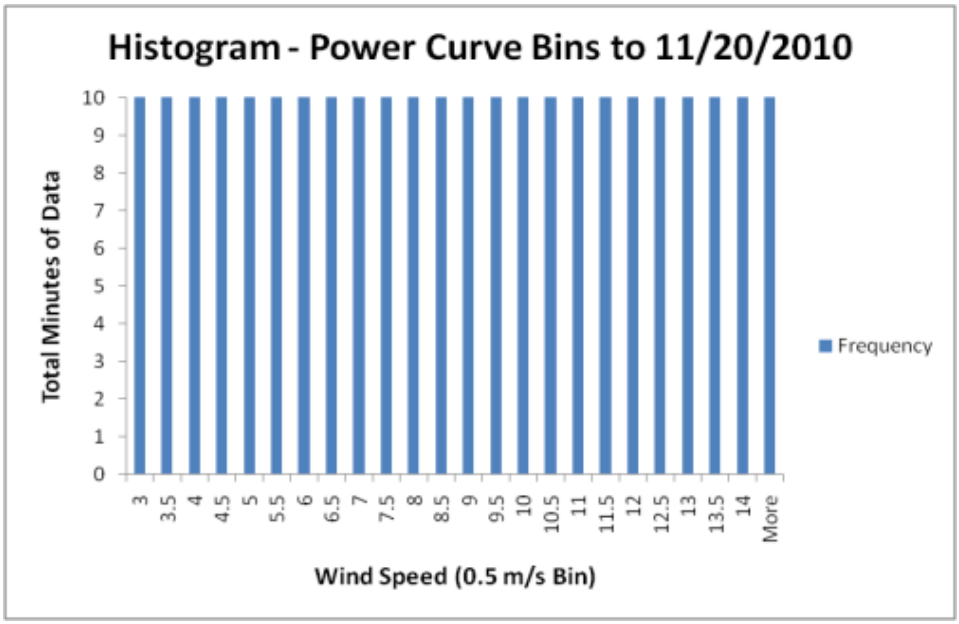

Figure 28: Histogram of Power Curve Wind Speed Bins.

4.1g Yaw Control & Off-axis Gust

The objective of the yaw mechanism research was primarily to research and develop a yaw mechanism for the Briza MEWT turbine. The yaw mechanism is what allows the turbine to rotate and is an integral part of the power transmission between the generator and the tower. Figure 29 presents a schematic of yaw system designed by FDWT engineers using slip rings and a friction damping clutch. The Briza turbine operated in a variety of wind conditions with the yaw friction clutch device. The yaw friction clutch allows for a variable mechanical resistance and allows the turbine to yaw out of the wind in extreme events. The Briza design allows for this

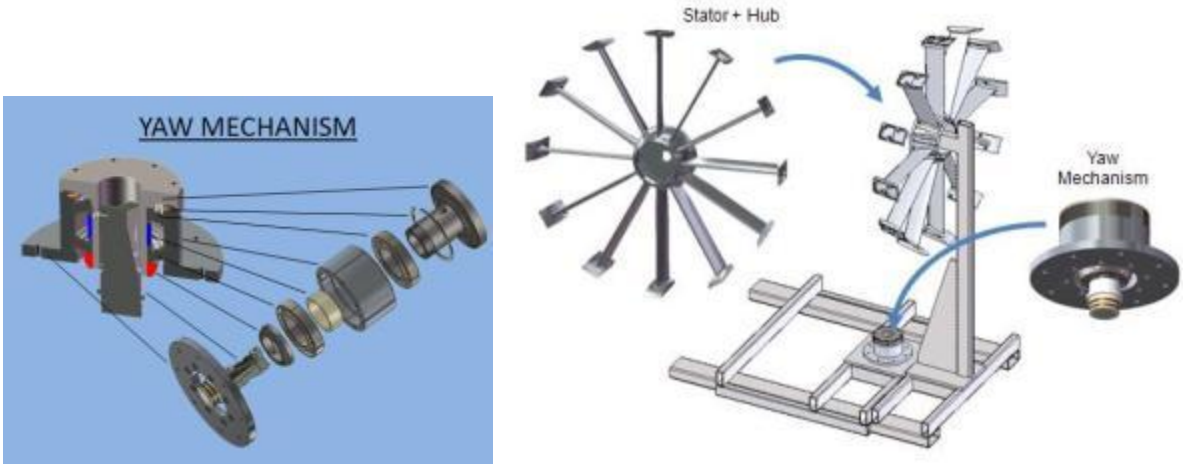

Figure 29: Yaw Design

passive yaw direction control where no electro-mechanical systems are required to align the turbine heading with the wind direction. This task also investigated the off-axis performance and structural loads of the Briza. The Briza was tested with a yaw damping clutch system. Figure 30 shows engineers working on the Briza yaw mechanism, and the measured power obtained

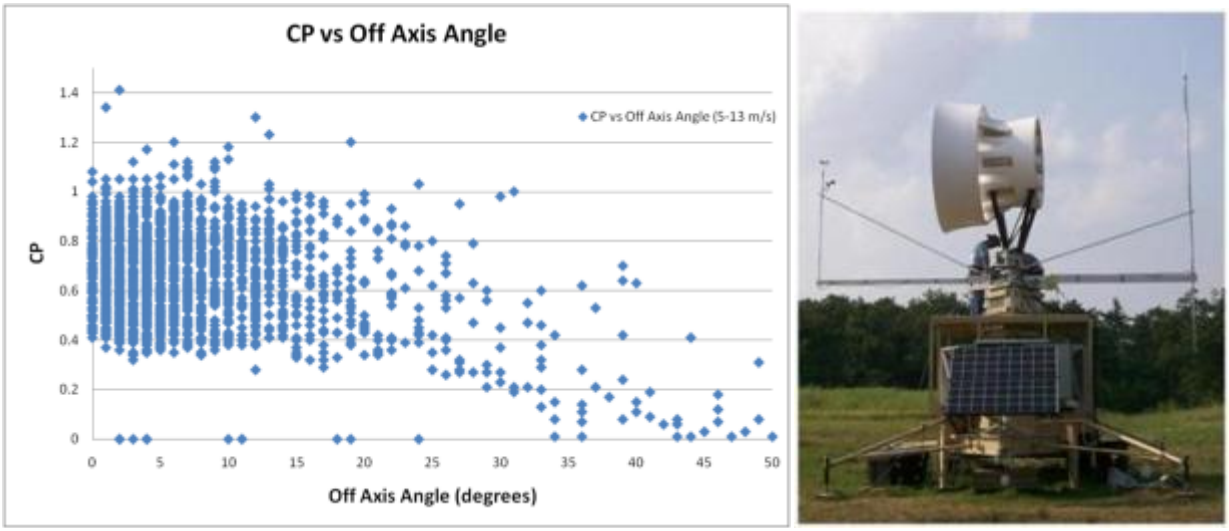

Figure 30: Coefficient of Performance vs. Off Axis Wind Direction

with yaw angle variations up to 50 degrees. The power is unaffected by off axis wind up to approximately 25 degrees. This is a major advantage of the MEWT design over traditional HAWT's. It is believed that the flow acceleration into the turbine shroud straightens the flow out before reaching the stator/rotor station. A free yaw test was also conducted with a locked rotor on the Briza. This condition reflects how the system might act in extreme winds. Figure 31 presents the wind tracking capability of Briza. The blue line represents a history of the wind direction. The yellow line represents a history of yaw mis-alignment of Briza to the wind direction. It is seen that Briza tracks the wind direction very well.

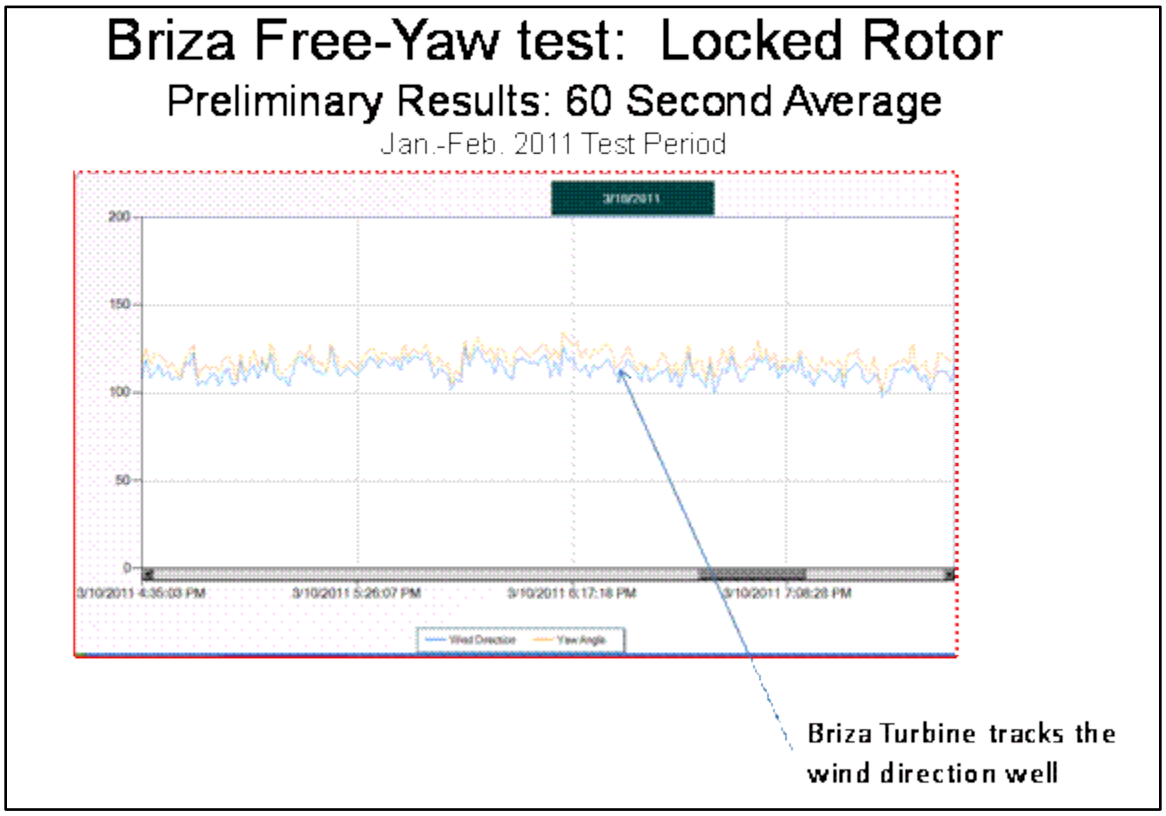

Figure 31: Tracking Ability of Briza.

4.1h Briza Alternate Component Tests

Several Briza component variations were designed and fabricated by FDWT Engineers for testing on a tower to determine their performance with real wind conditions. These component variations included the following:

- composite rotor
- stators with flaps
- fabric shroud

The original rotor on the Briza had 10 blades. It was machined out of solid aluminum and was extremely heavy. The rotor by itself weighed sixty pounds. As a result, it was thought that the large inertia of the blade had to be reducing gust response of the Briza during normal operation. A composite rotor was made using carbon fiber with a foam core to reduce weight and improve gust response. The number of blades was reduced from 10 to 7. The blade number reduction was designed into the system to further reduce the amount of material used. Figure 32 presents a photograph of both the original Briza rotor and the new composite rotor. The weight of the composite rotor was 26.6 pounds which is close to a 60% weight reduction from the original rotor. Figure 33 presents the power test results with and without the composite rotor. The seven bladed, composite rotor increased gust response, but was found to have a slightly lower efficiency. The lower efficiency of the composite rotor is probably a result of the reduction in number of blades. Also, the tests were conducted with actuator stator flaps. It was very difficult

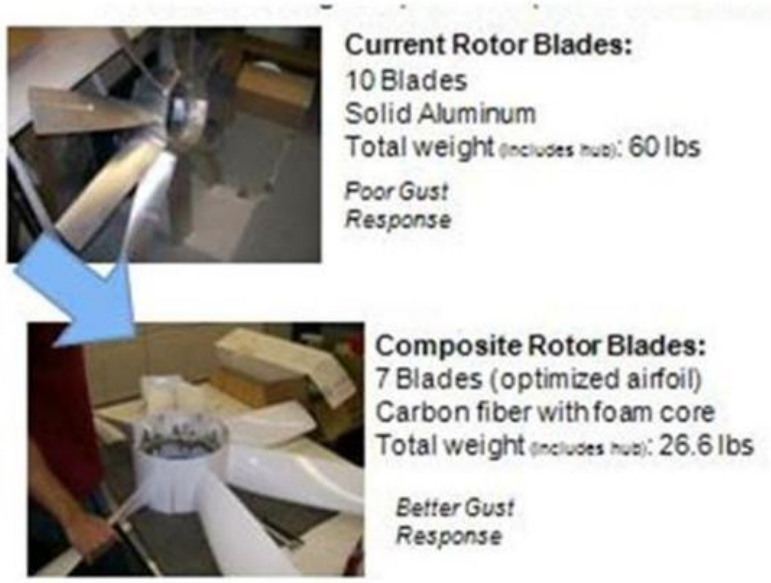

Figure 32: Composite Rotor Blades

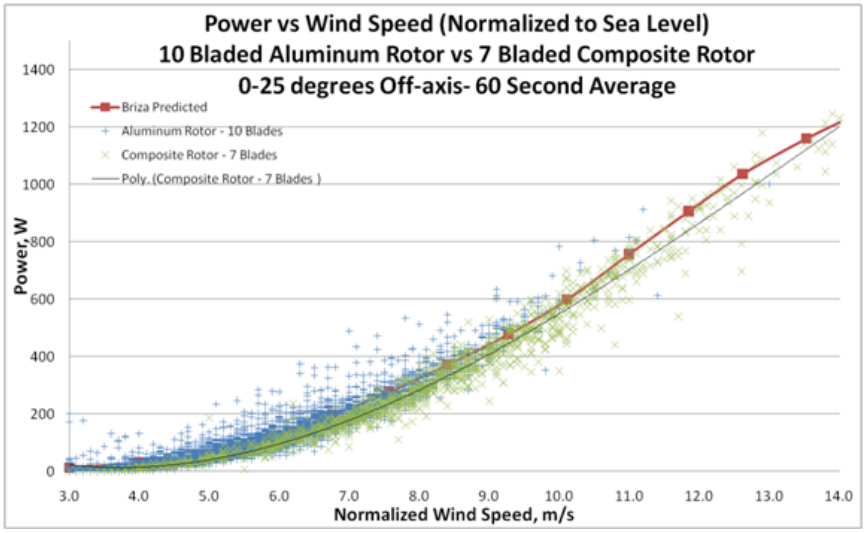

Figure 33: Composite Rotor Blade Performance

to perfectly align the flaps in the null position with the actuators. This could have been another source for the lower efficiency. Figure 34 presents a schematic and a photograph of the stator flap configuration. Individually servo controlled flaps were installed on nine of the twelve stator blades in the original Briza stator rotor system. This configuration was tested to determine the feasibility of using the flaps for aerodynamic braking. Figure 35 presents CFD predictions which indicate that aerodynamic braking was possible. Briza test results using aerodynamic braking were very successful and verified the CFD predictions. Figure 36 presents a photograph of the

Figure 34: Stator Flaps

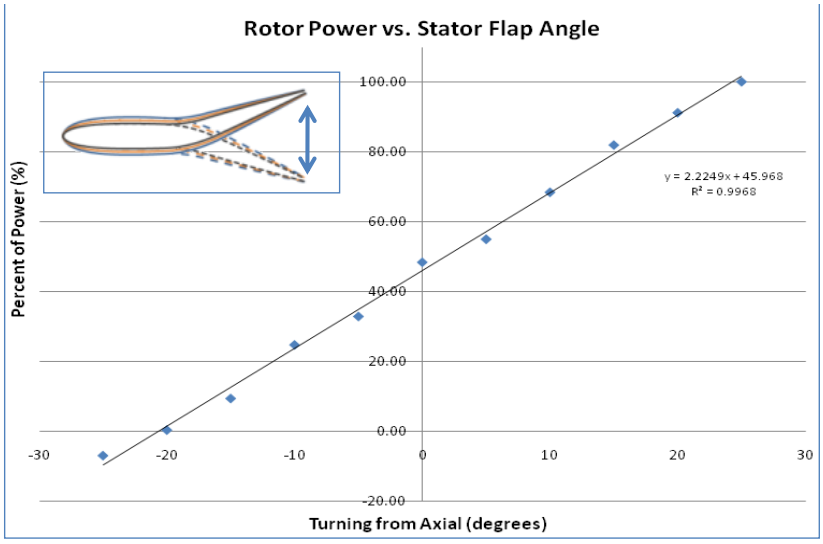

Figure 35: Stator Flap for Aerodynamic

construction of a fabric shroud. The fabric shroud was slightly shorter than the original Briza shroud as seen in Figure 37. It was mounted on the Briza system and tested over several days. Performance test results showed no difference between the fabric shroud and the conventional fiberglass shroud. These results indicate significant weight and cost savings can be accomplished by using fabric ejector shrouds.

Figure 36: Fabric Shroud Construction

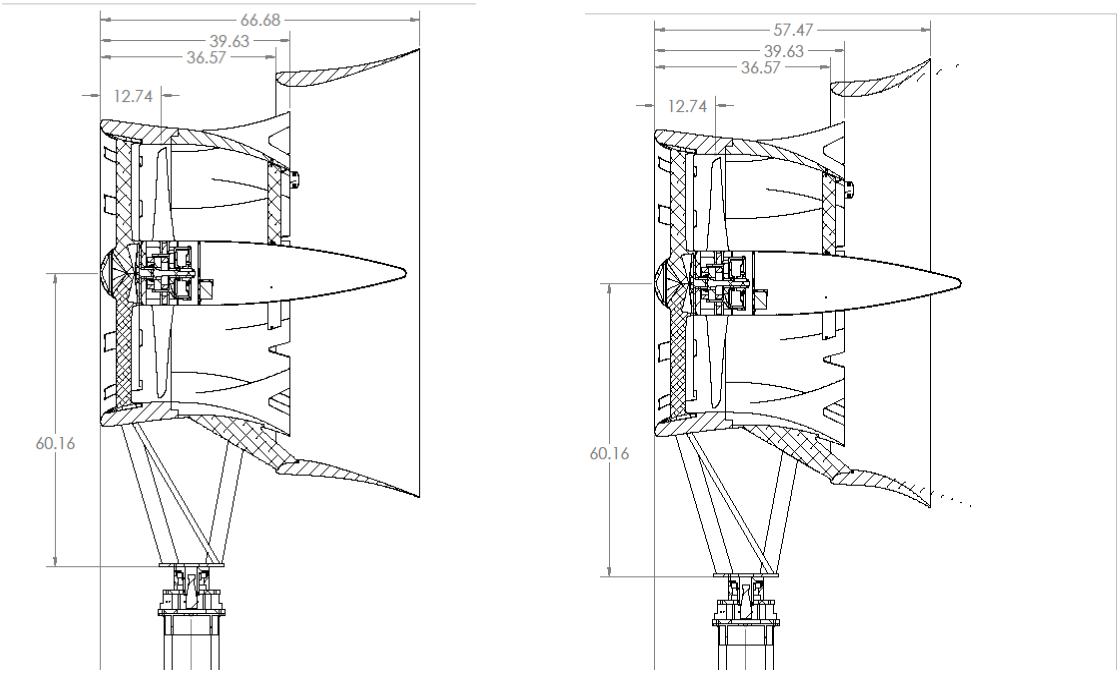

Figure 37: Fabric Shroud Dimensions

4.1i Acoustic Testing

The objective of this part of the project was to perform a noise analysis of the "Briza" 1kW mixer ejector turbine. All the testing was done at the site in Rutland, Massachusetts at an approximate address of 88 Maple Avenue, Rutland Ma 01543. The test turbine is located at the former Rutland Heights State Hospital site in Rutland, MA, which is 10 miles Northwest of Worcester, MA. The terrain consists of an open field with a slight slope towards the west and sloping off towards the east. The field is open except for a few deciduous trees, two evergreens, and thick forest on the perimeter. The trees are generally 60 ft tall. The site has prevailing winds bearing 290 degrees relative to true north. Figure 38 presents an aerial photograph of the Rutland site. For measurements for which it is important to accurately measure wind speed, FDWT uses data obtained when the wind direction is from all directions except between 20 and 160 degrees true. All testing was taken downwind of the turbine at specified locations. The testing distance(s) were acquired using the IEC 61400-11 standard. It was calculated that we test at 86 feet from the center of the turbine to perform a certified measurement. Also for the chance that the Briza turbine shields' noise we performed testing at 120 feet as well. The other issue that needed to be taken into account was the fact that the turbine may show signs of spherical spreading, which basically is that the sound maybe stronger or weaker off axis from the tail cone. In order to check for this, tests were conducted at 0 degrees (downwind, on axis), -15 degrees (downwind, off axis), and 15 degrees (downwind, off axis).

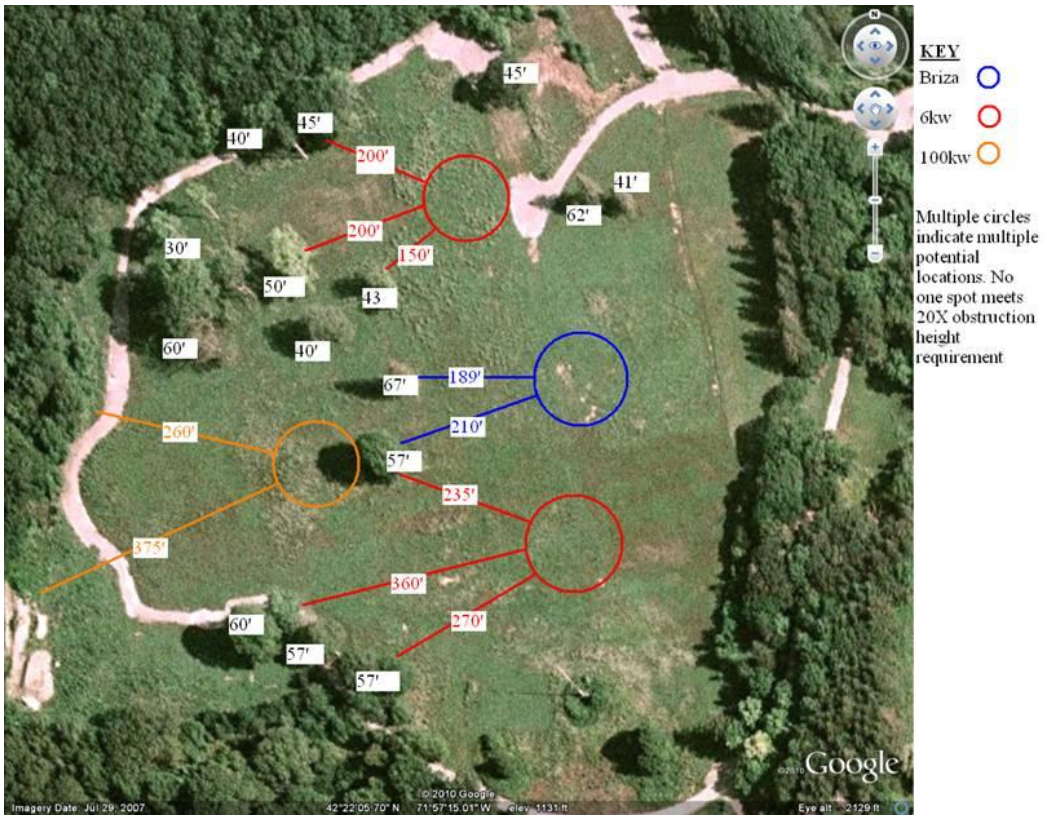

Figure 38: Google Sky Screenshot of Rutland Test Site with Pertinent Distances and Heights

The actual testing of the noise of the turbine was performed using techniques and equipment as close to the IEC standard as possible. In order to qualify as a certified test it was required that we

have 30 data points taken at integer wind speeds of 6, 7, 8, 9 and 10 m/s with a tolerance of +/- 0.5 m/s. All the equipment for a certified test can be seen in Table 2. However during the test used for this analysis, the type 1, Casella CEL-495 microphone and preamplifier which is used to plug into the data recorder was not used. A Casella Type 2 microphone was used for this test because the analysis program was calibrated for the type 2 microphone and the calibration had not yet been completed for the Type 1 microphone.

Table 2: Equipment Specifications

Instrument	Manufacturer	Model Number	Serial Number
Microphone	Casella USA	Cel-495	1001
Preamplifier	Casella USA	Cel-495	1002
Microphone	PCB	377B20	112193
Preamplifier	PCB	378B20	105112
Digital Recorder	Zoom	H4	70839
Sound Level Meter	Casella USA	Cel-440	42842
Signal Conditioner	PCB	480C02	10305

Also worth mentioning, all tests were completed on a 1 meter in diameter ¾" thick plywood circle. This "sound board" is to prevent inaccuracies from the various ground and soil types. Another precaution taken at the site was the grass and weeds were taken down with a weed whacker to minimize noise effects of the whistling grass. Figure 39 is a representation of a test location at the Rutland Site.

Figure 39: 86 ft and 0° Test Location-Rutland, MA.

Testing of the turbine was performed at one of the specified locations for about 30 minutes with the turbine on, and then another 30 minutes with the turbine's brake applied to get an ambient data set. At the specified location, data was recorded continuously through the Zoom digital recorder and when a high stream of wind came, short bursts of one to two seconds were recorded through the Casella sound level meter to get Lmin, Lmax, and Lequivalent values. Having the redundancy of the digital recorder and being able to match them with a correlated value off the sound level meter was a great attribute to guarantee correct results. Several software programs were written to facilitate the processing of the recorded data and the post-processing of the data. Most programs were written in Labview and several others were written in Matlab. Figure 40 presents a schematic of the acoustic measurement setup. The effort focused on the 1 kW, Mixer

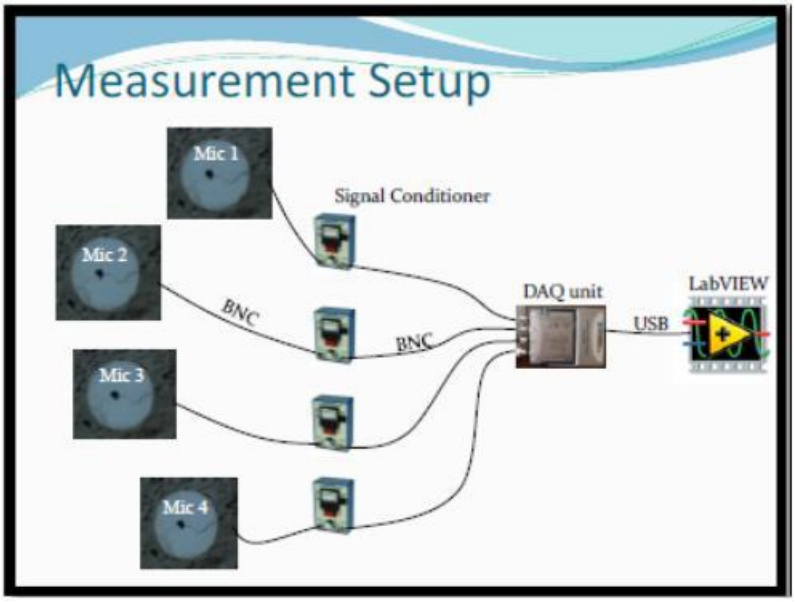

Figure 40: Acoustic Measurement Setup

Ejector Wind Turbine of FloDesign. In order to do this, a level of understanding about acoustics and noise control needed to be acquired. Using these developed skills and knowledge about acoustical noise measurement procedures and acoustic processing, specific acoustic hardware and LabView operated data acquisition systems were developed for data processing. The majority of the effort focused on characterizing the noise emissions of the Briza 1 kW mixer ejector wind turbine located in Rutland, Massachusetts, and compare it to radiated noise of the 1 kW Bergey wind turbine located at Western New England College. The Bergey 1 kW wind turbine located at Western New England University is attached to a 60 foot pole that is attached to the side of Sleith Hall on the Western New England University campus, as shown in Figure 41. The turbine hub is roughly 60 feet above the ground, and the anemometer is roughly 50 feet above the ground. Prevailing winds are typically from the west, which means that a downstream measurement location corresponds to a position on the roof of Sleith Hall. Several measurements were taken. There were several issues with the measurements. First, we did not have access to the wind speed data; therefore we can only do a qualitative assessment at this time. Second, during the wind turbine noise recordings, the hvac equipment that is situated on the roof of Sleith Hall was operational. When the hvac systems were running, the background noise increased significantly which made it more difficult in distinguishing the wind noise from

the general elevated background noise. Several sets of data were recorded and used to determine the Bergey acoustics.

Figure 41: View from the Roof of Sleith Hall of the Bergey 1 kW Wind Turbine

The noise measurements for both the Briza and the Bergey were collected and analyzed in accordance with the IEC standard for acoustic noise measurement techniques, IEC 61400-11 (Ref. 1) and the AWEA standard for small wind turbines. As mentioned above, turbine and background data were collected using 4 microphones simultaneously and Labview was used to acquire the data collected from the microphones.

Figure 42: Briza Quieter Than Bergey

A weighted sound pressure level measurements were used to measure the sound power of the Briza at various wind speeds. Figure 42 presents the measured sound power level of both the Briza in Rutland and the Bergey at Western New England University. This is a very good apples

to apple comparison since the Briza uses the same generator and power transmission as the Bergey. The measurements indicate that the Briza sound power level is over 10 dB lower than the Bergey, and is typically less than comparable wind turbines at the range of wind speeds measured. Figure 43 shows Briza sound pressure level measurements over a range of frequencies. These results definitely show tonal noise measurements related to the rotor rotational speed and its

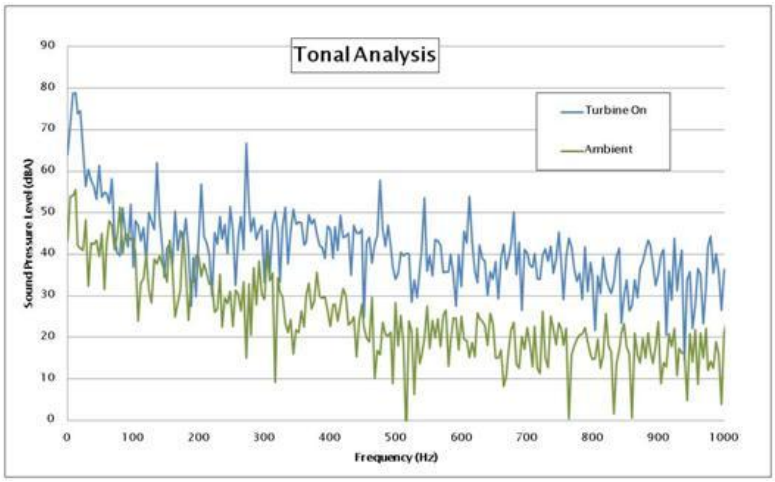

Figure 43: Tonal Analysis

Harmonics. An interesting fact is that the measurement of the ambient sound pressure level downstream of the wind turbine with the wind turbine rotor locked in place seems to indicate an increase in background level compared to other locations. This measurement seems to indicate a presence of a noise source other than the spinning rotor. In addition to sound power measurements, one third octave band and narrow band fast fourier transforms were performed to further investigate the characteristics of the radiated noise. Figure 44 presents results of the 1/3

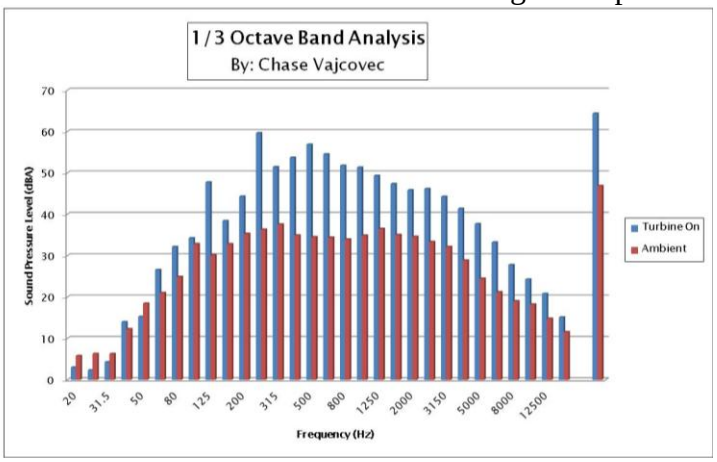

Figure 44: 1/3 Octave Band Analysis

octave band analysis. From these acoustic tests, a few conclusions can be made. First and foremost, smaller sized wind turbines especially in the 1 kW power range produce loud and high frequency tones at higher wind speeds which can be either frequency based or sporadic. The

Briza was consistently quieter than the Bergey, or its HAWT counterpart. At higher wind speeds, the noise created by the Briza wind turbine would not only increase in SPL but in frequency as well. The tonal noise was in multiples of the blade passing frequency of the stator and rotors. At this point the turbine sounds very much like a remote controlled plane flying or more commonly a quieter jet engine. Also after analyzing the four microphones that were place along the perimeter of the test circle on the date of July 21, it was determined that the noise propagation seemed to be more omni-directional as the sound power level for all four microphones seemed very similar. Appendix B presents more details of the Briza Acoustic testing efforts.

4.1j Dynamic FEA Analyses

The Briza turbine sits upon a mount that couples it to the tower and controls the yaw. This mount is the focus of this effort. To begin analyzing the structural integrity of the mount, Finite Element Analysis (FEA) was used to analyze the Load Beam. This piece is equipped with strain gages and is used to determine the loads on the turbine. Using FEA and applying the critical loads caused by an 80 mph wind, the strength of the load beam was determined. This work included developing an MS Excel program to calculate the effects of wind loads on turbines and their towers. Calculations were done to assess the loading conditions on turbine towers exposed to different wind conditions. The Briza is mounted on top of an 80 foot collapsible tower with three guide wires for stability seen in Figure 45.

Figure 45: Briza Prototype in Rutland

In between the tower and the Briza is the turbine mount that is the main focus of the project. This mount consists of a small electric motor and appropriate gearing which controls the yaw of the

Figure 46: Load Beam Instrumented with Strain Gages

turbine. Mounted at its base is the load beam which has been instrumented with strain gages in order to determine the loads that the turbine is subjected to as seen in Figure 46.

The load bearing capabilities of this piece were to be investigated along with the subsequent tresses that are induced. This is a critical component in the tower mount because the yaw assembly and turbine sit atop this piece. To determine the resulting stresses a finite element analysis program called Abaqus was used. Abaqus is a powerful engineering simulation program that utilizes the finite element method, to solve anything from simple linear analysis to the most complex nonlinear jobs. Finite element method is a numerical technique for finding approximate solutions to partial differential equations as well as integral equations. This routine is what allows Abaqus to solve very complex problems relatively easily. It has the capability of modeling several different types of materials such as, metals, rubbers, polymers, composites, reinforced concrete, etc. The program includes an extensive library of elements that allows for the modeling of complex components. The components can be either drawn in Abaqus using the sketch module or imported from a 3D modeling program, such as SolidWorks. The model can then be assigned a material type. This is done by creating a material and specifying if it is elastic or plastic. The final step is to input the applicable material properties such as, Modulus of Elasticity, Poisson Ratio, etc. The part that is being analyzed is divided into elements with nodes at each of its corners. These elements can be assigned different types in order to create an accurate mesh. The accuracy of the part mesh is critical to obtaining accurate results in the analysis. A mesh can range from coarse to fine, referring to the number of elements along each edge of the part. The finer the mesh, generally the more accurate the results will be. Having this type of accuracy causes the job to have to run for a longer time. Therefore the mesh refinement is reduced in areas where the stress is known to not be that significant. It is important to increase it in high stress areas like, bolt holes, fillets, and sharp corners. The types of elements that are utilized in the routine are also an important factor in the certainty of the results. The two most common types of elements are linear and quadratic. Linear elements are 8-node bricks where as quadratic are 20-node bricks. The 20-node type are more accurate than the 8-node because the computation is more extensive with twenty nodes, this causes the job to take longer to complete. Although the time to process is greater the accuracy that is obtained is sometimes required. The next steps would be to apply the appropriate loads and boundary conditions to the model. These need to simulate the actual loading and fixing points of the piece. There are numerous different

types of loadings that can be used, for example, concentrated forces, pressures, surface traction, moments, bolt loads, etc. The boundary conditions need to mimic how the part is restrained in its real world application. Contour plots showing the resulting stress, strain, reaction forces, and deformation are presented in Figure 47 below as a Von Mises stress contour plot. The processes described are what were used to conduct the analysis on the turbine mount. It was found that the highest stress at an angle of 225 degrees was 53,020 psi. The yield stress of the material is 40,000 psi. The severe loads caused by an 80 mph wind that were applied to the load beam suggest that the part needs more attention. The maximum stress induced by these loads at wind directions varying from, 0- 360 degrees in 45 degree increments range from 42,530 psi to 53,020 psi. These values are all above the yield stress of Aluminum 6061- T6, which is 40,000 psi. Therefore the need for further analysis is required to be certain that this is not a potential problem. It is further recommended that the Briza turbine be brought down using the telescopic tower in the event of any potential extreme wind conditions. More details of this Load Analysis is presented in Appendix C.

4.1k Briza Load Tests:

Calculations were done to assess the loading conditions on MEWT's lattice turbine towers exposed to different wind conditions. Towers were modeled in MS Excel using standard Fluids theory and in SolidWorks for use in Abaqus for finite element analysis. It was determined that the mixer ejector wind turbine (MEWT) created 1/3 the load on a typical monopole (tubular)

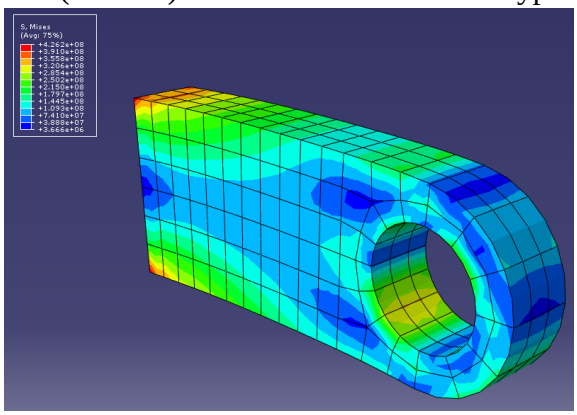

Figure 47: Von Mises Stress Contour Plot

tower while creating the same power output as a horizontal axis wind turbine (HAWT). It was also found that the side load of a HAWT was very large compared to the potential drag force due to a cross wind on the shroud of the MEWT. Through FEA analysis, the steel lattice tower design was found to be much better suited to handle any loads or torques compared to the steel tubular tower. Calculations also showed that the MEWT exerted a much smaller torque from gyroscopic loads than the HAWT due to its much smaller mass moment of inertia and overhang.

Several tests were conducted with load cells on Briza to measure actual loading under normal operation on a tower. Figure 46 presented the load beam mounted directly under the Briza at the tower interface. Figure 48 presents loads measured during normal operation. The data is seen to

have significant scatter, but has a trend which varies as wind velocity squared. These results are

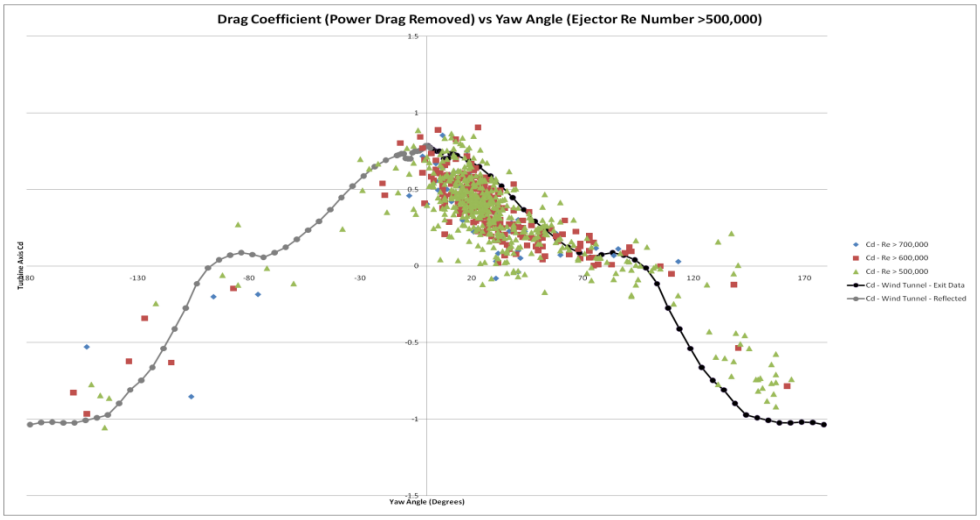

consistent with predictions and expected load data. Figure 49 presents a comparison of measured Briza Cd from the load cell data and University of Maryland wind tunnel test results. Cd is presented as a function of yaw angle. The two test results have very similar trends with the Briza loads significantly lower. These results could be directly related to the lower Reynolds numbers associated with wind tunnel testing.

Figure 48: Load Cell Measurements

Lower Reynolds number usually mean higher losses and higher drag. Also, the turbulence levels associated with tower testing are significantly higher than in a wind tunnel. Higher turbulence levels will tend to lower any separation drag occurring on the MEWT systems. More details of this study are presented in Appendix D.

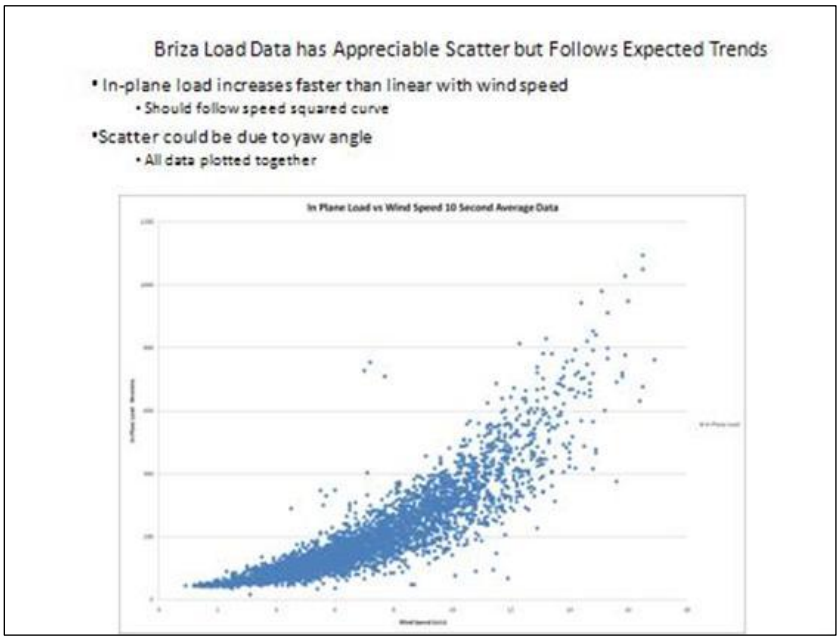

Figure 49: Briza Cd Comparison With UMD Wind Tunnel Results

4.1l Downstream Wake Modeling:

Interns and FloDesign Wind Turbine Engineers participated in a wake study program. This program included taking preliminary wake measurements on the Briza during power operation on the tower. The photograph in Figure 50 shows the measurement setup. A wind anemometer traverse rig was built and supported in the wake downstream of the Briza during normal operation. This wake traverse rig was moved to various axial distances from the ejector exit plane. Figure 50 presents measured velocity, non dimensionalized using wind velocity, for several different axial positions in the wake. The axial distance is non dimensionalized by MEWT exit diameter. The results show typical flow profiles measured in the MEWT wake. These preliminary wake profiles show very rapid mixing between the 1.0 and 2.0 axial distance locations downstream of the Briza. This is a very encouraging result, since the faster the wake mixes out, the closer wind turbines can be placed effectively on a wind farm. Most HAWT's require a spacing between five and ten diameters for effective power generation in a wind farm.

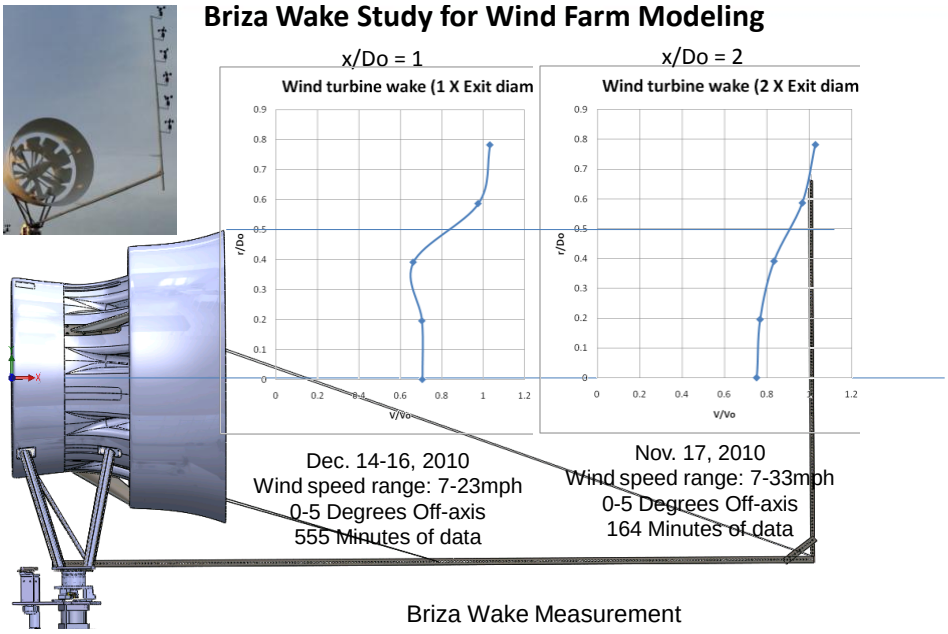

Figure 50: Sample Wake Measurements on Briza

4.1m Briza Summary:

The Briza was used to demonstrate the feasibility of FDWT's Mixer Ejector Wind Turbine in real world conditions. It consists of a rotor with a roughly five feet in diameter producing up to 1kW of power limited by its generator size. This turbine was installed onto a telescoping tower located upon a mobile trailer allowing for it to be deployed and stowed quickly at various locations in order to investigate multiple aspects of the system performance. This joint University and Industry program allowed many students and faculty to participate in various field tests with the Briza which demonstrated the following;

- Briza power performance was consistent with predictions indicating that MEWT concepts can have significantly higher performance than HAWT designs
- Off-axis gust performance was improved over HAWT designs
- Briza was significantly quieter than HAWT designs
- Briza wake measurements showed rapid mixing benefits
- Performance studies with alternate aerodynamic components demonstrated the feasibility of improving performance and the operation capability of the Briza design.

Each of the efforts performed provided valuable information in the process of developing and demonstrating FDWT's new and innovative MEWT concept, and provided on site engineering work experience for numerous Western New England (WNE) University Professors and Student Interns while bringing real-world wind turbine experience into the classroom further enhancing the Green Engineering Program at WNE University. The next two sections of this report describe the wind tunnel test efforts conducted to evaluate and improve MEWT components, and the feasibility study conducted to investigate using MEWT designs for home wind turbine application.

4.2 Small Scale MEWT Model Test Programs

Background

Small scale wind tunnel testing is used extensively at the early stages of product design as a way to quickly and costs effectively investigate the major effects of various conceptual ideas. The result of the conceptual testing provides valuable information and new ideas for future iterations which would otherwise never be discovered since a majority of the concepts cannot feasibly be integrated into a larger scale prototype.

There is however limitations to the small scale testing which also must be understood so that the results are not incorrectly applied or prematurely dismissed. These limitations include blockage effects due to the tunnel walls, the testing of incomplete models that do not include all of the installation effects, velocity profile variations across the wind tunnel diameter, and the inability to achieve Reynolds numbers consistent with larger scale prototypes.

Despite these limitations, many advances in the MEWT technology have been made during this testing program allowing for benefits to subsequent larger scale prototypes, such as the Briza, to incorporate these advanced concepts into the next level of development. Throughout this program various versions of the MEWT geometries were tested to understand their effectiveness in terms of performance as well as the magnitude of structural loads which will be generated at a larger scale. In the process of analyzing these concepts, it also provided an opportunity for the Interns to interact with WNU faculty and FDWT staff on a project that puts fluid dynamic theory into practice.

Test Setup

Dual Flow Wind Tunnel System

The wind tunnel was designed by FDWT along with the help of numerous Interns, to test MEWT components in an open jet, unrestricted from wall effects, in order to simulate an actual wind turbine installation. The same wind tunnel must also allow the flexibility of performing more focused tests on specific components such as mixer nozzles to investigate their flow parameters. This testing flexibility was achieved through the development of FDWT's Dual Flow Test Facility shown in Figure 51.

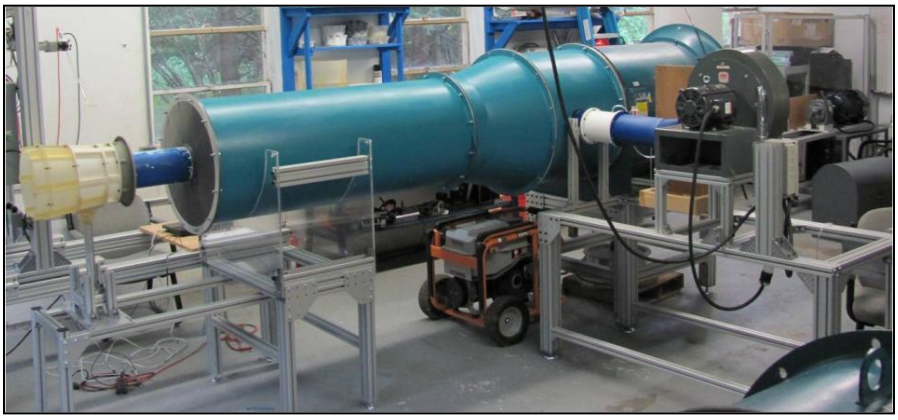

Figure 51: Dual Flow Wind Tunnel Test Setup

It provides the option of simulating a MEWT installation by mounting a small-scale MEWT model onto a load balance tower located downstream of the exit plane in order to measure aerodynamic drag with respect to yaw angle (Open Jet Configuration), or the MEWT can be mounted directly to the core-flow duct, as seen in Figure 52, which simulates the flow being delivered to the rotor of the MEWT providing a method to determine mixer effectiveness and ejector pumping (Core Flow Configuration).

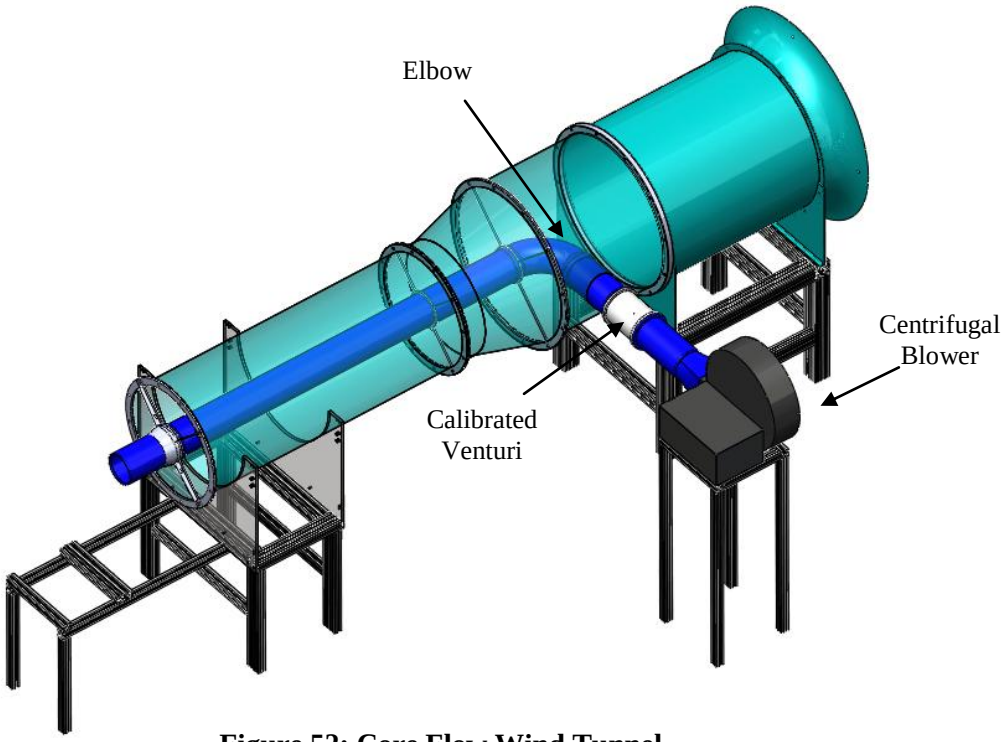

Figure 52: Core Flow Wind Tunnel

In the open jet configuration, shown in Figure 52, flow is delivered by an axial flow fan driven by a motor with a power output of approximately 20 horsepower. This fan supplies flow velocities of up to 80 feet per second through a converging duct, into a 29 inch diameter outlet

duct with an approximate length of 7 feet, before reaching its' exit plane to interact with the MEWT models.

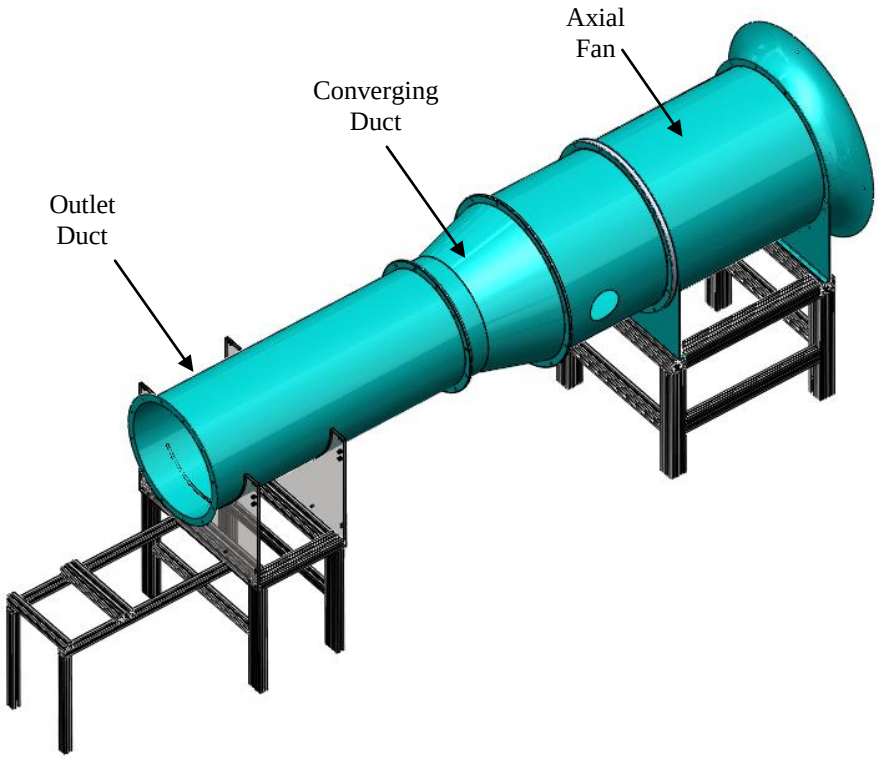

Figure 53: Open Jet Wind Tunnel Configuration

The core flow configuration, shown in Figure 52, utilizes a second fan and elbow-duct system independent of the open jet configuration's axial fan to produce flow velocities of greater than 140 feet per second at the mixer nozzle. A 5 horsepower centrifugal blower supplies this flow through a sheet metal square-to-round transition duct that interfaces with a calibrated venturi for flow rate measurements through the core flow system. Continuing downstream, the venturi interfaces with a 6 inch inner diameter PVC tube which pierces the open jet axial fan duct at right angles before entering a 90 degree elbow and continuing down the centerline of the open jet outlet duct for approximately 8 feet until reaching its' exit plane where a mixer nozzle can be installed.

Automated Traverse System

For both of the dual flow wind tunnel configurations it is necessary to measure and record the velocity profiles downstream of the MEWT components. This process utilizes an automated traverse system, shown in Figure 54, consisting of two independent lead screw rails and stepper motors that precisely position a pitot-static probe, shown in Figure 55, in a plane perpendicular to the outlet stream, measure a total and static pressure value for each position, and record it in the data acquisition system to be used for further analysis.

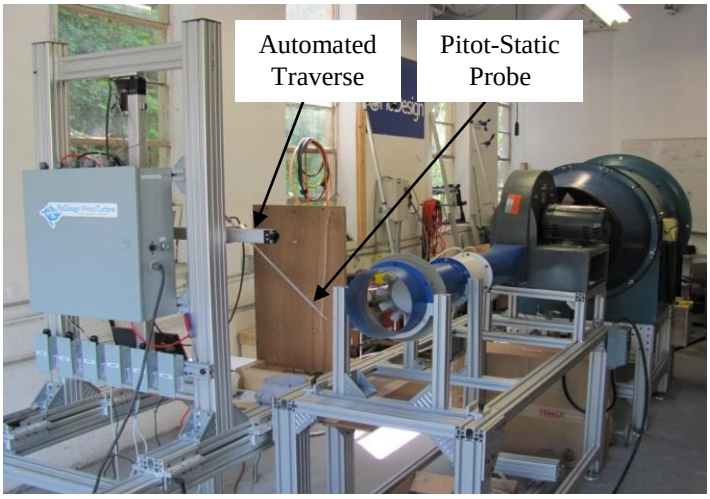

Figure 54: Automated Traverse System

Pitot Static Probe

A pitot static probe is used to sample the total and static air pressure values in either the ambient air or while the MEWT is operating. Figure 55 presents the measurement stations on a probe.

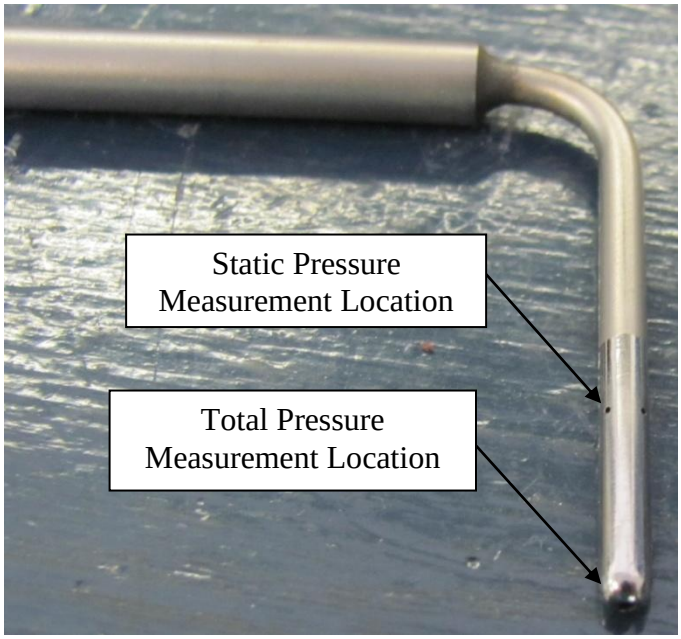

Figure 55: Pitot-static Probe Measures Both Static and Total Pressure

A uniform velocity profile across the entire flow plane is desired in order to simulate a steady-state flow condition but in practice this is difficult to achieve and is generally documented and referred to as a potential source of error. Assuming small variations in the velocity profile are present, the impacts on the major effects being studied in this small-scale testing program are considered negligible.

Each pressure measurement can be converted to velocity to create a velocity profile using Equation 1 below:

$$V = \sqrt{\frac{2*\Delta P}{\rho}} \qquad [1]$$

Where: V = Tunnel Exit Velocity (Ft/s)
ΔP = (Total Pressure-Static Pressure)*5.2023 (lbf/ft2)
ρ =density of air (0.00238 slug/ft3)

Load Balance System

The load balance system shown in Figure 56 simulates a MEWT tower by attaching the mixer/ejector geometry to load balance base. The base contains a load cell which measures the aerodynamic drag forces exerted on the MEWT components by the flow. The MEWT components can also be rotated to any angle relative to the flow direction and a resulting aerodynamic force can be measured and recorded within the data acquisition system to be used for further analysis.

Figure 56: Load Balance and Yaw Measurement System

Mixer/Ejector Test Setup

The MEWT components tested using the wind tunnel were designed to allow for interchangeability as well as ease of installation to reduce test setup time. Figure 57 identifies the components used to assemble the mixer/ejectors and attach them to the wind tunnel. The mixer nozzles are designed to be flush on the inner and outer diameter of the core flow outlet duct to minimize flow disturbances entering the nozzle section. In addition, radial screws are installed through the nozzle and into the core flow duct to counteract the plug loads and eliminate the possibility of the mixer being forced out by the flow. The shroud mount allows for various ejector configurations to be located concentrically with the mixer nozzle. The bellmouth at the inlet of the ejector allows for the aerodynamic inlet to the ejector to be interchangeable with the diffusing sections of the ejector.

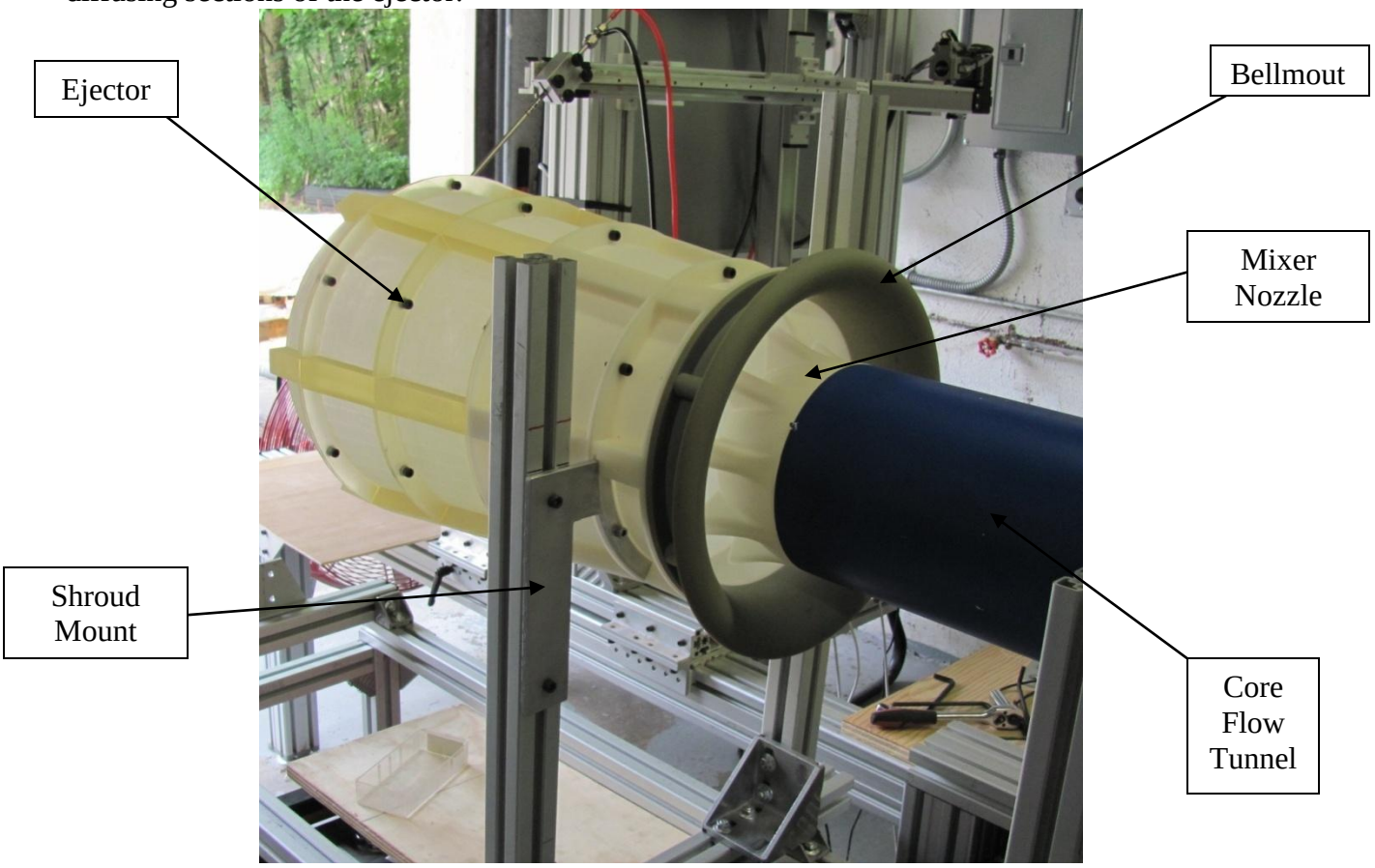

Figure 57: Mixer-Ejector Test Setup

Analog Manometer

An analog manometer is used to read the true pressure inside of the tunnel when the fan is turned on. It must be properly zeroed by using the attached bubble level to make sure the fluid level readings will be accurate.

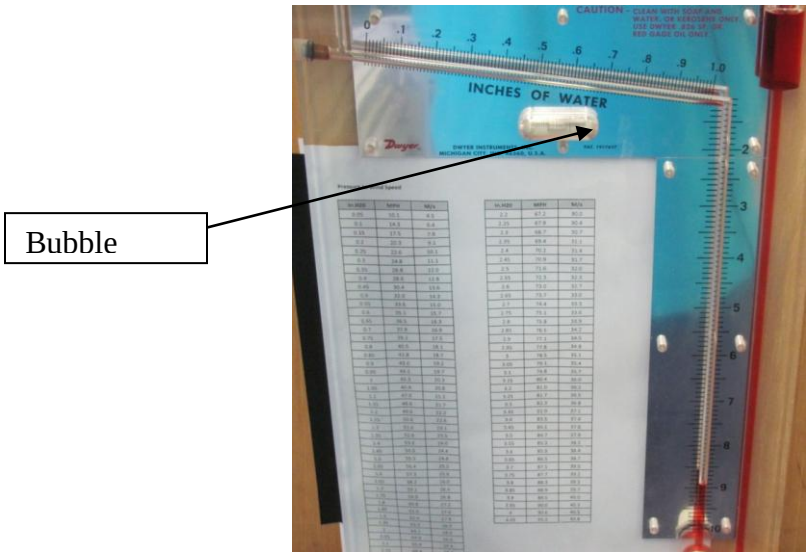

Figure 58: Manometer used During MEWT Testing

Laptop

A laptop computer is used to run the program titled, Windflow Traverse, which serves as the data acquisition interface for the Automated Traverse System. Each pressure measurement and location are recorded and stored in a data file for further analysis.

Figure 59: Laptop with Windflow Traverse Program

4.2a Wind Tunnel Characterization:

The data measured and recorded from the Small Scale Test Program was used to estimate performance and loads of much larger future turbine designs. In order make sure this measured data is valid for these estimates the wind tunnel's flow characteristics were measured to verify that the wind tunnel setup is not creating any aerodynamic phenomenon that might invalidate the results. A uniform velocity profile across the entire flow plane is desired in order to simulate a steady-state flow condition.

The following section describing the characterization process that was carried out by Interns Andrew Ross and Michael Wheeler under supervision of Dr. Walter Presz and Robert Dold of the FloDesign Wind Turbine Co. outlines the process used to assess the velocity profile and validate the wind tunnel for testing of the small-scale models

Open Jet Outlet Duct Traverse Testing

To verify the wind tunnel produces a uniform velocity profile at the MEWT test section, a traverse was performed at the exit plane of the 29 inch diameter open jet outlet duct in both the X and Y directions as shown in Figure 60. The x-direction traverse path begins at the left side of the duct as viewed looking upstream of the tunnel and is identified as x:y coordinate [-14.5:0]. A pressure measurement is recorded every 0.5 inch interval across the tunnel ending at tunnel coordinate [14.5:0].

Similarly, the y-direction traverse path begins at the top of the duct as viewed looking upstream of the tunnel and is identified as x:y coordinate [0:14.5]. A pressure measurement is recorded every 0.5 inch interval vertically across the tunnel ending at tunnel coordinate [-14.5:0].

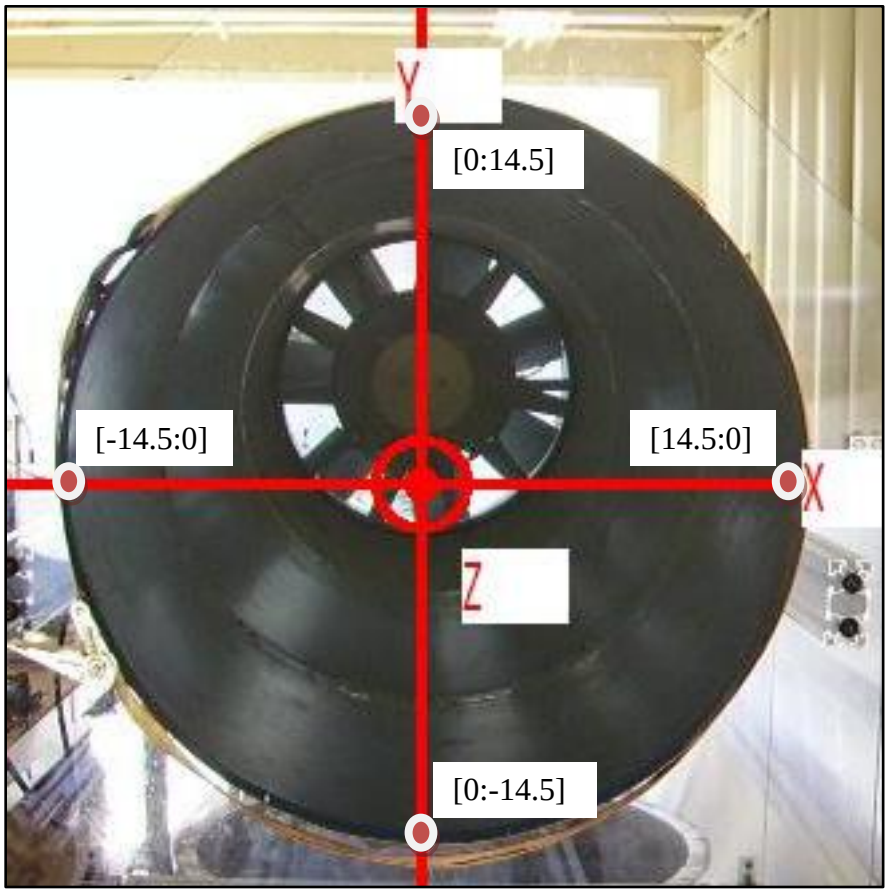

Figure 60: Open Jet Outlet Duct Exit Plane

In total, (5) traverses were performed at varying z-direction distances from the outlet duct exit plane which is considered position z=0 inches. The first traverse was located at z=2.0 inches, subsequent traverses were taken at 12 inch increments ending at traverse location z=50 inches downstream.

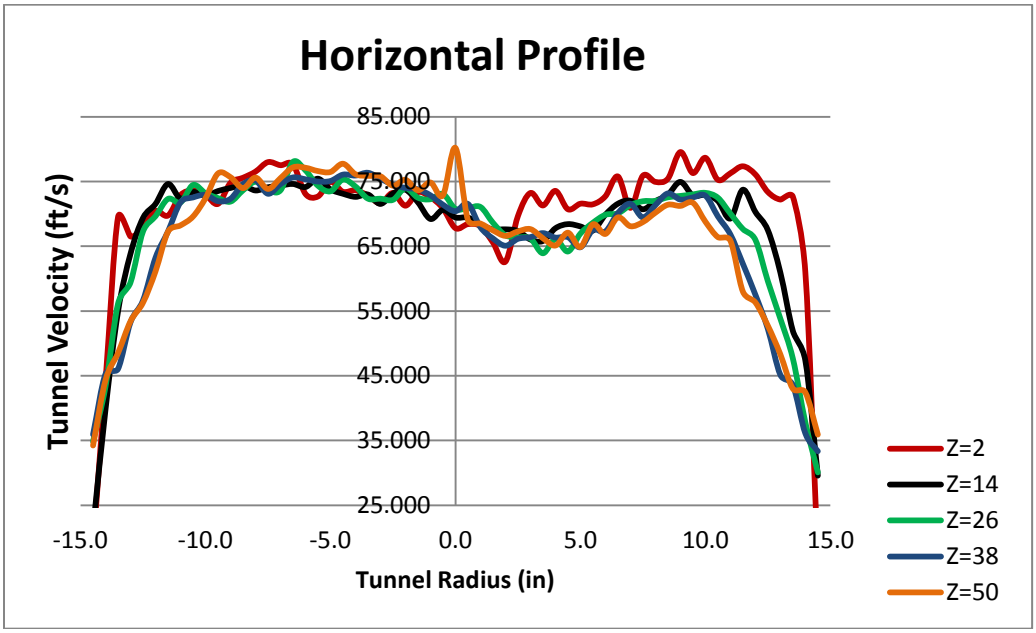

Figure 61: Open Jet Traverse of X-Direction

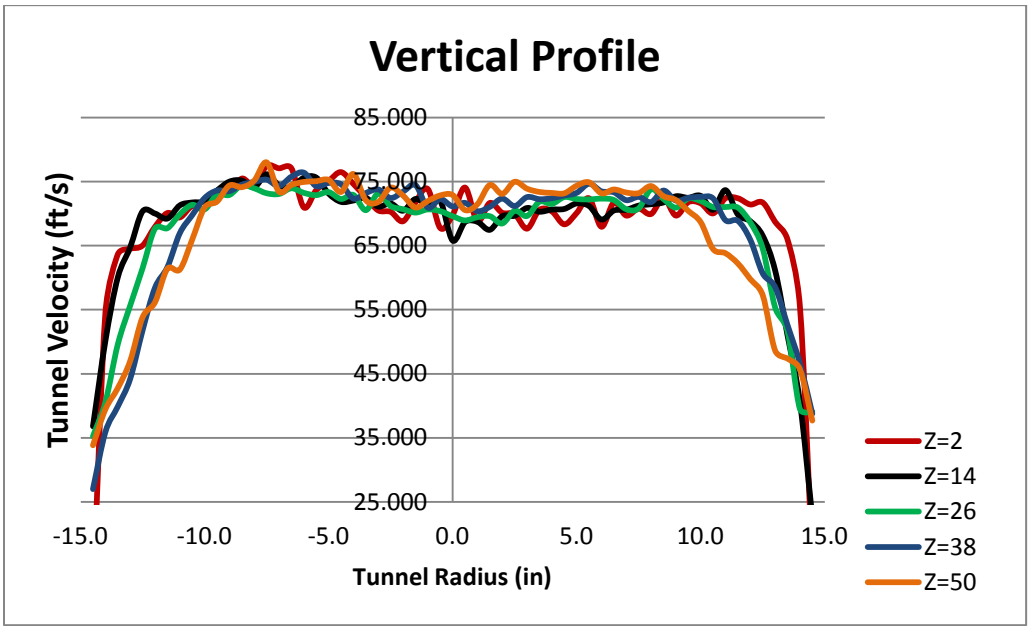

Figure 62: Open Jet Traverse of Y-Direction

The resulting plots, shown in Figure 61 and Figure 62, show that velocity profile decreases symmetrically towards the edges of the tunnel, and that this effect becomes more dramatic at greater distances from the outlet. This effect is due to the open jet mixing with the stationary air. At longer distances from the outlet, this mixing region will become larger. Also, some variation in velocity can be seen in the horizontal traverse but after review this variation was considered adequate to use for MEWT component testing. The goal of wind tunnel component testing is to evaluate major improvements or changes to the MEWT design. As such, most of the results are

compared to a baseline configuration. This reduces the requirement to measure absolute values of drag exactly.

Flow velocity versus motor frequency

The axial flow fan is powered by 3-phase electric power and is controlled by a variable frequency controller. This controller alters the frequency of the 3-phase power thereby varying the velocity of the flow through the wind tunnel. In order to correlate the frequency and the flow velocity, a test was performed to determine this relationship.

A radial exit plane traverse was performed on the open jet outlet duct to determine the velocity of the flow across the exit plane. This traverse radius ranged from 0 inches at the center of the duct to 14 inches at the outer diameter in increments of 2 inches. A total of 11 traverses were performed at varying 3-phase frequencies. The test began at a motor frequency of 10 Hz and was increased to 60 Hz in 5 Hz increments.

It was necessary to have a single velocity value corresponding to a single frequency value in order to create a correlation curve. However since the flow velocity varies across the profile and is typically lower at the outer diameter of the duct, taking a velocity measurement at a single point in the flow would not have given an accurate picture of overall flow velocity. Therefore, the velocity values calculated at each point within a given frequency were averaged. It should be noted that since the radius of the traverses started at duct position [0:0], there were four values for this position, one for each frequency. When calculating the average velocity, the values at [0:0] were averaged first, and then this average was used when calculating the overall average. These resulting flow velocities were plotted against the corresponding frequency values and can be seen in Figure 63.

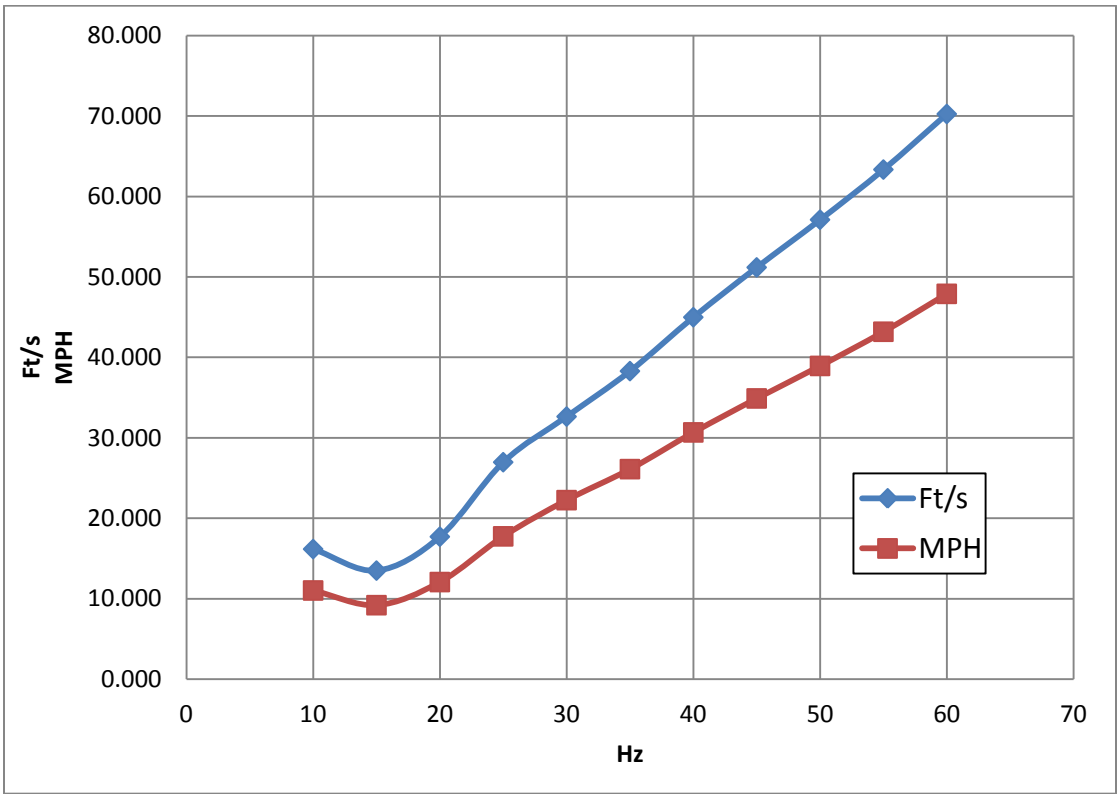

Figure 63: Average Flow Velocity versus Motor Frequency

The relationship between wind speed and 3-phase power is generally linear in the range of 25 Hz to 60 Hz. However, at lower frequencies, the plot shows that the wind velocity decreases from 10 Hz to 15 Hz, then increases from 15 Hz to 60 Hz. Also, the maximum flow velocity in the above plot is lower than that in previous tests because it shows averaged flow velocities.

Core Flow Traverse Testing

To verify the wind tunnel produces a uniform velocity profile at the entrance to the mixer nozzle , a traverse was performed at the exit plane of the 6.4 inch diameter core flow outlet duct in both the X and Y directions as shown in Figure 64. The x-direction traverse path begins at the left side of the duct as viewed looking upstream of the tunnel and is identified as x:y coordinate [-3.2:0]. A pressure measurement is recorded every 0.25 inch interval across the tunnel ending at tunnel coordinate [3.2:0].

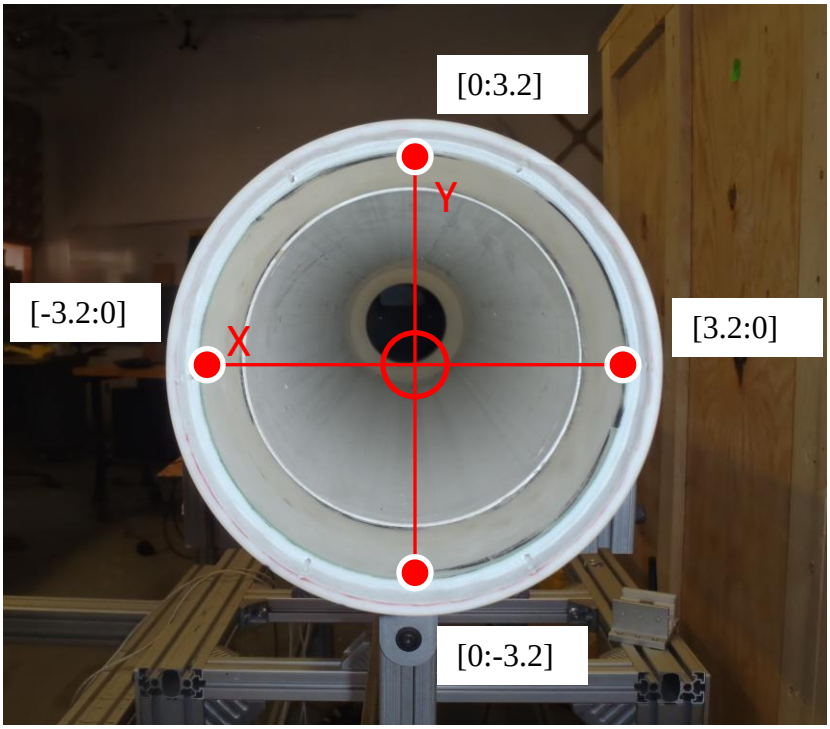

Figure 64: Core Flow Outlet Duct Exit Plane

Similarly, the y-direction traverse path begins at the top of the duct as viewed looking upstream of the tunnel and is identified as x:y coordinate [0:3.2]. A pressure measurement is recorded every 0.25 inch interval vertically across the tunnel ending at tunnel coordinate [-3.2:0].

Multiple traverses were performed at the exit plane of the core flow outlet duct and the average of the x and y direction results are shown in Figures X and Figure X respectively.

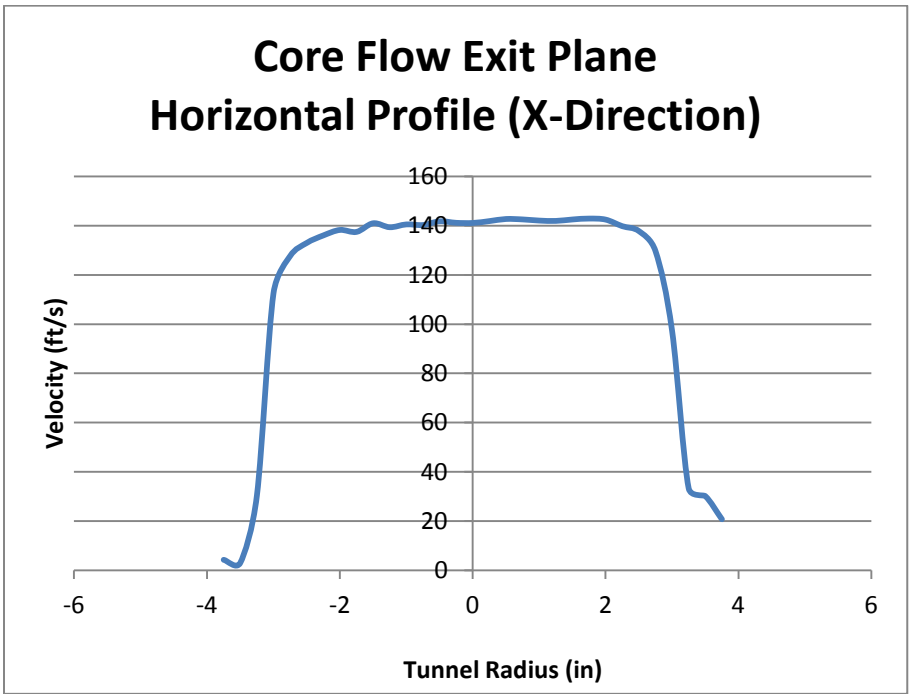

Figure 65: Core Flow Traverse of X-Direction

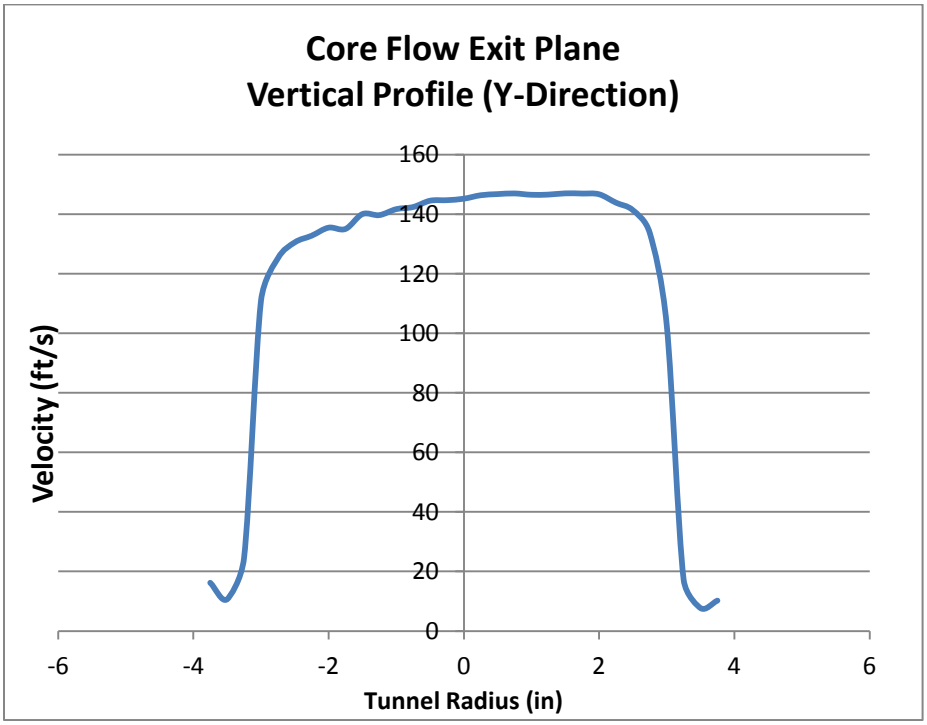

Figure 66: Core Flow Traverse of Y-Direction

Similar to the patterns seen in the open duct flow traverses, the resulting plots shown in Figure 65 and Figure 66 show that velocity profile decreases symmetrically towards the edges of the

tunnel. Some minor variation in velocity can be seen in the vertical traverse but after review this variation was considered adequate to use for MEWT component testing.

4.2b MEWT Component Testing and Evaluation

The process of creating the scale models used throughout the Small-Scale Model Test Program begins with a computational fluid dynamics (CFD) analysis which predicts the performance. This CFD model is then generated within a different computer aided design software program referred to as (CAD). This CAD design is created based on the design guidelines of mixer/ejector technology along with iterative feedback from computational fluid dynamics analysis. From this design process, multiple designs are created in CAD and then fabricated using a process called Stereolithography or SLA. The SLA process will convert the electronic CAD file into a physical hardware by exposing layers of photopolymer resin to a concentrated ultraviolet light leaving each successive layer of resin solidified on top of one another until the final geometry is completed. This process allows for extremely rapid and cost effective physical models to be fabricated and installed upon the FDWT wind tunnel for testing.

The following section describes the MEWT component testing and evaluation process carried out by Interns Patrick Nadeau and Derrick Barnagian under the supervision of Dr. Walter Presz and Robert Dold of the FloDesign Wind Turbine Co. Patrick and Derrick tested each of the fabricated SLA mixer/ejector configurations to assess the pumping performance and compare their measured values to the ideal predictions. This performance metric is used to verify and calibrate the CFD predictions for future analysis as well as identify which configuration of mixer and ejector are well suited for further testing on a larger scale.

Theory

The mixer/ejector system is a pump that mixes primary stream and secondary streams of air at the exit of jet engines and wind turbines. The streams are mixed through using the lobes on the mixer nozzle depicted in Figure 67.

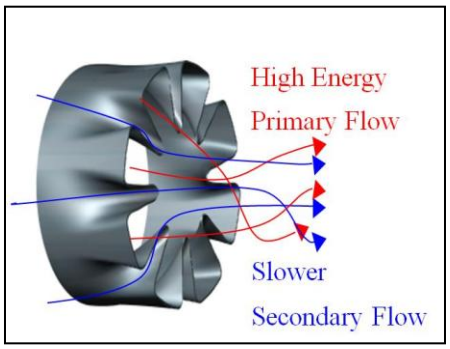

Figure 67: Mixing of Primary and Secondary Flows

Once mixed, the ejector shroud allows for continued mixing as the combined vortex leaves the mixer/ejector system. However, different ejector shrouds have different limitations. Straight ejectors provide mixing with higher L/D ratios, but can get very long in order to fully mix the two streams.

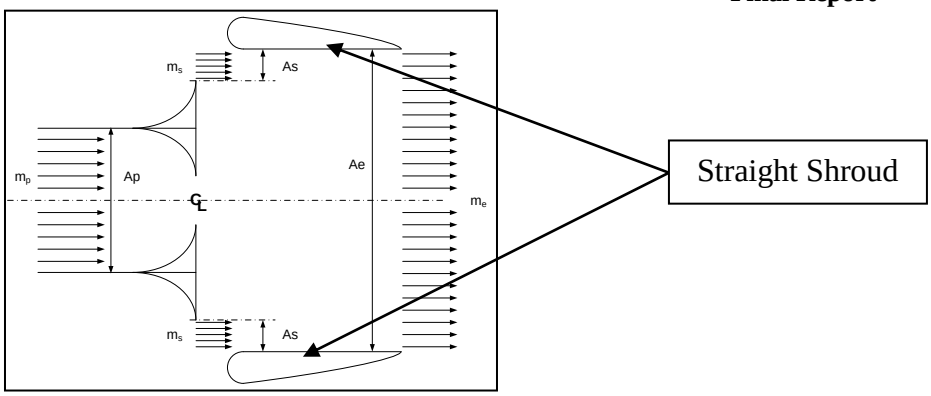

Figure 68: Diagram of a Straight Ejector

Diffusion can increase the performance of the mixers. This is because diffusion allows for the vortex to leave through a larger exit area, which can provide for more thorough mixing and power extraction. The diffusion also lowers the mixing losses that occur in the energy transfer in the ejector as noted in Reference 18. This allows for near ideal energy transfer in an ejector. However, if the angle at which the shroud increases its area is greater than six degrees, separation along the shroud can occur. This will defeat the purpose of increasing the exit area of the system.

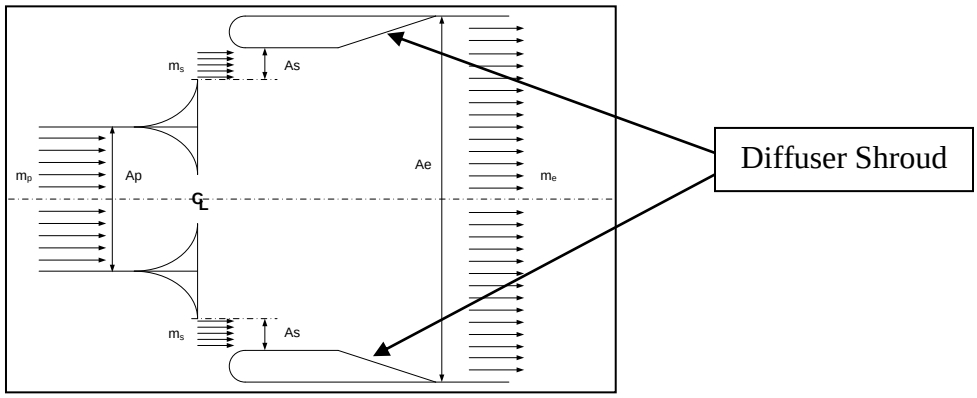

Figure 69: Diagram of a Diffused Shroud

Cambered shrouds allow for the flow to diffuse after it passes through the exit plane of the ejector. The camber keeps the flow attached and introduces turning in the flow. This turning keeps the flow diffusing downstream of the ejector outer diameter. By varying the degree and length of the shroud, it will make it possible to verify the physics of the concept and the downstream diffusion benefits. This type of shroud has the benefits of diffusion without its normal wall limitations.

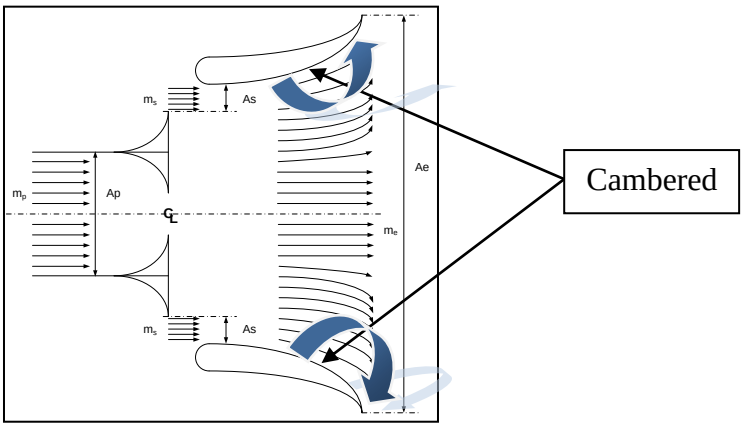

Figure 70: Diagram of a Cambered Shroud

A complete profile view of a mixer/ejector system is shown in Figure 70. This diagram again shows the diffusion beyond the shroud effect of the camber and the primary and secondary stream entrances in regards to the mixer and shroud.

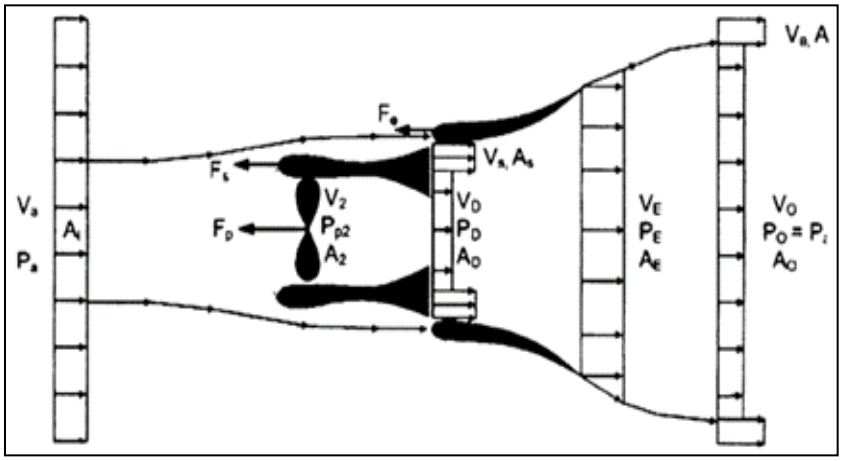

Figure 71: Mixer/Ejector System with Cambered Shroud

In order to measure the differences between mixers and ejectors and determine which combinations perform well, the pumping (m_s/m_p) is calculated through the system. Pumping is important because the higher this value is, the more effective the mixer/ejector system is, and the more quickly the flow returns to the ambient air. So, the higher pumping causes efficient MEWT system. Pumping, or $\left(\frac{\dot{m}_s}{\dot{m}_p}\right)$, is calculated using Equation 2 which was derived for an ejector diffuser using conservation of mass, momentum and energy, as presented in Reference 18.

$$\left(\frac{\dot{m}_s}{\dot{m}_p}\right)^2\left[\left(\frac{A_2}{A_3}\right)^2+\left(\frac{A_p}{A_s}\right)^2\right]+2\left(\frac{\dot{m}_s}{\dot{m}_p}\right)\left(1+\left(\frac{A_2}{A_3}\right)^2\right)+\left(\frac{A_2}{A_3}\right)^2-2\left(\frac{A_s}{A_p}\right)-1=0 \qquad [2]$$

Where:

$\dot{m}_s$ = Mass flow rate of secondary

$\dot{m}_p$ = Mass flow rate of primary

A_2 = Area before diffusion

A_3 = Area after diffusion

A_p = Area of primary flow

A_s = Area of secondary flow

Using this equation, the experimental pumping calculated from each test run is compared to the ideal pumping for the specified area ratio and a percent difference is calculated and recorded.

Procedure

The goal of this procedure is to test and record the ejector pumping values for various fabricated SLA mixer nozzles and ejectors. In this test, the core flow wind tunnel was used to force flow through the mixer nozzle which will entrain a secondary flow through the ejector. This secondary flow rate is measured using the automated traverse system and compared to the primary flow rate through the mixer nozzle, the ratio of these two flow rates is ejector pumping.

Although the flow is inverted from what the MEWT will be exposed to in a turbine installation, the testing of these concepts provides valuable information to improve mixer/ejector systems for future use in the MEWT. The ejectors to be tested included a range of L/D ratios for the straight shrouds, diffusers with a range of area ratios, as well as cambered airfoil ejectors. Inverted and scalloped mixer nozzle designs were fabricated and tested in conjunction with the new ejectors.

The automated traverse system was used to measure and record the pressure profile at the exit of mixer and ejector models. The flow rate through each measured position of the pitot-static probe can be integrated across the entire profile resulting in the flow rate through the entire mixer/ejector system. The total mass flow rate of the system is then calculated by converting the pressure to velocity, and summing the flow rates of each position. This process uses the Equation 3:

$$\dot{m}_t = A_p \sum_{i=1}^{k} V_i \qquad [3]$$

Where:

$\dot{m}_t$ = Volume flow rate

A_p = Area of each position

V_i = Velocity at each position

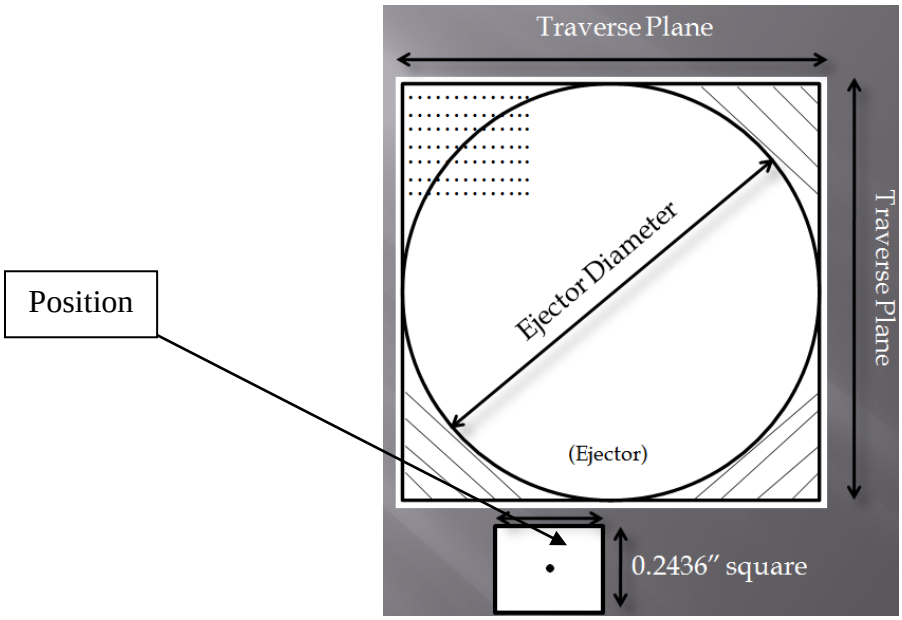

Figure 72: Diagram of Traverse Data Collection

Once the total mass flow rate is known, the mass flow rate of the primary is calculated by measuring the pressure difference across the Venturi and substituting into the following Equation 4:

$$\dot{m}_p = (DC)(A_{Throat})\left(\sqrt{\frac{1}{1-(DR)^4}}\right)\left(\sqrt{2\rho\Delta P_v}\right) \quad [4]$$

Where:

$\dot{m}_p$ = Mass flow of the primary

DC = Discharge coefficient

A_{Throat} = Throat area of Venturi

DR = Diameter ratio of throat to pipe

ρ = Density

ΔP_v = Venturi pressure

After these two variables are known, the following calculation is made to find the mass flow rate of the secondary:

$$(\dot{m}_t) - (\dot{m}_p) = (\dot{m}_s) \quad [5]$$

Where:

$\dot{m}_t$ = Total mass flow rate

$\dot{m}_p$ = Mass flow rate of primary

$\dot{m}_s$ = Mass flow rate of secondary

Finally, the secondary mass flow rate is divided by the primary mass flow rate to determine the experimental pumping ratio (m_s/m_p).

Results:

The following figures show a photograph of each tested mixer nozzle along with a table containing the results of each mixer and ejector combination.

The L2 Inverted mixer nozzle has a lobe geometry that is not optimized for use on a MEWT. It is instead optimized for applications similar to the test conditions, where the high energy flow is being forced through the mixer nozzle and entraining a secondary flow through the ejector. Even though it is not an ideal mixer geometry for the MEWT, observations can be made by testing this configuration and comparing the results to lobes which are optimized for the MEWT.

L2 Inverted

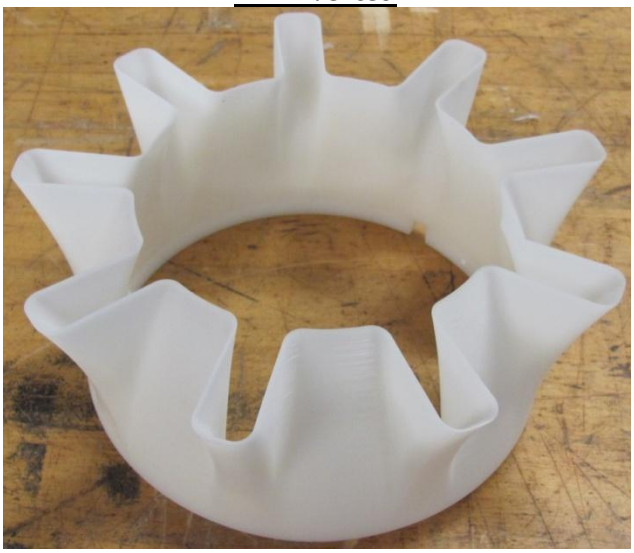

Ejector	ms/mp	Ideal	% Difference
L/D = 0.25	0.086	0.699	87.7%
L/D = 0.25	0.080	0.699	88.5%
L/D = 0.25	0.081	0.699	88.5%
L/D = 0.50	0.267	0.699	61.8%
L/D = 0.50	0.273	0.699	60.9%
L/D = 0.50	0.277	0.699	60.4%
L/D = 0.50	0.273	0.699	61.0%
L/D = 0.75	0.455	0.699	34.8%
L/D = 0.75	0.464	0.699	33.6%
L/D = 1.00	0.539	0.699	22.9%
L/D = 1.00	0.541	0.699	22.6%
L/D = 1.00	0.516	0.699	26.1%
L/D = 1.00	0.503	0.699	28.0%
A3/A2 = 1.25	0.694	0.913	23.9%
A3/A2 = 1.25	0.693	0.913	24.1%
A3/A2 = 1.25	0.708	0.913	22.4%
A3/A2 = 1.25	0.700	0.913	23.3%
A3/A2 = 1.75	0.988	1.196	17.4%

Figure 73: L2 Inverted Mixer/ejector Pumping Results

The pumping results of the L2 Inverted mixer improved as the ejector length increased. This is an anticipated result since a longer ejector provides more distance for the flow to mix within and will generally increase its ability to pump flow. The performance is further improved as diffusion (A3/A2) is added to the ejector.

The C144 L2 Scalloped mixer nozzle is unique because it effectively eliminates the side walls of each mixer lobe in an effort to reduce weight, material usage, and ultimately cost if applied to a MEWT.

C144 L2 Scalloped

Ejector	ms/mp	Ideal	% Difference
L/D = 0.50	0.192	0.332	42.0%
L/D = 0.50	0.192	0.332	42.0%
L/D = 0.50	0.166	0.332	49.9%
L/D = 0.50	0.165	0.332	50.2%
L/D = 1.00	0.293	0.332	11.5%
L/D = 1.00	0.298	0.332	10.2%
A3/A2 = 1.25	0.366	0.459	20.3%
A3/A2 = 1.25	0.369	0.459	19.6%
A3/A2 = 1.25	0.383	0.459	16.5%
A3/A2 = 1.50	0.430	0.544	20.9%
A3/A2 = 1.50	0.423	0.544	22.2%
A3/A2 = 1.50	0.441	0.544	19.0%

Figure 74: C144 L2 Scalloped Mixer/ejector Pumping Results

The pumping results of the C144 L2 Scalloped mixer nozzle improved as the ejector length increased. This is an anticipated result since a longer ejector provides more distance for the flow to mix within and will generally increase its ability to pump flow. Also, it can be noted that the pumping for diffused ejectors is larger than for the straight walled ejectors but the percent difference as compared to their ideal values is less.

The C144 L2 mixer nozzle geometry contains the same mixer area ratios as the C144 L2 Scalloped version but does not have the mixer lobe material removed.

C144 L2

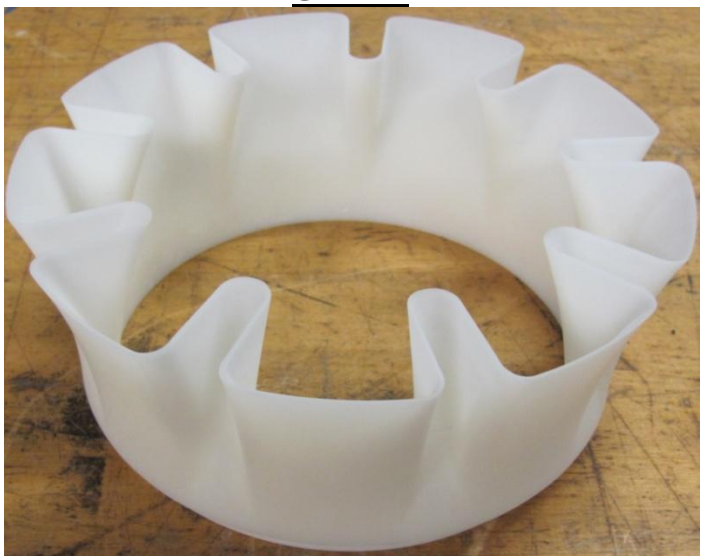

Ejector	ms/mp	Ideal	% Difference
L/D = 0.50	0.153	0.343	55.3%
L/D = 0.50	0.170	0.343	50.5%
L/D = 0.50	0.166	0.343	51.7%
A3/A2 = 1.25	0.273	0.473	42.2%
A3/A2 = 1.25	0.279	0.473	41.0%
A3/A2 = 1.25	0.285	0.473	39.6%
A3/A2 = 1.25	0.291	0.473	38.4%

Figure 75: C144 L2 Mixer/Ejector Pumping Results

The C144 L2 was only tested with the straight walled ejector with L/D equal to 0.5 and therefore does not have a comparison to the L/D equal to 1.0. Also this mixer was only tested with one diffused ejector configuration. When comparing the C144 L2 to the C144 L2 Scalloped mixer at each of these two configurations it can be noted that scalloped version performed slightly better in both cases. This observation will allow for additional future testing on scalloped lobes to be tested at FDWT potentially allowing for a reduction in material, weight and cost when applied to the MEWT.

The C120 L4 ALMEC contains a lobe geometry which alternates between a deep lobe penetration and a shallow lobe penetration. This concept was conceived based on previous mixer designs for applications other than a MEWT.

C120 L4 ALMEC

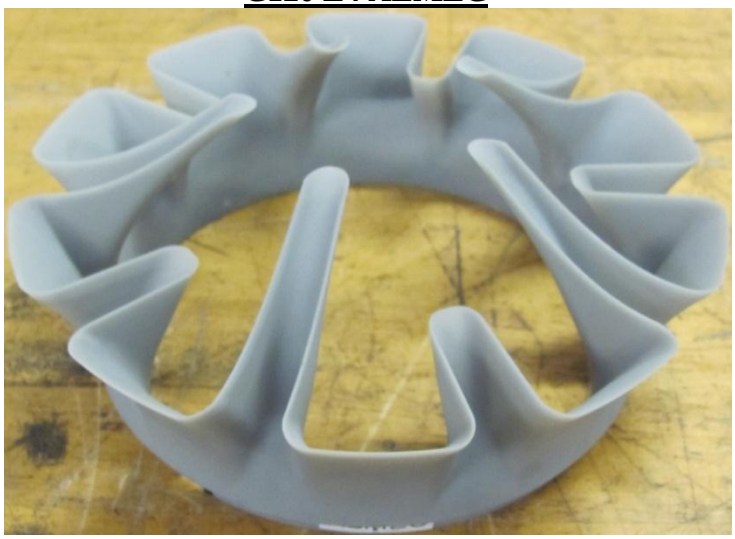

Ejector	ms/mp	Ideal	% Difference
L/D = 0.50	0.227	0.388	41.5%
L/D = 0.50	0.234	0.388	39.8%

Figure 76: C120 L4 ALMEC Mixer/Ejector Pumping Results

The C120 L4ALMEC concept was only tested with one straight walled ejector with an L/D ratio of 0.5. When compared to the other configurations tested with this same ejector combination, it performs better than some mixer nozzles but is not the best performing mixer tested.

The C120 L3, L2, and L1 mixer geometries are all variations of the same concept with varying exit plane areas from larger to smaller respectively.

C120 L3

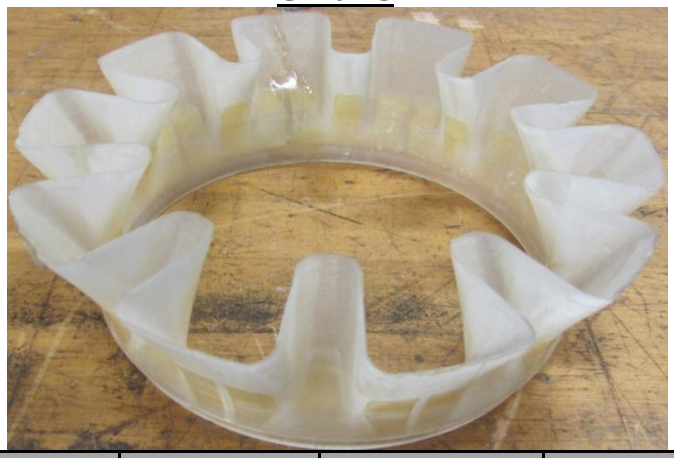

Ejector	ms/mp	Ideal	% Difference
L/D = 0.50	0.207	0.284	27.3%
L/D = 0.50	0.218	0.284	23.3%
L/D = 1.00	0.307	0.284	-8.0%
L/D = 1.00	0.301	0.284	-5.6%

Figure 77: C120 L3 ALMEC Mixer/Ejector Pumping Results

C120 L2

Ejector	ms/mp	Ideal	% Difference
L/D = 0.50	0.231	0.350	34.0%
L/D = 0.50	0.225	0.350	35.7%
L/D = 0.50	0.221	0.350	37.0%
L/D = 0.50	0.233	0.350	33.6%

Figure 78: C120 L2 ALMEC Mixer/Ejector Pumping Results

C120 L1

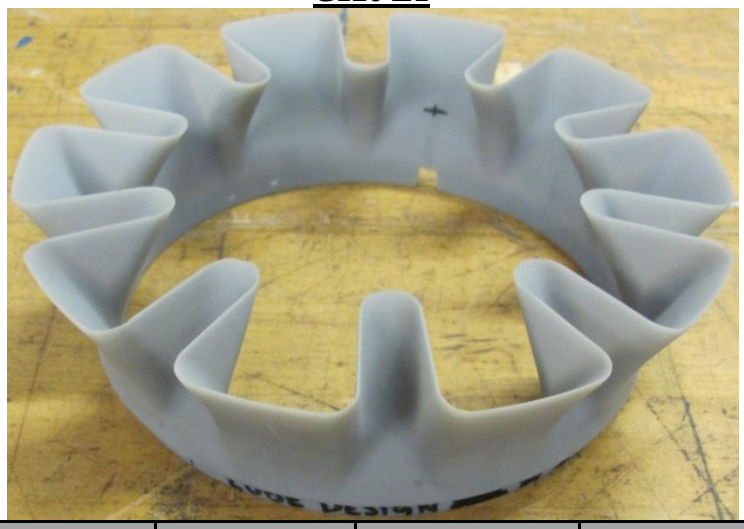

Ejector	ms/mp	Ideal	% Difference
L/D = 0.50	0.236	0.347	32.2%
L/D = 0.50	0.233	0.347	32.9%

Figure 79: C120 L1 ALMEC Mixer/Ejector Pumping Results

A table containing each mixer/ejector configuration that was tested along with the ejector area ratio or length/diameter ratio and the averaged experimental and ideal pumping ratios has been compiled in Figure 80. This table also calculates the percent difference from ideal as a way to quickly see which configurations performed better in terms of pumping secondary flow through the system.

Lobe	Ejector	Average Experimental Pumping	Ideal	% Difference From Ideal
L2 Inverted	L/D = 0.25	0.082	0.699	88.2%
L2 Inverted	L/D = 0.50	0.272	0.699	61.0%
L2 Inverted	L/D = 0.75	0.460	0.699	34.2%
L2 Inverted	L/D = 1.00	0.525	0.699	25.0%
L2 Inverted	A3/A2 = 1.25	0.697	0.913	23.7%
L2 Inverted	A3/A2 = 1.75	0.988	1.196	17.4%
C144 L2 Scalloped	L/D = 0.50	0.179	0.332	46.0%
C144 L2 Scalloped	L/D = 1.00	0.296	0.332	10.9%
C144 L2 Scalloped	A3/A2 = 1.25	0.372	0.459	19.0%
C144 L2 Scalloped	A3/A2 = 1.50	0.432	0.544	20.7%
C144 L2	L/D = 0.50	0.163	0.343	52.5%
C144 L2	A3/A2 = 1.25	0.281	0.473	40.5%
C120 L4 ALMEC	L/D = 0.50	0.230	0.388	40.7%
C120 L3	L/D = 0.50	0.213	0.284	25.3%
C120 L3	L/D = 1.00	0.304	0.284	-6.8%
C120 L2	L/D = 0.50	0.228	0.350	35.0%
C120 L1	L/D = 0.50	0.234	0.347	32.5%

Figure 80: Ejector Pumping results and comparison to ideal

Note that the tested configurations with larger ejector L/D ratios generated pumping closer to their ideal limit. In addition, the tested configurations with diffusion (A3/A2 > 1.0) improved their measured pumping values with respect to their ideal limit. These results can also be viewed graphically in Figure 81 where orange points correspond with straight ejectors; red points correspond with diffuser area ratios of 1.25, and so on.

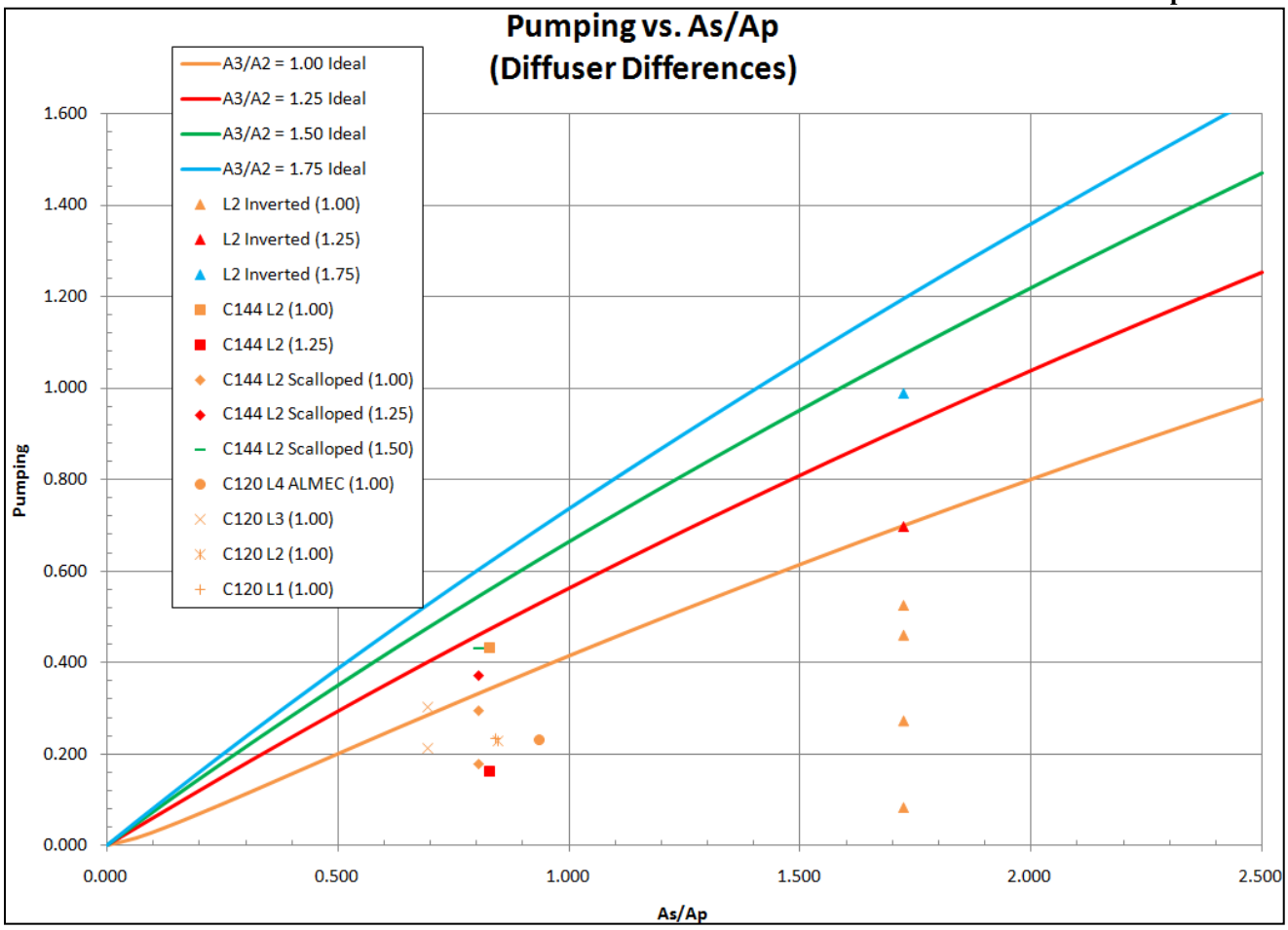

Figure 81: Ejector Pumping vs. Ideal Results

From all of the lobes that were tested, the L2's performed the closest to their ideal limit. The L2 Inverted especially stood out, due to the fact that it was designed for the primary air flow through the duct and mixer center and not between the mixer and ejector as will a MEWT wind turbine installation. From Figure 81, it can be noted that the C120 L3 was tested using an L/D of 1.00 and the average pumping value exceeded the ideal value for that particular mixer. This configuration will need to be retested in the future to identify any errors which arose during testing.

Although some mixers performed better than others in the averaged results, they may not have surpassed the other mixers in different areas. For example, the C144 L2 Scalloped had an average percent difference of 46% from its ideal value when using an L/D of 0.5. The C144 L2 had an average difference of 52.5% when under the same conditions. However, the C144 L2 developed a more thoroughly mixed flow exiting the mixer/ejector system. Figure 82 shows the velocity profile for the C144 L2. It can be observed that the velocity as it exits the reaches a velocity of 120 feet per second (fps) at each of the lobes (depicted in orange), and up to 160 fps at the center of the ejector (pink).

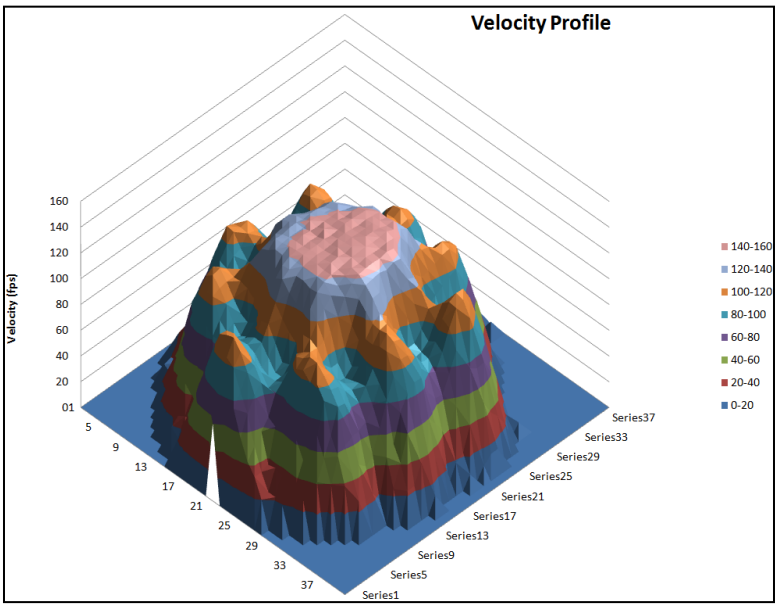

Figure 82: Velocity Profile for C144 L2 using an L/D = 0.50

When the profile above is compared to that of the C144 L2 Scalloped, shown in Figure 83 below, it is clearly evident the flow leaving the system does not mix as well. The two streams do not mix as thoroughly compared to the C144 L2.

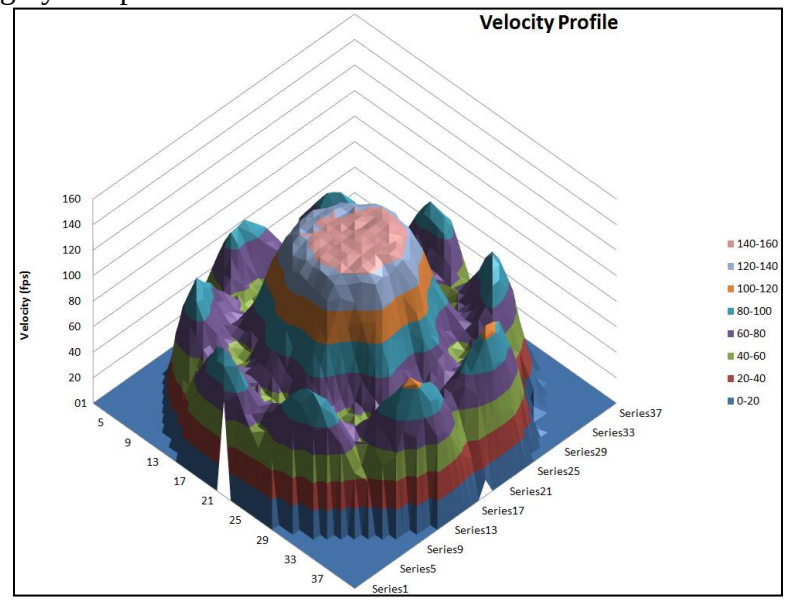

Figure 83: Velocity Profile for C144 L2 Scalloped using an L/D = 0.50

Figure 84 shows a velocity profile of the L2 Inverted while under the same conditions as the previous examples. It can be seen that this lobe model does not mix the streams thoroughly, however out of all the lobe sets, the L2 Inverted produces the highest exiting wind speeds (close to 180 fps).

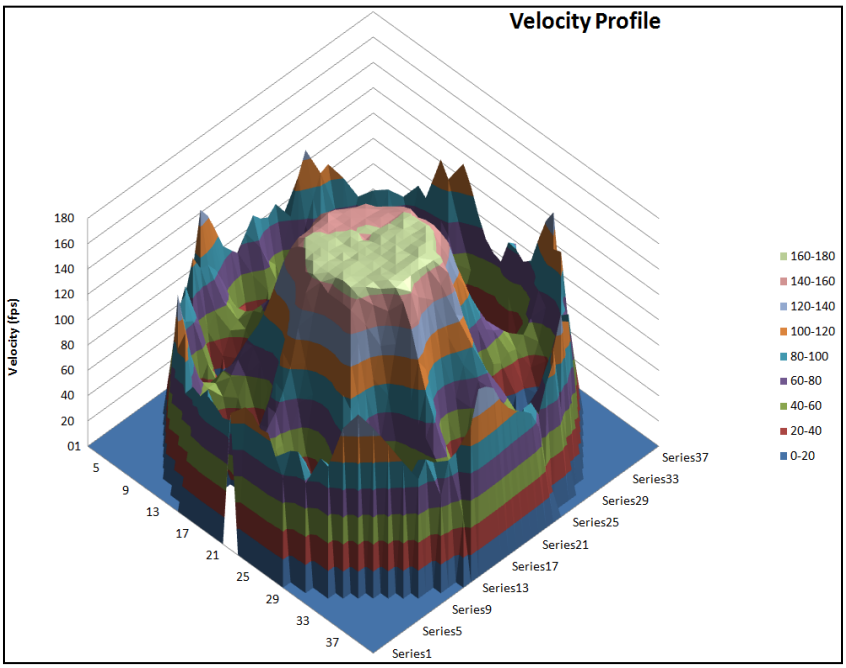

Figure 84: Velocity Profile for L2 Inverted using an L/D = 0.50

Conclusions:

The ejector pumping tests were performed on a wide variety of mixer and ejector concepts in an effort to generate an array of valuable data and observations for the improvement of future MEWT concepts. Although the best performing mixer/ejector configuration when compared to its ideal limit was the C144 L2 Scalloped mixer mated with a straight walled ejector (L/D=1.0), (10.9% difference from ideal), it does not however generate the largest quantity of ejector pumping. The mixer series which generated the most ejector pumping was the L2 Inverted. As noted, the L2 inverted was simply tested as a comparison to the other mixer concepts in order to provide an observational difference during the testing effort and does not contain area ratios that would be optimized for the MEWT. Second to the L2 Inverted series, the highest quantity of ejector pumping was generated by the C144L2 Scalloped mated with a diffused ejector (A3/A2 = 1.5). This result (ms/mp = .432) provides an interesting area to be investigated further by FDWT. If the scalloped lobe design can be optimized further, it may provide a valuable design compromise which can reduce weight, material, and most importantly cost for future MEWT prototypes.

4.2c Drag Reduction Testing

In the previous section, ejector pumping tests were performed as a way to identify high performance mixer/ejector configurations which should be investigated in more detail for future MEWT designs. Although MEWT performance is important as a means to maximize electric

power generation, this performance must be balanced by other requirements such as structural loading. The following section written by Michael Wheeler under supervision by Dr. Walter Presz and Robert Dold of FDWT outlines the theory and wind tunnel test procedure used to investigate aerodynamic loads and various ways to reduce them on the MEWT.

Insert into Drag & Balance Measurements

The purpose of this effort was to investigate the ability to quickly test MEWT loads using FDWT's open jet wind tunnel with its available force balance. Although small-scale wind tunnel testing has proven to be low cost and have much greater availability, the issue of the validity of test results is questioned due to scaling, and Reynolds number effects. These effects arise due to the need to test smaller models at higher wind speeds to match Reynolds numbers of larger scale models. One goal of this series of tests is to demonstrate the usefulness of the FDWT facility for quickly evaluating the benefits of novel concepts to reduce loads in MEWT designs. Comparisons of FDWT test results with University of Maryland results are made to demonstrate reasonable accuracy. FDWT has conducted numerous load tests at the University of Maryland. The data is consistent and has been verified against tower load measurements. The problem is that such tests are much more costly and require longer lead times than tests on FDWT's Dual Flow Wind Tunnel. Thus, this load test effort was conducted on the Dual Flow Wind Tunnel to determine feasibility of using it for quick tests in conjunction with Maryland tests. Western New England Interns were involved in the tests. A 15.4cm (6-inch) scale model of the L15s C481 was used as the test configuration. Figure 85 presents a photograph of the L15s C481 turbine shroud.

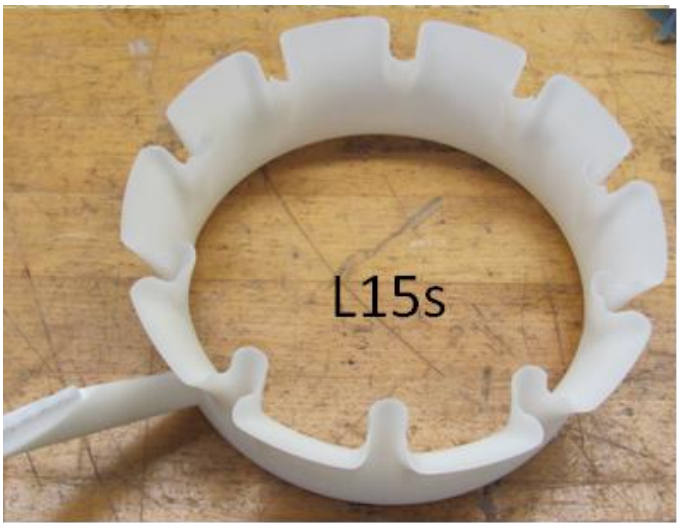

Figure 85: Scale model of the L15s C481 Turbine Shroud

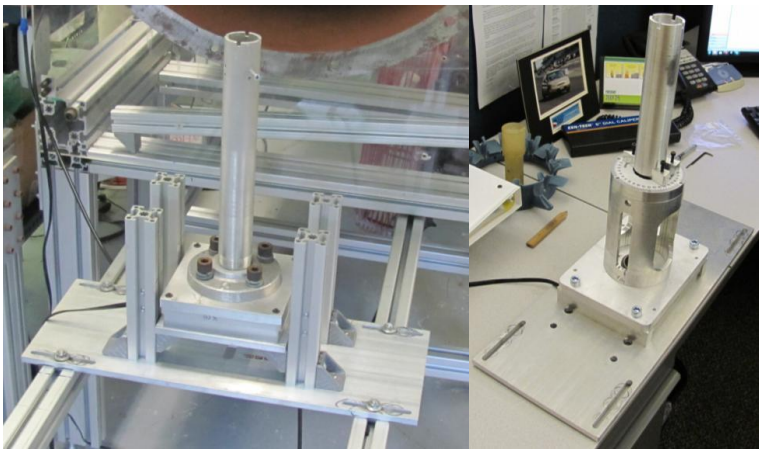

Figure 86: Model Mount with Force Balance. New Yawing Force Balance on Right

Figure 86 presents photographs of the test balance mount used. Testing involved obtaining force measurements from the force plate in the model mount. The scale model MEWT was mounted on the balance structure downstream of the exit of the Dual Flow Open Jet Wind Tunnel as shown in Figure 87. The model position was varied to produce different yaw angles. Balance force measurements were used to calculate measured drag coefficients versus yaw angle for the c481 L15s configuration. Drag coefficients are used since it represents a non dimensionalized drag load that is dependent on Reynolds number only. In most cases, drag variation with turbulent Reynolds number variations is small. This allows a more accurate projection of the test results to full scale results. These drag coefficients are needed to evaluate yaw mechanisms and to determine stability and safety

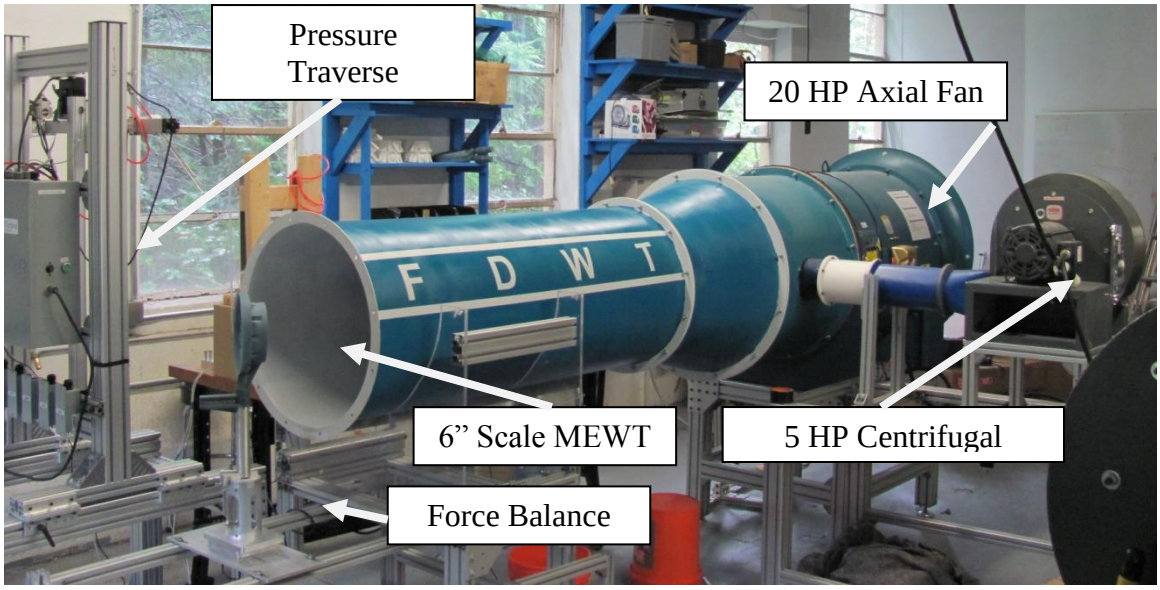

Figure 87: FDWT Ejector Facility, Shown in Open-Jet Configuration

of the design installation. Figure 88 shows typical measured drag coefficients versus yaw angle for the C481 L15s MEWT configuration. Figure 88 presents the drag coefficients along the wind axis. The Dual Flow Wind Turbine results are compared to University of Maryland data on the figure. Both results have similar variations with yaw angle. Maryland consistently predicts the lowest drag occurs at a yaw angle of 90 degrees.

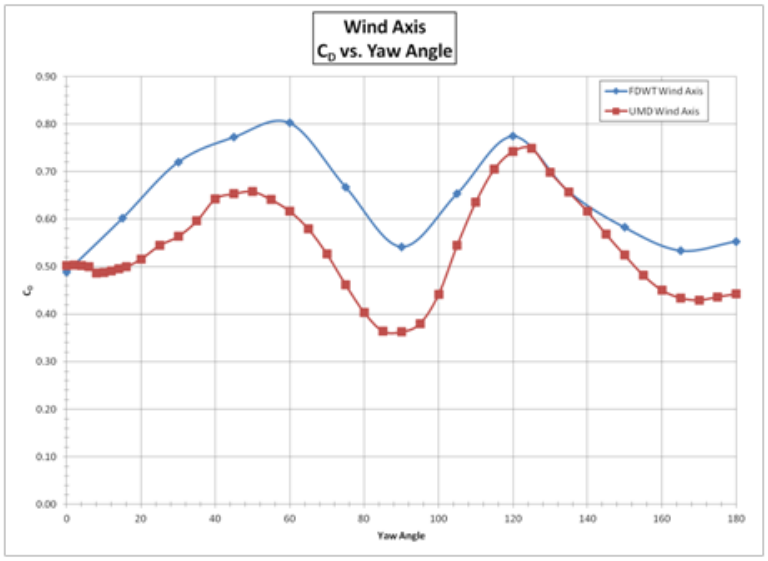

Figure 88: MEWT Drag versus Yaw Angle

4.3 Small Wind Turbine Feasibility Study

A feasibility study was done with the FloDesign Mustang (FDM), a conceptual state of the art MEWT system for residential and distributed wind. The belief is that the next big boom in the wind market is going to come from distributive wind due to the difficulties of large scale wind farms. Large scale wind farms are difficult because they require such a large amount of infrastructure as well as the dramatic initial costs and huge structures needed. They can also pose as safety hazards. The MEWT offers solutions to the typical distributed wind market. Typical HAWT's have issues in small wind due to the major losses that are seen on the small scale as well as the noise and safety concerns. There are also problems with ice slinging on non shrouded turbines which in an urban area could be detrimental to people's safety. This research effort was performed by summer Interns at Western New England University as well as Mechanical Engineers at FloDesign Inc. The effort was focused on investigating the use of the MEWT technology for the distributed wind market. Interns utilized previously tested shrouds to estimate the potential performance of the 1kW MEWT compared to current small wind turbines. Interns also worked on a current market study to be able to present information on the market and current products available. A full report done by student Interns on the small wind turbine feasibility study can be found in the Appendix E.

4.3a. MEWT Benefits for Distributive Wind

FloDesign Wind Turbine Corp has developed a new shrouded, axial flow wind turbine that has significant potential benefits over conventional HAWT designs. Many of the benefits are more significant at the smaller size required for distributive wind applications. The following sections discuss some of these benefits in more detail.

- No Tip Losses even with very small aspect ratio

There are many benefits to using a MEWT for distributive wind market. For example, on a HAWT, the shorter the wing span is the greater the tip losses are. So to the fact that distributive wind requires much smaller blades as compared to full size wind turbines, naturally the losses increase drastically as you decrease the span of the blades. The shroud on a MEWT eliminates tip losses simply because the MEWT blade tips are covered by the shroud. As you scale wind turbines down they have much greater loss in performance but with the MEWT system doesn't create any tip losses.

- Accelerates air through rotor

The high camber shrouds enhance flow pumping and increases the velocity at the rotor station allowing for higher available energy extraction levels. The mixer/ejector system pumps more flow through the rotor while using the bypass flow to energize the turbine exit flow allowing more turbine power extraction without wake stall. It provides energy transfer from the bypass flow to the rotor wake flow thus changing the wind turbine cycle and allowing more energy generation for a given system size. This also produces an increase in the turbines C_p value. The greatest advantage is that typical HAWT cannot surpass Betz Limit, which says that you can only capture as much power as 59.3% of the winds kinetic energy. The MEWT system by accelerating the velocity through the rotor plane there is potential to get up to possibly 3 to 4 times the Betz Limit.

- Acoustics benefits

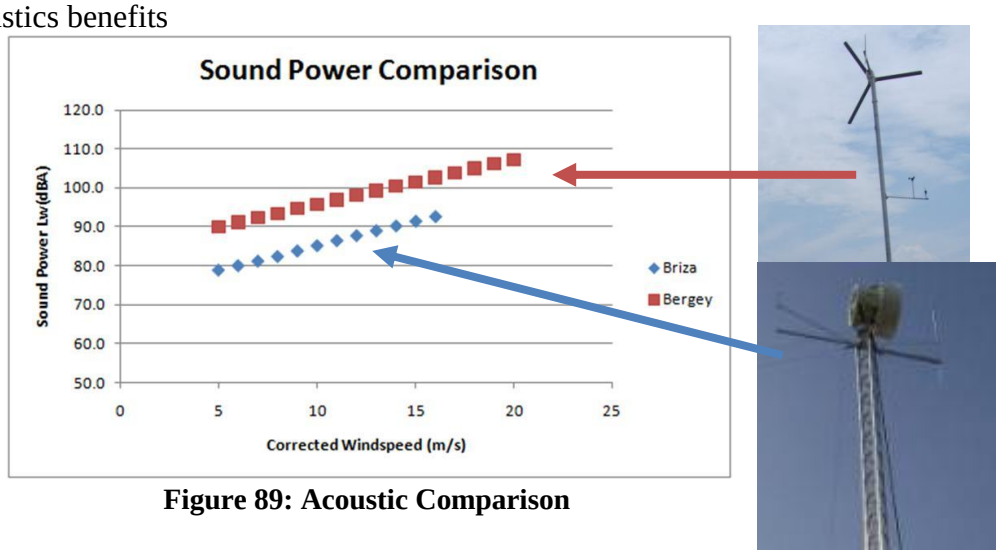

Figure 89: Acoustic Comparison

The shrouded rotor creates a shield around the rotor and you get lower acoustic levels as well as lower radar levels which can open up the market sizably. Having lower acoustic and radar noise

allows for the turbines to possibly be installed in a variety of other places such as near airports where current HAWT cannot be installed due to their high acoustic and radar noise levels. As you can see in the Figure 89 below, the MEWT has an 11 dBA noise reduction when compared to a HAWT.

- Safety Benefits

There are safety benefits that go along with having shrouded blades. The shroud shifts a significant portion of the loading from the rotating components to the static structure of the machine. In a typical HAWT system birds and bats fly into the blade path and are hit by the fast moving blades which is dangerous for the blades and wildlife. Due to the stator-rotor/shrouded rotor configurations, it allows for the MEWT to be seen by birds and bats giving them time to change the trajectory of their flight and decreasing the bird/bat strikes. Also, the rotor swept area size on a MEWT is one-quarter of the area of a HAWT with similar power Other safety benefits include no ice slinging due to the shrouded blades. On an archetypal HAWT when moisture attaches itself to the turbine blades it freezes and can be slung from the blade causing damage to whatever it hits in its path. Due to the shrouding of the MEWT rotor, this is not an issue.

- Lower cut in speeds

One of the greatest advantages to using the MEWT in the distributive wind market is its ability to have a lower cut in speed for the rotor. This is a key factor because in crowded and urban environments there is often lower average velocity of wind. Crowded areas have a greater blockage to the wind flow, as opposed to open fields were wind farms are located so having a lower cut in speed allows for a greater capacity factor because the turbine will start producing power at a lower wind speed.

These are some of the reasons why in the future the MEWT system can bring distributed wind to the front of the green energy distribution in the world.

4.3b. Research Wind Classifications:

Researching wind classifications is important because that's how to determine if the small wind market is viable market wind speed maps of the surrounding areas, as well as at a global level, were investigated but primarily the research focused towards the New England region. The rating scale, which is an area based average, is complimented by the International Electrotechnical Commission Wind Turbine Classification. This scale puts wind turbines into four different classes based on the annual average wind speed that they see or will see.
This wind turbine class system was designed for utility wind turbines: these are the ones rated above 100 kilowatts. Small wind turbines, turbines under 100 kilowatts, do not have a standard scale. There are no certification or standardization procedures for small wind turbines.

Table 4: Turbine Classes

Turbine Class	IEC I High Wind	IEC II Medium Wind	IEC III Low Wind
Annual average wind speed	10 m/s	8.5 m/s	7.5 m/s
Extreme 50-year gust	70 m/s	59.5 m/s	52.5 m/s
Turbulence classes	A 18%	A 18%	A 18%
	B 16%	B 16%	B 16%

Table 3: General Wind Classifications

General wind classifications			
Beaufort scale	10-minute sustained winds (knots)	(m/s)	General term
0	<1	<.5	Calm
1	1–3	0.5-1.5	Light air
2	4–6	2.1-3.1	Light breeze
3	7–10	3.6-5.1	Gentle breeze
4	11–16	5.7-8.2	Moderate breeze
5	17–21	8.7-10.8	Fresh breeze
6	22–27	11.3-13.9	Strong breeze
7	28–29	14.4-14.9	Moderate gale
	30–33	15.4-17	
8	34–40	17.5-20.6	Fresh gale
9	41–47	21.1-24.2	Strong gale
10	48–55	24.7-28.3	Whole gale
11	56–63	28.8-32.4	Storm
12	64–72	32.9-37	Hurricane
13	73–85	37.6-43.7	
14	86–89	44.2-45.8	
15	90–99	46.3-50.9	
16	100–106	51.4-54.5	
17	107–114	55.0-58.6	
	115–119	59.4-61.2	
	>120	>61.7	

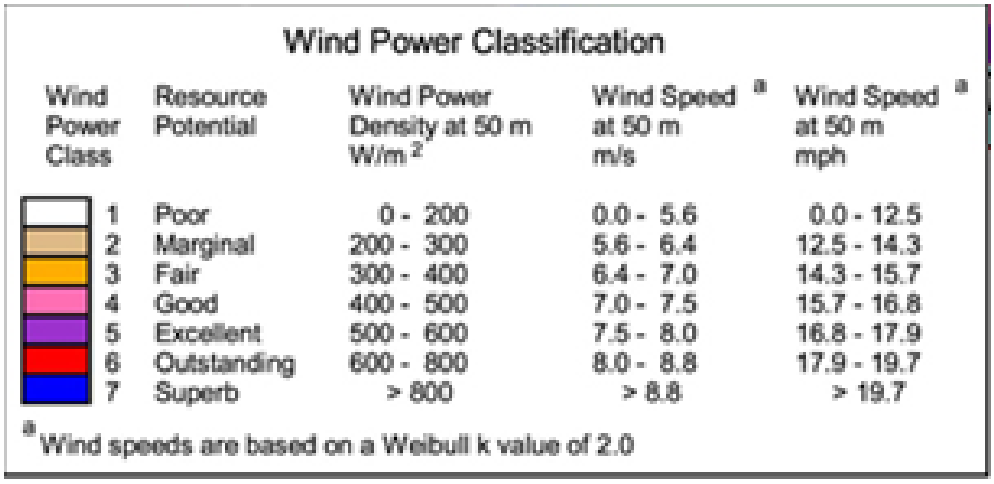

Figure 90: Wind Power Classification Key for the Following Maps

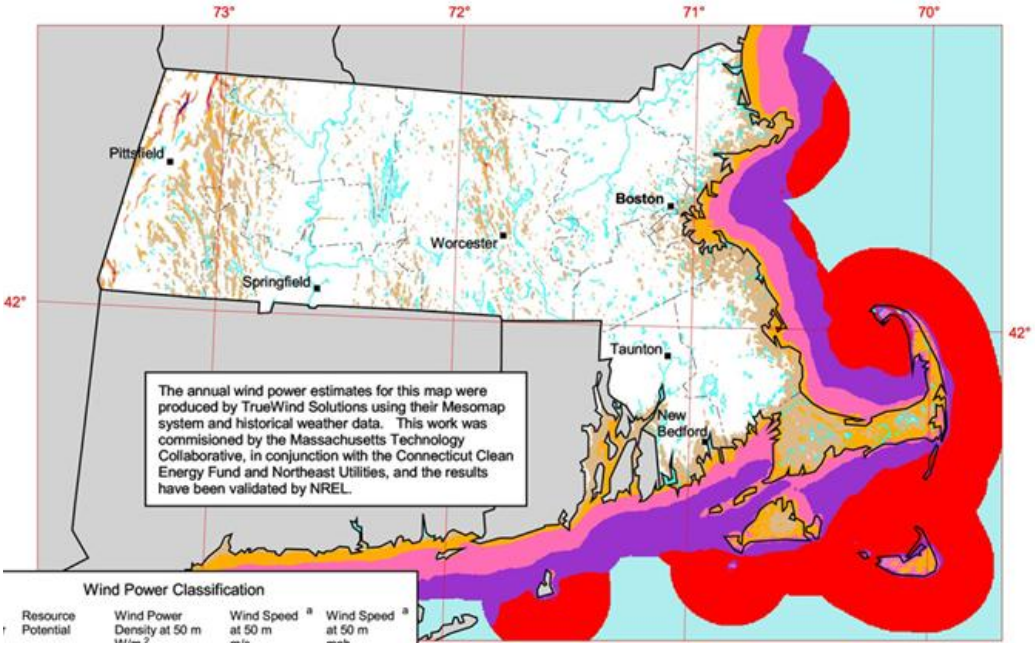

Figure 91: Wind Map of Massachusetts Showing Annual Average Wind Speeds at 50 m High

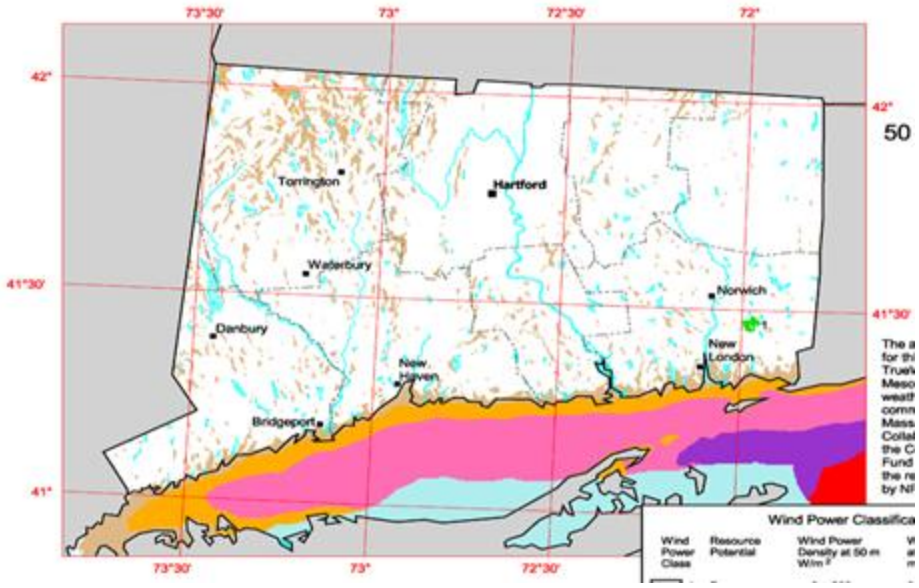

Figure 92: Wind Map of Connecticut Showing Annual Average Wind Speeds at 50 m High

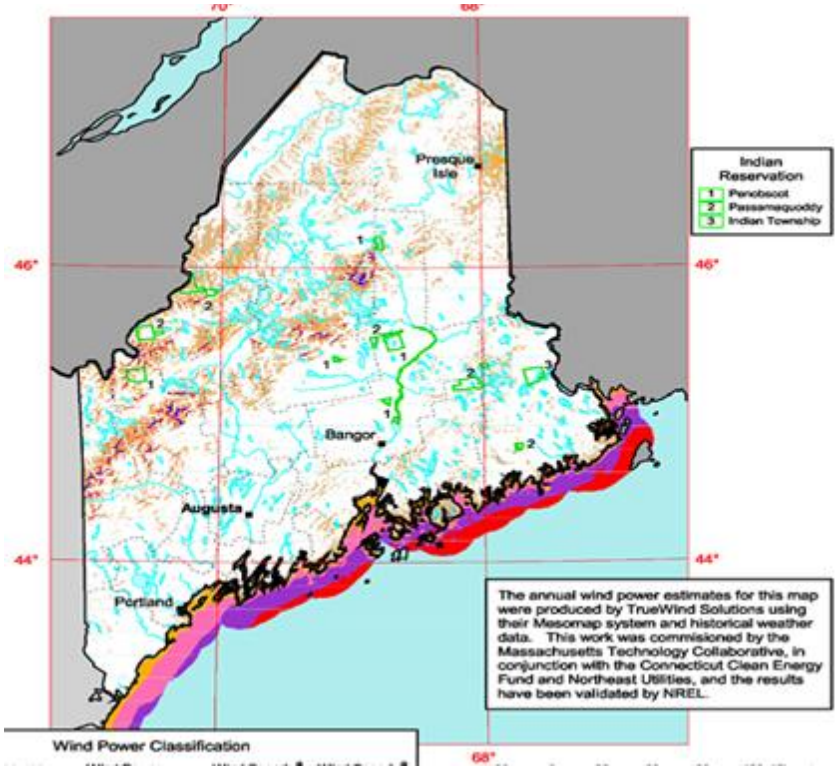

Figure 93: Wind Map of Maine Showing Annual Average Wind Speeds at 50 m High

Figures 90 through 93 present wind maps for the Northeast region of the United States. As these figures indicate, New England states do not have the best winds for producing power from a wind turbine since they fall into the "poor" or "marginal" categories listed in Figure 90. Since these states generally do not have the wind power to drive the current small turbines on the market, there is a need for a turbine which can operate in these smaller average winds. The average wind speeds across the entire US at a height of 80 meters is presented in Figure 94.

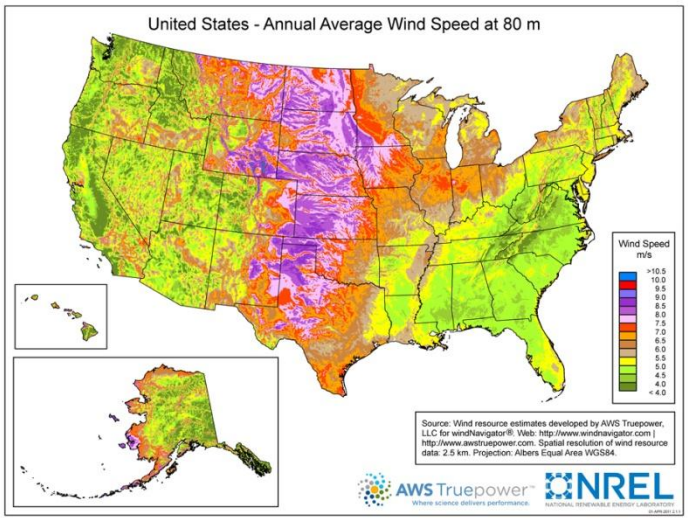

Figure 94: Annual Average Wind Speed at 80m [reference 26]

4.3c Market Research study of competitor landscape:

Preliminary studies were conducted around an updated Briza size, 1kW, wind turbine. The new MEWT distributed wind concept was named "Mustang". Exact size was to be evaluated. The desire was to have a concept that could be low cost while transported and installed easily by a home owner. One of the first studies conducted was a market research study. The market research study consisted of researching current available turbines that would compete with the FloDesign Mustang (FDM). There was also research done on the future small wind turbine market trends.

Small Wind Turbine Comparison

After the list of small wind turbines currently available on the global market was compiled, graphs were made to compare the different turbines. The categories in which they were compared were mass, power in kilowatts, and rotor diameter. The performance coefficient was compared as well but realized the accuracy of the calculated C_p values that were found in the literature was minimal so the comparison was not extensive. Each of these comparisons started as a full comparison of all the turbines. Then the comparison was narrowed down to turbines under three kilowatts because that is closer to the size range being explored for the Mustang.

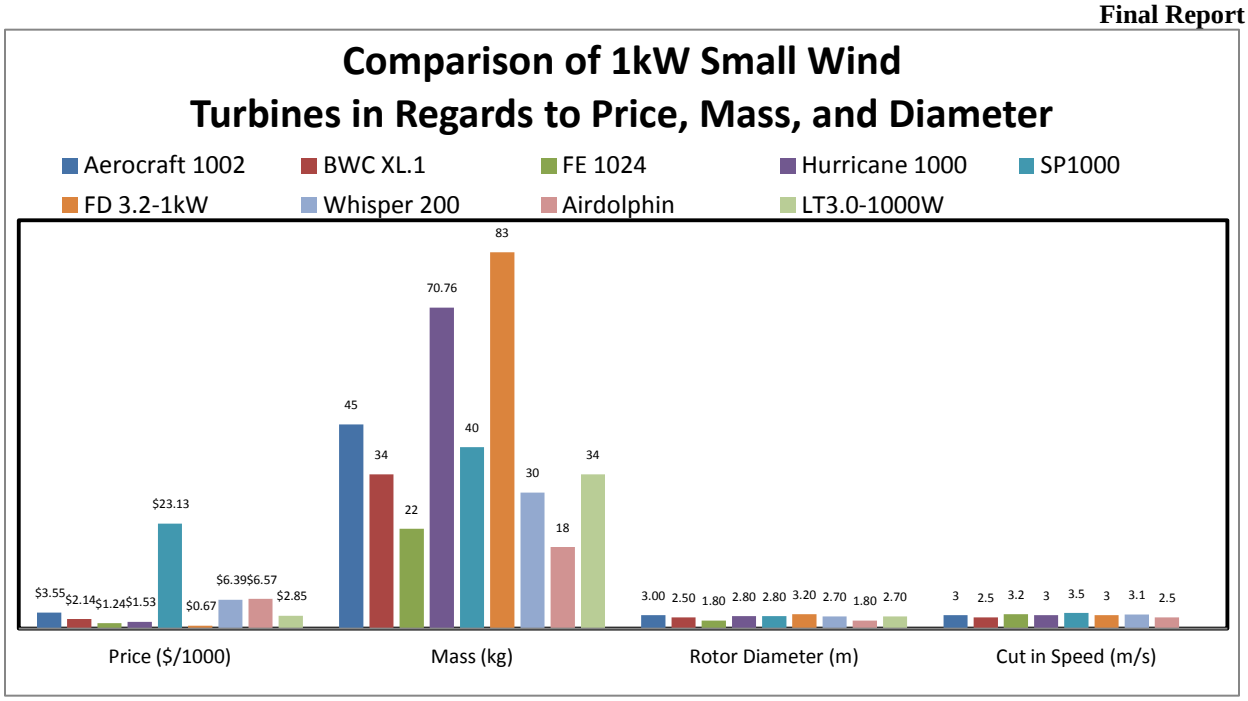

Figure 95: Comparison of All 1kw Turbines Found Regarding Price, Mass, and Diameter

Once each category was compared a final comparison was made against all the one kilowatt wind turbines.

Table 5: Available C_p Estimates for Small Wind Turbines

Name	Cp
Old Briza	0.69
FloDesign Mustang	1.38
Bergey XL.1	0.25
Whisper 200	0.18
SunEco	0.27
Hummer	0.3
Skystream 3.7	0.17

Figure 95 presents a comparison of price, mass, rotor diameter and cut in speed of different small wind turbines advertised as 1 kW. Again, it is important to emphasize that there are no standard requirements for advertising small wind turbine power generation. Much of the documentation is questionable at best. Table 5 presents a best estimate of the C_p values (non-dimensionalized performance) for key 1kW wind turbines. The C_p values are seen to be in the .15-.30 range except for FloDesigns MEWT concept. A C_p value of .15-.30 would be expected for any HAWT designed at this small size. The performance is very poor at the 1Kw size because of tip losses, low Reynolds flow effects, and frictional effects. The MEWT concept eliminates these problems as discussed previously. The Mustang has a much higher projected C_p than the Briza, since it is based on new technology advancements on shroud, rotor and mixer/ejector designs. The Briza is actual, measured power generation on a tower using three year old MEWT design technology.

The importance of Figure 95 is that it gives an idea of what the average available small wind turbine would cost. It is believed that to be competitive in the small wind market one would have to sell the product for between $5000 and $6000.

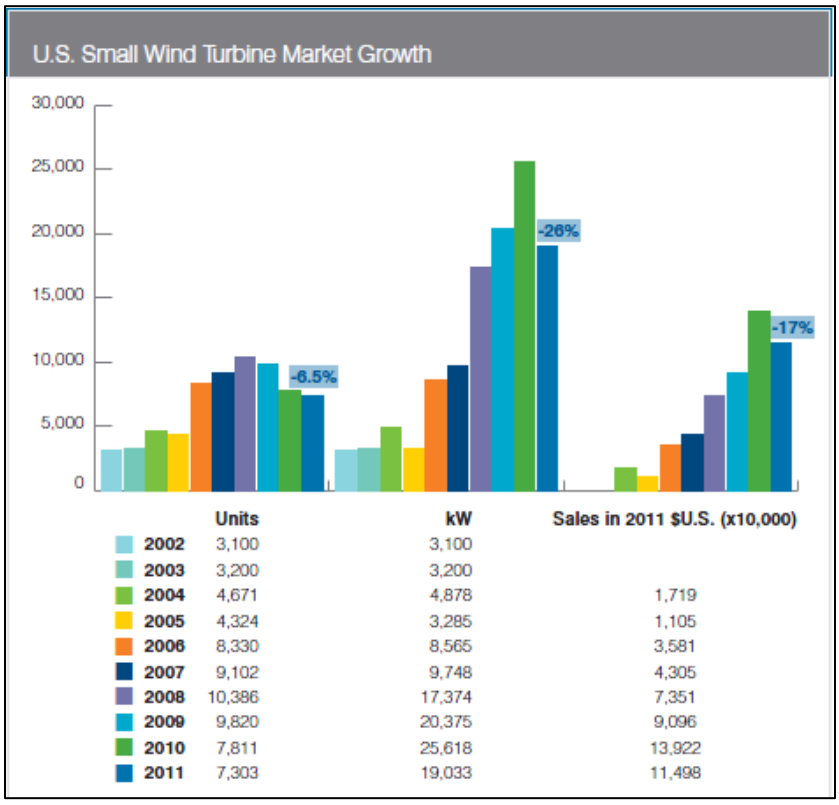

	Units	kW	Sales in 2011 $U.S. (x10,000)
2002	3,100	3,100	
2003	3,200	3,200	
2004	4,671	4,878	1,719
2005	4,324	3,285	1,105
2006	8,330	8,565	3,581
2007	9,102	9,748	4,305
2008	10,386	17,374	7,351
2009	9,820	20,375	9,096
2010	7,811	25,618	13,922
2011	7,303	19,033	11,498

Figure 96: U.S. Small Wind Turbine Market Growth

Figure 96, which was taken from the AWEA 2011 small wind turbine market report, shows there was a significant drop in the small wind market in 2011, but there are reports that show the growth of the market in the future could be extremely high. A report done by http://www.pikeresearch.com [reference 22] says:

> The cleantech market intelligence firm forecasts that the global market for small wind systems will more than double between 2010 and 2015, rising from $255 million to $634 million during that period. Within the same forecast horizon, small wind system installed capacity additions will nearly triple to 152 megawatts, and average installed prices of small wind systems will decline to just over $4,150 per kilowatt.
> "The payback period for a small wind system can be 5 to 10 years in a region with adequate wind resources," says senior analyst Peter Asmus. "These economics provide a strong value proposition for a variety of commercial, industrial, and residential applications. Small wind turbines are currently more efficient than solar photovoltaic (PV) systems and, therefore, more economical from a levelized cost of energy perspective."

Figures 98 and 99 look at the growth of the wind market in the US over the previous decade. [reference 26]

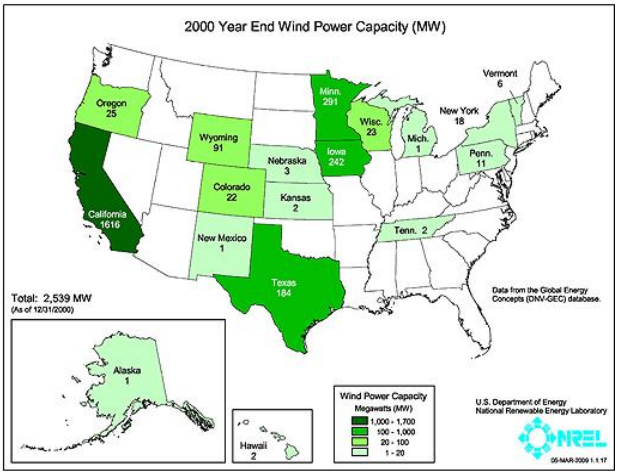

Figure 97: USA year 2000 Wind Power Capacity

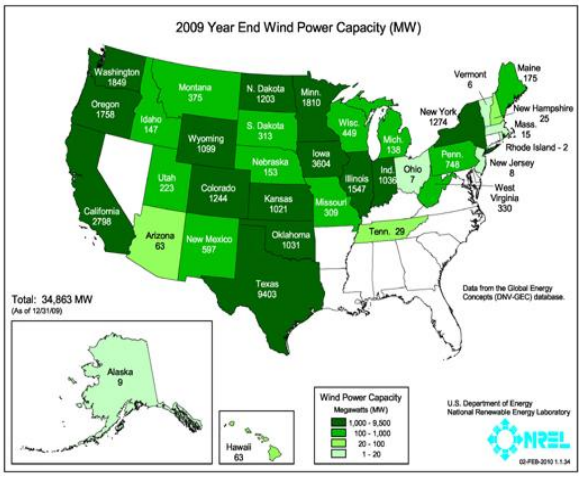

Figure 98: USA year 2009 Wind Power Capacity

Due to the fact that small wind is more economical from a levelized cost of energy it allows for the belief that in the near future with raising oil prices and diminishing fossil fuels that people will start to turn to small wind as a viable option to lower their electric bills. There are also

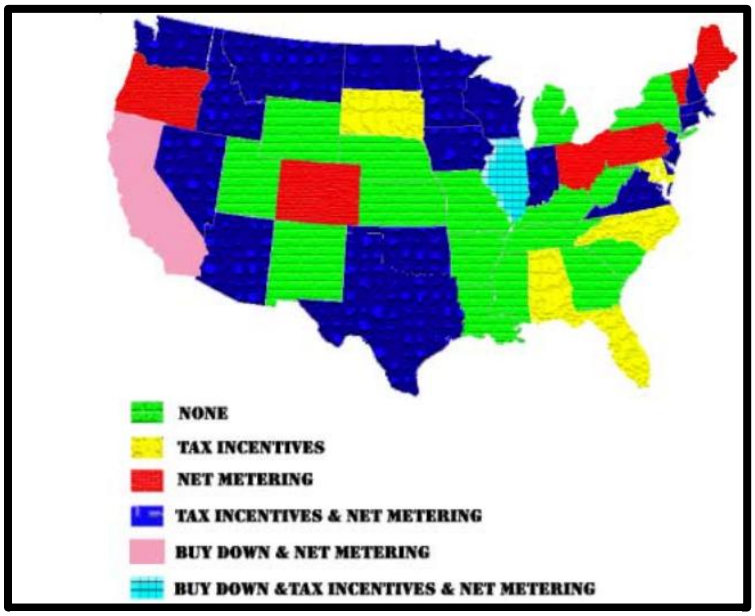

Figure 99: US Tax Incentives [reference 23]

many new government incentives and programs available for people willing to install wind turbines on their property. Figure 99 presents tax incentives across the US which is from a NREL report of the status of small wind. As the government incentives grow so will the small wind market. These incentives have the ability to cut payback periods way down and will allow for more people to afford small wind turbines.

4.3d Annual Energy Production (AEP):

Annual energy production is the amount of energy a wind turbine can produce in a year. It is a function of the mean power of a turbine and the number of hours in a year. By multiplying the two together, annual energy production is yielded. Table 7Table 6 presents AEP results for four wind turbines.

Table 6: AEP and Energy Cost Comparison

AEP prediction from calculator

AEP Comparison					
Modify Cells in Green					
Cost of energy based on 20 year lifespan					
	Chosen Turbine...	Compared to...	Compared to...	Compared to...	Compared to...
Turbine Name	Custom Parameter:	*Honey Well 6500*	*Bergey XL.1*	*Skystream 3.7*	*FDMustang 1000*
Cost of Turbine ($)	*$6,000*	$5,995	$3,560	$6,200	$3,500
AEP (kWhr/Year)	8,518	2,750	2,000	4,800	2,850
Cost of Electricity ($/kWhr)	0.12	0.12	0.12	0.12	0.12
Cost of Energy ($/kWhr)	$0.0352	$0.1090	$0.0890	$0.0646	$0.0614
Energy Usage (kWhr/year)	11,000	11,000	11,000	11,000	11,000
Electric Bill Per Year ($)	$1,320	$1,320	$1,320	$1,320	$1,320
Money Saved by Turbine ($)	$1,022	$330	$240	$576	$342
Payback Period (Years)	5.9	18.2	14.8	10.8	10.2

This table of AEP comparison is linked with an AEP calculator shown in Figure 100. The first turbine on the left is a custom turbine that the user can input values for site information and come up with a Weibull wind speed distribution and in tandem with that information, there is information about the turbine as well, such as its rated wind speed, rotor diameter, C_p, cut in speed and cut out speed. The calculator will then produce a power curve and AEP prediction for the custom turbine. That AEP prediction then is automatically placed into Table 6. This then allows the user to compare AEP and simple payback period for common market small wind turbines. This is an effective tool because it allows a design team to look at their potential production and understand how they compare to the actual market. Values for the market turbines are found from their respective websites. This chart uses some simple assumptions such as the cost of electricity and energy usage, but due to the fact that it is just a comparison allows for the assumptions. The results presented in Table 6 show a significant cost benefit of purchasing FloDesign's proposed Mustang. It should be emphasized that these results are based on projections of Mustang cost reduction due to high volume, mass production which could provide a $3000 price tag for the Mustang.

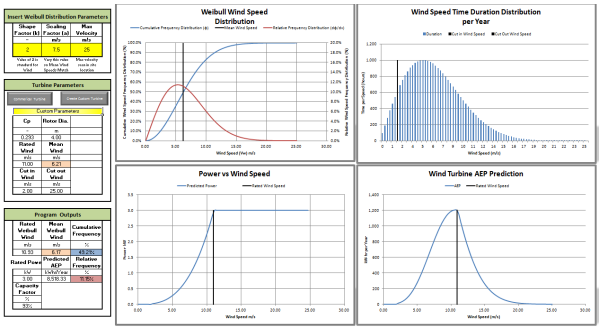

FIGURE 100: AEP CALCUATOR

4.3e. Identify optimal target size:

The FloDesign Mustang (FDM) was designed to be a 1kW MEWT. The reasons for choosing this size are that a good entry to the small wind market could be a home assembly kit. In other words the idea is that the consumer can buy the FDM as a kit at major department/construction stores and assemble it themselves at home. With the advantages that the MEWT provides in the small wind market, the belief is that the FDM would only need to be a 1kW but would be smaller than competitors 1kW making it a more versatile product. As can e seen in Table 7, the FDM has a slightly larger rotor diameter than the Briza prototype, but it also produces the same power as Briza but at a lower rated wind speed. This is important due to the fact that in urban areas and for household operations, the typical wind speed is less than what is to be expected on a wind farm. 1kW was also chosen due to the lessons learned from Briza. From the testing done on Briza, there was a familiarity with the 1kW system. Also with the small scale testing that was done, it brought forward newer geometries that produced greater efficiencies than the shroud system used for Briza. With the advances in the shroud geometries, it allows for them to be shorter, hence using less material meaning more cost effective to produce.

Table 7: Small Wind Turbine Specs

Wind Turbine Name	Rated Power (kW)	kWhr/Year	Rated Wind Speed (m/s)	Cut in Speed (m/s)	Cut Out Wind Speed (m/s)	Rotor Diameter (m)	Swept Area (m2)	Cp	Rotor Diameter (ft)	Cost
Old Briza	1	-	11.90	1.00	25.00	1.34	1.41	0.69	4.40	Choose
FDMustang 1000	1	2,850	8.99	1.00	25.00	1.44	1.63	1.38	4.73	Choose
Honey Well 6500	2	2,750	11.41	0.90	16.99	1.83	2.63	0.84	6.00	$5,995.00
Bergey XL.1	1	2,000	11.00	3.67	13.00	2.50	4.91	0.25	8.20	$3,560.00
Whisper 200	1	2,400	11.62	3.13	25.00	2.74	5.91	0.18	9.00	$3,015.00
SunEco	1	-	10.00	3.00	25.00	2.80	6.16	0.27	9.19	$806.00
Hummer	1	8,640	8.99	4.39	20.00	3.08	7.44	0.30	10.10	$3,225.00
Skystream 3.7	2.4	4,800	12.96	3.50	25.00	3.66	10.51	0.17	12.00	$6,200.00

4.3f FloDesign Mustang (FDM) Concept Design:

Figure 101: Students Final FDM Design

Most of the FDM design work was done by the student Interns Team. They started with a shroud geometry and some direction from FloDesign Wind Turbine. They did research on

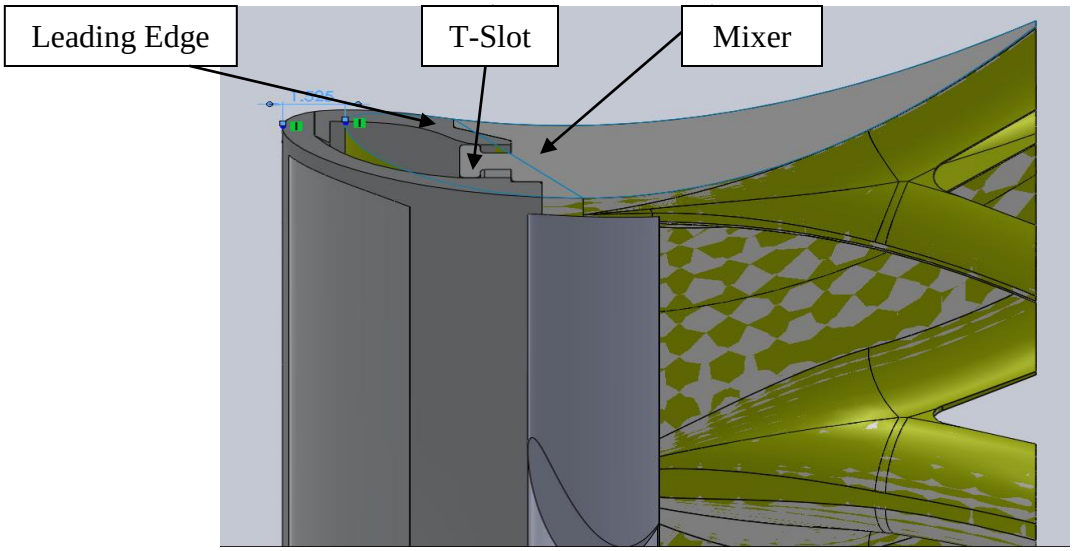

Figure 102: T-Slot Connection of Mixer to Leading Edge

which generators would be most effective for the distributed wind application; they also performed a study on different ways to fabricate the shroud, whether it should be made from foam or out of a SLA plastic. They worked on deciding the type of materials that would be used and the process in which all the components would be fabricated. The key part of their design was that the mixer sections would attach to the leading edge with a T-slot connection to be able to easily assemble the FDM.

The Students were also instrumental in the design of the elongated C481 shroud. It was decided that the FDM should come with a stator-rotor configuration; the C481 had to be modified so that it had enough room to house both a stator and a rotor, shown in Figure 103. The students had the FDM designed when the project concluded, but never had the opportunity to have the prototype created. A full report detailing the extent of the project submitted by the student Interns can be found in the Appendix E.

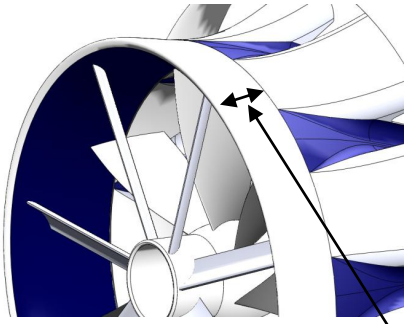

Figure 103: Shroud with Elongated Leading Edge

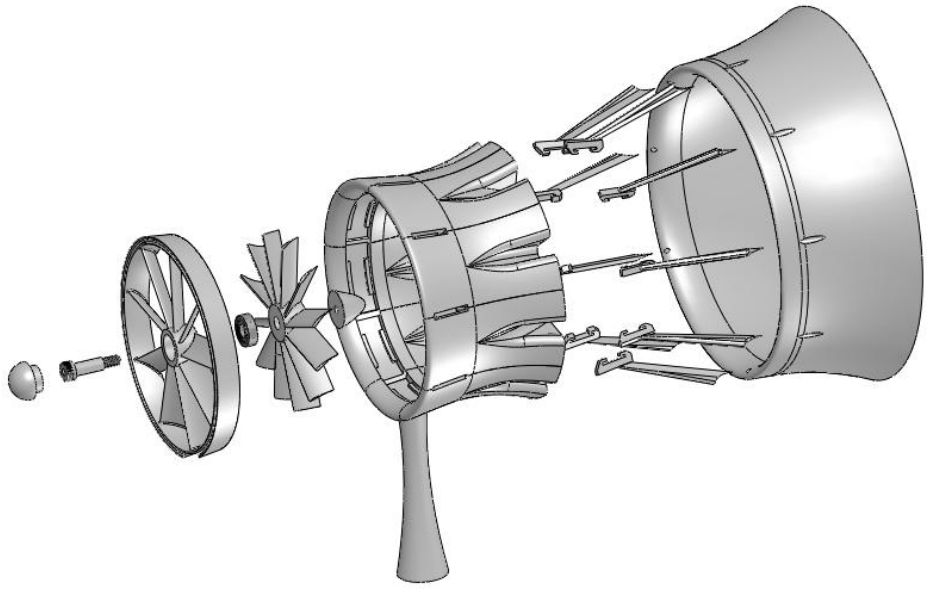

Figure 104: Student Interns Exploded 3D Model of FDM

A preliminary final design produced by the student Interns was constructed in a 3D solid modeling program called SolidWorks, shown in Figure 104. Two FloDesign Engineers continued the effort from this point and finished off the tasks required. These final design tasks were to design a new tower mount and fabric shroud as well as develop a bill of materials and an estimate cost of the prototype. Once updates to the FDM, such as incorporating a tower mounting system for the solid ejector model as well as designing the fabric shroud and struts were completed, the bill of materials was created along with a cost estimate. The tower mounting system was designed with a focus on not decreasing the FDM performance. For example, the tower was designed to limit the flow blockage that the tower causes on the flow that goes through the rotor as well as the flow through the ejector. The tower mount consists of four legs attaching to the front and back of the leading edge, this design was found to create less

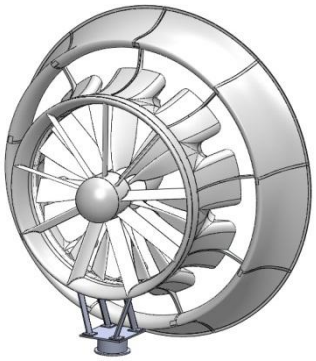

Figure 106: Four-legged Stand

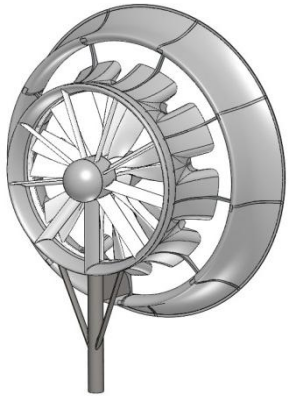

Figure 105: Tubular Stand

blockage in flow than a single strut to the center of the bottom of the leading edge. Creating a fabric shroud concept was the primary design goal for the ejector shroud, mainly due to the drop in manufacturing costs that this option offers. It is more cost effective to produce a fabric shroud than it is to fabricate one from plastic or foam. Another benefit of the fabric shroud is that it can be turned into a home assembly kit which could potentially drop the price well below competitors; however the consumer would have to assemble parts on their own and the fabric is more likely to become damaged in severe weather.

4.3g. Feasibility Cost Estimate:

There were two studies performed for the feasibility cost estimate, one of which was done on the cost estimate for a single prototype to be fabricated and the other cost estimate was done if we were to be manufacturing a couple hundred them. The total cost to produce a single prototype unit would be slightly over $26,000 shown in Figure 107, whereas if they were being manufactured the initial cost per turbine would be around $3,400 shown in Figure 108. The cost breakdown for each is shown below. From these studies, it is believed that mass producing

Bill of Materials for FloDesign Wind Turbine "Mustang 1kW Turbine"Prototype

$25,730.65	Total Weight (lbs):	268.767	Total Volume (in^3):	6,547.5	Total Surface Area (in^2):	20,394.3
$25,610.00	Stand Weight (lbs):	51.827	Turbine Weight (lbs):	215.7	Components:	48

Part	Material	Qty	Volume (in^3)	Surface Area (in^2)	Density (lbs/in^3)	Weight (lb)	Total Weight (lb)	Cost	Total Cost	Manufacture Process
Stator Inner	HDPE	1	1556.24	6665.92	0.03500	54.47	54.47	$7,020.00	$7,020.00	Injection Mold
Stator Outer	Aluminum	1	383.08	2125.25	0.09838	37.69	37.69	$2,340.00	$2,340.00	Investment Cast
Rotor	HDPE	1	1029.05	3481.26	0.03500	36.02	36.02	$3,480.00	$3,480.00	Injection Mold
Nose Cone	Foam	1	218.31	672.73	0.00174	0.38	0.38	$600.00	$600.00	Injection Mold
Tail Cone	Foam	1	225.15	1351.1	0.00174	0.39	0.39	$600.00	$600.00	Injection Mold
PMG Mount	Aluminum	1	52.27	239.49	0.09838	5.14	5.14	$400.00	$400.00	Machine
PMG	Generator	1	109.52	-	0.14061	15.40	15.40	-	-	-
C481 Lobe	Foam	9	810.567	1108.157	0.00174	1.41	12.67	$666.67	$6,000.00	Mold
Lobe T-insert	HDPE	9	37.567	185.886	0.03500	1.31	11.83	$20.00	$180.00	Injection Mold
Ejector Strut	HDPE	9	57.73	267.48	0.03500	2.02	18.18	$110.00	$990.00	Laser Cut
Ejector	Foam	9	1505.57	1624.01	0.00174	2.61	23.52	$444.44	$4,000.00	Mold
Stand	-	-	-	-	Assembly	N/A	N/A	-	-	-
5" Dia. Tube	Aluminum	1	280.61	1136.69	0.09838	27.61	27.61	$0.00	$0.00	Machine
Front Strut Right	Aluminum	1	76.99	250.98	0.09838	7.57	7.57	$0.00	$0.00	Sand Cast
Front Strut Left	Aluminum	1	76.99	250.98	0.09838	7.57	7.57	$0.00	$0.00	Sand Cast
Gusset Plate	Aluminum	1	92.22	328.51	0.09838	9.07	9.07	$0.00	$0.00	Sand Cast
Gurney Ring	HDPE	1	35.61	705.89	0.03500	1.25	1.25	$0.00	$0.00	Stamp

Part	Description	Head	Qty		Size	Per Pack	Cost	Packs	Total
Rim Bolts	Bolt outer and Inner Rim	Low Profile Socket	27		8-32 x 3/4"	25	$13.79	2.00	$27.58
Key Bolts	Bolts thru key bar to inner rim an	Low Profile Socket	36		6-32 x 3/8"	25	$9.20	2.00	$18.40
Top Blade Bolts	Bolts rim to blade	Socket	18		10-32 x 9/16"	50	$6.10	1.00	$6.10
Bot. Blade Bolts	Bolts hub to blade	Flat	18		10-32 x 5/8"	100	$12.90	1.00	$12.90
Hub Bolts	Bolts hub to PMG Plate	Socket	9		1/4-20 x 1.5"	50	$7.92	1.00	$7.92
Ejector Bolt	Bolts Ejector to struts	Flat	9		1/4-20 x 2"	25	$8.37	1.00	$8.37
Thrust Bearing	Between PMG and Rotor	-	1		20 mm	1	$4.21	1.00	$4.21
Washers	For thrust bearing	-	2		20 x 2.75 mm	1	$9.32	2.00	$18.64
Shaft Collar	To hold on rotor	-	1		20 mm	1	$2.61	1.00	$2.61
Set Screws	Hold on rotor Blades	-	7		10-32 x 1/2"	$25.00	$13.92	1.00	$13.92

Figure 107: Bill of Materials and Cost Estimate for FDM Prototype

thousands of units could reduce the cost another 50%

Bill of Materials for FloDesign Wind Turbine "Mustang 1kW Turbine" Manufacture

Total Cost:	$3,383.78	Total Weight (lbs):	59.422	Units Needed:	235.00	Final Lead Time:			
Process	**Part**	**Material**	**Qty**	**Volume (in^3)**	**Density (lbs/in^3)**	**Weight (lb)**	**Total Weight**	**Cost**	**Total Cost**
Mold	FDM_Mixer Lobe	Foam	9	318.9	0.00174	0.55	4.98	$75.00	$675.00
Cast	FDM_Stator Outer	SLS	8	11.65	0.03443	0.40	3.21	$50.00	$400.00
Cast	FDM_Stator Inner	SLS	8	22.03	0.03443	0.76	6.07	$50.00	$400.00
Cast	FDM_Stator Outer Slot	SLS	1	9.9	0.03443	0.34	0.34	$50.00	$50.00
Cast	FDM_Stator Inner Slot	SLS	1	20.93	0.03443	0.72	0.72	$50.00	$50.00
Extruded	FDM_Stator Blade	SLS	9	11.51	0.03443	0.40	3.57	$10.00	$90.00
Cast	FDM_Stator Hub	SLS	1	10.26	0.03443	0.35	0.35	$120.00	$120.00
Cast	FDM_Leading Edge Key	Aluminum	9	0.15	0.09838	0.01	0.13	$5.00	$45.00
Cast	FDM_T-Slot Key	Aluminum	9	0.15	0.09838	0.01	0.13	$5.00	$45.00
Cast	FDM_Stator Outer Key	Aluminum	9	0.28	0.09838	0.03	0.25	$5.00	$45.00
Cast	FDM_Rotor Hub	SLS	1	104.25	0.03443	3.59	3.59	$100.00	$100.00
Cast	FDM_Rotor Blade	SLS	7	27.57	0.03443	0.95	6.65	$50.00	$350.00
Cast	FDM_PMG Plate	Aluminum	1	29.67	0.09838	2.92	2.92	$25.11	$25.11
Molded	FDM_Nose Cone	SLS	1	55.1	0.03443	1.90	1.90	$34.26	$34.26
Molded	FDM_Tail Cone	SLS	1	45.59	0.03443	1.57	1.57	$24.26	$24.26
Stamped	FDM_Strut	Aluminum	9	8.46	0.09838	0.83	7.49	$25.00	$225.00
Molded	FDM_Ejector	Foam	9	995.53	0.00174	1.73	15.56	$75.00	$675.00

Company	**Part**	**Description**	**Head**	**Qty**	**Size**	**Per Pack**	**Cost**	**Packs**	**Total**
McMaster	Rim Bolts	Bolt outer and Inner Rim	Low Profile Socke	27	8-32 x 3/4"	25	$13.79	2.00	$6.90
McMaster	Key Bolts	Bolts thru key bar to inner rim an	Low Profile Socke	36	6-32 x 3/8"	25	$9.20	2.00	$4.60
McMaster	Top Blade Bolts	Bolts rim to blade	Socket	18	10-32 x 9/16"	50	$6.10	1.00	$1.53
McMaster	Bot. Blade Bolts	Bolts hub to blade	Flat	18	10-32 x 5/8"	100	$12.90	1.00	$3.23
McMaster	Hub Bolts	Bolts hub to PMG Plate	Socket	9	1/4-20 x 1.5"	50	$7.92	1.00	$1.98
McMaster	Ejector Bolt	Bolts Ejector to struts	Flat	9	1/4-20 x 2"	25	$8.37	1.00	$2.09
McMaster	Thrust Bearing	Between PMG and Rotor	-	1	20 mm	1	$4.21	1.00	$1.05
McMaster	Washers	For thrust bearing	-	2	20 x 2.75 mm	1	$9.32	2.00	$4.66
McMaster	Shaft Collar	To hold on rotor	-	1	20 mm	1	$2.61	1.00	$0.65
McMaster	Set Screws	Hold on rotor Blades	-	7	10-32 x 1/2"	$25.00	$13.92	1.00	$3.48

Figure 108: Bill of Materials and Cost Estimate to Manufacture the FDM

4.3h. Summarize all Findings and Incorporate Feasibility Study into course Curriculum for WNU:

During the FloDesign Inc. effort there was a classroom presentation and homework assignment presented to the Wind Water Turbine Course (ME 415) at Western New England (WNE) University. Below is the homework assignment given to the class. The presentation was focused on using Weibull/Rayleigh distribution to identify annual wind speeds to create power curves as well as Annual Energy Production. The presentation also covered wind speed classifications and typical wind turbine sizing as well as a brief discussion on common small wind turbine competitors. Given along with the homework assignment shown in Figure 109 there was a excel program utilized for Weibull wind speed analysis and AEP calculations shown in Figure 110.

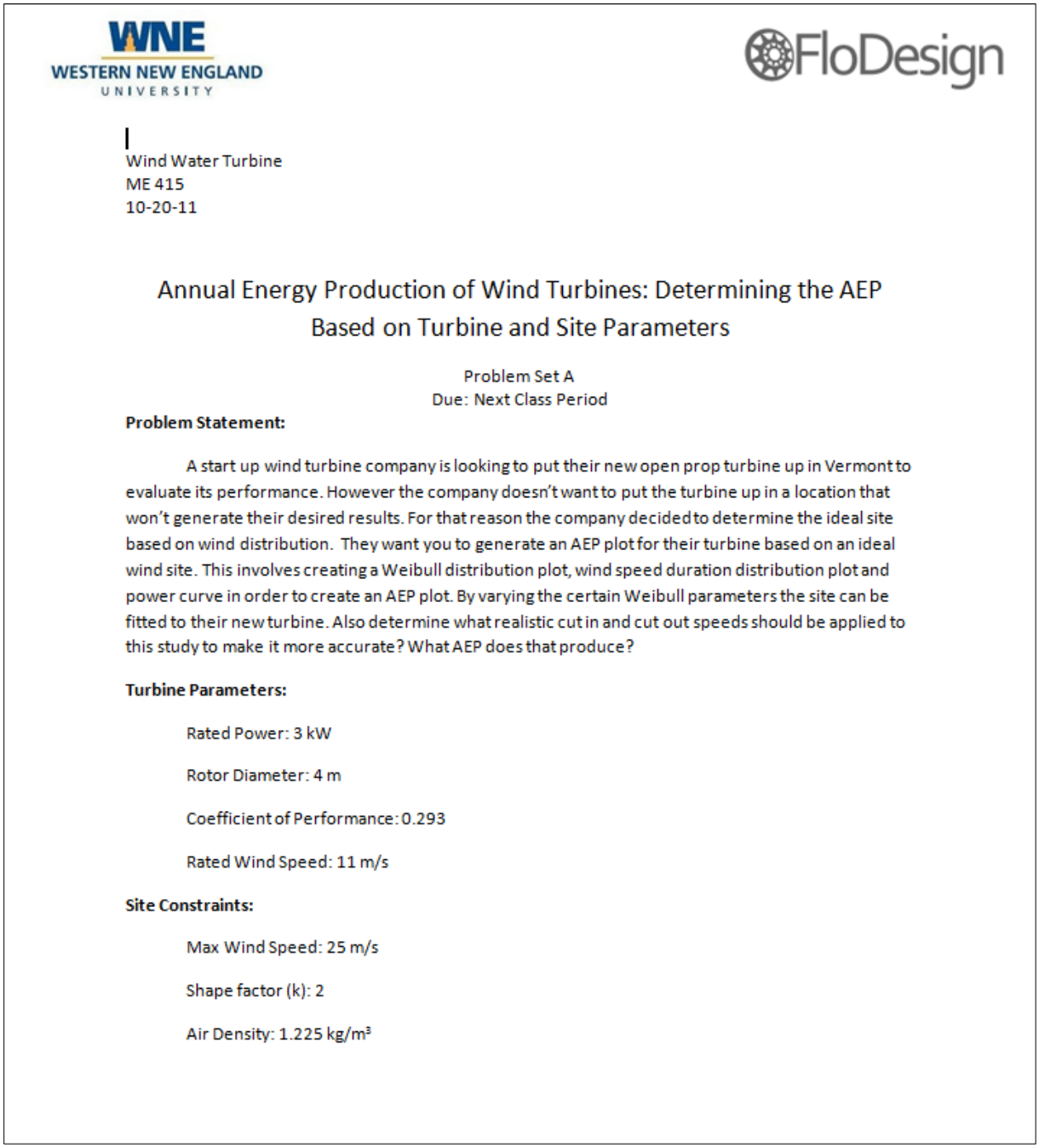

WESTERN NEW ENGLAND UNIVERSITY

FloDesign

Wind Water Turbine
ME 415
10-20-11

Annual Energy Production of Wind Turbines: Determining the AEP Based on Turbine and Site Parameters

Problem Set A
Due: Next Class Period

Problem Statement:

A start up wind turbine company is looking to put their new open prop turbine up in Vermont to evaluate its performance. However the company doesn't want to put the turbine up in a location that won't generate their desired results. For that reason the company decided to determine the ideal site based on wind distribution. They want you to generate an AEP plot for their turbine based on an ideal wind site. This involves creating a Weibull distribution plot, wind speed duration distribution plot and power curve in order to create an AEP plot. By varying the certain Weibull parameters the site can be fitted to their new turbine. Also determine what realistic cut in and cut out speeds should be applied to this study to make it more accurate? What AEP does that produce?

Turbine Parameters:

Rated Power: 3 kW

Rotor Diameter: 4 m

Coefficient of Performance: 0.293

Rated Wind Speed: 11 m/s

Site Constraints:

Max Wind Speed: 25 m/s

Shape factor (k): 2

Air Density: 1.225 kg/m^3

Figure 109: Homework Assignment Given to Class (ME415)

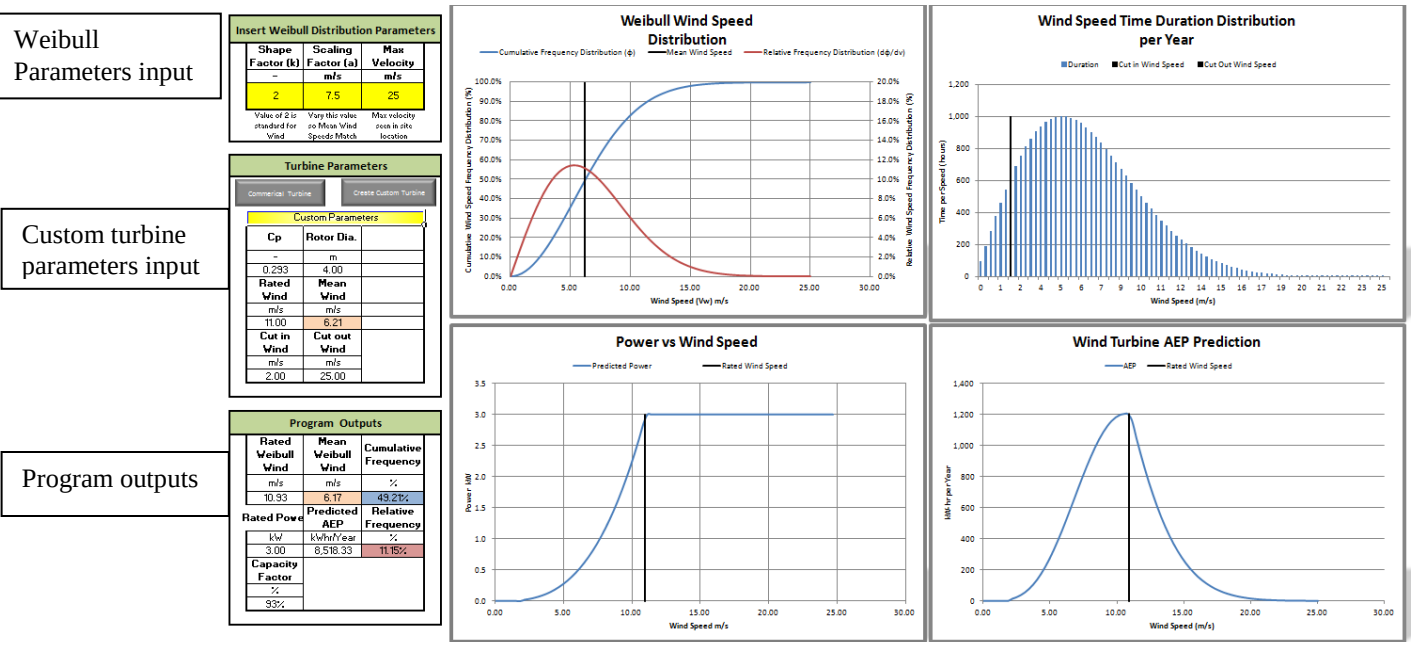

Figure 110: Weibull Wind Speed Distribution and AEP Calculator

The Weibull wind speed and distribution and AEP calculator was designed by FloDesign Inc. as a study tool for the students in WNE wind water turbine class. Its function is to be able to predict the annual wind speeds as well as the duration of time at those wind speeds and coupled with some specifications of a wind turbine the program will produce a power curve as well as an Annual Energy Production. The way that it calculates these values is with a few simple input values such as mean wind speed of the turbine as well as the rotor diameter, and the cut in and cut out speeds of the turbine.

The Weibull wind speed distribution chart is based on three values. The three inputs are shape factor (k), scaling factor (A), and max wind velocity. The shape factor (k) value for common wind applications is 2, but can typically range from 1 to 3. For any max velocity wind speed, a lower shape factor will produce a wide distribution of wind speeds whereas as higher shape factor specifies a narrow distribution of wind speeds. Typically a lower shape factor grants a higher energy production. So as the shape factor changes the peak of the curve is affected or in other words, the height of the Y-axis is shifted up or down. The scaling factor is what adjusts the X-axis value of the plot. There are multiple ways of estimating this number or numerically solving for this number using the gamma function. Typically its value is close to the average wind speed. The max wind velocity is just the highest wind speeds seen at a given location. There are two curves on this chart, one of which is a probability density function (pdf) which is shown mathematically below:

$$\frac{d\varphi}{dv} = \left(\frac{k}{A}\right) * \left(\frac{V_w}{A}\right)^{k-1} * e^{-\left(\frac{V_w}{A}\right)^k} \qquad [6]$$

This equation gives you the probability density function (pdf) which tells the user the percentage that the wind will be at any given speed. The other curve on the chart is a cumulative density function (cdf) which is mathematically described below:

$$\varphi = 1 - e^{-(\frac{V_w}{A})^k} \qquad [7]$$

This function describes the percent of time that the wind will be at a given speed. For example, in Figure 111 below, the pdf or, relative frequency distribution, says that at the wind will blow at 6 (m/s) around 56% of the time and the (cdf) says that 50% of the time the wind will blow at 6 m/s or less.

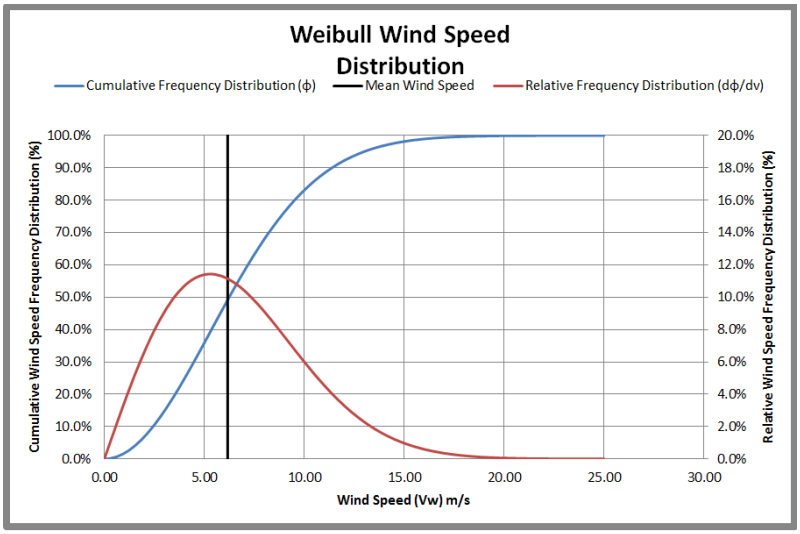

Figure 111: Weibull Wind Speed Distribution Example

The next chart that the excel program calculator prepares is a power curve of the given turbine with the specified wind parameters.

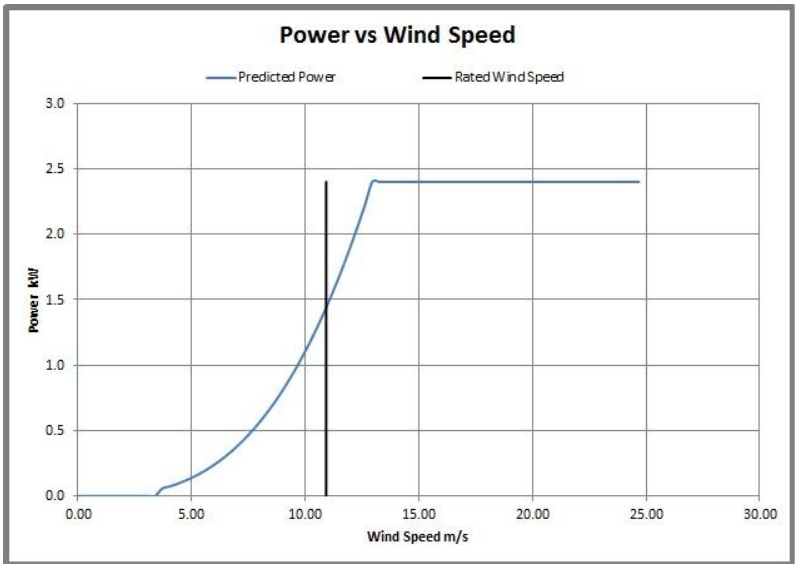

Figure 112: Power Curve Example

The power curve is a rather simple calculation and it's mathematically described below:

$$P = \frac{1}{2} * \rho * A * V_w^3 * C_p \quad [8]$$

Basically what the excel calculator does is it plots the values of power at multiple wind speeds. Excel compiles all of the wind speeds from the weibull plots and puts them into the equation above, so based on the chosen turbine's swept rotor area and C_p value it gives you power (kW) value and when shown graphically it looks like a plot in Figure 112.

The final chart is the AEP prediction. This is the value (kW-hr/year) that the specified turbine should output. This value is calculated by:

$$AEP = 8760 * P \quad [9]$$

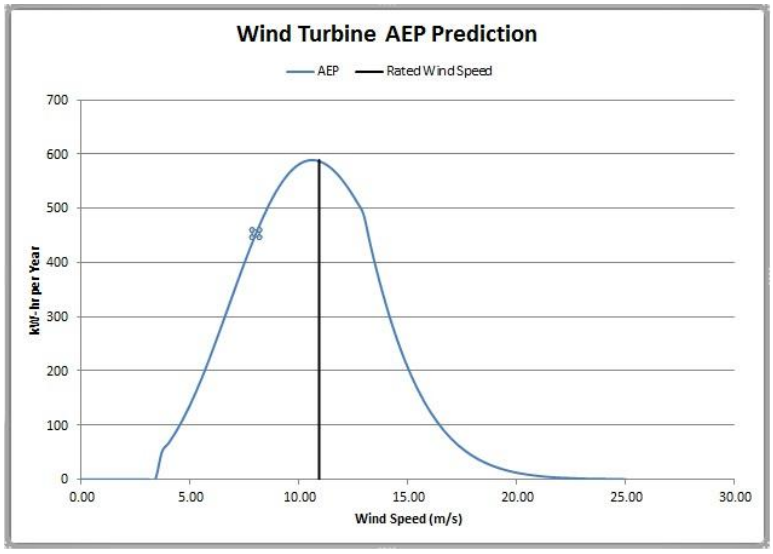

Figure 113: AEP Prediction Plot Example

Excel takes the power supplied at each individual wind speed and multiplies it by 8760 hours, which are the amount of hours in a year. This is how the curve is created, and then the program calculates the area under the curve to predict the total AEP of the turbine for a year.

This was designed purely as a learning tool for the students of Western New England University. The purpose was to have them go through the process of determining what would be the best turbine to install at particular locations. The goal was to have the students do the calculations out by hand then apply all of the information to the excel program to check their work. When the homework assignment was given the excel calculator was given to the students but it was password protected not to allow any of them to use the program without first completing the project by hand.

4.3i Feasibility Study Summary

The FloDesign Mustang feasibility study was performed by WNE University's student Interns as well as a couple of FloDesign Inc. employees under the direction of FloDesign Wind Turbine Corp. The focus of the study was to determine the feasibility of the FloDesign Mustang (FDM), a conceptual state of the art MEWT system for residential and distributed wind. There were FDM design studies, cost estimates, AEP comparisons as well as a market study of the current state and future trends of the small wind turbine. These studies provide data that supports the development of the Mustang as a viable product for residential and distributed wind. With the advantages of the MEWT design, the Mustang can revolutionize the small wind market.

5.0 REFERENCES

1. Provisional Patent Application No. 60/919,588 – Presz, W.M. Jr., Werle, M.J.,"Mixer-Ejector Power/Propulsion System", March 23, 2007.

2. Patent Application No. 12/054,050 – Presz, W.M., Werle, M.J., "Wind Turbine with Mixers and Ejectors", March 24, 2008.

3. Igar, O., Shrouds for Aerogenerators, AIAA Journal, October 1976, pp 1481-83. See also AIAA paper # 76-181 presented at the AIAA 14th Aerospace Conference, Washington DC, January
1976.

4. Hansen, M.O.L, Sorensen, N.N.: and Flay, R.G.J.: Effect of Placing a Diffuser around a Wind Turbine, Wind Engineering, Vol. 3, 2000, pp 207-213, see also Hansen, M.O.L.:AERODYNAMICS OF WIND TURBINES Cromwell Press, 2000

5. Gashe, R. and Twele, J,: WIND POWER PLANTS, Solarpraxis, 26.0 0 2

6. Werle, M.J., and Presz, Jr., W, "Ducted Wind/Water Turbines and Propellers Revisited", Technical Note, AIAA Journal of Propulsion and Power, Vol. 24, No. 5, Sept-Oct 2008, pp 1146-51.

7. Jamieson, J., Beating Betz—Energy Extraction Limits in a Uniform Flow Field, paper presented at the European Wind Energy Conference, Brussels, March, 2008.

8. Werle, M.J., and Presz, Jr., W.M., "Shroud and Ejector Augmenters for Subsonic Propulsion &Power Systems", AIAA Journal of Propulsion and Power, Vol. 25, No. 1, Jan-Feb, 2009.

9. Presz, Jr, W., Reynolds, G and Hunter, C: Thrust Augmentation with Mixer/Ejector Systems, AIAA Paper # 2002-0230, presented at 40th AIAA Aerospace Sciences Meeting & Exhibit 14-17, January 2002 / Reno, NV17.

10. Presz, W. and Reynolds, G., Alternating Lobed Mixer/Ejector Concept Suppressor, ALMEC Suppressor, United States patent 5,884,472, March 1999

11. Presz, W., "Mixer/Ejector Noise Suppressors," Paper No. 91-2243, AIAA 27th Joint Propulsion Conference, June, 1991

12. Presz, W. and Reynolds, G., Alternating Lobed Mixer/Ejector Concept Suppressor, ALMEC Suppressor, United States patent 5,884,472, March 1999

13. Presz, W., Morin, B., and Blinn, R., "Short Efficient Ejector Systems," Paper No. 87-1837, AIAA 23rd Joint Propulsion Conference, June, 1987.

14. Skebe, S., McCormick, D., and Presz, W., "Parameter Effects on Mixer-Ejector Pumping Performance," Paper No. 88-7018, AIAA 26th Aerospace Science Meeting, January, 1988.

15. Presz, W., Morin, B., and Blinn, R., "Short Efficient Ejector Systems," Paper No. 87-1837, AIAA 23rd Joint Propulsion Conference, June, 1987.

16. Werle, M.J., and Presz, Jr., W, New Developments in Shrouds and Augmenters for Subsonic Propulsion Systems, AIAA Paper No. 2008-4962, presented at the AIAA Joint propulsion Conference, Hartford CT, July 21-23, 2008.

17. Werle, M., "WindTurbine Wall Blockage Performance Corrections", Technical Note submitted to the AIAA Journal of Propulsion and Power, March 2009.

18. Presz, W.M., Jr., Reynolds, G., and McCormick, D., "Thrust Augmentation Using Mixer-Ejector-Diffuser Systems,"AIAA Paper No. 94-0020, Jan. 1994.

19. Presz, W.M., Morin, B.L. and Blinn, R.F., "Mixer-Ejector Performance Study." UTRC Report No.87-26, Dec. 1987

20. Presz, W., Morin B., and Gousy, R., "Forced Mixer Lobes in Ejector Designs," Paper No. 86-1614, AIAA 22nd Joint Propulsion Conference, June, 1986

21. "Home of the Small Wind Turbines." *All Small Wind Turbines - Portal to the World of Small Wind Turbines*. Web. 8 June 2011. <http://allsmallwindturbines.com>.

22. Small Wind Power Market to Double in Size to $634 Million by 2015 Pike Research. (2011, September 30). Pike Research. Retrieved August 6, 2012, from http://www.pikeresearch.com/newsroom/small-wind-power-market-to-double-in-size-to-634-million-by-2015

23. United States. National Renewable Energy Labratory. Department of Energy Labratory. By Trudy L. Forsyth, Peter K.C Tu, and Jeff Gilbert. N.p.: n.p., n.d. Web. 3 Aug. 2012. <http://www.nrel.gov/docs/fy00osti/26975.pdf>.

24. Heiser, W.H., "Ejector Thrust Augmentation", submitted for publication as a Technical Note in Journal of Propulsion and Power, May, 2010.

25. Werle, M.J., and Presz, Jr., W.M., Shrouds and Ejector Augmentors for Subsonic Propulsion and Power Systems, AIAA Journal of Propulsion and Power, Vol 25, No. 1, Jan-Feb, 2009. (Also included in the Additional Information Section of this proposal)

26. "Wind Powering America: 80-Meter Wind Maps and Wind Resource Potential." *Wind and Water Power Program: Wind Powering America*. U.S. Department of Energy. Web. 10 June 2011. <http://www.windpoweringamerica.gov/wind_maps.asp>.

27. "Wind Speed Distribution Weibull - Wind." Renewable Energy UK. N.p., 8 Mar. 2007. Web. 12 Oct. 2011. <http://www.reuk.co.uk/Wind-Speed-Distribution-Weibull.htm>.

28. Bennet, Alec, *Design and Research of Wind Turbine Tower Loads*, ME 440, Senior Design Project, Western New England College, Springfield, MA, Spring 2010.

29. "Wind Turbine Design Cost and Scaling Model." Web. www.nrel.gov/wind/pdfs/40566.pdf, July 2010.

30. Mindek, Richard, "Gyroscopic Forces," Lecture, Western New England College, Springfield, MA, August 2010.

31. Mikey. "Basic gyroscope equations." Gyroscopes. 2 February 2007 <http://www.mariner.connectfree.co.uk/html/gyro.htm>.

32. "Wind Energy: Facts." *Mass.Gov*. Department of Energy Resources. Web. 02 Aug. 2011. <http://www.mass.gov/?pageID=eoeeaterminal>.

33.http://www.mass.gov/?pageID=eoeeaterminal&L=4&L0=Home&L1=Energy%2C+Utilities+%26+Clean+Technologies&L2=Renewable+Energy&L3=Wind&sid=Eoeea&b=terminalcontent&f=doer_renewables_wind_wind-energy-facts&csid=Eoeea

34. Metzger, F. Bruce. "A Review of Propeller Noise Prediction Methodology." (1995). Rpt. in Hampton: National Aeronautics and Space Administration. Print.

35. Migliore, P., and A. Huskey. "Acoustic Tests of Small Wind Turbines." (2003). Rpt. in By J. Van Dam. Golden: National Renewable Energy Laboratory. Print.

36. W Z Shen and J N Sørensen 2007 *J. Phys.: Conf. Ser.***75** 012085 doi: 10.1088/1742-6596/75/1/012085.

37. Vick, Brian D. "AFFECT OF NEW BLADES ON NOISE REDUCTION OF SMALL WIND TURBINE WATER PUMPING SYSTEMS." Print. Rpt. in By R. Nolan.Bushland: USDA-Agricultural Research Service. Print.

38. Brooks, Thomas, and Michael Marcoloni. "Airfoil Self Noise and Prediction." (1989). Rpt. in By D. Stuart Pope. NASA Reference. Print.

39. Oerlemans, Stefan. "Detection of Aeroacoustic Sound Sources on Aircraft and Wind Turbines." (2009). Rpt. in Thesis University of Twente, Enschede. Print.

40. Woodward, Richard P. "Far-Field Acoustic Characteristics of Multiple Blade-Vane Configurations for a High Tip Speed Fan." (2004). Rpt. in By John A. Gazzaniga. National Aeronautics and Space Administration. Print.

41. Crocker, Raju P. "Eversman Comparison of Radiated Noise from Shrouded and Unshrouded Propellers." (1992). Rpt. in Vol. 1.University of Missouri. Print.

42. Thomas, Russell H. "Flow and Noise Control: Review and Assessment of Future Directions." (2002). Rpt. in By Meelan M. Choudari. National Aeronautics and Space Administration. Print.

43. Moccia, Antionio. "INDUSTRIAL CFD SIMULATION OF AERODYNAMIC NOISE." Print. Rpt. in 2007. Print.

44. Zhu, Wei Jun. "Modeling Of Noise From Wind Turbines." (2004). Rpt. in MechenicalDepartment,DTU. Print.

45. Klug, H. "NOISE FROM WIND TURBINES STANDARDS AND NOISE REDUCTION PROCEDURES." (2002). Rpt. in Wilhelmshaven, Germany;: DEWI (German Windenergy Institute). Print.

46. Fokkerweg, Anthony. "NOISE: Computation of Ducted Fan and Propeller Noise." (2002). Rpt. in National Aerospace Laboratory. Print.

47. Schulten, J.B.H.M., and M. Namba. "Numerical Results of Lifting Surface Theory." (2000). Rpt. in National Renewable Energy Laboratory. Print.

48. Leloudas, Giorgos. "Optimization of Wind Turbines with Respect to Noise." (2006). Rpt. in Master's Thesis Project Supervised by Jens N. Sørensen. Print.

49. G Leloudas. " Prediction and Reduction of Noise from a 2.3 MW Wind Turbine "*et al* 2007 *J. Phys.: Conf. Ser.***75** 012083doi: 10.1088/1742-6596/75/1/012083

50. Grosveld, Ferdinand W. "Prediction of Broadband Noise from Horizontal Axis Wind Turbines." (1985). Rpt. in 4th ed. Vol. 1. Hampton: Bionetics Corporation. Print.

51. Oerlemans, S., and J.G. Schepers. "Prediction of Wind Turbine Noise and Validation against Experiment." (2009). Rpt. in National Aerospace Laboratory. Print.

52. Hodgson, Ernest V. F. "Residential Wind Turbines and Noise Emissions." Web.

53. Sacks, A. H. "Ducted Propellers- A Critical Review of the State of the Art." (1962). Rpt. in By J. A. Brunell. Vol. 3. Oxford: Pergamon, 1961. Print.

54. Duane, Oleson R., and Patrick Howard. "SMALL AIRCRAFT PROPELLER NOISE WITH DUCTED PROPELLER." (1998). Rpt. in American Institues of Aeronautics and Astronautics, 1998. Print.

55. Grosveld, Ferdinand, Brenda Sullivan, and Stephen Rizzi. "TEMPORAL CHARACTERIZATION OF AIRCRAFT NOISE SOURCES." (2004). Rpt. in American Institute of Aeronautics and Astronautics. Print.

56. G.P.van Den Berg. "The Beat Is Getting Stronger: The Effect of Atmospheric Stability on Low Frequency Modulated Sound of Wind Turbines." Print. Rpt. in 4th ed. Vol. 4.University of Groningen. Print.

57. Vlterna, Larry. "The NASA-LeRC Wind Turbine Prediction Code." (1981). Rpt. in U.S. Department of Energy. Print.

58. Migliore, Paul G. *Microsoft Powerpoint*. Computer software. *Wind Turbine Aeroacoustic Issues*. National Renewable Energy Laboratory, Dec. 2002. Web.

59. Huskeys, A., and M. Meadors. *Wind Turbine Generator Systems Acoustic Noise Test Report*.Tech. National Renewable Energy Lab, 2001. Print.

60. Rogers, Anthony, and James Manwell. "Wind Turbine Noise Issues." (2002). Rpt. in Huskeys, A., and M. Meadors.Wind Turbine Generator Systems Acoustic Noise Test Report.Tech. National Renewable Energy Laboratory. Web.

61. Hubbard, Harvey H. "Wind Turbine Acoustics." (1990). Rpt. in By Kevin Sherperd.U.S. Department of Energy. Web.

62. Rogers, Anthony, and James Manwell. "Wind Turbine Noise Issues." (2002). Rpt. in Huskeys, A., and M. Meadors.Wind Turbine Generator Systems Acoustic Noise Test Report.Tech. National Renewable Energy Laboratory. Web.

63. Metzger, F. Bruce. "A Review of Propeller Noise Prediction Methodology." (1995). Rpt. in Hampton: National Aeronautics and Space Administration. Print.

64. W Z Shen and J N Sørensen 2007 *J. Phys.: Conf. Ser.* **75** 012085
doi: 10.1088/1742-6596/75/1/012085

65. Vick, Brian D. "AFFECT OF NEW BLADES ON NOISE REDUCTION OF SMALL WIND TURBINE WATER PUMPING SYSTEMS." Print. Rpt. in By R. Nolan. Bushland: USDA-Agricultural Research Service. Print.

66. Brooks, Thomas, and Michael Marcoloni. "Airfoil Self Noise and Prediction." (1989). Rpt. in By D. Stuart Pope. NASA Reference. Print.

67. Woodward, Richard P. "Far-Field Acoustic Characteristics of Multiple Blade-Vane Configurations for a High Tip Speed Fan." (2004). Rpt. in By John A. Gazzaniga. National Aeronautics and Space Administration. Print.

68. Crocker, Raju P. "Eversman Comparison of Radiated Noise from Shrouded and Unshrouded Propellers." (1992). Rpt. in Vol. 1. University of Missouri. Print.

69. Thomas, Russell H. "Flow and Noise Control: Review and Assessment of Future Directions." (2002). Rpt. in By Meelan M. Choudari. National Aeronautics and Space Administration. Print.

6.0 APPENDICES:

Appendix A: Design of an Ethernet based Data Collection System for Modern Wind Turbines

Design of an Ethernet Based Data Collection System for Modern Wind Turbines

By:
Justin Beach
Faculty Advisor:
Professor Mohammad Khosrowjerdi

Table of Contents:

Abstract……3
Purpose……3
Introduction……..3
Theory……..6
Experimental Procedure……10
Data and Results……21
Conclusions……23
Appendices……25

Abstract

In their development of a new prototype wind turbine FloDesign Wind Turbine has acquired the need to verify the proposed advantages of the prototype design over those of conventional wind turbines. The process of benchmarking their Briza Mixer Ejector Wind Turbine (MEWT) against a known competitor the Bergey XL1 Horizontal Axis Wind Turbine (HAWT) is the objective of this project. The MEWT design would prove revolutionary to modern wind turbine technology if it were shown to be superior to the conventional HAWT design. To prove or disprove this hypothesis data must be accrued on the performance of each turbine design. This was accomplished via a Data Acquisition System (DAS) developed in the graphical programming language Visual Basic combined with the output of sensors, which gathered pertinent data on turbine performance. The project resulted in a functioning user interface, which provided all relevant data recorded by the DAS, which will aid FloDesign in benchmarking their Briza prototype. The following report details the procedure that was utilized to construct the functioning DAS as well as the outputs that the system displays to the user.

Purpose

The overriding goal of this project was to develop a data collection system for the purpose of benchmarking the Briza Prototype Wind Turbine, in development by FloDesign Wind

Turbine of Wilbraham, Massachusetts. This system will compile data on wind speed, wind direction, air temperature, relative humidity, and barometric pressure at two separate sites. The Briza prototype wind turbine is located at a test site in Rutland Massachusetts and the control, a Bergey model XL1 wind turbine has been installed at Sleith Hall of Western New England College in Springfield Massachusetts. Both turbines are rated as being capable of generating 1kW of electrical power under optimum conditions. The purpose of benchmarking the prototype Briza model is to determine whether the new MEWT concept will yield any advantages over the conventional three bladed HAWT design. These two geographic locations vary in average wind speed, prevailing wind direction, and surface exposure, as well as elevation and hence air density. To be able to accurately compare (benchmark) the power developed by the two turbines data must be taken from both locations so that the variances between locations can be accounted for in the comparison. FloDesign hopes that the resulting comparison will reveal an increase of efficiency of the Briza prototype design over the conventional Bergey design, and perhaps a lower cut in speed or better high speed/high wind performance.

Introduction

Interest in renewable energy is growing rapidly as there is an increased concern for the environment as well as speculation that production of fossil fuels, mainly oil, has peaked. The use of solar and wind energy to supply electrical power has become a viable and often environmentally and politically savvy alternative to fossil fuels like coal. Harnessing energy from the wind is no new idea and has been implemented in various ways for thousands of years from the sailing ships to wind mills. Many countries have taken to construction of wind farms to generate electrical energy where hundreds or even thousands of wind turbines will be located in a region of high wind and little interference. A wind turbine is a rotary device that extracts potential energy from the wind, converts it first into mechanical energy, and then into electrical energy by the use of a generator. Deserts, mountain passes, and even the ocean have become ideal locations for these turbines, so as to generate power with little or no impact on populated areas. Worldwide power generation using wind energy is an ever increasing trend as shown in the Figure 1 below, and will only increase in the years to come.

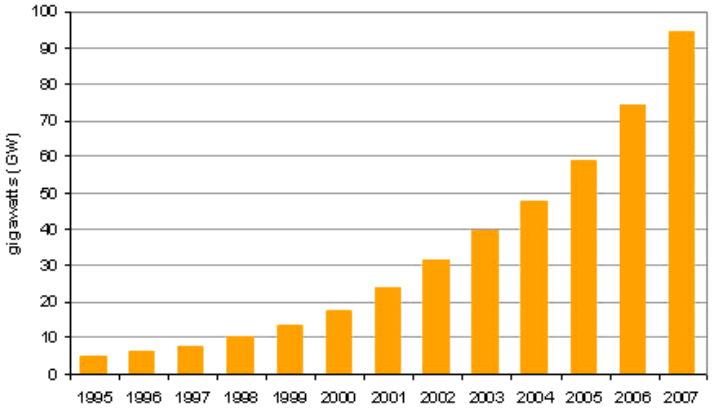

Figure 1. Global wind energy generation capacity trends. Source: International Energy Agency, Key World Statistics 2007

In the United States alone the use of wind energy is expected to increase due to government initiatives over the next few decades as shown in Figure 2. As such it is desirable to create and market products that generation electric power from wind energy. FloDesign, based in

Wilbraham Massachusetts, wishes to revolutionize this market segment with new conceptual wind turbine design.

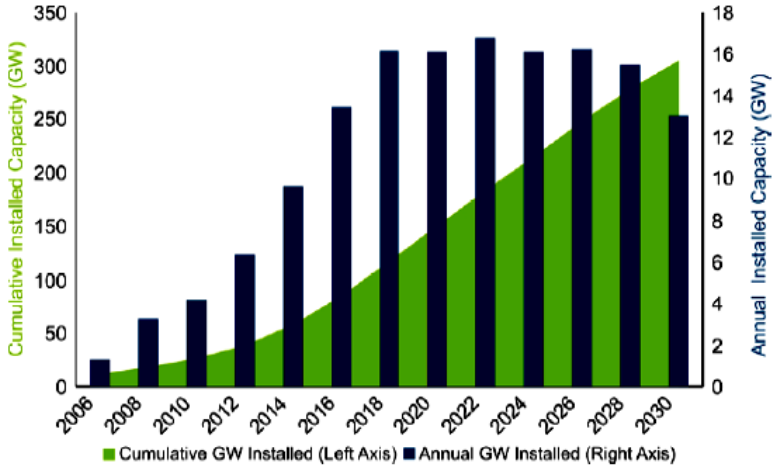

Figure 2. US projected wind energy growth under 20% by 2030 program. Source: U.S. Dept. of Energy

The most prolific design for modern wind turbines is that of the Horizontal Axis Wind Turbine (HAWT). This design dominates most wind farms worldwide and has become somewhat of an accepted standard for the wind turbine industry. The most commonly viewed HAWT is the three bladed variant which utilizes three blades of airfoil type geometry to extract energy from the wind. This energy is used to turn the hub, to which the blades are attached, which is connected to a gearbox located in the nacelle. This gear box is connected to a generator which converts the rotational motion, by means of generating a magnetic field by passing current through windings, into electrical energy. The electricity is then transmitted to the grid and consumed by the public.

FloDesign wishes to improve the wind turbine offerings for the growing renewable wind energy market. Their design, a Mixer Ejector Wind Turbine (MEWT), integrates technology taken from jet engine design that incorporates a shroud and mixer ejector to the turbine geometry. The Briza prototype, seen in Figure 3 below, displays the shrouded design. Addition of these elements results in pumping between the shroud and the mixer ejector cowling which serves to increase the amount of mixing in the exit stream of the turbine increasing the efficiency of the design. The prototype Briza design also incorporates the use of a stator and rotor design common to jet engines. The fluting of the shroud also aids in the mixing of the exit flow of the turbine decreasing the chance of separation in the flow and the associated loss of energy.

Figure 3, Briza Prototype MEWT

The fixed stator, enclosed by the shroud, first encounters the wind and functions to turn the flow as it passes through the blades of the stator. The rotor located directly behind the stator on a central hub has blades which catch the swirl induced by the stator. This swirl causes the rotor to rotate about the hub thus extracting the energy of the flow contained in the swirl. The rotation of the rotor turns the windings of an electro magnet in the generator creating electric power.

To determine if the MEWT design is more advantageous than conventional HAWTs performance data from both turbines needed to be collected. Having better high speed performance, being more efficient in a smaller package, producing more power, and having a lower cut in speed would be indicators that FloDesign's MEWT is superior to conventional HAWTs. The data collected at both sites included wind speed, wind direction, air temperature, air pressure, and relative humidity. Measurement of these quantities were made by the use of sensors installed on the Bergey turbine tower itself as well as on a ground mast located approximately ten feet off the ground adjacent to the Bergey turbine at Sleith Hall at WNEC. All of the data was collected by the data collection system and is stored in a database as well as being available for viewing by the user in the Visual Basic user interface.

Theory

The design of modern three bladed wind turbines stems from the theoretical limit on their efficiency called the Betz Limit, proposed by the German physicist Albert Betz. This limit allows for only 59% of the kinetic energy in the swept area of a HAWT to be captured by the turbine. The power generated by a HAWT is a function of the mass flowrate through the swept area of the rotor and the total pressure drop. These two factors, however, are opposing effects as an increase in total pressure drop (yielding more power extraction) results in a decrease in the mass flowrate through the rotor. The more energy the turbine extracts from the flow the greater the decrease between the free upstream velocity and the downstream exit velocity of the wind. Eventually if too much energy is extracted from the flow the flow will stop, as will the turbine and thus the generation of power. The efficiency of the HAWT is further influenced by the gear box, generator, and frictional losses as well. There is also a major loss of energy to the larger wake regions produced by the HAWT as shown below in the schematic in Figure 4.

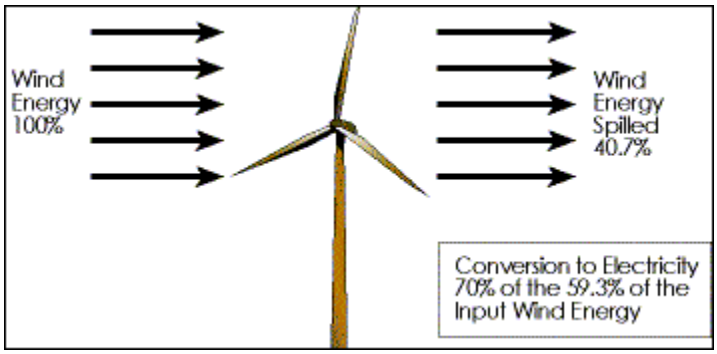

Figure 4, Betz Limit Schematic

Based on the Betz Limit the efficiency of modern HAWTs is contingent on the scale of the application. The larger the swept area of the rotor of a HAWT the closer the design will approximate the efficiency of the Betz Limit. The largest turbines today capture nearly 53% of the potential energy of the wind yet they have grown to monstrous sizes with rotor diameters in excess of 110m on average. This obviously creates design issues with respect to the strength of the blades, hub, actuators (to adjust the angle of attack of the blades), and tower support structure as well as logistical issues with regards to transportation and construction of the units.

FloDesign has created a new generation of turbines called Mixer Ejector Wind Turbines (MEWTs) which theoretically allow for three to four times the energy potential as the Betz Limit states. The design incorporates chambered shrouds which function together to produce the effect of a mixer ejector which creates a pumping effect as it mixes the flow. This increases the efficiency of the turbine by using energy from the flow, which is not captured by the swept area of the turbine, to energize the exit flow, i.e. pumping. This augments the thrust on the rotor blades by reducing the resulting pressure drop through the turbine. The actual performance of the MEWT is unknown however, and the prediction of three to four times the efficiency of the HAWTs has not yet been verified. This is the goal of the development and use of data acquisition systems for both the Briza prototype (MEWT) and the Bergey (HAWT). These systems will allow the two different turbine designs to be compared head to head so as to determine what advantage in efficiency the MEWT design has over that of the HAWT.

Data Acquisition (DAQ) is the process of sampling real world conditions and converting these analogue quantities into digital numeric values/data to be stored and analyzed later. The use of sensors allowed for the sampling of critical data, at both the Rutland site (Briza prototype) and WNEC (Bergey XL1), which in turn was received and recorded with the use of the DAQ. Sensors permit the collection of environmental and performance data from each turbine so as to benchmark one against the other. A sensor is a device which converts a physical property or event into a corresponding analogue electrical signal. The sensors installed at WNEC included two separate anemometers to measure wind speed, two wind direction sensors, a combined temperature and humidity sensor, and a barometric pressure sensor.

These sensors were hardwired, linked via wires run directly from the sensor, to a Data Acquisition System (DAS) constructed in the mechanical engineering laboratory at Western New England College. The system also incorporated the use of a multitude of thermocouples mounted on the solar collectors outside of Sleith Hall as well as on the pipes of the solar system inside the mechanical engineering laboratory. The output of each of these thermocouples was also read in to the system for collection and recording purposes as part of the new Green Engineering curriculum at Western New England College. The DAS collected the analogue signal outputs

from all of the sensors and converted them to digital signals which were then recorded through a user interface developed in the graphical programming environment Visual Basic.

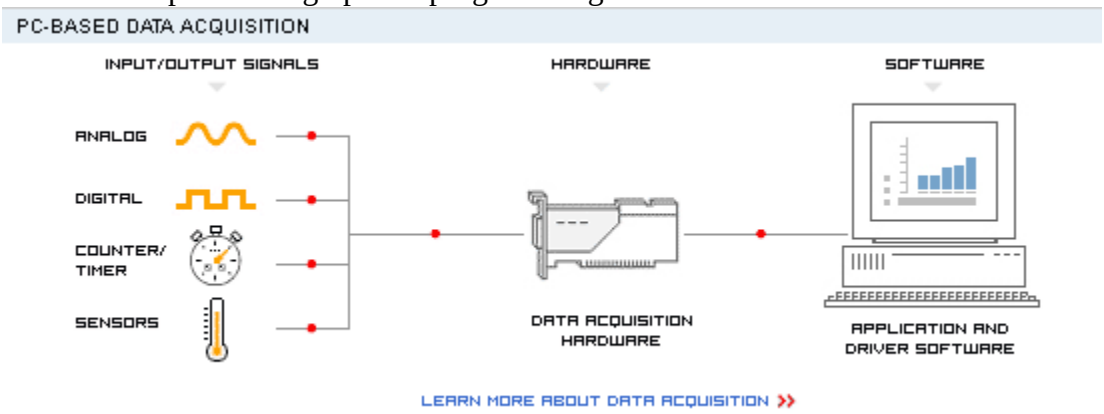

Figure 5, Data Acquisition System (DAS)

Figure 5, above, shows the process of Data Acquisition in which sensors convert physical properties into voltage or current and send that data to the DAQ hardware where it is digitized for storage and analysis.

The two types of anemometers that were installed at WNEC were a three cup design and that of a propeller type. The propeller type anemometer functioned in the same way the HAWT does in that it catches the wind with airfoil shaped blades which cause it to rotate. This rotation is used to calculate the wind speed; also this model happened to incorporate a tail section which acts as a wind vane giving the wind direction as well. The three cup anemometer is required by IEC standards, and consists of three cups attached to a central shaft. The cups are spaced 120 degrees from each other producing equal and consistent torque to the main shaft when acted upon by the wind. The cups capture the air and turn at the same velocity as the wind. The Riso three cup anemometer we are using came from Denmark and is of the switch-closure type. The rotation of the shaft causes a switch to open or close producing an output signal with two pulses per revolution. The wind direction sensor is simply a wind vane which is a bladed structure that self aligns itself with the direction the wind is blowing from in the same fashion as a wind vane on a house would. The base of the wind vane is instrumented with a rotary potentiometer which gives the radial position in degrees of the wind vane. The temperature sensing was combined with a humidity sensor, and was in essence a thermocouple with two wires, made of dissimilar material, that had a dielectric constant between them. A change in the temperature creates a voltage difference that can be reported as a temperature change. This principle guides the use of the thermocouples attached to the solar system as well. The thermocouples utilized for temperature measurement on the solar system were T-type thermocouples. Type T (copper–constantan) thermocouples are suited for measurements in the −200 to 350 °C range. Type T thermocouples have a sensitivity of about 43 µV/°C. The humidity sensor functions by utilizing a dielectric layer shielded by polymer layers, as seen in Figure 6, so as to absorb moisture from the air without foreign material such as dirt skewing the data. The dielectric response of the material varies with temperature and humidity.

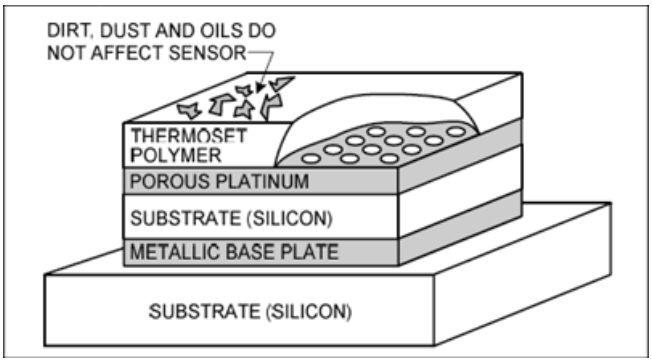

Figure 6, Humidity sensing material

This necessitates the need for temperature compensation for the temperature dependence. The sensor then outputs a linear voltage that is a function of the relative humidity of the air. The barometric pressure sensor is a pressure transducer which produces a linear analogue voltage of 6 to 30v proportional to the ambient pressure of the air.

Perhaps the most important measurement used to compare the two turbines was the power that each produced. Both were designed and rated at 1kW with the maximum power generation potential of the Bergey being rated at 1300 watts and the Briza prototype, being a prototype, was unknown. To measure the power produced by the Bergey wind turbine the AC power produced by the turbine was fed through a rectifier circuit. In Figure 7 below the operation of a rectifier circuit can be viewed. The figure shows that positive and negative current, from an AC power source (in our case the turbine), being split and forced to go down two separate paths by the use of a bridge of diodes. This bridge rectifies the AC current so that the entire waveform is positive. Using capacitors the rectifier circuit reduces the peaks of the AC voltage to a constant DC voltage. The beginning and ending waveforms can be viewed in Figure 8, depicting three separate AC waveforms and the resultant DC waveform post rectifier.

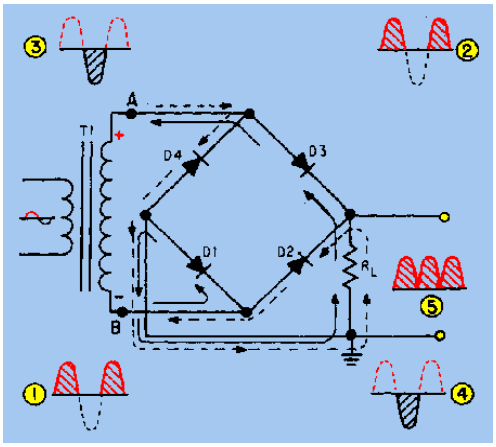

Figure 7, Rectifier Circuit

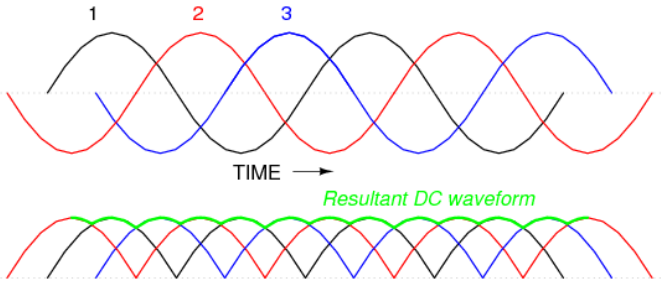

Figure 8, Rectified Waveform of Three AC sources

Power measurement is accomplished with the use of a watt transducer, which utilizes a Hall Effect sensor. A Hall Effect sensor determines the power being generated by measuring the magnetic field produced by current passing through its windings and converting that output into a power figure. This is then stored and reported as a particular value in watts of power.

Experimental Procedure

This project began with research into wind energy generation and especially to research the Bergey XL1 wind turbine which was installed outside of Sleith Engineering Hall at Western New England College. The addition of two photovoltaic arrays, two solar collectors, and the Bergey Wind Turbine were accompanied by subsequent senior projects aimed at aiding future students in WNEC's Green Engineering Program. As such the logbooks of seniors, last semester, Dan Goodwin and Adam Desmaris proved to be very useful in the beginning stages of the project. The researched specifications of the Bergey XL1 wind turbine, seen in Figure 9, can be found in Appendix A.

Figure 9, Bergey XL1 HAWT outside of Sleith Engineering Building

The goal of the project was to construct a data collection system that mirrored the one built by Dr. Khosrowjerdi for FloDesign, for the Briza prototype, located at the test site in Rutland, MA. This system can be seen in Figure 10 below, and the photo was taken on site in Rutland and is of the DAS attached to the trailer mount for the Briza.

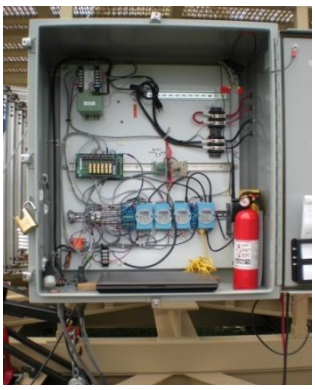

Figure 10, Briza DAS, located on tower base trailer

FloDesign is currently testing a new prototype wind turbine and therefore for the data to be accepted the testing and data must conform to the International Electrotechnical Commission (IEC) standards. To match the data being taken from the Briza prototype the data collection system for the Bergey would need to record wind speed data, wind direction, air temperature and relative humidity, and the barometric pressure. The power generated by the photovoltaic panels as well as the amount of solar energy (solar irradiance) had to be measured for use in the Green Engineering program. Based on the IEC standards the Bergey wind turbine would need to be reinstrumented and the data collection system would need to take data once every ten seconds and average that data over a ten minute period. Dan Goodwin had previously instrumented the Bergey XL1 for wind speed and direction and had power meters in place to register what kind of power the turbine was producing. These sensors lacked analogue outputs however and thus could not be used by the proposed Ethernet based data collection system which Dr. Khosrowjerdi was developing. The need for more accurate measurement of wind speed, temperature, humidity, and

barometric pressure to conform to the IEC standards required the purchase of new sensing equipment.

The first purchase was that of a new three cup type anemometer for installation on the Bergey support tower itself. The anemometer that was chosen was a Riso P2546A from Denmark which measures wind speed from 0-70 m/s with an uncertainty of 0.08-0.14m/s. This unit was a direct replacement for the existing three cup anemometer which had been installed on the Bergey support tower. The specifications of the Riso anemometer can be found in Appendix B along with those of all the other sensors utilized during this project. The installation of the new anemometer merely required a new fixture which Peter Bennett, our machinist, was able to fashion for us. The installation and new bracket can be seen in Figure 11 through 13 below.

Figure 11, New Bracket for anemometer

Figure 12, New Riso three cup anemometer next to existing wind vane

The existing wind direction sensor (in black) is near the end of the mounting mast and is an NRG 1904 #200 unit. This unit has an analogue DC output, measures 360 degrees, and has an accuracy of within 1% potentiometer linearity. Again the specifications of this device are found in Appendix B of this report.

Figure 13, Bergey XL1 tower and instrument mast

To manage this installation the Bergey had to be lowered outside of Sleith Hall which was made possible by its tilting cantilever tower support. The lowering of the turbine was not difficult and was accomplished from the roof of Sleith Hall by way of an apparatus designed by Curt Freedman. The process can be seen in Figures 14 and 15 as the Bergey is slowly lowered into a waiting cradle for access from the ground.

Figure 14, Lowering the Bergey

Figure 15, Bergey on the ground

The second stage of reistrumentation was that of reinstrumenting the ten foot ground mast. IEC standards require that the wind speed must be taken at hub height as well as ten feet off the ground. To accomplish this, a mast was attached to the photovoltaic array nearest Sleith Hall. This mast had already been instrumented for wind speed, using a three cup anemometer, temperature and relative humidity, using a combined sensor, and solar irradiance (the amount of sun able to be absorbed for energy) using a pyranometer. The existing anemometer was deemed inaccurate and thus was replaced by a propeller type anemometer which incorporated a wind vane for wind direction sensing. After mounting the new anemometer it was necessary to calibrate the device. This was done by connecting leads to the outputs on the device and observing the current. When the wind vane turned the current would change. Once the vane was in a direction which yielded no current (north) on the digital multimeter it was temporarily fixed in place. Then the base of the device was oriented so that it matched the orientation of the wind vane thus syncing the two halves and the device. This allowed for a reading of 0 amperes when the wind vane faced due south and a maximum of 5 amperes when it faced due north. This way the data acquisition system could distinguish which direction the wind vane was facing, and hence which direction the wind was blowing. Also attached to the T shaped tip of the ground mast was a temperature and humidity sensor. This unit was shielded and produced a linear analogue voltage output proportional to the temperature and humidity of the surrounding air. The T shaped top of the ground level instrument mast can be seen in Figure 16, noting the three sensors visible; the anemometer and incorporated wind vane, the temperature and relative humidity combined sensor, and the pyranometer.

Figure 16, Instrumented Ground Mast

Below the three sensors located on the top of the ground mast was the 2046 NRG BP-20 barometric pressure sensor which was mounted directly to the mast itself as seen in Figure 17.

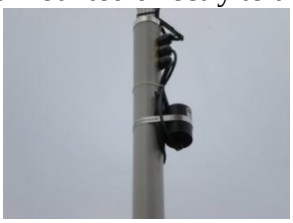

Figure 17, Barometric Pressure Sensor

All of these sensors reused existing wiring that had already been feed through conduit from the ground mast into Sleith Hall and into the mechanical engineering laboratory. It is there where the Data Acquisition System (DAS) resides.

As part of the newly formed Green Engineering program the photovoltaic arrays and solar collector systems were also instrumented. This was done so as to allow students a better learning opportunity to become engaged in actual applications of the theories which they learn. The photovoltaic arrays as well as both the Flat Panel and Evacuated Tube Solar Collectors can be seen outside of Sleith Hall and in Figure 18.

Figure 18, from left to right; Evacuated Tube Solar Collector, Flat Panel Solar Collector, and then the two Photovoltaic Arrays

The data collected from the photovoltaic arrays is merely the power they develop as well as the solar irradiance given by the pyranometer. The pyranometer is again located on the ground mast seen above the right hand side of the PV array furthest on the right. The solar collectors are instrumented to determine the temperature at each inlet and outlet at the collectors as well as

throughout the network of pipes they are connected to in the mechanical engineering laboratory. The solar collectors both function to harness the energy of the sun and transfer it to a working fluid (in this case propylene glycol) which is then pumped through a pipe network to mixing tanks and heat exchangers within the mechanical laboratory. This system is represented by the schematic in Figure 19, which represents the two solar collectors and their respective pipe networks.

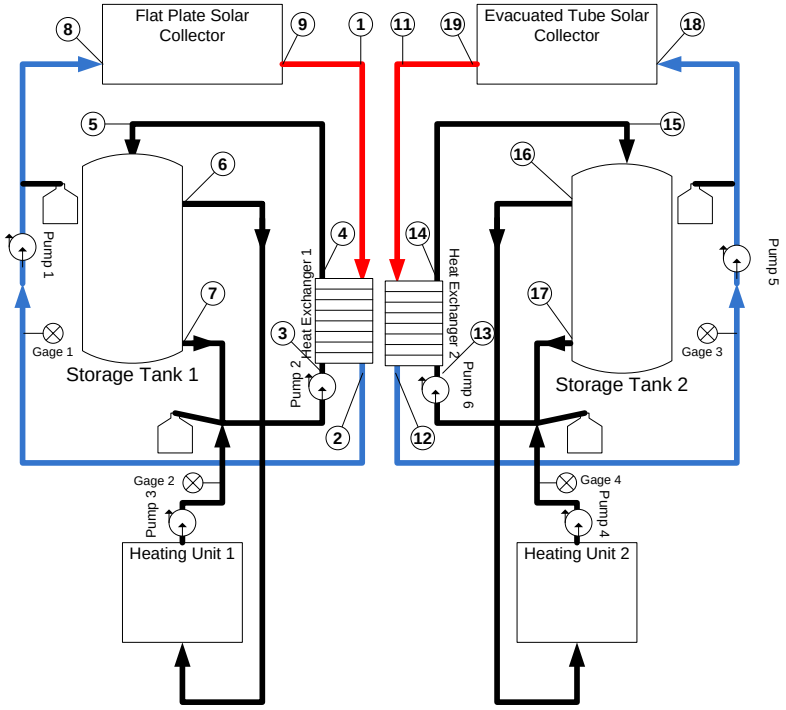

Figure 19, Solar Collector Networks

Here the red lines indicate the flow of heated fluid from the solar collectors into the network and the blue lines indicate the flow exiting the network and going into the collectors to receive energy. The schematic above in Figure 19 is a representation of the pipe network seen below in Figure 20, located in the mechanical engineering laboratory.

Figure 20, solar pipe network, heat exchangers, and mixing tanks in ME lab

Each numbered circle represents a T type thermocouple which has been attached to monitor the temperatures at various points of interest in the pipe network. The thermocouples that were used had an adhesive backing that was thermally conductive yet non-electrically conductive and, allowed for easy attachment to the piping. There are two separate systems displayed in Figure 18, and the thermocouples are labeled so that numbers 1-9 are dedicated to the Flat Plate Collector and numbers 11-19 are for the Evacuated Tube Collector. This was done so as to remove any chance of misunderstanding when taking data on the two separate systems. Each is numbered sequentially yet separated by a factor of ten, making the numbering system intuitive. The temperature is monitored on the inlets and outlets of the two heat exchangers as well both mixing tanks. The inlet and outlet temperature of the system is also monitored outside of the building on the collectors themselves.

There are thermocouples attached to each solar collector at its inlet and outlet totaling four thermocouples placed outside. The thermocouples labeled 8 and 9 are the inlet and outlet, respectively, from the Flat Plate Solar Collector. Numbers 18 and 19 again represent the inlet and outlet respectively of the Evacuated Tube Solar Collector. Each thermocouple is attached via an electrical junction to wires leading into Sleith Hall. The connections were made in the junction boxes located on support structures of the two collectors. These wires were then painstakingly snaked through conduit to a main electrical box on the side of Sleith Hall. This box mirrors one on the inside of Sleith, in the machine shop, which functions as a DAS for the outside thermocouples alone. The signals from the thermocouples on the collectors are sent to the main DAS, in the ME lab, via Ethernet cable from a remote DAS located in the machine shop.

Finally the main Data Acquisition System (DAS) is fed all the information either directly from the sensors themselves or, in the case of the thermocouples attached to the collectors, via Ethernet. The system collects all the data from all the analogue sensors and converts it through the ADAM modules into digital signals that are then transferred to the PC for display as can be seen in the Data and Results section. The ADAM 6017 module can accept up to eight separate analogue inputs and output two separate digital outputs. This module is the backbone of the data collection system and can be seen in both systems in Figures 21 and 22.

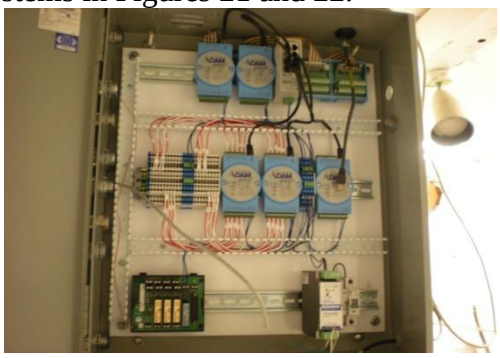

Figure 21, ADAM modules in blue at Briza, Figure 22, ADAM modules in ME DAS

In each case, the DAS at the Briza site in Rutland and in the mechanical laboratory at WNEC, the DAS is enclosed in a large electrical box so as to protect its sensitive components and wiring.

Power generated by the turbine is 3 phase AC which must then be transformed into DC power by a rectifier circuit. The rectifier circuit, as shown before in Figure 7, removes the power

spikes and delivers a constant DC waveform of 24 volts DC. This current is then passed through the power sensor, Hall Effect sensor, and on to the inverter. Once the power generated by the turbine is sent to the inverter it is then transformed back in to AC current so as to be used by the lights in the mechanical engineering laboratory. This is shown in schematic form in Figure 23, which also displays the various sensors which send data to the Data Acquisition System (DAS).

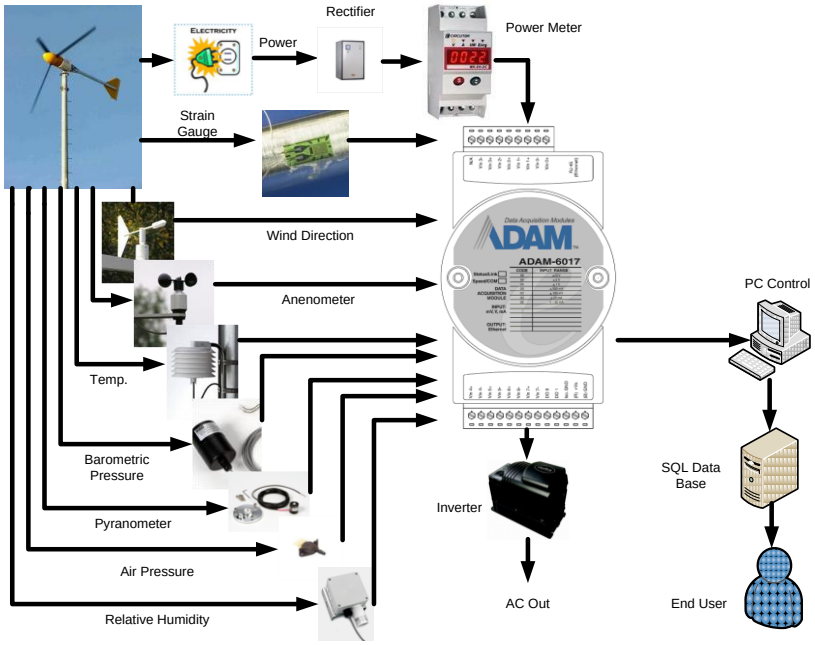

Figure 23, Schematic of DAS inputs and current flow from turbine

The photovoltaic arrays outside of Sleith Hall also produce power that is fed into the system in the form of 24 volts DC. Both the power generated by the Bergey turbine as well as the photovoltaic arrays is fed into the Bergey Power Controller. This controller, seen in Figure 24 below, collects the power and feeds the power from both turbine and PV arrays either to the inverter or, keeping it as DC power, directly to the battery banks for storage.

Figure 24, Bergey Power Controller

The power can also be fed through a dump load resistor so as to dissipate the energy produced. If the power created by the Bergey turbine and the PV arrays is not completely used

by the system, to either charge the batteries or to power the lights in the mechanical laboratory, then the DAS is unable to determine the amount of power being produced. Thus a one ohm dump resister was attached to the Bergey Power Controller to absorb any potentially unused energy. Once all the electrical connections were made the system was fully functional, and the DAS could report the output of all the sensors and the amount of power being produced by the entire system of combined solar and wind turbine power. The final step in the project was to allow the end users, the students, easy access to the output of the DAS. This was done by fitting two large plasma screen televisions in the mechanical engineering laboratory that constantly present the Visual Basic programs which display the DAS output. The output is shown below just as it is displayed on screen for the users in Figure 25 through 27 below.

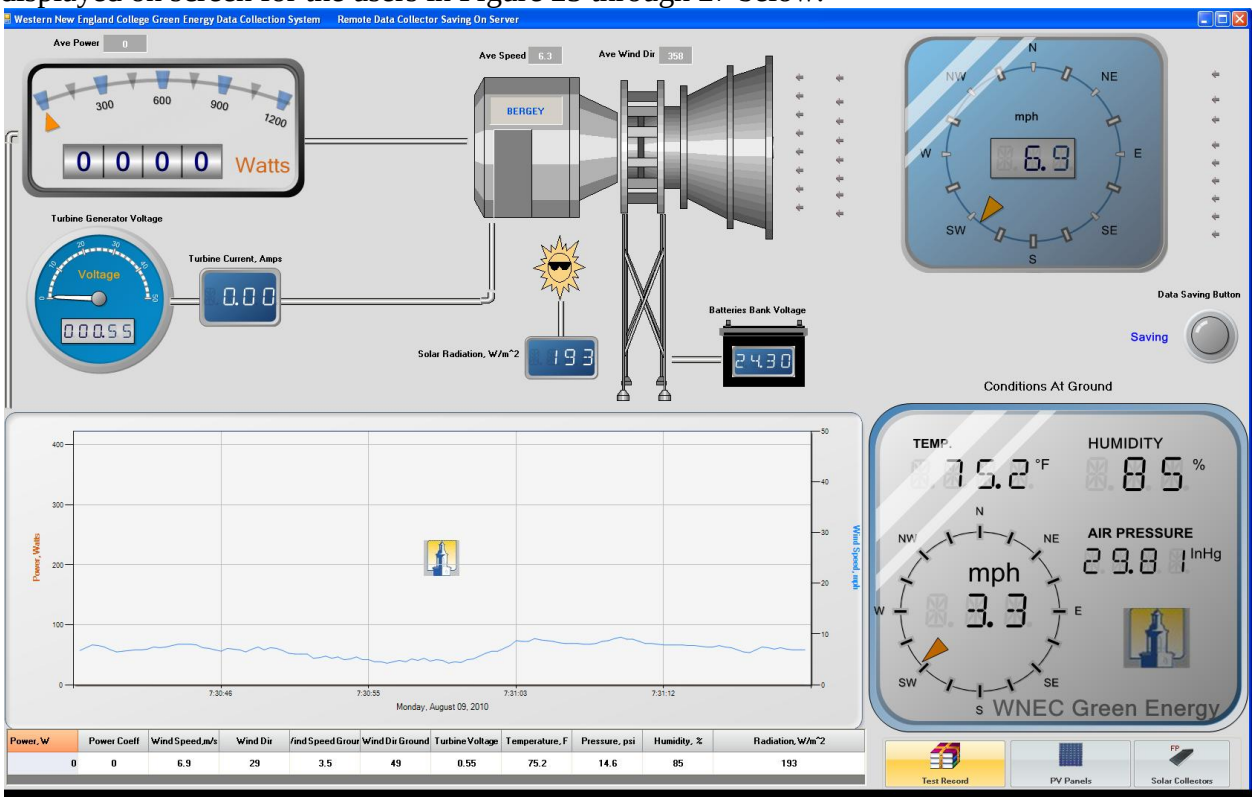

Figure 25, Visual Basic display of Bergey Wind Turbine Data

Figure 25 above displays the power being generated by the Bergey wind turbine in watts in the upper left hand corner. It also shows the total voltage being produced and plots the power generation versus wind speed. It naturally also displays both the wind speed and direction at both the tower mast elevation as well as at the ground level. The ground level output in the bottom right hand side of the display also gives the temperature of the air, the relative humidity, and the barometric pressure of the site at WNEC. To aid the students in utilizing the photovoltaic arrays the pyranometer data for solar irradiance is also shown towards the middle of the display.

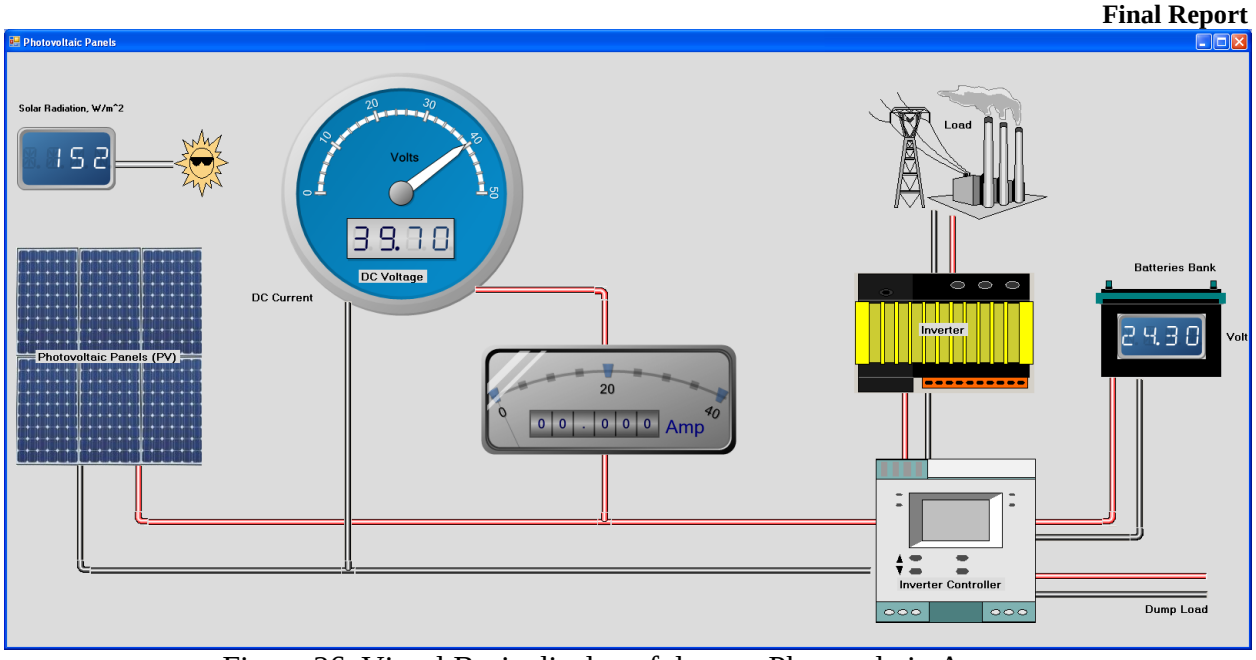

Figure 26, Visual Basic display of data on Photovoltaic Arrays

The display above serves as the DAS display for the photovoltaic arrays. The display pictorially displays the generation and transmission of solar power and also displays the amount of power being generated. Again the values for solar irradiance are displayed to aid in efficiency calculations oriented towards the photovoltaic arrays.

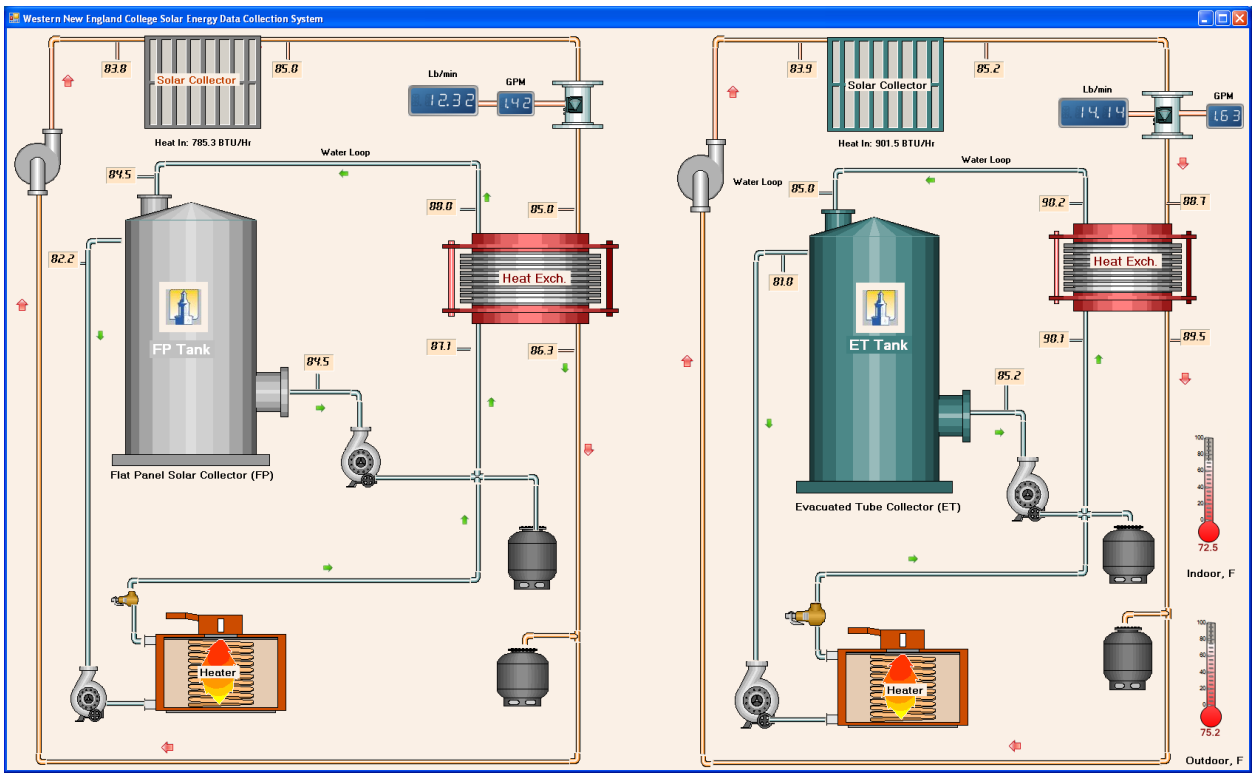

Figure 27, Visual Basic display of Solar Collector system data

Figure 27 represents the Solar Collector systems, both the Flat Plate and Evacuated Tube Collectors, in the graphical user interface provided by Visual Basic. This interface allows for the user to monitor the temperature at various points in the solar collector system by viewing the temperatures reported by numerous thermocouples. Each system is pictorially depicted allowing for ease of use by students as they can easily determine visually where each temperature is being taken. These displays are the end product of the entire project, and will allow FloDesign to view the data on the Bergey wind turbine as well as benefitting future Green Engineering students in the study of their curriculum.

Data and Results

Data recording is accomplished by the DAS taking samples four times a second and displaying that data. The data is saved once a second for further review and post processing analysis later allows for one minute or ten minute averages to be found. This data is then stored in a relational database called MYSQL which is resident on one of the Western New England College servers. All data is protected and secured by being on this server and only those with access rights can view the proprietary information, such as the data collected for FloDesign's prototype Briza turbine.

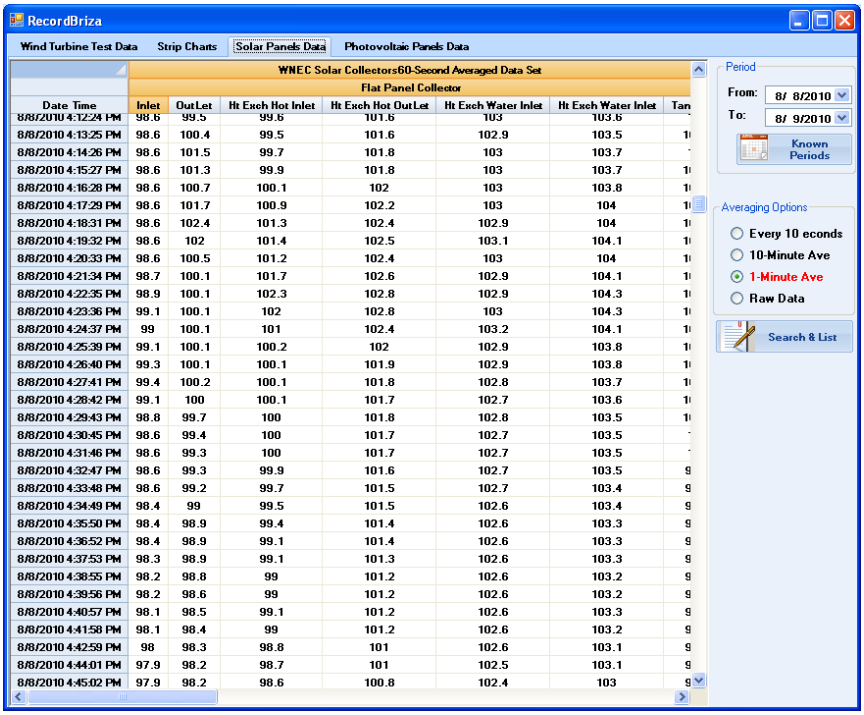

Figure 28, Thermocouple data from Solar Collector System

The outputs of the thermocouples which were installed to monitor the temperatures of the solar collector system are shown above in Figure 28. This is the output of the DAS and displays the time at which the data was taken as well as the temperatures at the inlets and outlets of the solar collectors themselves.

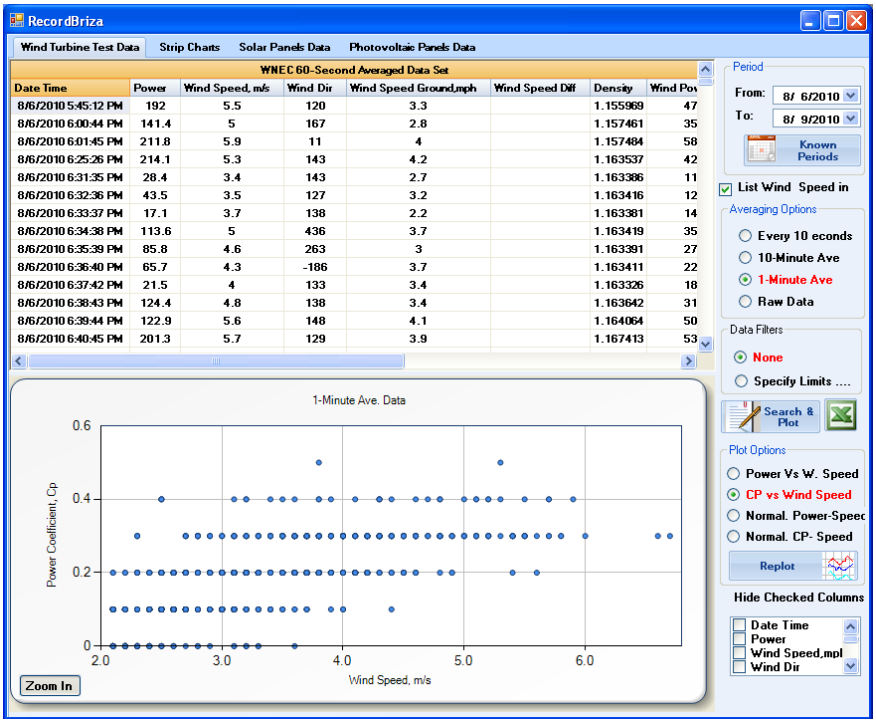

Figure 29, Wind Speed data and Cp

Both Figure 29 and 30 display wind speed data including the wind speed at the Bergey tower and also at the ground level. The date stamp is shown again on the right side with the next column being the power produced at that time. The further columns in Figure 29 display wind speed data, air density, and other information used to calculate the Coefficient of Power (Cp) of the system. Figure 30 also displays wind speed as well as a plot of the power produced versus wind speed as averaged per minute. The trend of the data shows that power increases with proportionally with wind speed. This is expected of the Bergey as all wind turbines up until the turbine reaches its peak power production and then the power falls off dramatically. The Bergey turbine actually has a folding tail section which will “auto-furl” to prevent over-speed of the turbine which could prove harmful to the turbine and generator assembly.

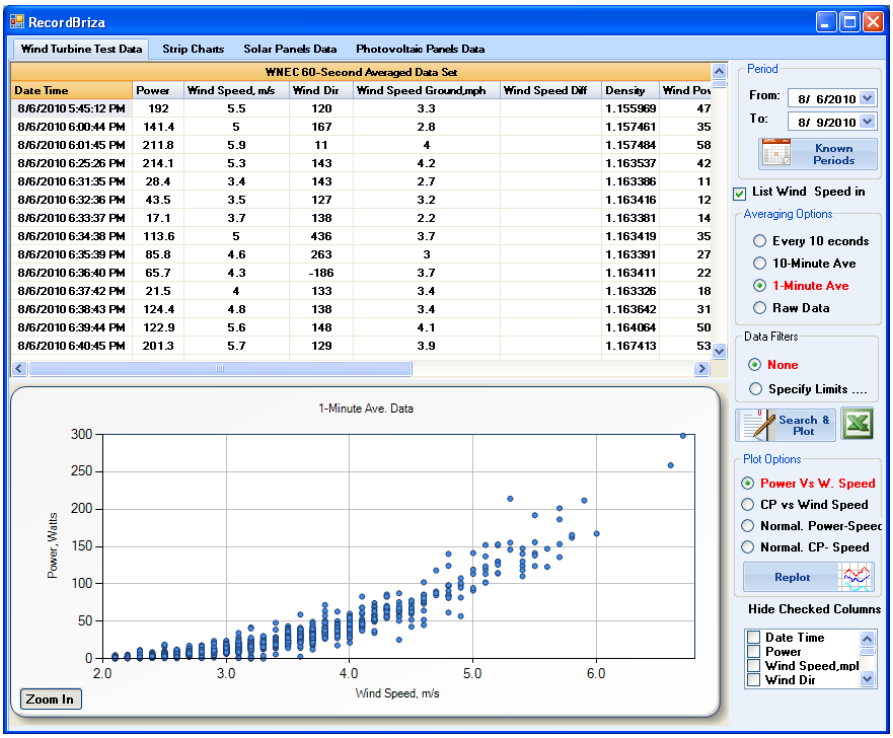

Figure 30, Wind Speed data

The resulting displays for the project were depicted in the figures presented earlier, Figures 25-27. These figures show the data which was desired by FloDesign and by the faculty for the Green Engineering program. These are the real tangible results for which the project was conceived. The data recorded by the Data Acquisition System (DAS) is viewable to students via the displays screens in the mechanical engineering laboratory, as pictured in Figures 25-27, and also by users such as FloDesign remotely via the MYSQL server hosted by the Western New England College server.

Conclusions

As this time no conclusions can be drawn due to the lack of data recorded and lack of analysis of the data. It will take time to collect sufficient data over perhaps a few months to compare the different locations of the two turbines (Briza prototype at Rutland test site and the Bergey at WNEC). The locations differ in elevation as well as in the characteristics of the wind which they receive and utilize for power. Variances in local elevation, air temperature, relative humidity of the air, and the density and pressure of the air will affect the coefficient of performance (Cp), and hence the power output of the turbines. As such they must first be compared purely based on their differences in the location. Then the performance data on power production collected from both turbines will be analyzed to determine if indeed a gap in performance and efficiency between the Briza prototype and the Bergey XL1. Conclusions as to what gains in efficiency or power production exist with the new MEWT design as opposed to the conventional HAWT design will only be known after a thorough analysis which was not within the scope of this project. This project allowed for the next step to be taken in that it was aimed at providing the tools (sensors) and the system (DAS) necessary to benchmark the turbine against each other. The actual process of comparing the two turbines based on the data collected is the next step and will hopefully yield the confirmation of our hypothesis that we desire.

Appendix A: (Bergey HAWT Specifications)

XL.1 Specifications

Type: 3 Blade Upwind
Rotor Diameter: 2.5 m (8.2 ft.)
Start-up Wind Speed: 3 m/s (6.7 mph)
Cut-in Wind Speed: 2.5 m/s (5.6 mph)
Rated Wind Speed: 11 m/s (24.6 mph)
Rated Power: 1000 Watts
Maximum Power: ~ 1,300 Watts
Cut-Out Wind Speed: None
Furling Wind Speed: 13 m/s (29 mph)
Max. Design Wind Speed: 54 m/s (120 mph)
Blade Pitch Control: None, Fixed Pitch
Overspeed Protection: AutoFurl
Gearbox: None, Direct Drive
Temperature Range: -40 to +60 Deg. C (-40 to +140 Deg. F)
Generator: Permanent Magnet Alternator
Output Form: 24 VDC Nominal
Functional Features: Low-End Boost, Slow-Mode, Electric Brake, 30A Solar Regulator, 60A Dump Load, Timed Battery Equalization, Watt Meter Display Mode, Polarity Checker

Predicted Energy Production

Wind Speeds Taken at Top of Tower

Annual Average Wind Speed (m/s)		3.5	4	4.5	5	5.5	6	6.5
Annual Average Wind Speed (mph)		7.8	8.9	10.1	11.2	12.3	13.4	14.5
Production in kWh (24 VDC)	Daily	1.9	2.8	3.9	5.1	6.4	7.7	8.9
	Monthly	55	85	115	155	195	235	270
	Annually	680	1,010	1,410	1,850	2,320	2,790	3,260

Wind Speeds Taken at 10 meters (per standard wind resource maps)

US-DOE Wind Power Class		1	2	3	4	5	6	7
Annual Average Wind Speed (mph)		~ 8.9	~ 10.7	~ 12.1	~ 13.0	~ 13.9	~ 15.0	~ 18.8
Annual Average Wind Speed (m/s)		~ 4.0	~ 4.8	~ 5.4	~ 5.8	~ 6.2	~ 6.7	~ 8.4
Production in kWh (24 VDC)	30 ft (9m) Tower Daily	2.6	4.3	5.8	6.8	7.8	9.1	12.7
	30 ft (9m) Tower Monthly	80	130	175	205	240	275	385
	64 ft (20m) Tower Daily	4.1	6.4	8.2	9.3	10.4	11.7	14.7
	64 ft (20m) Tower Monthly	125	195	250	285	320	355	445
	104 ft (32m) Tower Daily	5.2	7.8	9.7	10.9	12.0	13.1	15.4
	104 ft (32m) Tower Monthly	160	235	295	330	365	400	465

Assumptions: Inland site, Rayliegh Wind Distrubution, Shear Exponent = 0.20, Altitude = 1000ft (300m).
Note: Battery charge regulation (batteries full) and wire run losses will reduce actual XL.1 performance.
Your Performance May Vary.

Appendix B: (Sensor and Hardware Specifications)

NRG #200P Wind Direction Vane, 10K, With Boot

SPECIFICATIONS

Description	
Sensor type	continuous rotation potentiometric wind direction vane
Applications	• wind resource assessment • meteorological studies • environmental monitoring
Sensor range	360° mechanical, continuous rotation
Instrument compatibility	all NRG loggers
Output□si□nal	
Signal type	Analog DC voltage from conductive pla□tic potentiometer, 10K ohms
Transfer function	Output signal is a ratiometric voltage
Accuracy	potentiometer linearity within 1%
Dead band	8° Maximum, 4° Typical
Output signal range	0 V to excitation voltage (excluding deadband)
Response characteristics	
Threshold	1 m/s (2.2 miles per hour)
Power requirements	
Supply voltage	Regulated potentiometer excitation of 1 V to 15 V DC

Installation	
Mounting	onto a 13 mm (0.5 inch) diameter mast with cotter pin and set screw
Tools required	0.25 inch nut driver, petroleum jelly, electrical tape
Environmental	
Operating temperature range	-55 °C to 60 °C (-67 °F to 140 °F)
Operating humidity range	0 to 100% RH
Lifespan	50 million revolutions (2 to 6 years normal operation)
Physical	
Connections	4-40 brass hex nut/post terminals
Weight	0.14 kg (0.3 pounds)
Dimensions	• 21 cm (8.3 inches) length x 12 cm (4.3 inches) height • 27 cm (10.5 inches) swept diameter
Materials	
Wing	black UV stabilized injection molded plastic
Body	black UV stabilized static-dissipating plastic
Shaft	stainless steel
Bearing	stainless steel
Boot	protective PVC sensor terminal boot included
Terminals	brass

NRG #BP20 Barometric Pressure Sensor
SPECIFICATIONS

Description	
Sensor type	micromachined integrated circuit absolute pressure sensor
Applications	• wind resource assessment • meteorological studies • environmental monitoring
Sensor range	15 kPa to 115 kPa (4.43 inches to 34.0 inches Hg)
Instrument compatibility	• NRG Symphonie equipped with a BP SCM + any iPack
Output signal	
Signal type	linear analog voltage
Transfer function	Absolute Pressure in kPa = (Voltage x 21.79) + 10.55 typical
Accuracy	+/- 1.5 kPa (15 mb) max. uncorrected offset (+/- 0.443 inches Hg)
Calibration	calibration sheet included with each sensor specifies offset correction
Turn on time	15 ms
Power requirements	

Supply voltage	7 V to 35 V DC
Supply current	15 mA max. (8 mA typical)
Installation	
Mounting	mounts directly to tower or inside steel shelter box with hose clamps (included)
Tools required	8mm (5/16 inch) nut driver or flat blade screwdriver
Environmental	
Operating temperature range	• 10 C to 50 C at full accuracy • At cold temperatures, offset increases by 3 kPa (30 mb) worst case at -30 C.
Physical	
Connections	wire leads, 3 conductor shielded cable: • Red: sensor power • White: output signal • Black: sensor ground • Shield wire: to earth ground
Cable length	• 1.5 m (5 feet) • cable diameter 4.8 mm (3/16 inches)
Weight	0.1 kg (0.2 pounds)
Dimensions	• 57 mm (2.25 inches) diameter • 112 mm (4.4 inches) length (including cable bushing)
Materials	
Cable	3 conductor 22 AWG, with overall foil shield and drain wire, chrome PVC jacket
Enclosure	weatherproof black ABS

Li-Cor #LI-200SZ Pyranometer
SPECIFICATIONS

Description	
Sensor type	total solar radiation sensor - cosine corrected
Applications	• solar resource assessment • meteorological studies • environmental monitoring
Sensor range	0 W/m^2 to 3000 W/m^2
Instrument compatibility	• NRG Symphonie PLUS w/ Solar SCM • NRG Symphonie w/ Solar SCM • Logger measurement range 0 to 1300 W/m^2, typical
Output signal	
Signal type	microamp current proportional to total solar radiation
Transfer function	• included on calibration certificate • typical is 90 µA per 1000 Watts/m^2
Accuracy	maximum deviation of 1% for sensor range
Calibration	• calibration sheet included with each sensor defines output in microamps per 1000 Watts/square meter

	• calibrated against Eppley Precision Spectral Pyranometer under natural daylight conditions.
Output signal range	0 µA to 270 µA (typical)
Drift	+/- 2% change over a 1 year period
Response characteristics	
Threshold	0.1 W/m^2
Installation	
Mounting	mounts to tower with custom NRG side mounting boom and hose clamps
Tools required	• sheet metal shears or similar for hose clamps • 5/16 inch hex driver or flat blade screwdriver • 0.05 inch hex key (included); metric #4 allen wrench for level adjustment
Environmental	
Operating temperature range	-40 °C to 65 °C (-40 °F to 149 °F)
Operating humidity range	0 to 100%
Physical	
Connections	2 bare wire leads from coaxial cable
Cable length	3 m (10 feet)
Weight	28 g (1.0 ounces)
Dimensions	• 23.8 mm (0.94 inches) diameter • 25.4 mm (1 inch) length
Materials	
Cable	shielded coaxial
Detector	high-stability silicon photovoltaic
Enclosure	weatherproof anodized aluminum case with acrylic diffuser and stainless steel hardware

Email page

ADAM-6017 RoHS

8-ch Isolated Analog Input Modbus TCP Module with 2-ch DO

Main Features

10/100 Mbps communication rate
I/O type: 8 AI / 2 DO
Input type: mV, V, mA
Provide default/customized web page
Provides math. Functions: Max., Min., Avg.

Configure your system now

Datasheet (PDF) 3D model online view Download 3D Model Manual/ Driver/ BIOS/ FAQ

Introduction

The ADAM-6017 is designed with 8 analog inputs and 2 digital outputs to satisfy all plant needs. Each analog channel is allowed to configure an individual range for variety of applications.

Specifications

Part Number		**ADAM-6017-BE**
Analog Input	**Channels**	8
	Voltage Input	±150 mV ±500 mV ±1 V ±5 V ±10 V
Analog Output	**Channels**	-
	Voltage Output	-
Digital I/O	**Digital Input Channels**	-
	Digital Output Channels	2 (Sink)
General	**Interface**	10/100 Mbps Ethernet
	Peer-to-Peer1	Yes
	GCL1	Yes

Appendix B: Measurement and Analysis of Shrouded and Unshrouded Wind Turbine Noise

Final Report

Measurement and analysis of shrouded and unshrouded wind turbine noise

Dr. Bart Lipkens, Chase Vajcovec

August 2010

Abstract:

The objective of this project was to characterize the noise emissions of the Flodesign Briza 1 kW mixer ejector wind turbine located in Rutland, Massachusetts, and compare it to radiated noise of the 1 kW Bergey wind turbine located at Western New England College. Noise measurements were collected and analyzed in accordance with the IEC standard for acoustic noise measurement techniques, IEC 61400-11 (Ref. 1) and the AWEA standard for small wind turbines. Turbine and background data were collected for the Briza wind turbine on June 29, 2010 and July22, 2010. Data for the Bergey turbine were taken on. A weighted sound pressure level measurements were used to measure the sound power of the Briza at various wind speeds. The measurements indicate that the Briza sound power is typically less than comparable wind turbines at the range of wind speeds measured. An interesting fact is that the measurement of the ambient sound pressure level downstream of the wind turbine with the wind turbine rotor locked in place seems to indicate an increase in background level compared to other locations. This measurement seems to indicate a presence of a noise source other than the spinning rotor. In addition to sound power measurements, one third octave band and narrow band fast fourier transforms were performed to further investigate the characteristics of the radiated noise.

Introduction:

Our summer project as part of the DOE Appropriations Funding between Western New England College and Flodesign revolved around the noise generated by small wind turbines. Specifically, we measured and analyzed the wind turbine noise of a traditional three bladed propeller turbine such as the Bergey XL versus that of the Flodesign shrouded wind turbine, i.e., the Briza model. Our main goals for the summer project were:

a. Perform a literature survey:
    a. Wind turbine noise of traditional wind turbines
    b. Noise from shrouded fans, propellers, and compressors
    c. Comparison of shrouded and unshrouded fan noise
b. Measurements of wind turbine noise:
    a. According to the IEC 61400-11 standard
    b. On the Bergey 1 kW unit at Western New England College
    c. On the Briza turbine located in Rutland, MA
    d. Report the data according to the standard
        I. Overall sound pressure level
        II. 1/3 octave band levels
        III. Tone analysis
        IV. Sound power level
c. Initiate wind turbine noise modeling efforts
        I. Determine scaling laws for wind turbine noise
        II. Come up with a model to predict wind turbine noise
        III. Predict 100 kW Flodesign wind turbine noise

I. Literature Survey:

Our summer project as part of the DOE Appropriations Funding between Western New England College and Flodesign revolved around the noise generated by small wind turbines. A literature survey was done in order to review the state of the art of noise of small wind turbines, the modeling of wind turbine noise, and the noise generation of shrouded and unshrouded fans. Below is a compilation of the results of our survey.

A REVIEW OF PROPELLER NOISE PREDICTION METHODOLOGY 1919-1994

Since 1919 attempts have been made to predict the noise of propellers. Early hampered by a lack of computers for processing the complex calculations of theoretical formulations of complete prediction methods. Also, these early efforts were hampered by limitations in experimental equipment for measuring noise. Some progress was made in the time period up the early 1950's but the advent of computers at that time led to the development of methods which addressed a significant portion of the propeller noise generation process. Between the 1950s and early 1970's some progress was made in refining the prediction methods. Empirical methods were also developed in this time period that provided an indication of the effects on noise of many operating and geometric parameters without having to use computer calculations.

Since the early 1970's there has been a renewal of interest in propeller noise prediction. This has been driven first by interest in the control of noise of General Aviation and commuter airplane propellers and second (in 1980's) by interest in the control of the noise of the Prop fan advanced high cruise speed turboprop. Both empirical and theoretical methods were developed in this time period. The empirical methods were generally refinements of earlier methods but some also used regression analysis of propeller aircraft data bases to define improvements. Most of the theoretical methods have been based on the acoustic analogy proposed by Light hill in 1952. However some attempts have been made to use numerical technologies based on the Euler equation to predict noise at high cruise speed for the Prop fan.

In this report, the emphasis is on review of methods that exist in a form that they can be used for propeller noise prediction. However, many theoretical developments have been reported that describe improved equations for predicting noise but in many cases the computer program is not available for use of the method. Some of these theoretical developments are discussed as the findings reported may be of interest to researchers who are attempting to make further improvements in existing propeller noise prediction tools.

The empirical methods discussed in this report exist in graphical, equation or computer program form. The early methods exist primarily as graphs or equations. The most recent methods have been converted to computer or hand calculator programs to speed up the prediction process, particularly for preliminary design studies where the effect of many design variables on noise produced is being studied.

ACOUSTIC TEST OF SMALL WIND

Eight small wind turbines ranging from 400 watts to100 kW in rated power was tested for acoustic emission sat the U.S. Department of Energy's National Renewable Energy Laboratory. Rigorous test procedures based on International standards were followed for measurements and data analyses. Results are presented in the form of sound pressure level versus wind speed,

Where the sound was recorded downwind of the turbine at a distance equal to the hub height plus half the rotor diameter. When there was sufficient separation between wind turbine noise and background noise, the apparent sound power level was calculated. In several cases, this was not possible. The implications of this problem are discussed briefly. Some of the configurations tested were specifically developed to reduce the noise level of their predecessors. Test data for these machines demonstrate marked progress toward quieter turbines.

AERO-ACOUSTIC MODELING USING LARGE EDDY SIMULATION

Computational aero-acoustics (CAA) is now becoming a common tool for predicting noise generated from aerodynamic flows, such as helicopter and wind turbine flows. Since such flows are complex and turbulent, the generated noise is broadband. To predict the noise, a simple way is to employ semi empirical modeling in which noise formulae obtained from the Light hill acoustic analogy [1] and scaled on a set of experimental data are used. Semi-empirical models [2-8] are easy to run on a personal computer and can be used to design low-noise blades. Since semi-empirical models are based on limited sets of experimental data, many fundamental questions may arise, such as the applicability of the model and the accuracy of the experimental

data. In order to resolve the problem, one possibility is to solve the 3D compressible Euler/Navier-Stokes equations using Large Eddy Simulations (LES). In the recent years, computer resources have been improved significantly and this now becomes possible.

In this context, the splitting technique developed by Shen and Sørensen [9] will be used for computing the noise from turbulent flows. In the first step, the flow solution is obtained by solving the incompressible Navier-Stokes equations together with a suitable sub-grid-scale model. In our simulations, the mixed model developed by Ta Phuoc [10] is used. The mixed model exploits the advantages of the vorticity turbulence model and the small scale turbulence model and it has been shown that it is superior to usual SGS models. After the flow stabilizes, the perturbed compressible equations are solved. Since the flow and the acoustic equations are solved separately in two steps, they can be discretized on two different meshes with two different time-steps. For this reason, the splitting technique is faster than the more conventional method of directly solving the compressible Euler/Navier-Stokes equations.

AFFECT OF NEW BLADES ON NOISE REDUCTION OF SMALL WIND TURBINE

WATER PUMPING SYSTEMS

Acoustical noise data were collected on small wind turbines used for water pumping – different blade designs were tested on each wind turbine. Three different blade designs were tested on 1 kW wind turbines and each successive blade design was shown to produce less noise with respect to rotor speed. All three blade designs, however, produced acoustical noise above 80 dB during part of their operation due to wind turbine blade fluttering which occurred when a specific rpm was exceeded for each blade design. Two radically different blade designs were tested on a 10 kW wind turbine. For the loaded condition (online) the average acoustical noise measured for both blade designs was within a few dB of each other (noise under 70dB), but for the unloaded condition the average acoustical noise measured for the newer blade design was 4 to 8 dB less.

The acoustical noise for both blade designs of the 10 kW wind turbine usually ranged between 70 and 80 dB in the offline condition, but occasionally exceeded 80 dB. Binning the measured sound data in terms of rotor or tip speed instead of wind speed greatly reduced the scatter in the data and enabled better evaluation of the noise emission for the different blade designs. A recommendation for obtaining an acceptable noise emission from a small stand-alone wind turbine can be found in the conclusions.

AIRFOIL SELF-NOISE AND PREDICTION

An overall prediction method has been developed for the self-generated noise of an airfoil blade encountering smooth flow. Prediction methods for individual self-noise mechanisms are semiempirical and are based on previous theoretical studies and the most comprehensive self-noise data set available. The specially processed data set, most of which is newly presented in this report, is from a series of aerodynamic and acoustic tests of two- and three-dimensional airfoil blade sections conducted in an anechoic wind tunnel. Five self-noise mechanisms due to specific boundary-layer phenomena have been identified and modeled: boundary-layer turbulence passing the trailing edge, separated-boundarylayer and stalled-airfoil flow, vortex

shedding due to laminar-boundary-layer instabilities, vortex shedding from blunt trailing edges, and the turbulent vortex flow existing near the tips of lifting blades. The data base, with which the predictions are matched, is from seven NACA 0012 airfoil blade sections of different sizes (chord lengths from 2.5 to 61 cm) tested at wind tunnel speeds up to Mach 0.21 (Reynolds number based on chord up to 3 x 106) and at angles of attack from 0 ° to 25.2 °. The predictions are compared successfully with published data from three self-noise studies of different airfoil shapes, which were tested up to Mach and Reynolds numbers of 0.5 and 4.6 x 106, respectively. An application of the prediction method is reported for a large-scale-model helicopter rotor and the predictions compared well with data from a broadband noise test of the rotor, conducted in a large anechoic wind tunnel. A computer code of the methods is given for the predictions of 1/3-octave formatted spectra.

DETECTION OF AERO ACOUSTIC SOUNDS SOURCES ON AIRCRAFT AND WIND

TURBINES

Main idea: comparison of the noise from the wind turbine with the noise from an aircraft turbine.

This thesis deals with the detection of aero acoustic sound sources on aircraft and wind turbines using phased microphone arrays. The characteristics of flow-induced sound from aircraft wings and wind turbine blades are derived and summarized. The phased array technique is described in detail, and several aspects of the method are discussed, for example how to account for the effects of flow and moving sources, and how to quantify array results using a source power integration method.

The reliability of the integration method is assessed using airframe noise measurements in an open and a closed wind tunnel. It is shown that, although the absolute sound level in the open jet can be too low due to coherence loss, the relative levels are accurate within 1 dB for both test sections. Thus, phased arrays enable quantitative aero acoustic measurements in closed wind tunnels.

Next, the array technique is applied to characterize the noise sources on two modern large wind turbines. It is demonstrated that practically all noise emitted to the ground is produced by the outer part of the blades during their downward movement. This asymmetric source pattern, which causes the typical swishing noise during the passage of the blades, can be explained by trailing edge noise directivity and convective amplification. The test results convincingly show that broadband trailing edge noise is the dominant sound source for both turbines.

On the basis of this information, a semi-empirical prediction method is developed for the noise from large wind turbines. The prediction code, which only needs the blade geometry and the turbine operating conditions as input, is successfully validated against the experimental results for both turbines. Good agreement is found between predictions and measurements, not only with regard to sound levels and spectra, but also with regard to the noise source distribution in the rotor plane and the temporal variation in sound level (swish). Moreover, the dependence on wind speed and observer position (directivity) is well predicted.

The absolute sound levels are accurate within 1-2 dB and the swish amplitude within 1 dB.

The validated prediction method is then applied to calculate wind turbine noise footprints, which show that swish amplitudes up to 5 dB can be expected for cross-wind directions, even at large distance.

The influence of airfoil shape on blade noise is investigated through acoustic wind tunnel tests on a series of wind turbine airfoils. In quiescent inflow, trailing edge noise is dominant for all airfoils. At low Reynolds numbers (below 1 million), several airfoils exhibit pure tones due to laminar boundary layer vortex shedding, this can be eliminated by proper boundary layer tripping. In the presence of severe upstream turbulence, leading edge noise is dominant, and the sound level increases with decreasing airfoil thickness.

Finally, two noise reduction concepts are tested on a large wind turbine: acoustically optimized airfoils and trailing edge serrations. Both blade modifications yield a significant trailing edge noise reduction at low frequencies, which is more prominent for the serrated blade. However, the modified blades also exhibit increased tip noise at high frequencies, which is mainly radiated during the upward part of the revolution, and which is most important at low wind speeds due to high tip loading. Nevertheless, average overall noise reductions of 0.5 dB and 3.2 dB are obtained for the optimized blade and for the serrated blade, respectively. This demonstrates that wind turbine noise can be halved without adverse effects on the aerodynamic performance.

FAR-FIELD ACOUSTIC CHARACTERISTICS OF MULTIPLE BLADE VANE CONFIGURATIONS FOR A HIGH TIP SPEED FAN

The acoustic characteristics of a model high-speed fan stage were measured in the NASA Glenn 9- by 15-Foot Low Speed Wind Tunnel (LSWT) at takeoff and approach flight conditions. The fan was designed for a corrected rotor tip speed of 442 m/s (1450 ft/s), and had a powered core, or booster stage, giving the model a nominal bypass ratio of 5. A simulated engine pylon and nozzle bifurcation was contained within the bypass duct. The fan stage consisted of all combinations of 3 possible rotors, and 3 stator vane sets. The 3 rotors were (1) wide chord, (2) forward swept, and (3) shrouded. The 3 stator sets were (1) baseline, moderately swept, (2) swept and leaned, and (3) swept integral vane/frame which incorporated some of the swept and leaned features as well as eliminated the downstream support structure. The baseline configuration is considered to be the wide chord rotor with the radial vane stator. A flyover Effective Perceived Noise Level (EPNL) code was used to generate relative EPNL values for the various configurations. The swept and leaned stator showed a 3 EPNdB reduction at lower fan speeds relative to the baseline stator; while the swept integral vane/frame stator showed lowest noise levels at high fan speeds. The baseline, wide chord rotor was typically the quietest of the three rotors. A tone removal study was performed to assess the acoustic benefits of removing the fundamental rotor interaction tone and its harmonics. Reprocessing the acoustic results with the bypass tone removed had the most impact on reducing fan noise at transonic rotor speeds. Removal of the bypass rotor interaction tones (BPF and nBPF) showed up to a 6 EPNdB noise reduction at transonic rotor speeds relative to noise levels for the baseline (wide chord rotor and radial stator; all tones present) configuration.

FINITE ELEMENT MODEL EVERSMAN 1

A finite element model is created for the generation, propagation, and radiation of steady, rotor alone noise and rotor and exit guide vane interaction noise of a ducted fan. In the case of rotor alone noise the acoustic source is represented by a rotating lifting line of thrust and torque dipoles distributed radially on the blade. In the case of interaction noise the acoustic source is a stationary lifting line of torque and thrust dipoles which represent the fluctuating lift on the exit guide vane created by the velocity deficit associated with wakes in the steady velocity field behind the rotor. In the configurations considered in the present study, emphasis is on ducted fans or ducted propellers for which the by-pass ratio is very large. In this case the usual assumption is made that the fan, or propeller, is operating in a mean flow environment which is uniform and the same as the forward flight velocity. The flow acceleration in the inlet, acceleration in the fan duct, and jet free shear layer are not accounted for in the present model. The model accounts for the noise generation process, the propagation through the inlet and fan duct, and the radiation to the near and far field.

The major issue addressed in the computational examples is the relationship between the far field radiated Sound Pressure Level (SPL) and directivity and the fan tip speed. In the case of rotor alone noise it is shown that due to the effect of finite duct length and mean flow velocity in the duct there can be significant SPL in the far field at large angles to the duct axis, even for subsonic tip speeds. In the case of interaction noise it is found that the radiated field can be significant near the duct axis.

FLOW AND NOISE CONTROL REVIEW AND NOISE CONTROL REVIEW AND

ASSESSMENT OF FUTURE DIRECTIONS

The nineties have witnessed a changing of the guard in aeromechanics research, with an increased emphasis on harnessing the potential of active flow control as implemented in a fully integrated, multidisciplinary framework. Consequently, technologies for developing radically new aero vehicles that would combine quantum leaps in cost, safety, and performance benefits with environmental friendliness have appeared on the horizon. Transitioning these technologies to application requires coupling further advances in traditional areas of aeronautics with intelligent exploitation of nontraditional/interdisciplinary technologies, such as smart, distributed controls, novel actuators, and micro electromechanical systems. This report provides both an assessment of the current state of the art in flow and noise control and a vision for the potential gains to be made, in terms of performance benefit for civil and military aircraft and a unique potential for noise reduction, via future advances and novel application of flow and noise Technologies. Similar benefits for other transportation systems, especially toward reduced cost for space access, are also indicated wherever appropriate. It is hoped that this comprehensive vision will strongly dispel the prevailing notion that aerodynamics research has reached maturity. The report outlines and prioritizes specific areas of research that will enable the breakthroughs necessary to bring this vision to reality. Recent developments in many topics within flow and noise control are reviewed, including sensors, actuators, active control methods, and applications. The flow control overview provides succinct summaries of various approaches for drag reduction (viz., laminar flow control and compliant coatings for skin friction reduction;

active and passive vortex generators and riblets for separation control) and improved maneuvering (via thrust vectoring, fore body control, and passive porosity). Both exterior and interior noise problems associated with air transportation systems are examined, including dominant noise sources (viz., turbo machinery, jet, and airframe), physics of noise generation and propagation, and both established and proposed concepts for noise reduction. Synergy between flow and noise control is a focus and, more broadly, the need to pursue research in a more concurrent approach involving the classical disciplines of fluid mechanics, structural mechanics, material science, acoustics, and stability and control theory is pointed out. Also discussed are emerging technologies, such as nanotechnology, that may have a significant impact on the progress of flow and noise control. Finally, some recommendations and references to facility issues are made in order to provide a basis for NASA planning.

INDUSTRIAL CFD SIMULATION OF AERODYNAMIC NOISE

Real challenges to suppress undesirable fluid-excited acoustics are posed by a wide variety of engineering disciplines. Noise regulations, passenger comfort and component stability are motivators which are continuing to stimulate substantial efforts towards the understanding of aero acoustic phenomena, and not least to quantify the usability (practicability and value) of traditional and advanced prediction methods. The latter is the primary focus of this thesis, particularly as applied to the transportation industries, aerospace, automotive and rail.

Nowadays Computational Fluid Dynamics (CFD) is a tool well integrated into the industrial development and production life-cycles. This is possible now because of two main factors: the increase in the performance of relatively cheap personal computers and network facilities, and the progress made in general purpose CFD software between modeling complexity and practicability within the industrial environment.

While CFD methodologies are well established for lots of applications such as aerodynamics, heat exchange, etc., aero acoustic CFD simulations still represent a challenge, in particular their industrial practicability. In these years this has given rise to heavy investments by the automotive industry in International aero acoustics consortia, whereby all the major car companies' work together to study the limitations and advantages of aero acoustics CFD. The general aim of these consortia is to develop methodologies which fit into, and improve upon, current design processes.

The goal of the present work is to explore the multitude of different CFD modeling approaches for some typical industrial problems such as: cavity noise, vortex shedding noise, propeller and jet noise. Each of these problems has a particular mechanism for noise generation and different methods have been studied and tested, in order to develop and optimize a practical methodology for the analysis of each problem type. Furthermore each of the aero acoustics problems considered are representative of a variety of industrial applications. Cavity noise is at the origin of phenomena such as sunroof buffeting in convertibles or door-gap tonal noise. Vortex shedding noise is typical of any flows involving bluff bodies such as automobile antennas or aircraft landing gear. Propeller noise is typical to applications involving rotating machinery, such as fans, pumps and turbines.

Different approaches ranging from steady and transient RANS simulations with the acoustic analogy (including porous and solid surface formulations), to Computational

Aero Acoustics (CAA) and Large Eddy Simulation (LES) type computations have been studied and applied.

Classic theories already exist to predict aerodynamically generated noise, which are both computationally and economically less expensive than CFD methods. However aero acoustics CFD is the future, beginning as a promising present, for the following reasons:

- Industries are interested in modeling complex geometries.
- Many classic theories can be applied successfully but very often restrictions exist with respect to the configuration and flow conditions. For example, classic propeller theories cannot be used to model real-world configurations such as a propeller installed on a wing with some prescribed yaw or angle of attack.
- The progress of all other Computer Aided Design and Engineering tools, such as linear or nonlinear structural codes, are driving design towards a virtual multi-physics approach for the simulation of complex geometries. Due to previous experience and the wide availability of modeling options, it was decided to use the general purpose CFD software package ANSYS FLUENT for CFD investigations in this study.

MODELING OF NOISE FROM WIND TURBINES

Main ideas: Is that the analysis of the noise coming from the wind turbine.

The aim of this report is to give a new prediction model for the aero dynamical generated noise from wind turbines. A 2D wind turbine noise propagation model is also developed using acoustic sound ray theory.

Aerodynamic noise is generated when the rotor encounters smooth flow.

It contains airfoil self-noise and turbulence inflow noise. The present semi-empirical model is coupled with CFD and aerodynamic calculation so as to improve the accuracy of the prediction model. By doing CFD computations, boundary layer parameters for some relevant airfoil profiles are stored as a database which is used directly for the noise prediction model. The total noise spectrum for a given wind turbine is compared with experiment and encouraging result is obtained.

The sound pressure level at receiver point is further corrected by coupling with the sound propagation model. A wind turbine is regarded as a dipole sound source placed at the hub height. To determine the changes of sound pressure level, several factors are considered: Geometric spreading, Directivity, Air absorption, Wind effect, Temperature gradient effects and Ground effects.

NOISE FROM WIND TURBINE STANDARDS AND NOISE REDUCTION PROCEDURES

In many countries the noise radiation is still the major limitation in the tremendous development of wind energy over the last years. Within several European research projects, modifications of the rotor blade trailing edge (sharp or serrated) and the tip design (avoiding tip vortex-trailing edge interaction by ´trailing edge cutting´) resulted in considerable noise reductions in the range of several dB. Mechanical noise from gear box and generator was reduced significantly but tonal noise is still the crucial point concerning the acceptance of wind

turbines. The measurement procedures have been improved significantly as well. The IEC standard 61400-11

Wind Turbines – Part 11 ‚Acoustic Noise Measurement Techniques'was revised recently in order to present a procedure expected to provide accurate results that can be replicated by others.

NOISE-COMPUTATION OF DUCTED FAN AND PROPELLER NOISE

NREL NOISE TESTS (INCLUDING BERGEY XL.1)

Eight small wind turbines ranging from 400 watts to 100 kW in rated power were tested for acoustic emissions at the U.S. Department of Energy's National Renewable Energy Laboratory. Rigorous test procedures based on International standards were followed for measurements and data analyses. Results are presented in the form of sound pressure level versus wind speed, where the sound was recorded downwind of the turbine at a distance equal to the hub height plus half the rotor diameter. When there was sufficient separation between wind turbine noise and background noise, the apparent sound power level was calculated. In several cases, this was not possible. The implications of this problem are discussed briefly. Some of the configurations tested were specifically developed to reduce the noise level of their predecessors. Test data for these machines demonstrate marked progress toward quieter turbines.

NUMERICAL RESULTS OF LIFTING SURFACE THEORY

In many countries the noise radiation is still the major limitation in the tremendous development of wind energy over the last years. Within several European research projects, modifications of the rotor blade trailing edge (sharp or serrated) and the tip design (avoiding tip vortex-trailing edge interaction by ´trailing edge cutting´) resulted in considerable noise reductions in the range of several dB. Mechanical noise from gear box and generator was reduced significantly but tonal noise is still the crucial point concerning the acceptance of wind turbines. The measurement procedures have been improved significantly as well. The IEC standard 61400-11 Wind Turbines – Part 11 ‚Acoustic Noise Measurement Techniques'was revised recently in order to present a procedure expected to provide accurate results that can be replicated by others.

OPTIMIZATION OF WIND TURBINES WITH RESPECT TO NOISE

The purpose of this thesis is to examine the issue of noise from wind turbines and eventually optimize their operation settings. The tools used are both simulations and measurements.

The programming part was based on an existing model by Wei Jun Zhu developed in DTU as part of another master thesis. The code was expanded, combined with a BEM code and coupled to an optimization routine. All simulations and tests were made on a SIEMENS SWT-2.3-92 wind turbine equipped with a B45 blade.

Noise measurements were taken at the Risø test site for large wind turbines at Høvsøre. A total of eleven hours of data were obtained in two days and they featured measuring noise versus different pitch angles and rotational velocities.

The first aim of this project was to validate the code predictions against the measurements, in a way that it had not been possible to do before. In addition, to make a detailed study of the individual noise mechanisms along the blade and with changing wind speed.

Subsequently, the code was going to be used for optimizing the performance of the SWT-2.3-92 wind turbine with respect to noise. This is a variable speed, pitch regulated machine, so the project concentrated on looking for the combinations of these settings that would lead to a possible reduction in noise by keeping the power production at high levels. Alternatively, to find the settings that optimize power production by constraining the maximum allowed noise.

The ultimate ambition was to see whether the design of the blade itself could be modified for it to become more silent. This study concentrated on the chord, twist and relative thickness distributions.

PREDICTION AND REDUCTION OF NOISE FROM A 2.3 MW WIND TURBINE

We address the issue of noise emission from a 2.3 MW SWT-2.3-93 wind turbine and compare simulations from a semi-empirical acoustic model with measurements. The noise measurements were taken at the Høvsøre test site for large wind turbines. The acoustic model is based on the Blade-Element Momentum (BEM) technique and various semi-empirical acoustic relations. The comparison demonstrates a generally good agreement between predicted and measured noise levels. The acoustic model is further employed to carry out a parametrical study to optimize the performance/noise of the wind turbine by changing tip speed and pitch setting. We show that it is possible to reduce the noise level up to 2 dB(A) without sacrificing too much the power yield.

PREDICTION OF BROADBAND NOISE FROM HORIZONTAL NOISE FROM

HORIZONTAL AXIS WIND TURBINES

A method is presented for predicting the broadband noise spectra of horizontal axis wind turbine generators. It includes contributions from such noise sources as the inflow turbulence to the rotor, the interactions between the turbulent boundary layers on the blade surfaces with their trailing edges, and the wake due to a blunt trailing edge. The method is partly empirical and is based on acoustic measurements of large wind turbines and airfoil models. The predicted frequency spectra are compared with measured data from several machines, including the MOD-OA, MOD-2, WTS-4, and U.S. Wind power Inc. machine. The significance of the effects of machine size, power output, trailing-edge bluntness, and distance to the receiver is illustrated. Good agreement is obtained between the predicted and measured far-field noise spectra.

PREDICTION OF WIND TURBINE NOISE AND VALIDATION AGAINST EXPERIMENT

Problem area

The availability of fast and accurate wind turbine noise prediction methods is important for the design of quiet wind turbines and for the planning of wind farms.

Description of work

A semi-empirical prediction method for trailing edge noise is applied to calculate the noise from two modern large wind turbines. The prediction code only needs the blade geometry and the turbine operating conditions as input. The availability of detailed acoustic array and directivity measurements on the same turbines enables a thorough validation of the simulations.

Results and conclusions

The prediction code is successfully validated against the experimental results, not only with regard to sound levels, spectra, and directivity, but also with regard to the noise source distribution in the rotor plane and the temporal variation in sound level (swish).

The validated prediction method is then applied to calculate wind turbine noise footprints, which show that large swish amplitudes can occur even at large distance.

Applicability

This study provides a firm validation of the prediction method, which therefore is a valuable tool for the design of quiet wind turbines and for the planning of wind farms.

RESIDENTIAL WIND TURBINES AND NOISE EMISSIONS

The purpose of this project is to scientifically address the problem of noise emissions related to residential scale wind turbines. This will hopefully be accomplished in three areas: research, testing, and interviews. The purpose of the research phase is familiarizing the reader as well as myself with how this problem has been addressed to this point. This will include the studies done so far, manufacturers specs and claims for their individual turbines, and experiences with these turbines from experts in the field, such as Mick Sagrillo and Paul Gipe, as well as others who work with these machines ona daily basis. To me these testimonials are a key element because these are the folks who have installed them and watched them in the field under real world conditions. The testing will be a continuation of the work started by Adam Sacora last semester using a sophisticated decibel meter. This device is also a data logger, and can be connected to a laptop to insure all noise testing is saved as it is conducted. This is probably the toughest phase due to the large amount of variables. These include wind speed, distance, and orientation to the machine in question. This entails not only east west, etc... But whether you are downwind or upwind of the turbine correlated with the wind direction and speed at that time. Another hurdle to deal with is the type of noise you are recording: Ambient noise (the wind itself, any naturally occurring noise in the area), background (cars, noise from homes or anything mechanical) and the actual turbine emissions. Separating these will be a challenge indeed. Finally, I will be

conducting interviews with residents in the immediate area of the SWI research facility. Hopefully I will also be able to conduct 7 some sound testing from these residences as well, depending on their cooperation and weather conditions (open window testing, etc...). I am optimistic that by making the local residents a part of the research process, they will be open to giving their opinions and concerns and/or inquiries of the wind turbines currently in use. Hopefully, all these areas will result in a well rounded research project that can be a tool for the awareness and understanding of the relationship between residential wind turbines and the noise they generate.

REVIEW OF NOISE PREDICTION METHODS FOR AXIAL FLOW FANS

This paper will review some methods to predict aerodynamic noise produced by rotating blades in low Mach number, low to medium speed axial flow fans with an emphasis on broad band noise. The term 'method' used here indicates that the emphasis is put on schemes which include more or less the relevant source mechanisms. The literature surveyed is far from being complete and somewhat arbitrary. Some guidance was given by the idea that the methods should not be too complex and relatively easy to handle by a fan designer. To the knowledge of the authors none of the more advanced noise prediction methods is used routinely in fan design. A reason might be that the required inputs parameters as inflow and boundary layer parameters are not known in a traditional aerodynamic design procedure.

SACKS BURNELL SURVEY

A critical survey is made of the state of the art of ducted propellers. The survey is divided generally into theoretical and experimental research, and a comprehensive table of the latter is presented showing the type and extent of experimental investigations carried out. Specific reports are discussed where appropriate, and various aspects of the ducted propeller problem are considered in some detail. Finally, a summary of the state of the art is presented along with some recommendations for future research.

SMALL AIRCRAFT PROPELLER NOISE WITH DUCTED PROPELLER

The purpose of this paper was to document the results of initial testing of various configurations of a ducted propeller apparatus. Apparatus designed based combination acoustic principles and desire able applies knowledge gained to practical application such ultra light aircraft in an effort to reduce the overall noise levels emitted. The apparatus consisted of a 35 horsepower ultra light engine, a four bladed ultra light propeller, and a duct constructed foam core covered with fiberglass. Initial evaluations compared noise levels from the apparatus both with without shroud place, well as various engine silencer configurations. The data gathered proved apparatus actually about louder with shroud than without shroud a result of strong rotor-stator interactions. Based on the initial evaluations, this apparatus demonstrated its potential further testing acoustical work principles rotor-stator interactions, short duct acoustics, active

noise control applications with long range goal being reduce acoustic emissions from propeller driven aircraft.

TEMPORAL CHARACTERIZATION OF AIRCRAFT NOISE SOURCES

Current aircraft source noise prediction tools yield time-independent frequency spectra as functions of directivity angle. Realistic evaluation and human assessment of aircraft fly-over noise require the temporal characteristics of the noise signature. The purpose of the current study is to analyze empirical data from broadband jet and tonal fan noise sources and to provide the temporal information required for prediction-based synthesis. Noise sources included a one-tenth-scale engine exhaust nozzle and a one-fifthscale scale turbofan engine. A methodology was developed to characterize the low frequency fluctuations employing the Short Time Fourier Transform in a MATLAB computing environment. It was shown that a trade-off is necessary between frequency and time resolution in the acoustic spectrogram. The procedure requires careful evaluation and selection of the data analysis parameters, including the data sampling frequency, Fourier Transform window size, associated time period and frequency resolution, and time period window overlap. Low frequency fluctuations were applied to the synthesis of broadband noise with the resulting records sounding virtually indistinguishable from the measured data in initial subjective evaluations. Amplitude fluctuations of blade passage frequency (BPF) harmonics were successfully characterized for conditions equivalent to take-off and approach. Data demonstrated that the fifth harmonic of the BPF varied more in frequency than the BPF itself and exhibited larger amplitude fluctuations over the duration of the time record. Frequency fluctuations were found to be not perceptible in the current characterization of tonal components.

THE EFFECT OF ATMOSPHERIC STABILITY ON LOW FREQUENCY MODULATION

SOUND OF WIND TURBINES

Sound from wind turbines involves a number of sound production mechanisms related to different interactions between the turbine blades and the air. An important contribution to the low frequency part of the sound spectrum is due to the sudden variation in air flow which the blade encounters when it passes the tower: the angle of attack of the incoming air suddenly deviates from the angle that is optimized for the mean flow. Hitherto, low-frequency sound from wind turbines has not been shown to be a major factor contributing to annoyance. This seems reasonable as the blade passing frequency is of the order of one hertz where the human auditory system is relatively insensitive. This argument, however, obscures a very relevant effect: the blade passing frequency modulates well audible, higher-frequency sounds and thus creates periodic sound: blade swish. This effect is stronger at night because in a stable atmosphere there is a greater difference between rotor averaged and near-tower wind speed. Measurements have shown that additional turbines can interact to further amplify this effect. Theoretically the resulting fluctuations in sound level will be clearly perceptible to human hearing. This is confirmed by residents near wind turbines with the same common observation: often late in the afternoon or in the evening the turbine sound acquires a distinct ‘beating’ character, the rhythm

of which is in agreement with the blade passing frequency. It is clear from the observations that this is associated to a change toward a higher atmospheric stability. The effect of stronger fluctuations on annoyance has not been investigated as such, although it is highly relevant because a) the effect is stronger for modern (that is: tall) wind turbines, and b) more people in Europe will be living close to these wind turbines as a result of the growth of wind energy projects.

THE NASA-LeRC WIND TURBINE SOUND PREDICTION CODE

Main idea: NASA modeling of sound from a wind turbine.

Since regular operation of the OOE/NASA Mod-1 wind turbine began in October 1979 about 10 nearby households nave complained of noise from the machine. Development of the NASA-LeRC wind turbine sound prediction code began in May 1980 as part of an effort to understand and reduce the noise generated by Mod-1. Tone sound levels predicted with this code are in generally good agreement with measured data taken in the vicinity Mod-1 wind turbine (less than 2 rotor diameters). Comparison in the far field indicates that propagation effects due to terrain end atmospheric conditions may be amplifying the actual sound levels by shout 6 db. Parametric analysis using the code has shown that the predominant contributors to Mod-1 rotor noise are (1) the velocity deficit in the wake of the support tower. (2) The high rotor speed, (3) off-optimum operation.

TURBINE NOISE (POWERPOINT PRESENTATION)

In the future, wind turbines are likely to be deployed closer to people. Wind turbine noise is an issue if it becomes a deterrent to deployment – there is a tradeoff between cost effectiveness ($$$) and noise. Many complex noise sources need to be considered. Lowest noise emission level for large turbines is ≅ 99 dB(A) [600 m2/kW for 40 dB(A) at receptor location]. NREL field tests, wind tunnel tests and computer code development to understand and mitigate noise emissions. Improvements expected for small and large wind turbines.

WHISPER 100 NOISE REPORT

The objective of the test is to characterize the noise emissions of the Whisper H40 wind turbine. To meet this objective, the measurements were collected and analyzed in accordance with the IEC standard for acoustic noise measurement techniques, IEC 61400-11 (Ref. 1). This report documents the measurement techniques, test equipment, analysis procedures, results, and uncertainty for the following quantities:

- Apparent sound power level
- Dependence on wind speed
- Directivity

WIND TURBINE NOISE ISSUES

Attachment A-J

The main concept of this article is concerned about noise pollution.

WIND TURBINE ACOUTICS

Available information on the physical characteristics of the noise generated by wind turbines is summarized, with example sound pressure time histories, narrow- and broadband frequency spectra, and noise radiation patterns.

Reviewed are noise measurement standards, analysis technology, and a method of characterizing wind turbine noise. Prediction methods are given for both low-frequency rotational harmonics and broadband noise components. Also included are atmospheric propagation data showing the effects of distance and refraction by wind shear.

WIND TURBINE ACOUTIC NOISE

Wind turbines generate sound via various routes, both mechanical and aerodynamic. As the technology has advanced, wind turbines have gotten much quieter, but sound from wind turbines is still an important sitting criterion. Sound emissions from wind turbine have been one of the more studied environmental impact areas in wind energy engineering. Sound levels can be measured, but, similar to other environmental concerns, the public's perception of the acoustic impact of wind turbines is, in part, a subjective determination.

Noise is defined as any unwanted sound. Concerns about noise depend on:

1. The level of intensity, frequency, frequency distribution and patterns of the noise source;
2. Background sound levels;
3. The terrain between the emitter and receptor
4. The nature of the receptor; and
5. The attitude of the receptor about the emitter.

In general, the effects of noise on people can be classified into three general categories:

1. Subjective effects including annoyance, nuisance, dissatisfaction
2. Interference with activities such as speech, sleep, and learning
3. Physiological effects such as anxiety, tinnitus, or hearing loss.

In almost all cases, the sound levels associated with wind turbines large & small produce effects only in the first two categories, with modern turbines typically producing only the first. The third category includes such situations as work inside industrial plants and around aircraft. Whether a sound is objectionable will depend on the type of sound (tonal, broadband, low frequency, or impulsive) and the circumstances and sensitivity of the person (or receptor) who hears it. Because of the wide variation in the levels of individual tolerance for noise, there is no completely satisfactory way to measure the subjective effects of noise or of the corresponding reactions of annoyance and dissatisfaction.

Operating sound produced from wind turbines is considerably different in level and nature than most large scale power plants, which can be classified as industrial sources. Wind turbines are often sited in rural or remote areas that have a corresponding ambient sound character. Furthermore, while noise may be a concern to the public living near wind turbines, much of the sound emitted from the turbines is masked by ambient or the background sounds of the wind itself.

The sound produced by wind turbines has diminished as the technology has improved. As blade airfoils have become more efficient, more of the wind energy is converted into rotational energy, and less into acoustic energy. Vibration damping and improved mechanical design have also significantly reduced noise from mechanical sources.

The significant factors relevant to the potential environmental impact of wind turbine noise are shown in Figure 1 [Hubbard and Shepherd, 1990]. Note that all acoustic technology is based on the following primary elements: Sound sources, propagation

Paths and receivers. In the following sections, after a short summary of the basic principles of sound and its measurement, a review of sound generation from wind turbines, sound propagation, as well as sound prediction methods is given.

Human perception thresholds, based on laboratory and field tests, are given. Building vibration analysis methods are summarized. The bibliography of this report lists technical publications on all aspects of wind turbine acoustics.

II. Standards Review:

a. **IEC 61400-11 Summary**

Purpose

The purpose of the IEC 61400-11 standard [add reference] is to provide a uniform methodology that will ensure consistency and accuracy in the measurement and analysis of acoustical emissions by wind turbine generator systems. The standard has been prepared with the anticipation that it would be applied by:

- The wind turbine manufacturer striving to meet well defined acoustic emission performance requirements and/or a possible declaration system;
- The wind turbine purchaser in specifying such performance requirements;
- The wind turbine operator who may be required to verify that stated, or required, acoustic performance specifications are met for new or refurbished units;
- The wind turbine planner or regulator who must be able to accurately and fairly define acoustical emission characteristics of a wind turbine in response to environmental regulations or permit requirements for new or modified installations.

This standard provides guidance in the measurement, analysis and reporting of complex acoustic emissions from wind turbine generator systems. The standard will benefit those parties involved in the manufacture, installation, planning and permitting, operation, utilization, and regulation of wind turbines. The measurement and analysis techniques recommended in this document should be applied by all parties to insure that continuing development and operation of wind turbines is carried out in an atmosphere of consistent and accurate communication relative

to environmental concerns. This standard presents measurement and reporting procedures expected to provide accurate results that can be replicated by others.

The procedures present methodologies that will enable the noise emissions of a single wind turbine to be characterized in a consistent and accurate manner. These procedures include the following:

- Location of acoustic measurement positions;
- Requirements for the acquisition of acoustic, meteorological, and associated wind turbine operational data;
- Analysis of the data obtained and the content for the data report; and
- Definition of specific acoustic emission parameters, and associated descriptors which are used for making environmental assessments.

The standard is not restricted to wind turbines of a particular size or type. The procedures described in this standard allow for the thorough description of the noise emission from a wind turbine. If, in some cases, less comprehensive measurements are needed, such measurements are made according to the relevant parts of this standard.

Details

The method described in this International Standard provides the apparent "A" weighted sound power levels, spectra, and tonality at integer wind speeds from 6 to 10 m/s of an individual wind turbine. In order to qualify as an accurate reading; thirty data points at each whole wind speed (tolerance of +/- 0.5 m/s) is required. Optionally, directivity may also be determined. The directivity is determined by comparing the A-weighted sound pressure levels (which is explained in the following section) at three additional positions around the turbine with those measured at the reference position.

In order to successfully qualify as a certified measurement specific attention to the equipment used must be done. The equipment shall meet the requirements of a type 1 sound level meter according to IEC 60804. The diameter of the microphone shall be no greater than 13 mm. In addition to the requirements given for type 1 sound level meters, the equipment should have a constant frequency response over at least the 45 Hz to 11,200 Hz frequency range. The filters shall meet the requirements of IEC 61260 for Class 1 filters.

The measurements are made at locations close to the turbine in order to minimize the influence of terrain effects, atmospheric conditions or wind-induced noise. To account for the size of the wind turbine under test, a reference distance *R*o based on the wind turbine dimensions is used. Refer to Figure 1, on the following page, to complete the calculation.

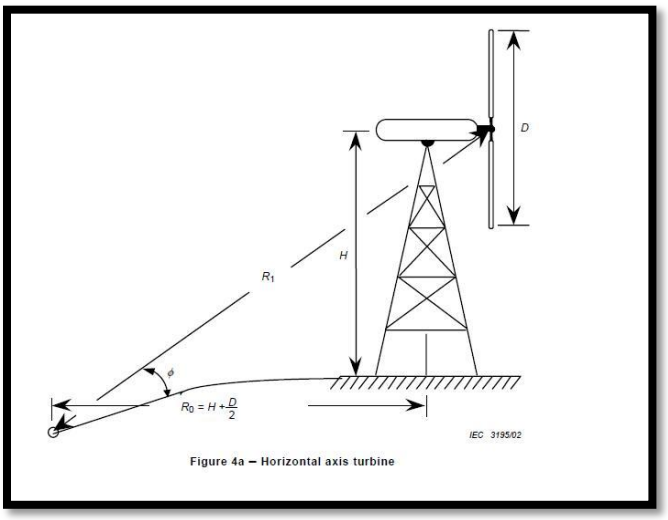

FIGURE 1: HORIZONTAL AXIS TURBINE, RO

Measurements are taken with a microphone positioned on a board placed on the ground to reduce the wind noise generated at the microphone and to minimize the influence of different ground types. The sound board layout can be seen in Figure 2 below. The microphone shall be mounted at the center of the sound board with the diaphragm of the microphone in a plane normal to the board and with the axis of the microphone pointing towards the wind turbine. A windscreen is used to aid in noise spikes caused by the wind. The windscreen to be used with the ground-mounted microphone shall consist of a primary and, where necessary, a secondary windscreen. The primary windscreen shall consist of one half of an open cell foam sphere with a diameter of approximately 90 mm, which is centered on the diaphragm of the microphone.

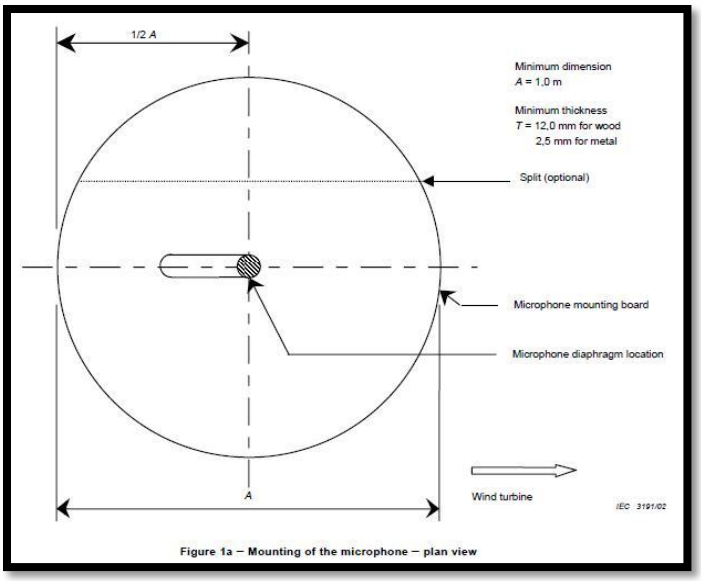

FIGURE 2: MOUNTING OF MICROPHONE ON SOUND BOARD

Measurements of sound pressure levels and wind speeds are made simultaneously over short periods of time and over a wide range of wind speeds. The measured wind speeds are converted to corresponding wind speeds at a reference height of 10 m and a reference roughness length of 0.05 m using equation 1 below. To find the roughness length, Z_o, use table 1 below.

$$V_s = V_z \left[\frac{\ln\left(\frac{z_{ref}}{z_{0ref}}\right) \ln\left(\frac{H}{z_0}\right)}{\ln\left(\frac{H}{z_{0ref}}\right) \ln\left(\frac{z}{z_0}\right)} \right] \quad \textbf{(1)}$$

where

z_{0ref} is the reference roughness length of 0,05 m;
z_0 is the roughness length;
H is the rotor centre height;
z_{ref} is the reference height, 10 m;
z is the anemometer height.

TABLE 1: ROUGHNESS LENGTH (IEC STANDARD)

Table 1 – Roughness length

Type of terrain	Roughness length z_0
Water, snow or sand surfaces	0,000 1 m
Open, flat land, mown grass, bare soil	0,01 m
Farmland with some vegetation	0,05 m
Suburbs, towns, forests, many trees and bushes	0,3 m

The sound levels at the standardized wind speeds of 6, 7, 8, 9, and10 m/s are determined and used for calculating the apparent A-weighted sound power levels. If the IEC 61400 is used for verification that actual noise emission is in accordance with a reference/declared noise level, the verification measurement shall be made in accordance with the present standard for a wind speed range given by:

– Annual average wind speed at 10 m height onsite ±1 m/s as a minimum. As a minimum, three integer wind speed values and 8 m/s shall be reported (i.e. site average = 4,8 m/s, use 4, 5, 6, and 8 m/s).

– If the declaration measurements indicate that audible tones are present at other wind speeds, these wind speeds shall be included as well.

b. AWEA Summary

Purpose

The purpose of the AWEA Small wind turbine performance and safety standard is to provide a uniform methodology and meaningful performance criteria to assess small wind turbines and

provide consumers a measure of confidence in the quality of the small wind turbine. The standard applies to wind turbines having a rotor swept area of 200 m^2 or less so it equates to a rotor diameter of 16m or 52 ft for a horizontal axis turbine.

For noise the AWEA Rated Sound Level is the sound level that will not be exceeded 95% of the time, assuming an average wind speed of 5 m/s (11.2 mph), a Rayleigh wind speed distribution, 100% availability, and an observer location 60 m (about 200 feet) from the rotor center. The sound level is calculated from the International standard IEC 61400-11 test results, except as modified by AWEA standard. In general wind turbine sound levels are measured according to the IEC 61400-11 standard but incorporating the following guidelines. The averaging period is 10 seconds rather than 1 minute. It is preferred to measure directly the wind speed rather than derive it from the power curve. The method of integer bins is used to determine the sound pressure levels at integer wind speeds. It is suggested to cover as wide a wind speed range as possible, as long as the wind screen remains effective. A tonality analysis is not required but the presence of prominent tones shall be observed and reported. Whenever there is an obvious change in sound level at high wind speeds because of activation of overspeed protection like furling or pitching, a description shall be added.

The AWEA rated sound level is calculated at a distance of 60m from the rotor hub and excludes and contribution of background sound. The overall sound level at any distance R from the turbine includes the contribution of the AWEA rated sound level and the background noise and can be calculated according to the following equation:

$L_{overall} = 10log_{10}\left(10^{L_{tur}/10} + 10^{L_{back}/10}\right)$, where $L_{overall}$ is the overall sound pressure level, L_{tur} is the sound pressure level of the turbine at distance R, and L_{back} is the background noise level. The turbine sound pressure level at a distance R is calculated from the rated AWEA sound pressure level measured at a distance of 60 m as:

$L_{tur} = L_{AWEA} + 10log_{10}(4\pi 60^2) - 10log_{10}(4\pi R^2)$.

III. Briza Wind Turbine Noise:
   a. Rutland Site
   b. Measurement Instrumentation and Calibration
   c. Software Development

All acoustical testing of the "Briza" 1kW mixer ejector turbine was done at the site in Rutland, Massachusetts at an approximate address of 88 Maple Avenue, Rutland Ma 01543. The test turbine is located at the former Rutland Heights State Hospital site in Rutland, MA, which is 10 miles Northwest of Worcester, MA. The terrain consists of an open field with a slight slope towards the west and sloping off towards the east. The field is open except for a few deciduous trees, two evergreens, and thick forest on the perimeter. The trees are generally 60 ft tall. The site has prevailing winds bearing 290 degrees relative to true north. For measurements for which it is important to accurately measure wind speed, FDWT uses data obtained when the wind direction is from all directions except between 20 and 160 degrees true. All testing was taken downwind of the turbine at specified locations. The testing distance(s) were acquired using the IEC 61400-11 standard. It was calculated that we test at 86 feet from the center of the turbine to perform a certified measurement. Also for the chance that the Briza turbine shields's noise we performed testing at 120 feet as well. The other issue that needed to be taken into account for was the fact that the turbine may show signs of spherical spreading, which basically is the sound maybe stronger or weaker off axis from the tail cone. In order to check for this, tests were

conducted at 0 degrees (downwind, on axis), -15 degrees (downwind, off axis), and 15 degrees (downwind, off axis).

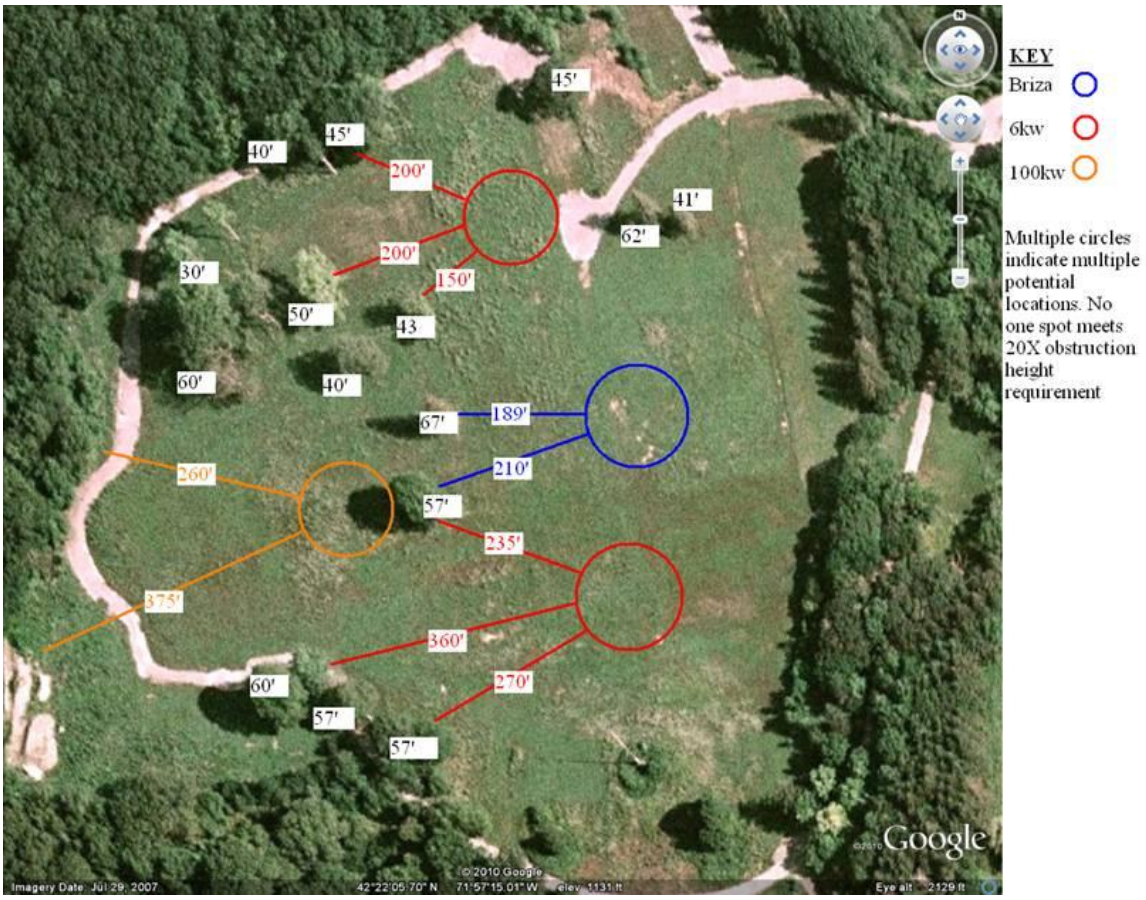

FIGURE 3: GOOGLE SKY SCREENSHOT OF RUTLAND TEST SITE WITH PERTINENT DISTANCES AND HEIGHTS

The actual testing of the noise of the turbine was performed using techniques and equipment as close to the standard as possible. In order to qualify as a certified test it was required we have 30 data points taken at integer wind speeds of 6, 7, 8, 9 and 10 m/s with a tolerance of +/-0.5 m/s. All the equipment for a certified test can be seen in Table 2 on the following page. However during the test used for this analysis, the type 1, Casella CEL-495 microphone and preamplifier which is used plug into the data recorder was not used. A Casella Type 2 microphone was used for this test because the analysis program was calibrated for the type 2 microphone and the calibration had not yet been completed for the Type 1 microphone.

TABLE 2: EQUIPMENT SPECIFICATIONS

Instrument	Manufacturer	Model Number	Serial Number
Microphone	Casella USA	Cel-495	1001
Preamplifier	Casella USA	Cel-495	1002
Microphone	PCB	377B20	112193
Preamplifier	PCB	378B20	105112
Digital Recorder	Zoom	H4	70839
Sound Level Meter	Casella USA	Cel-440	42842
Signal Conditioner	PCB	480C02	10305

Also worth mentioning, all tests were completed on a 1 meter in diameter ¾" plywood circle. This "sound board" is to prevent inaccuracies from the various ground and soil types. Another precaution taken at the site was the grass and weeds were taken down with a weed whacker to minimize noise effects of the whistling grass. Figure 4 is a representation of a test location at the Rutland Site.

FIGURE 4: 86 FT AND 0° TEST LOCATION-RUTLAND, MA.

Testing of the turbine was performed at one of the specified locations for about 30 minutes with the turbine on, and then another 30 minutes with the turbine's brake applied to get an ambient data set. At the specified location, data was recorded continuously through the Zoom digital recorder and when a high stream of wind came, short bursts of one to two seconds were recorded through the Casella sound level meter to get Lmin, Lmax, and Lequivalent values. Having the redundancy of the digital recorder and being able to match them with a

correlated value off the sound level meter was a great attribute to guarantee correct results. All the required values needed to compare the sound readings with respect to wind speed and direction can be found in the excel files Dr. Khosrowjerdi developed.

Several software programs were written to facilitate the processing of the recorded data and the post-processing of the data. Most programs were written in Labview and several others were written in Matlab. Here we discuss briefly each of the programs written, their operation, and the output files that they create.

The first Labview program is called Analyze_wind_sound.vi. The graphical user interface is shown in Figure 5. This program is used to read in all the recorded sound level meter readings that were taken during a particular measurement session. As such the user can input the initial file number and the total number of files to be read. The program will read in the start time stamp, end time stamp, the maximum sound level recorded during that period, the minimum sound level, and the equivalent sound level during that period, i.e., the energy averaged sound level. All the sound level data are then stored as arrays with the time stamp converted into seconds. The second portion of the program reads in the MS Excel measurement file for the Briza for that particular measurement day. This file was provided by Robert Cunningham from Flodesign. The program automatically reads in all the recorded data of that day and stores it as arrays including the time stamp of each measurement. The program creates several outputs. The first is to correlate the wind speed and sound level measurement. For each sound level measurement, which has a specific start and end time, the program retrieves all the wind speed measurements that occur within that time range. The program then calculates the average, maximum, and minimum wind speed that occurred in that time period. The program then creates three graphs and three MS Excel output files. The first one is that of the equivalent or average sound level versus average wind speed for each sound measurement interval. The second and third ones are similar, but this time we plot the minimum sound level versus the minimum wind speed during the recorded time span and the maximum sound level versus the maximum wind speed. The program also provides the user the opportunity to input a desired wind speed value. The program then finds all wind speed measurements that have a measured wind speed within 0.5 m/s from the desired wind speed. In addition it also keeps track of how many consecutive wind speed data points fall within the desired range. This data is then available for later use, especially for sound analysis, since it provides the time intervals were a specific wind speed was obtained.

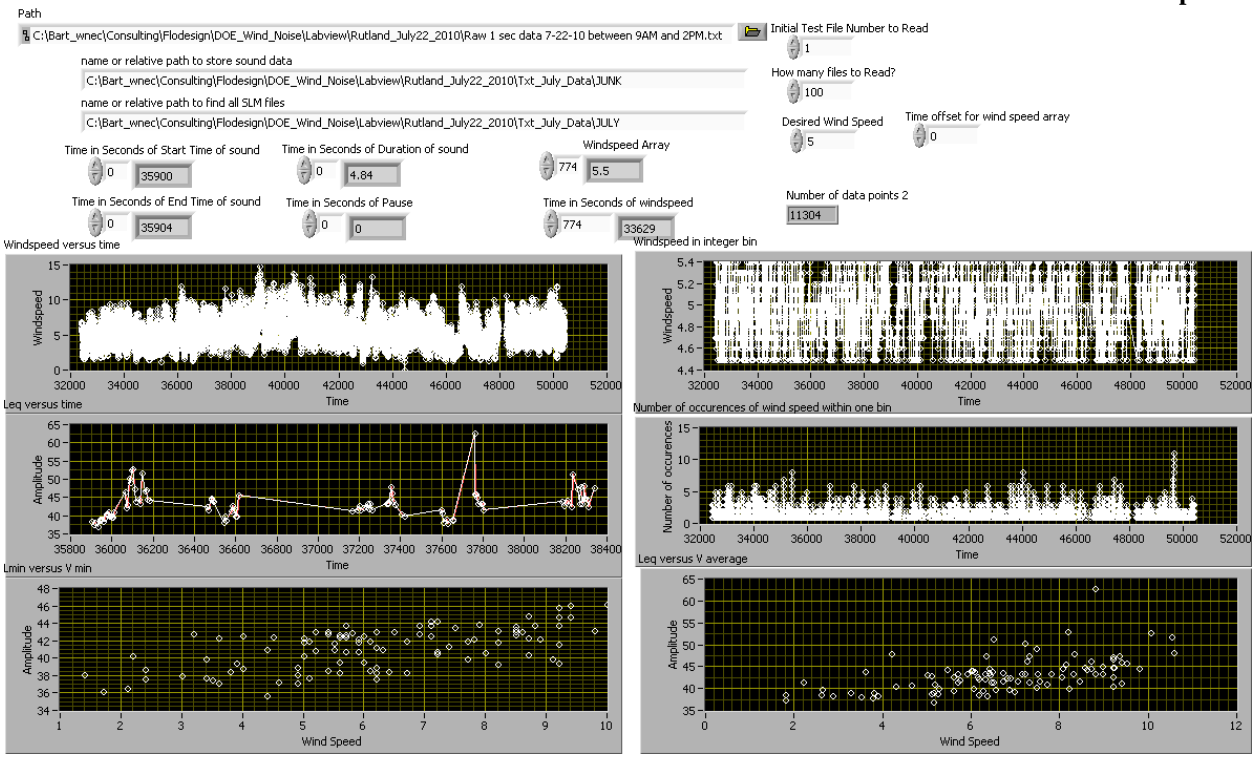

FIGURE 5: GUI FOR ANALYZE_WIND_SOUND_V1.VI PROGRAM

The second Labview program is WindNoiseAnalysis_V1.vi. This program reads in a recorded sound waveform recorded during measurement of wind turbine noise. The waveform is stored in a wav file format and is recorded by the digital recorder. The program converts the voltage amplitude into a pressure amplitude in Pascal once the user inputs the recorder sensitivity and the microphone sensitivity. The user also specifies the length of each segment of the wav file used for analysis. This program performs several sound analysis operations. First, it includes a simple limit test, a measurement to see whether the recorded signature exceeds a certain level. Second, it functions as a sound level meter. It calculates the average sound level during each time segment that is analyzed. The user has the capability of specifying filters such as the A, B, or C weighted sound levels. Our measurements typically include A weighted sound levels. The sound level meter function also calculates the 1/3 octave band sound levels. All the sound level data is stored in Excel files for later analysis. Next, the program calculates a narrow band power spectrum of the waveform. A spectrum is calculated for each time segment of the waveform. All spectra are stored in an Excel file for later analysis. The frequency resolution is determined by the length of the time segment. The longer the time segment the better frequency resolution is obtained. As an example, for a time segment of 250 ms, the frequency resolution is 4 Hz. Finally, the program has the capability to do zoom fast fourier transforms and the display of all spectra in a waterfall format.

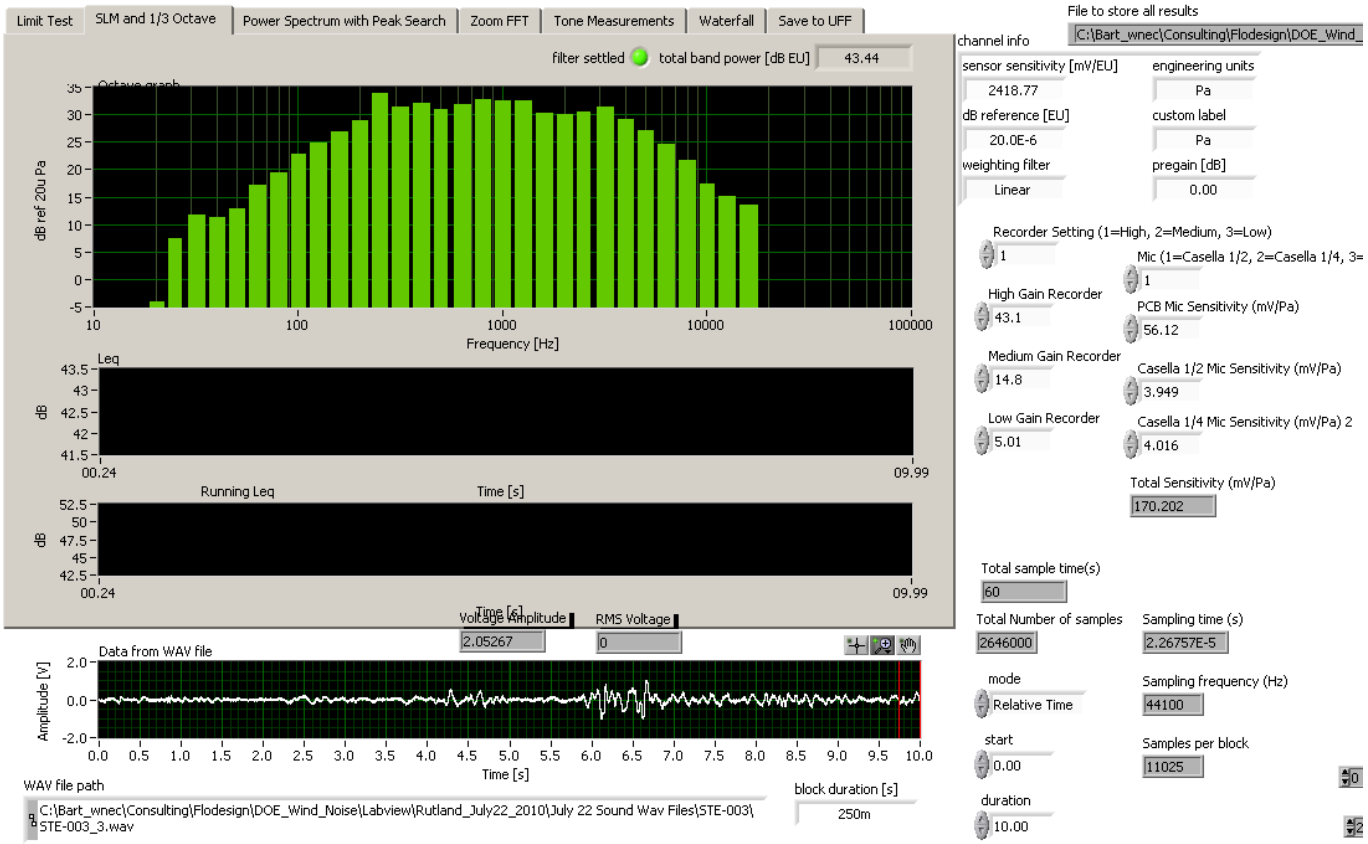

FIGURE 6: GUI OF THE LABVIEW PROGRAM WINDNOISEANALYSIS_V1.VI

Several programs were written in Matlab to deal with wav files that were of large size, typically hundreds of MB. A first program was written to read in large wave files and chop it into segments of a particular duration, e.g., one minute, and then write the one minute segments into new wav files. The second program reads in the wav files, plots the waveforms, and plays it through the audio device for a quick inspection of the recorded signal. This is useful in determining the contents of a particular wav file, such as the occurrence of spurious background noises.

d. Results

Our discussion of results relate to the measurements that were taken at the Rutland site on July 22, 2010. A total of 443 sound level measurements were taken, spread out over three positions. The three positions were all at a horizontal distance of 86 feet from the center of the tower. Position 1 is directly on axis downwind from the turbine. Positions 2 and 3 are resp. +/- 15 degrees from the turbine axis. We also recorded the sound signals of two microphones, the Casella type II microphone and the type I PCB microphone, on the digital recorder. Eleven wav files were recorded with a total of more than an hour of recorded sound. Measurements were taken at all three positions with the turbine running and then again with the turbine stopped. In the stopped position the rotor was locked. Before measurements were started the time stamp of

the Casella sound level meter and the Flodesign laptop computer were equaled so that both time stamps read identical times. All sound level meter recordings were done with A weighting applied.

For the first set of results we correlated the wind speed as read by the anemometer with the sound level measurements that occurred at the same time. As explained in the previous section, for each sound level measurement that typically took place over a time span of several seconds, the sound level meter records the maximum, minimum, and average sound level that is measured during that span. Similarly, we calculated from the anemometer readings, the average, minimum, and maximum wind speed over the same time span. All wind speed data are then normalized to a standard height of 10 m and applying a surface roughness value of 0.5 m. For the Briza test site, this results in a reduction of measured wind speed by a factor of 0.84. Figure xx shows the average sound level L_{eq} as a function of average wind speed with the turbine running for all three recorded positions. Included in the graph are linear interpolation lines for the recorded data points. Several conclusions can be drawn from this figure. First, there is a significant scatter from the data. This is expected since the wind speed at Rutland is rarely steady and is typically highly unsteady with lots of gusts. Since the rotor has some inertia it takes a few seconds before it reaches steady state, therefore the measured sound level does not always directly correlate with the wind speed measured at the same time. Second, there is little difference between the three positions, indicating that with the turbine running, the recorded sound levels are very similar. Third, as indicated by the trend lines, there is a definite increase of sound pressure level with wind speed, on the order of 4 to 5 dB increase for an increase in wind speed of 4 m/s.

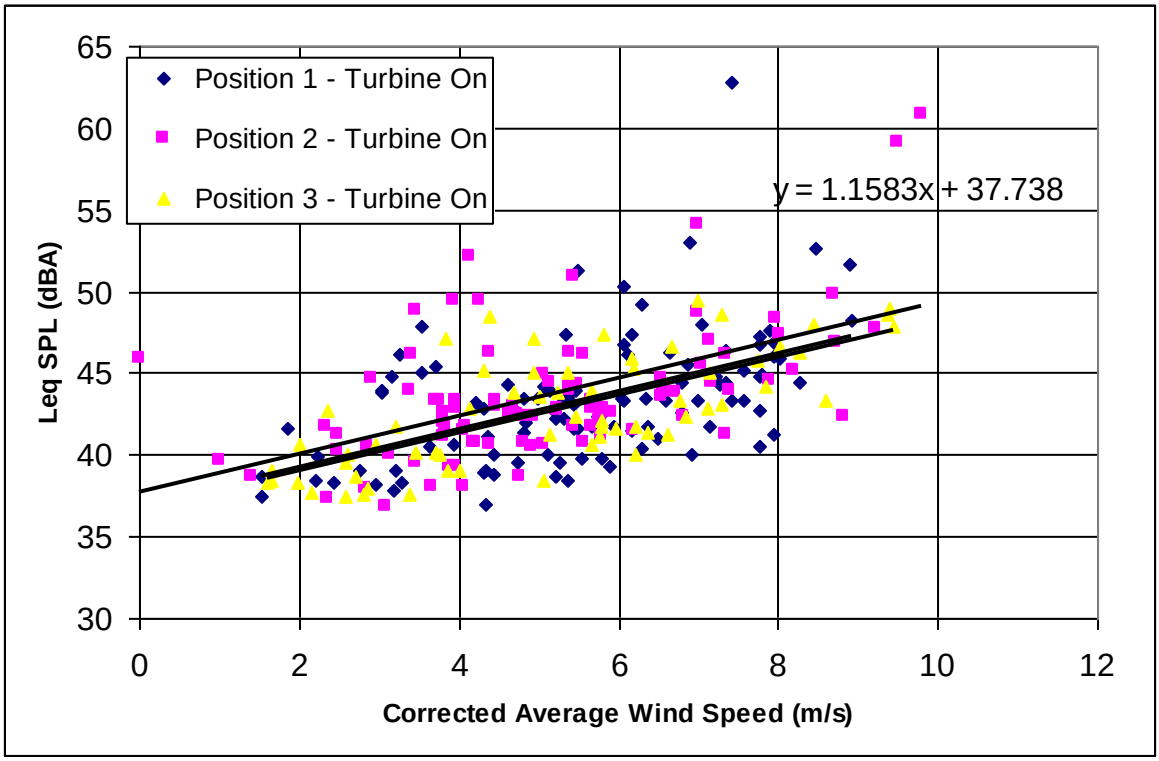

FIGURE 7:AVERAGED SOUND PRESSURE LEVEL (DBA) VERSUS NORMALIZED AVERAGED WIND SPEED FOR ALL THREE MEASUREMENT POSITIONS WITH THE TURBINE OPERATIONAL.

Figure 7 compares the ambient averaged sound level measured at the three positions, i.e., with the turbine stopped versus average wind speed. Several conclusions are apparent from this graph. First, there is a significant difference in sound pressure level between position 1 and positions 2 and 3. Remember that position 1 is directly downstream from the wind turbine. Clearly the sound pressure level at position 1 increases with wind speed. This behavior is however not observed for positions 2 and 3. At these positions the SPL still increases with the wind speed but at a much reduced rate. Second, as a result of the different sensitivities to wind speed, the SPL at positions 2 and 3 is typically lower than that at position 1. The difference increases with increasing wind speed. Since the IEC standard involves measuring the background noise, this brings up an interesting point, namely which background noise to use. The increased background noise in position 1, on axis, is probably caused by the presence of the wind turbine, and may come from noise generated by shedding off the stopped rotor blades or from a potential duct mode of the shroud, or from turbulent inflow over the shroud itself. This is certainly an area that deserves more attention. In general the background noise does increase with increasing wind speed. The background noise level as measured and varying between 40 dBA at low wind speeds and increasing to 45-50 dBA at higher windspeeds is similar to that reported in the literature.

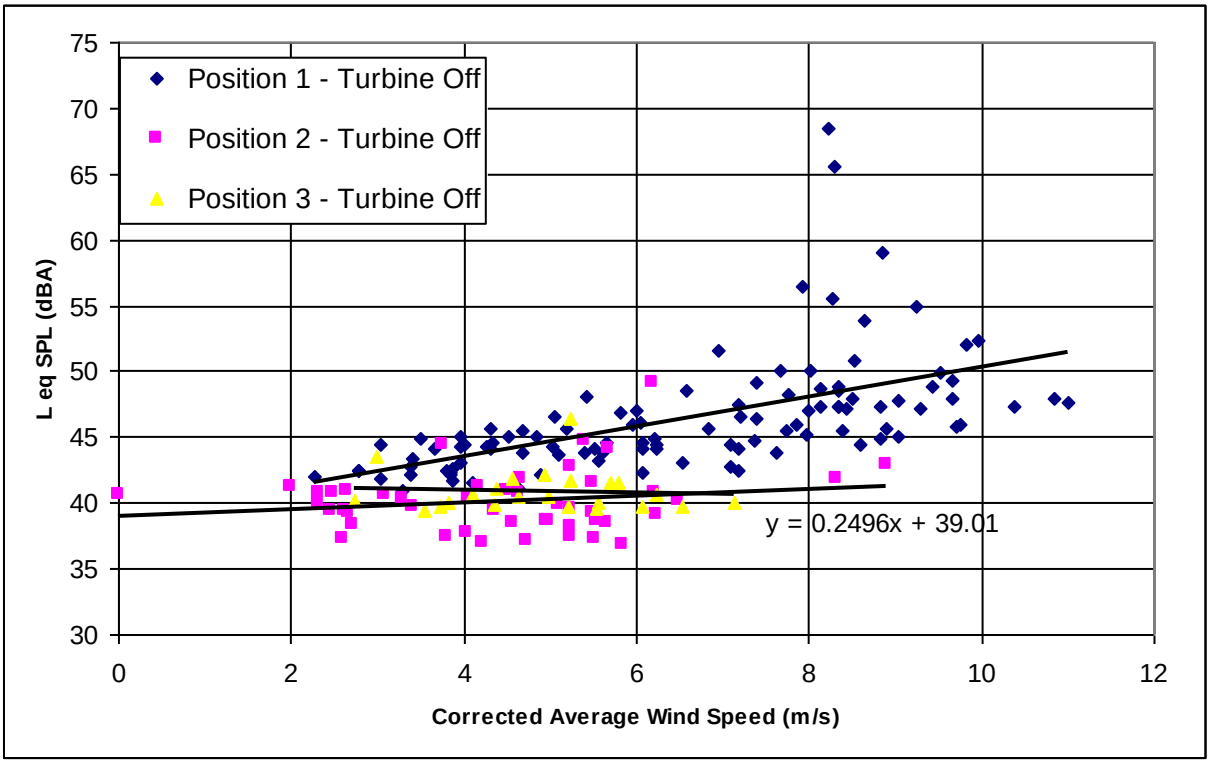

FIGURE 8: AVERAGED SOUND PRESSURE LEVEL (DBA) VERSUS NORMALIZED AVERAGE WIND SPEED FOR ALL THREE MEASUREMENT POSITIONS WITH THE TURBINE ROTOR STOPPED.

Next we compare the averaged SPL measured in position one, with the turbine rotor spinning and with the turbine rotor stopped. We also include the data for position 2 with the turbine stopped. The first observation is that there is not much difference in SPL between the case of the rotor stopped or running in position 1. This is an indication, that at most wind speeds measured, there is not a significant difference between the rotor spinning or not. The second observation is that the SPL in position one is higher than that at position 2, and that the difference increases with wind speed. A 6 dB difference between background noise and wind turbine noise would indicate that the wind turbine is adding additional noise to the environment and is a separate noise source.

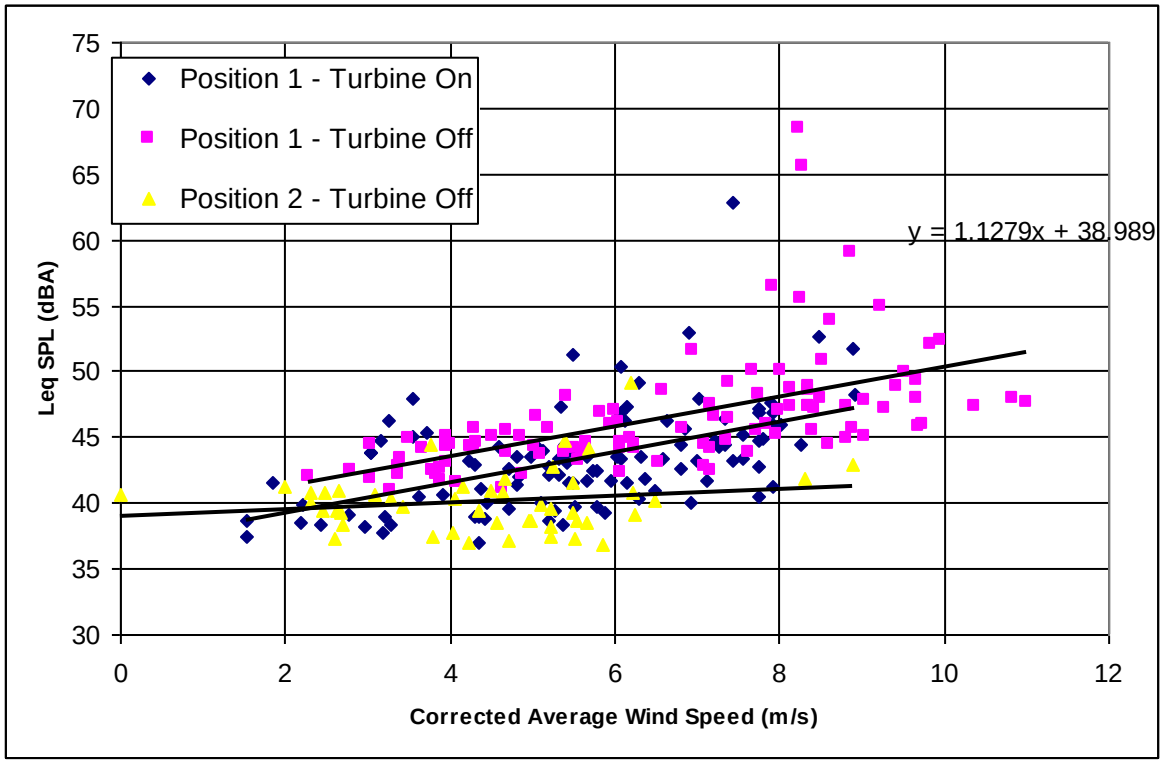

FIGURE 9: AVERAGED SOUND PRESSURE LEVEL (DBA) VERSUS NORMALIZED AVERAGE WIND SPEED FOR POSITION 1WITH THE TURBINE ROTOR RUNNING AND STOPPED, AND FOR POSITION 2 WITH THE TURBINE ROTOR STOPPED

The next three figures show similar results but this time the minimum SPL L_{min} is shown as a function of the minimum recorded wind speed during each acoustic measurement time span. Peak SPL are smaller since spurious ambient noises have probably been excluded from the data. Typical examples of loud noises that occur during the measurements are trucks passing by, birds singing near the microphone, crickets and other insects buzzing in the immediate vicinity of the microphone. In general the conclusions drawn during the previous analysis of the average SPL versus averaged wind speeds hold. Wind turbine noise increases as a function of wind speed.

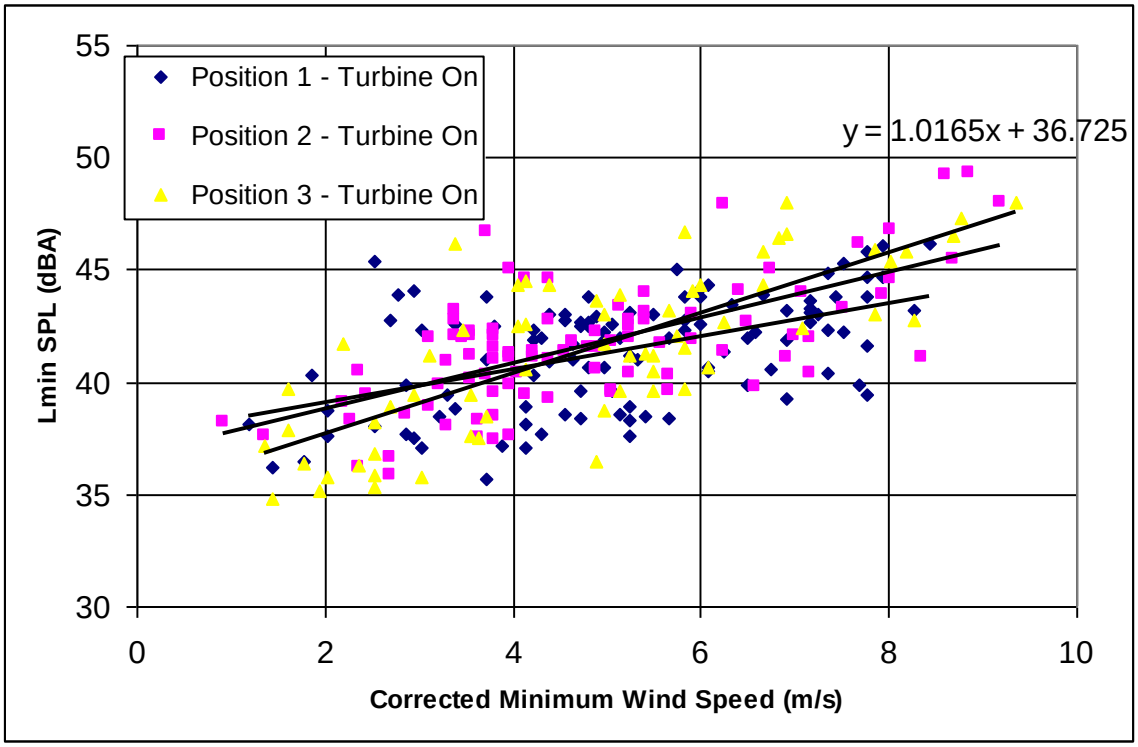

FIGURE 10:MINIMUM SOUND PRESSURE LEVEL LMIN (DBA) VERSUS NORMALIZED MINIMUM WIND SPEED FOR ALL THREE MEASUREMENT POSITIONS WITH THE TURBINE OPERATIONAL

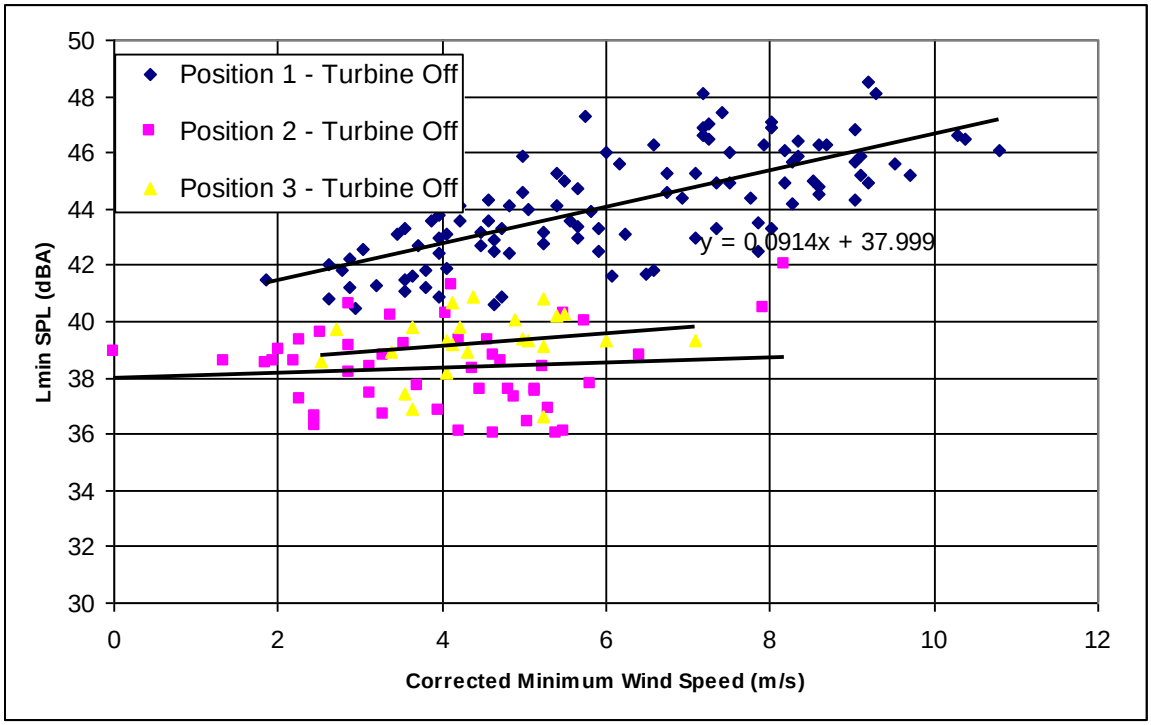

FIGURE 11: MINIMUM SOUND PRESSURE LEVEL LMIN (DBA) VERSUS NORMALIZED MINIMUM WIND SPEED FOR ALL THREE MEASUREMENT POSITIONS WITH THE TURBINE ROTOR STOPPED

The background noise in position 1 is significantly higher than compared with position 2 and 3. At higher wind speeds there is more than a 6 dB difference between wind turbine noise and off axis background noise.

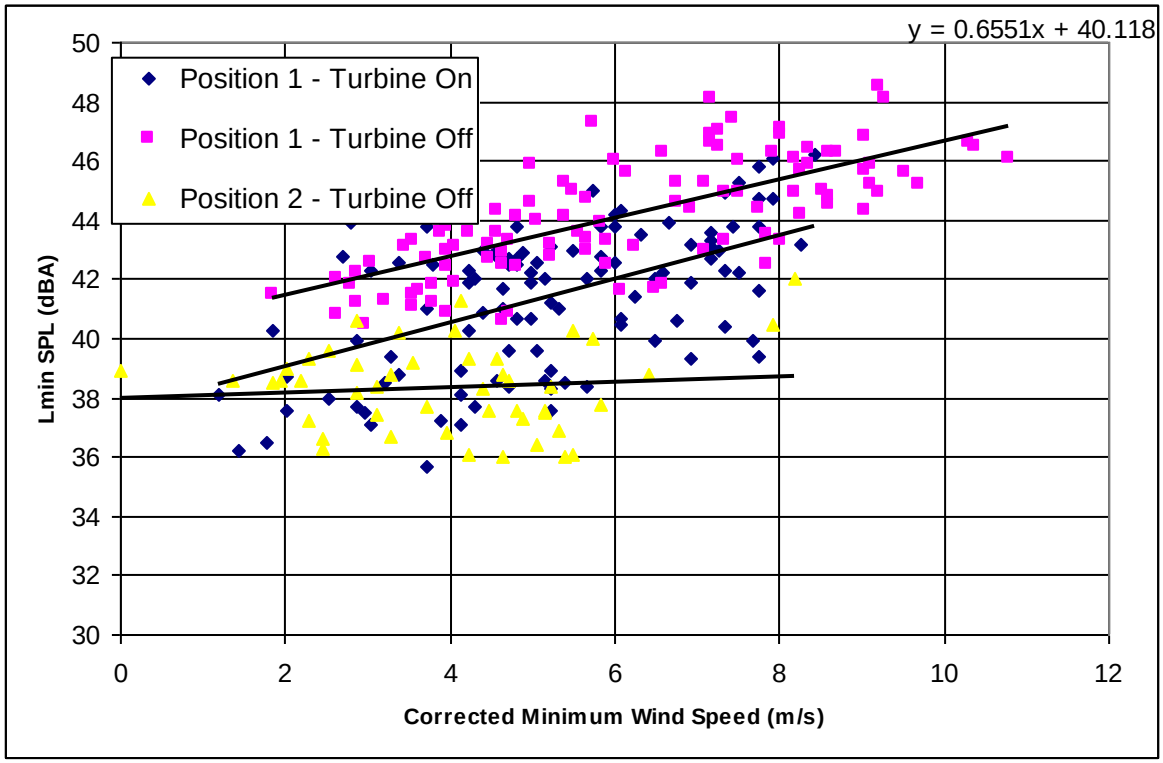

FIGURE 12: MINIMUM SOUND PRESSURE LEVEL LMIN (DBA) VERSUS NORMALIZED MINIMUM WIND SPEED FOR POSITION 1 WITH THE TURBINE SPINNING AND STOPPED, AND FOR POSITION 2 WITH THE TURBINE STOPPED

The next three graphs show similar information but this time the maximum SPL L_{max} is plotted as a function of the maximum measured wind speed. Again, the conclusions are similar to those obtained before. The scattering of the measured data is more severe, which is probably attributed to the presence of spurious sounds that distort the data. In addition, it is observed that typically at very high wind speeds, which occur as gusts or spikes in wind speed, there is a delay between the rotor reaching its maximum rotational velocity and the observed maximum velocity of the gust. Since our analysis is based on time-correlation some of the data may be skewed, in the sense that the maximum SPL that was measured may be attributed to a higher wind speed of a gust recorded several seconds earlier, but may be linked with a lower wind speed at the time of recording.

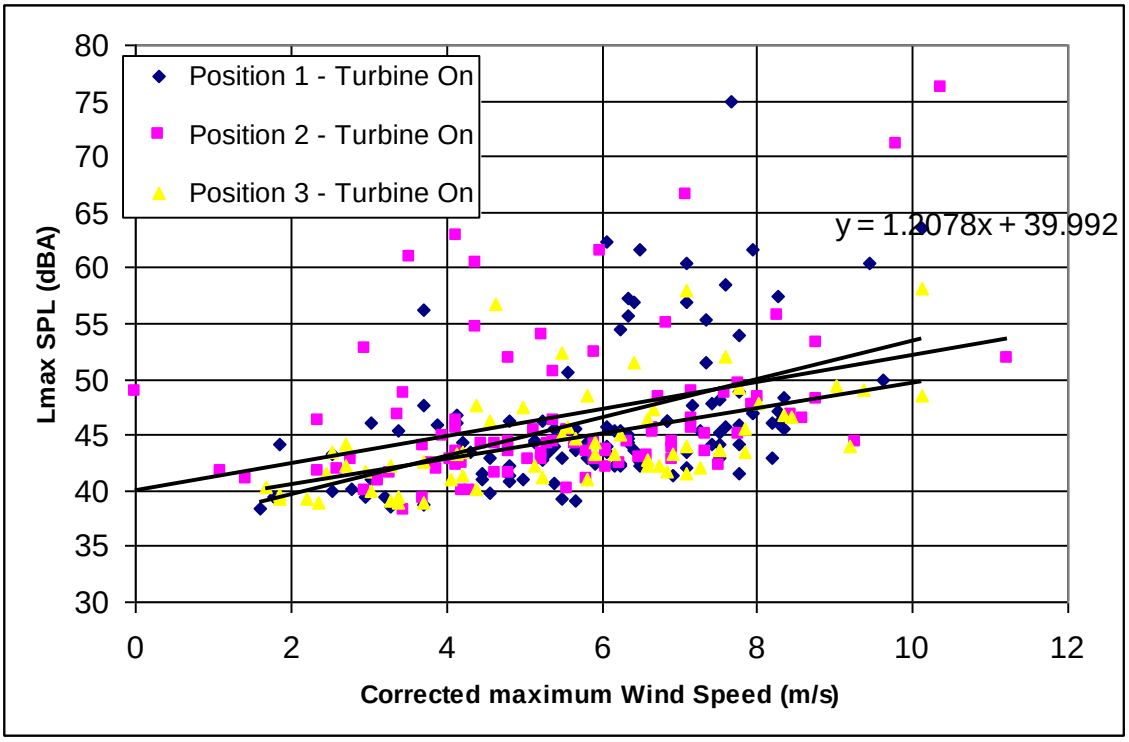

FIGURE 13: MAXIMUM SOUND PRESSURE LEVEL LMIN (DBA) VERSUS NORMALIZED MAXIMUM WIND SPEED FOR ALL THREE MEASUREMENT POSITIONS WITH THE TURBINE OPERATIONAL.

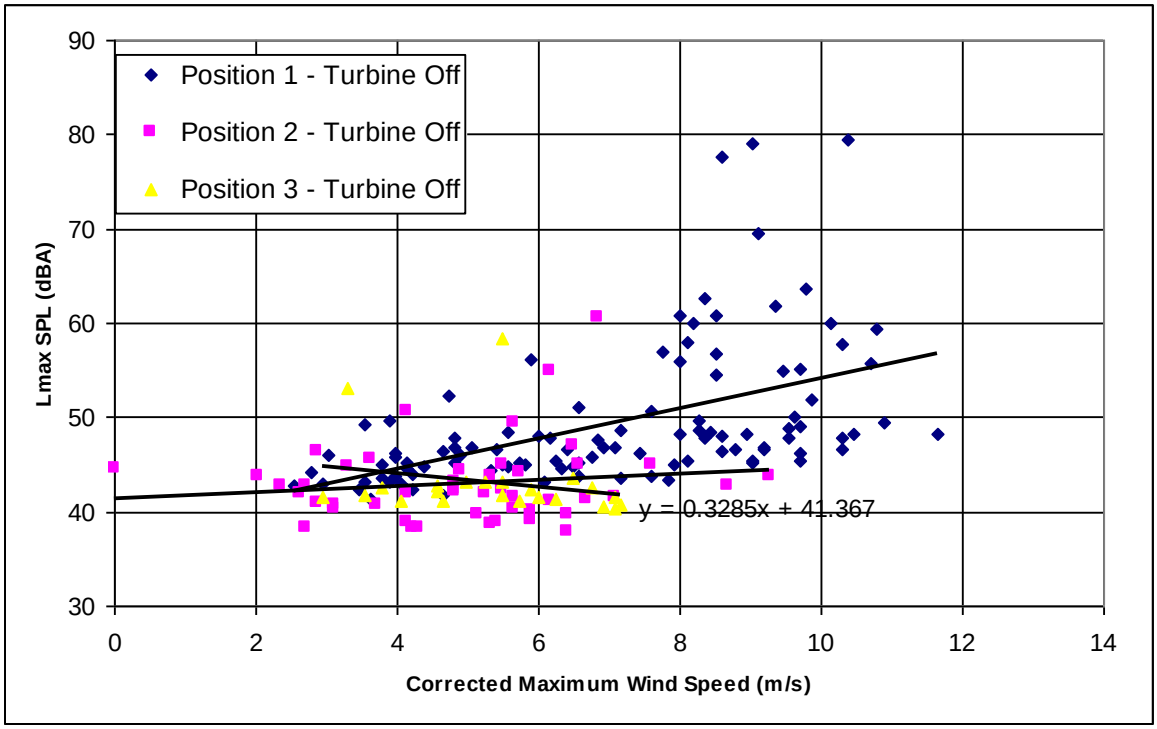

FIGURE 14: MAXIMUM SOUND PRESSURE LEVEL LMIN (DBA) VERSUS NORMALIZED MAXIMUM WIND SPEED FOR ALL THREE MEASUREMENT POSITIONS WITH THE TURBINE ROTOR STOPPED

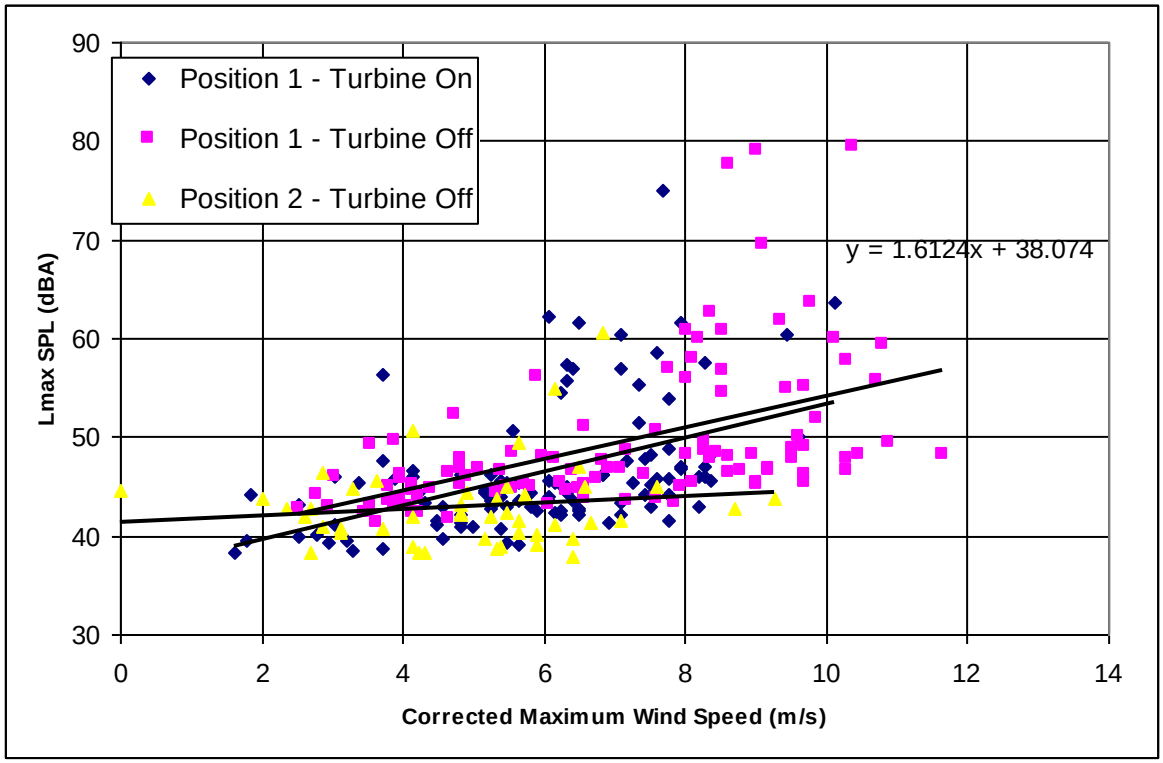

FIGURE 15: MAXIMUM SOUND PRESSURE LEVEL LMIN (DBA) VERSUS NORMALIZED MAXIMUM WIND SPEED FOR POSITION 1 WITH THE TURBINE SPINNING AND STOPPED, AND FOR POSITION 2 WITH THE TURBINE STOPPED

Next, we used the averaged SPL L_{eq} and averaged wind speed to determine the sound power of the turbine. We used the best fit equation for the turbine noise in position 1, which is given by L_{s+n} (dBA) = 1.16*V+37.74, where V is the standardized wind speed at reference height in m/s. L_{s+n} represents the sound level of the source (turbine) and background noise combined.

For the background noise itself we use position 2 with the turbine rotor in locked position. The background noise equation is L_n (dBA) = 0.250*V+ 39.01, where L_n is the background noise. The noise generated by the wind turbine itself is then determined as:

$L_s = 10 * log10(10^{\frac{L_{s+n}}{10}} - 10^{\frac{L_n}{10}})$. Table 1 lists the sound levels as a function of wind speed. According to the IEC standard there must be at least a 6 dB increase between the background noise level and the turbine running sound level for the turbine noise to be a distinct source. If the measurements are more than 3 dB above the background noise, 1.3 dB shall be deducted from the sound level L_{s+n} in order to find the turbine sound level. Table 1 shows that up to a normalized wind speed of 4 m/s, the difference between background noise and turbine noise is less than 3 dB. From 4 to 8 7 m/s the difference is more than 3 but less than 6 dB, and a 1.3 dB correction was applied. From 8 m/s to 12m/s the difference is at least 6 dB, and therefore we can calculate the sound power of the wind turbine. The A weighted sound power of the turbine is calculated by assuming that the wind turbine is a spherically radiating omni-directional sound source, and therefore we can back propagate the measured sound level to the source and determine the source power. This is done by the following equation:

$L_W\ (dB) = L_S - 6 + log10(4\pi R^2/1m^2\ \ )$+0.005*R,

where the 6dB takes into account the pressure doubling that occurs on the rigid plywood board that the microphone sits on. The third term represents the spherical propagation part, and R is the distance from the source to the microphone position. For Rutland, the microphone is located 86 feet from the turbine tower, and since the turbine is at a height of 86 feet, R is 37 m. The last term takes into account atmospheric absorption of the sound is a frequency averaged absorption term, which is proportional to propagation distance. For the limited distance this term does not provide a significant impact. The last column in Table 1 show the calculated sound power values for the Briza model.

TABLE 3: LS+N, LN, LS AND LW(A) AS A FUNCTION OF NORMALIZED WIND SPEED

Normalized Wind Speed (m/s)	L_(s+n) (dBA)	L_n (dBA)	L_s (dBA)	L_(w) (dBA)
2	40.1	39.5	na	na
3	41.2	39.8	na	na
4	42.4	40.0	na	na
5	43.5	40.3	42.2	78.8
6	44.7	40.5	43.4	79.9
7	45.8	40.8	44.5	81.1
8	47.0	41.0	45.7	82.3
9	48.2	41.3	47.2	83.7
10	49.3	41.5	48.5	85.1
11	50.5	41.8	49.9	86.4
12	51.6	42.0	51.1	87.7

Figure 16 shows a comparison of the sound power level of the Briza wind turbine compared to several other small wind turbines as measured by NREL. Included in the graph are the Bergey Exel-S a 10 kW turbine with both BW03 and SH3052 blades, Southwest windpower Air 403, a 400 W turbine, and a Air X turbine wind turbine flutter control, Bergey Xl.1 wind turbine rated at 1 kW, Southwest windpower Whisper H40, a 900 W turbine, and the 50 kW Atlantic Orient and the 100 kW Northwind turbines. We observe that the Briza is about 2-3 dB less in sound power than the 900W Whispher H40. The sound power level of Briza is similar to the Air X at lower wind speeds, and slightly less at higher wind speeds. The Bergey Xl.1 has a significantly lower sound power than the Briza, possibly because of the use of optimized airfol blades.

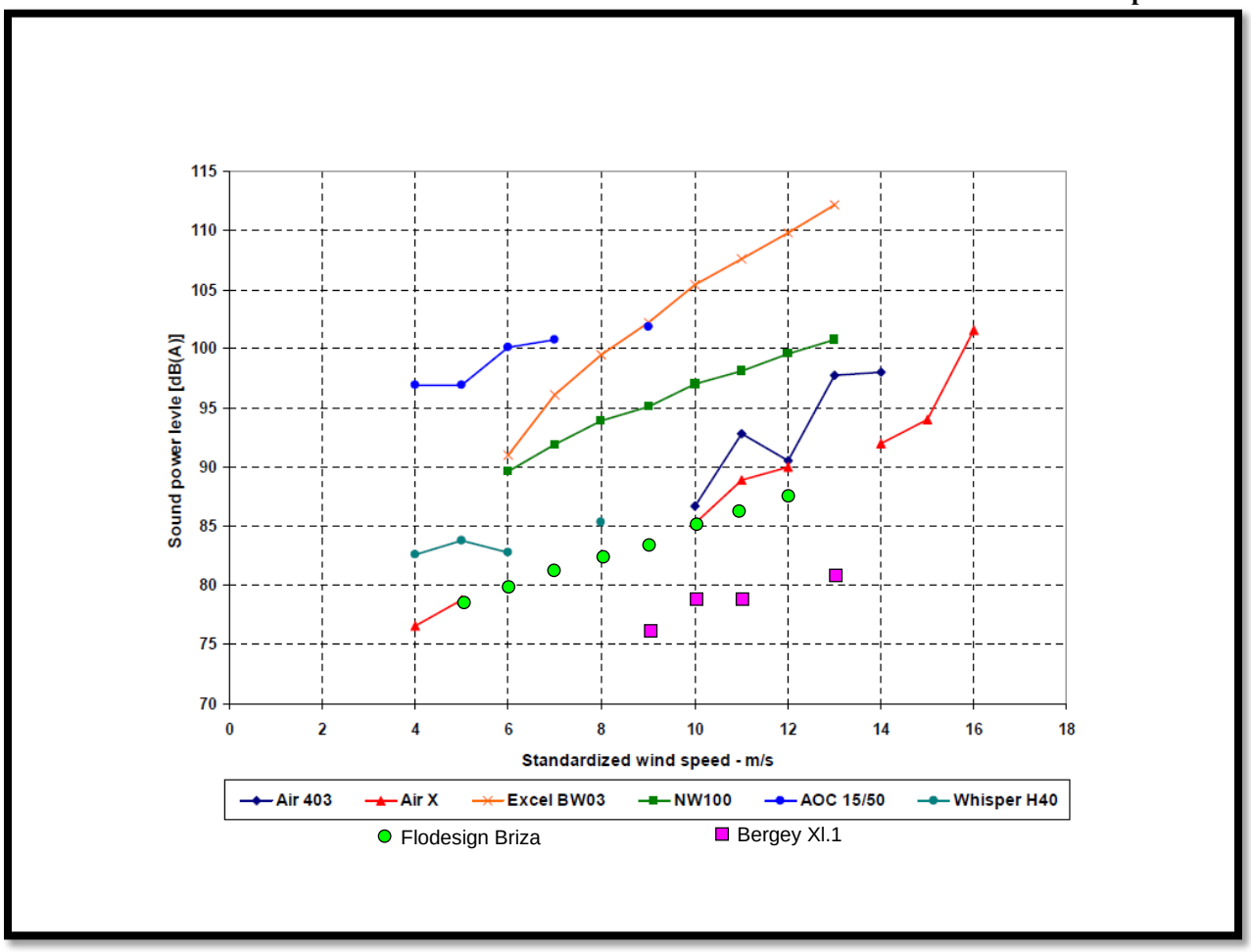

FIGURE 16: SOUND POWER LEVEL (DBA) OF SEVERAL SMALL WIND TURBINES

A second analysis is the integer wind speed bin analysis. In this case all the wind speed data are assigned to integer bins, with all wind speed values from x-0.5 < x <= x+0.5 and corresponding sound pressure levels being assigned to the integer wind speed x. Figure xx shows the measured sound levels for the turbine running in position one and the background noise in position 2 as a function of the integer wind speed bins. This representation of the data reduces the variability in the data. Trendlines are shown and used for calculation of sound level powers. The results show slightly elevated levels of sound power combined to the previous analysis, as shown in Table 2.

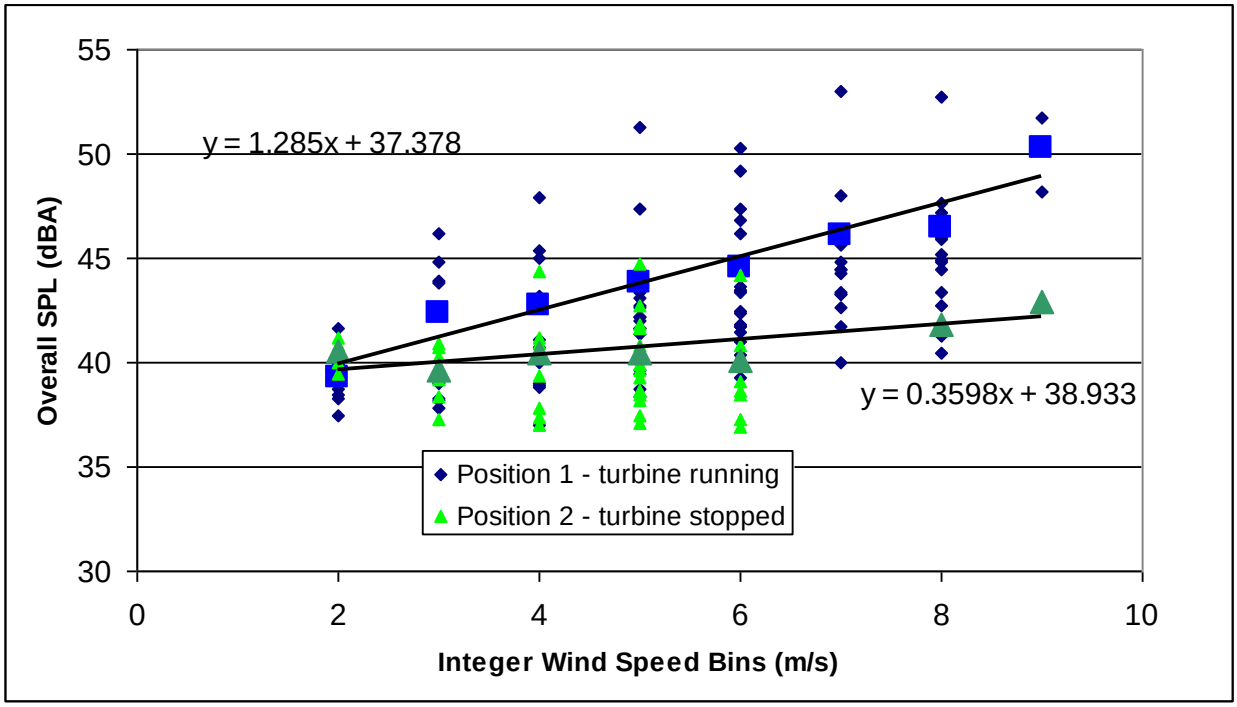

FIGURE 17: SOUND PRESSURE LEVELS AND THEIR AVERAGED VALUES VERSUS INTEGER WIND SPEED BINS (M/S) FOR THE TURBINE RUNNING AND MEASURED IN POSITION 1, AND FOR THE BACKGROUND NOISE MEASURED IN POSITION 2

TABLE 4: COMPARISON OF WIND TURBINE SOUND POWER CALCULATED ACCORDING TO THE INTEGER WIND SPEED BIN ANALYSIS AND THE RAW DATA ANALYSIS.

Normalized Wind Speed (m/s)	L_(w) (dBA) Integer Bin Analysis	L_(w) (dBA) Raw Data Analysis
2	na	na
3	na	na
4	na	na
5	79.1	78.8
6	80.3	79.9
7	81.6	81.1
8	82.9	82.3
9	84.5	83.7
10	86.0	85.1
11	87.4	86.4
12	88.8	87.7

The final analysis that was done was a tone analysis for the recorded sound signatures at the higher wind speeds. The IEC standard prescribes a procedure for the determination of the presence of tones, and the level of tonal audibility. For tonal audibilities larger than -3dB, the particular frequencies in question need to be reported as tonal with their levels of tonal audibilities. A preliminary analysis was performed on a segment of recorded sound corresponding to a strong gust of wind reaching peak wind speeds of about 11 m/s and peak rotational velocities of about 330 rpm. At these wind speeds, there is a very distinct “whirling” sound, similar to that of a propeller airplane. Several recordings were taken during such whirling. These recordings are used for the tonal analysis. Figures 18 show two narrowband spectra obtained from the recorded signal.

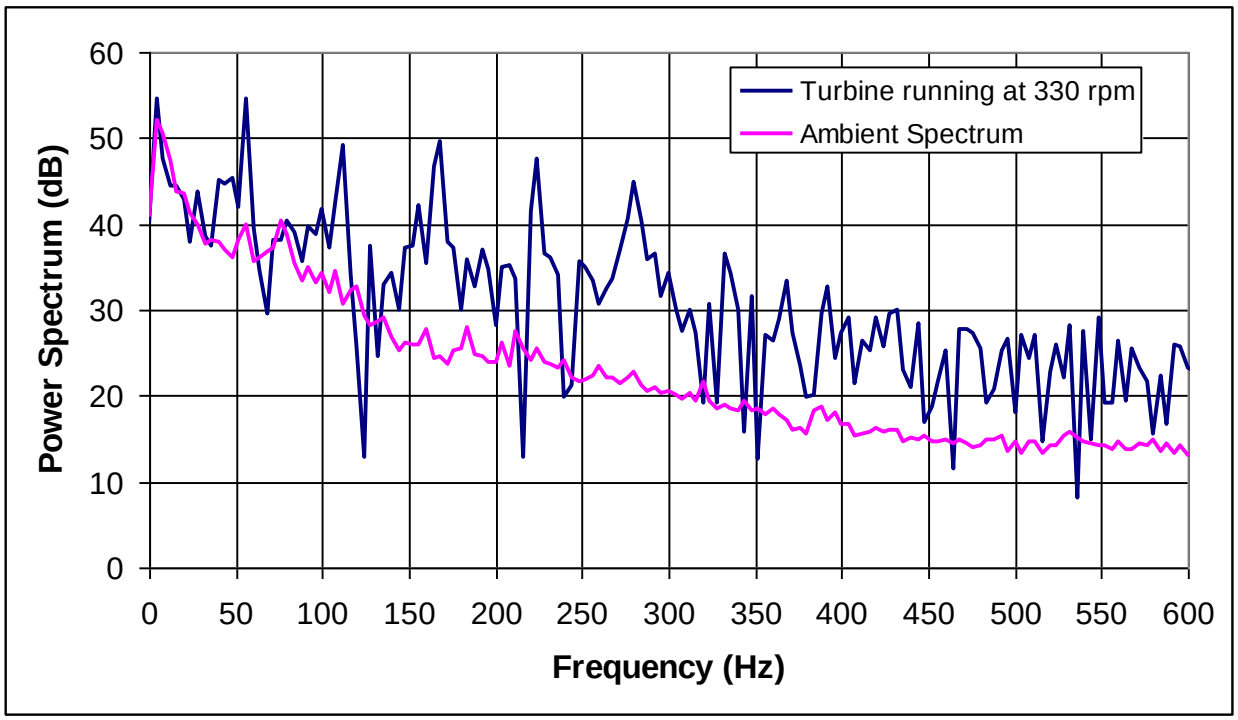

FIGURE 18: NARROWBAND POWER SPECTRUM OF TURBINE RUNNING AT ABOUT 330 RPM AND THAT OF THE BACKGROUND NOISE

It is clear from Figure 18 that at high wind speeds the blade passing frequency becomes the dominant noise source. For 12 rotor blades and a rotational velocity of 330 rpm, the fundamental frequency is 55 Hz. In the graph it is easy to see the fundamental harmonic and at least the next four higher harmonics. None of these components show up in the spectrum of the ambient sound. There is a dominant peak in the ambient spectrum at 4 Hz. We are unsure at this point what the dominant mechanism is for this peak. We think it is related to the large scale turbulence structure of the atmosphere. A tonal analysis was then performed at both the fundamental and second harmonic. For both frequencies it was determined that they do qualify as tones. The tonal audibility is 7 dB at 55 Hz and 5 dB at 110 Hz.

We also calculated an A weighted 1/3 octave band histogram of the noise signal recorded at these peak speeds. Figure 19 is an example of such a 1/3 octave band analysis.

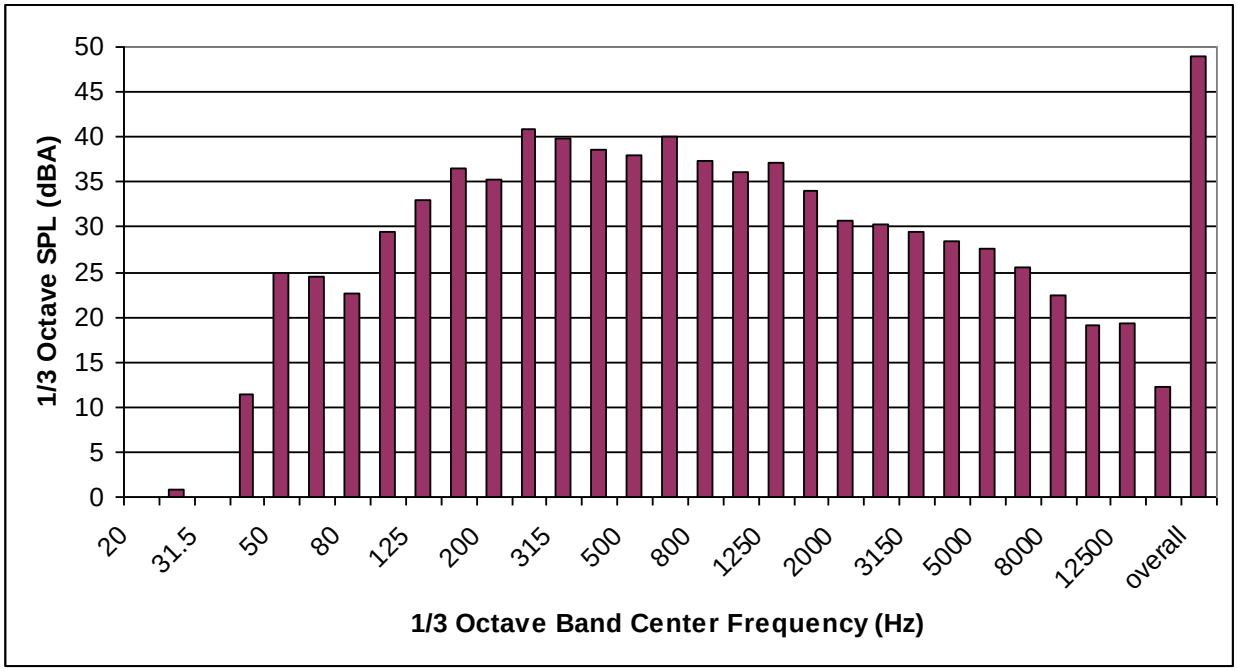

FIGURE 19: A WEIGHTED 1/3 OCTAVE BAND HISTOGRAM OF WIND TURBINE NOISE SIGNAL CORRESPONDING TO A "WHIRLING" SOUND AT ELEVATED WIND SPEED

Because of the A weighting, which affects the lower frequencies significantly more than the middle frequencies, we observe that the peak sound levels are obtained for the 250Hz and 630 Hz 1/3 octave bands. We also notice that there are peaks in the 1/3 octave band corresponding to the fundamental frequency of 55Hz and the harmonics at 110, 165, 220, 280 Hz.

In order to determine the AWEA sound pressure level, we used the maximum sound pressure levels recorded to come up with a sound power value of the turbine for these maximum values (rather than the averaged values). This calculated sound power level was then used to determine the AWEA sound level at a distance of 60m for a normalized wind speed of 5 m/s. The AWEA sound pressure level for the Briza is 33.4 dBA. Since the measured background sound pressure level at 5 m/s is about 43 dBA, we can generate a curve that shows the total sound pressure level of the Briza turbine and the background for various distances from the rotor. This curve is shown in Figure 20.

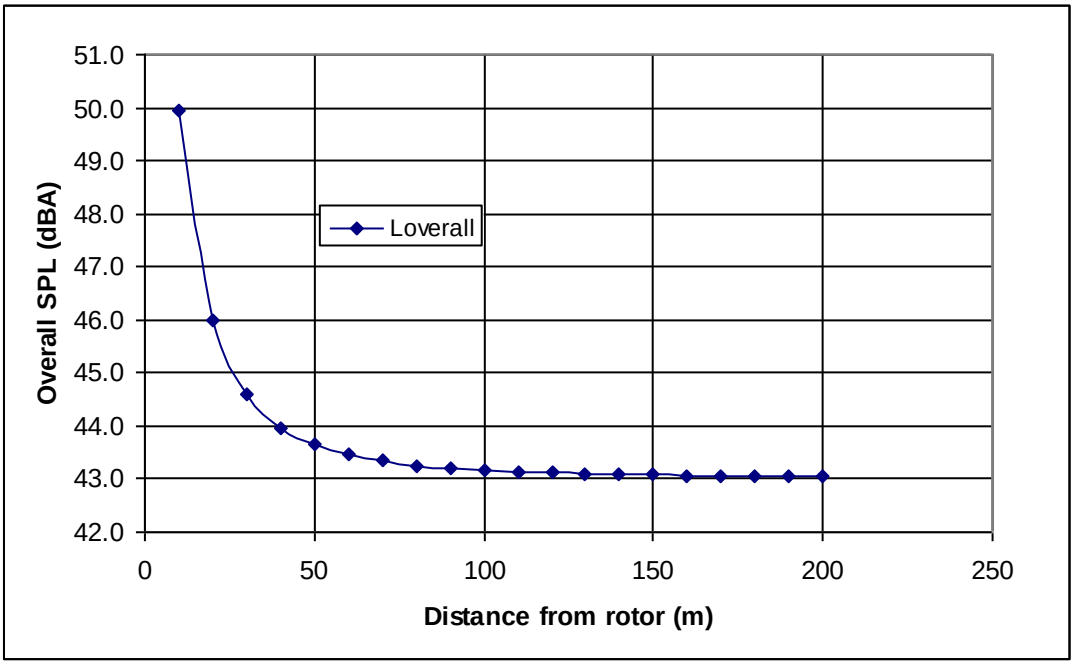

FIGURE 20: OVERALL SOUND PRESSURE LEVEL (DBA) AS A FUNCTION OF DISTANCE FROM THE ROTOR FOR THE BRIZA AWEA SOUND PRESSURE LEVEL AND A BACKGROUND NOISE LEVEL OF 43 DBA

IV. Bergey Wind Turbine Noise:

a. WNEC Site

The Bergey 1 kW wind turbine is located at Western New England College. The turbine is attached to a 60 foot pole that is attached to the side of Sleith Hall on the Western New England College campus, as shown in Figure 21. The turbine hub is roughly 60 feet above ground, and the anemometer is roughly 50 feet above ground. Prevailing winds are typically from the west, which means that a downstream measurement location corresponds to a position on the roof of Sleith Hall. Several measurements were done. There were several issues with the measurements. First, we did not have access to the wind speed data, therefore we can only do a qualitative assessment at this time. Second, during the wind turbine noise recordings, the hvac equipment that is situated on the roof of Sleith Hall was operational. When the hvac systems were running, the background noise increased significantly which made it more difficult in distinguishing the wind noise from the general elevated background noise.

FIGURE 21: VIEW FROM THE ROOF OF SLEITH HALL OF THE BERGEY 1 KW WIND TURBINE ATTACHED TO THE SIDE OF SLEITH HALL AT WESTERN NEW ENGLAND COLLEGE.

Several sets of data were recorded. The analysis that is described below is that of two sets of results. One set was taken during a particularly windy day where the turbine was exhibiting its typical whistling sound. We analyzed two portios of the recorded sound, one where the whistling sound is particularly evident, and another that corresponds to a temporary lull in the noise recordings. These two sections of recordings were then used to analyze the sound and come up with narrow band frequency spectra and 1/3 octave band analyses. A second set of data was analyzed in a similar way. From listening to the recording it was apparent that this section corresponded to a significant noise level of the wind turbine but not one where the whistling sound was a defined as in the first recording. We deduce from that that the windspeed was less than that of the first recording.

FIGURE 22: VIEW OF THE REFLECTING BOARD, SOUND LEVEL METER, AND RECORDER ON THE ROOF OF SLEITH HALL.

b. Results

Figure 23 shows the frequency spectrum of the sound recorded at high speed (blue) and the sound recorded during a calm period. The frequency range is from 0 to 5000 Hz. It is apparent that Bergey wind turbine creates an increase in high frequency noise in the range from 1000 to 5000 Hz, with a peak at about 3250 Hz. Figure 24 shows a zoom of Figure 23 for frequencies from 0 to 600 Hz. This graph shows that there is no difference in the low frequency part of the spectrum for the two cases, high wind and no wind. The conclusion is that the increase in noise for the wind turbine results in high frequency noise of the range of 2-4 kHz. This is the noise that we hear as the whistling noise. It is broadband in the sense that it extends over a wide range of frequencies and is certainly not resonance based, as in one dominant frequency.

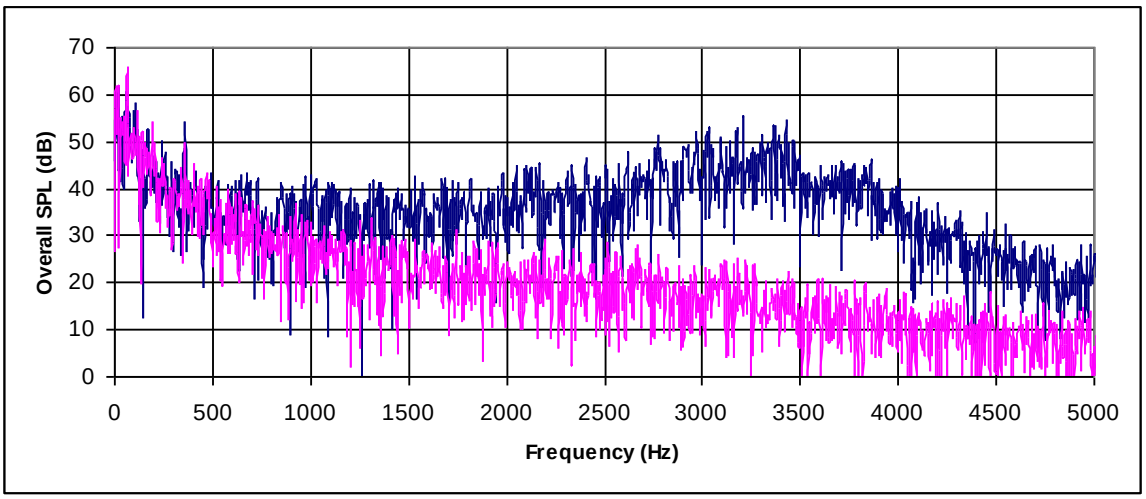

FIGURE 23: NARROW BAND FREQUENCY SPECTRUM (0-5000 HZ) OF THE SOUND AT HIGH WIND SPEED (BLUE) AND AT VERY LOW WIND SPEED (PINK) FOR THE BERGEY WIND TURBINE.

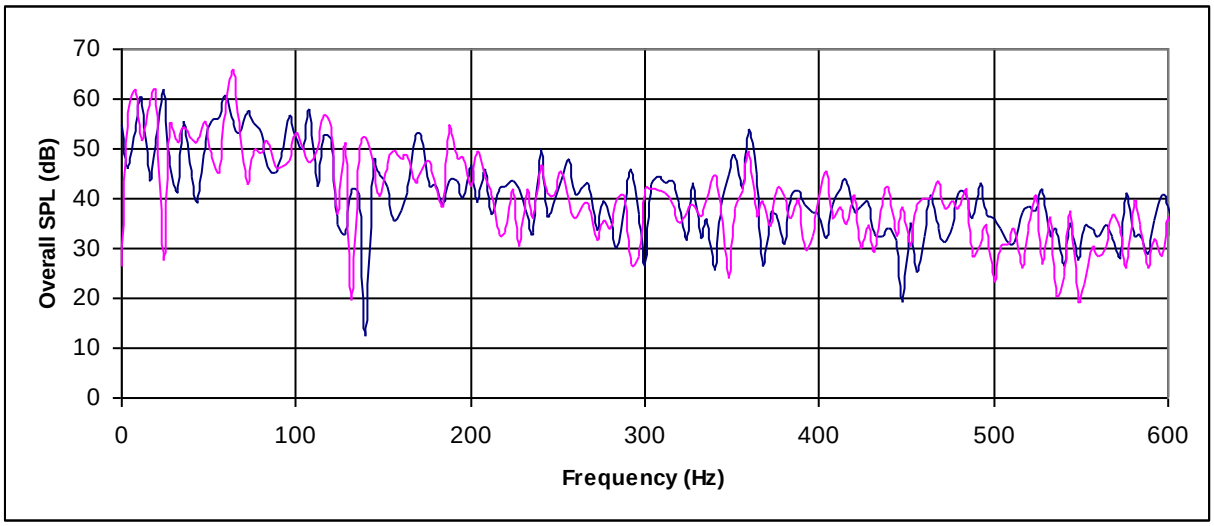

FIGURE 24: NARROW BAND FREQUENCY SPECTRUM (0-600 HZ) OF THE SOUND AT HIGH WIND SPEED (BLUE) AND AT VERY LOW WIND SPEED (PINK) FOR THE BERGEY WIND TURBINE.

Figure 25 shows the corresponding A-weighted 1/3 octave band analysis for the high wind speed and no wind speed. As expected, for the high wind speed case, there is a noticeable increases at the 1/3 octave bands starting at 1 kHz. The overall A-weighted sound pressure level for the high wind case is about 72 dBA, and for the no wind case it is about 57 dBA. This increase of 15 dBA is quite significant.

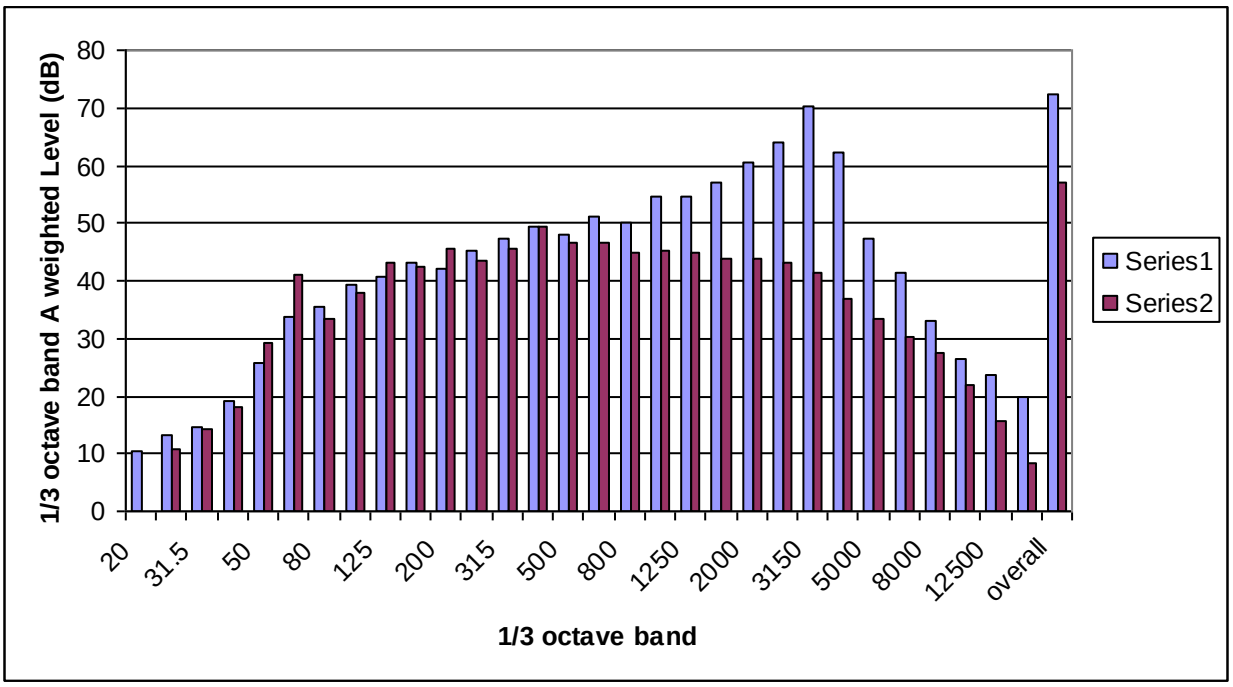

FIGURE 25: ONE THIRD A-WEIGHTED OCTAVE BAND ANALYSIS OF THE SOUND AT HIGH WIND SPEED (BLUE) AND AT VERY LOW WIND SPEED (PINK) FOR THE BERGEY WIND TURBINE.

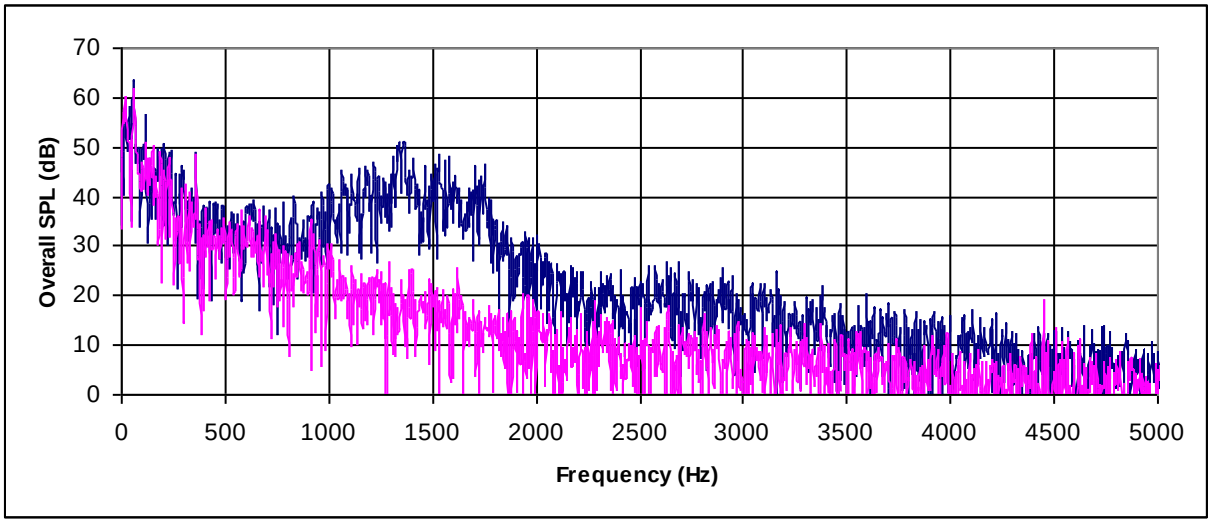

FIGURE 26: NARROW BAND FREQUENCY SPECTRUM (0-5000 HZ) OF THE SOUND AT MODERATE WIND SPEED (BLUE) AND AT VERY LOW WIND SPEED (PINK) FOR THE BERGEY WIND TURBINE.

Figure 26, 27, and 28 show similar results but this time for a second set of data corresponding to a more moderate wind speed. The narrow band frequency spectrum of

Figure 26 now shows that for the moderate wind speed the increase in noise is concentrated in the 600 to 3000 Hz range, with the peak occurring at about 1400 Hz. Therefore we conclude that a reduction in wind speed results in a decrease of the frequency range where we observe an increase of the sound pressure level. Figure 27 indicates again that there is no low frequency difference between the moderate wind speed sound data and the no wind sound data.

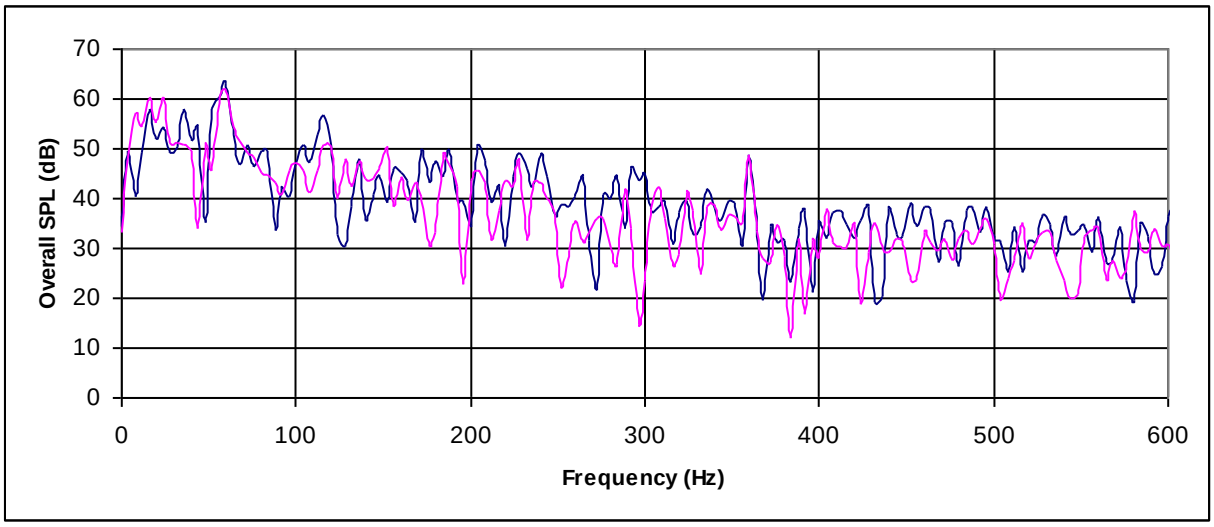

FIGURE 27: NARROW BAND FREQUENCY SPECTRUM (0-600 HZ) OF THE SOUND AT MODERATE WIND SPEED (BLUE) AND AT VERY LOW WIND SPEED (PINK) FOR THE BERGEY WIND TURBINE.

Finally, Figure 28 shows the 1/3 octave band graphs. At moderate wind speed the overall A weighted level is about 67 dBA and the no wind speed analysis shows a 54 dBA level. The 1/3 octave band analysis confirms the increase of levels from about 1000 to 3000 Hz. A preliminary sound power analysis indicates that the sound power of the Bergey turbine significantly exceeds that of the Briza. It is important to stress that this is a preliminary result since no wind speed data was obtained, and more detailed and accurate measurements are needed.

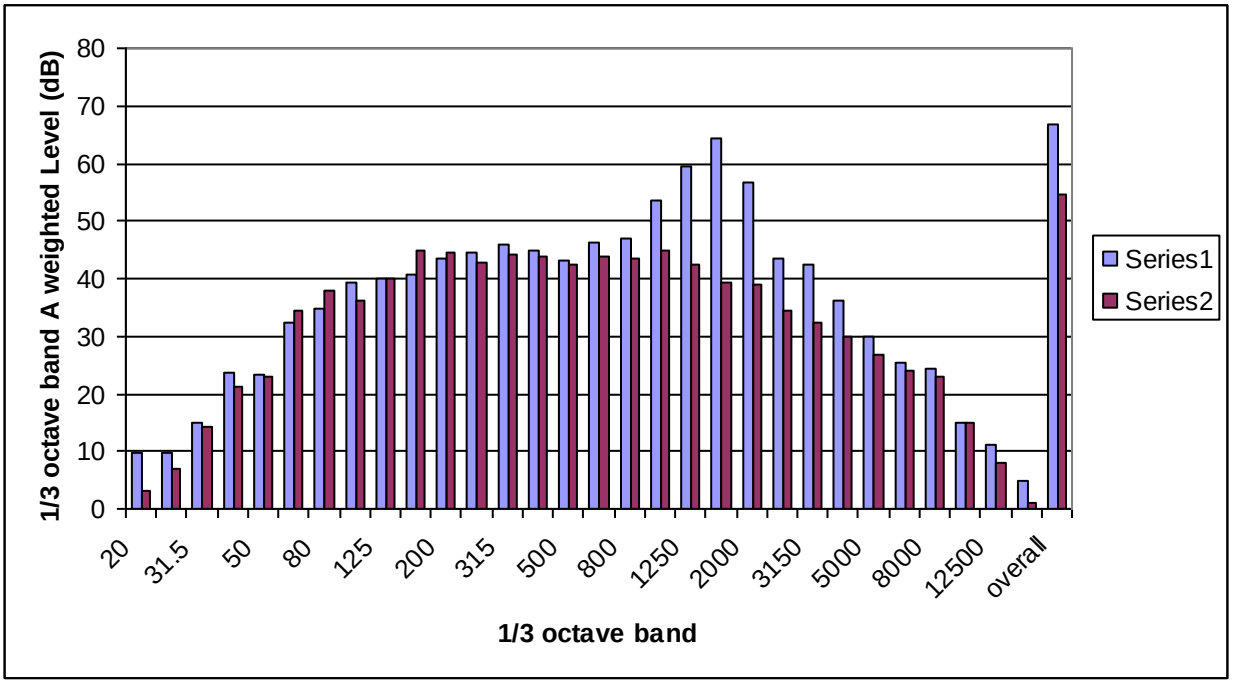

FIGURE 28: ONE THIRD A-WEIGHTED OCTAVE BAND ANALYSIS OF THE SOUND ATMODERATE WIND SPEED (BLUE) AND AT VERY LOW WIND SPEED (RED) FOR THE BERGEY WIND TURBINE.

V. Wind Turbine Noise Modeling:

a. Sources of noise and initial modeling efforts

Research into wind turbine noise has typically relied on literature concerning noise prediction from isolated air foils, propellers, helicopter rotors, and compressors. Typical sources of noise for traditional wind turbines are noise contributions from rotational harmonics associated with the blade passing frequency and broadband noise. The sources for broadband aerodynamic noise are primarily low frequency noise, inflow turbulence, interaction between turbulent boundary layer and blade trailing edge, laminar boundary layer vortex shedding noise, tip vortex formation noise, and the vortex shedding from the bluntness of the trailing edge. For the Flodesign Briza there are potentially new sources of noise such as the noise from the shroud surface, and stator-rotor interactions noise. We have made some initial attempts at modeling the various noise sources. In this discussion we do not include mechanical noise coming from components such as the gearbox. It is important to point out though that a reduction of mechanical noise for a typical Flodesign wind turbine would be a beneficial factor in evaluating and comparing the noise structure of a Flodesign wind turbine with a more traditional one.

i. Rotational harmonics

Modeling of rotational harmonics has not commenced yet.

ii. Inflow turbulence noise

We have made some initial modeling efforts for inflow turbulence noise. Several of the models we employ are described in the literature; especially the models by Grosveld, Wei Jun Zhu, Amiet, and Lawson are used. First we model the variation of the mean wind speed with altitude, then we model the variation of turbulence intensity with altitude, and finally we derive a model for the generation of noise from inflow turbulence.

The source for the inflow turbulence noise is contained in the instability of the atmosphere and the inherent turbulence of the atmospheric boundary layer. Atmospheric turbulence contains eddies of a range of length scales. When these eddies interact with the blades, noise will be generates, as shown in Figure xx. Large eddies create fluctuating forces on the blades resulting in a dipole type of acoustic radiation at low frequencies. Smaller eddies create more of a localized pressure fluctuation resulting in a high frequency acoustic pulse. The noise is therefore a function of turbulence intensity and length scale, and the geometry of the wind turbine. Turbulent inflow noise is one of the critical components of wind turbine noise and is represented by a broadband noise contribution. Assumptions are isotropic turbulence and a neutrally stable atmosphere.

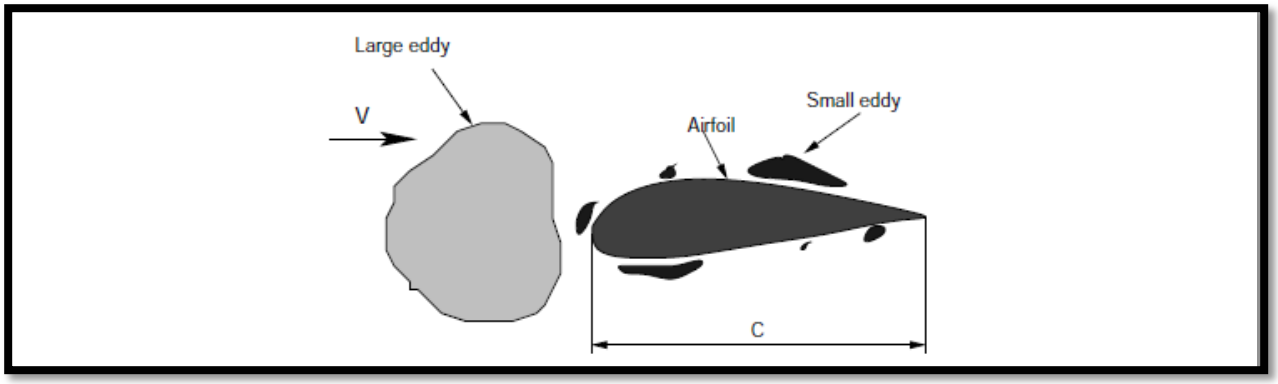

FIGURE 29: SCHEMATIC DEPICTING THE INTERACTION OF A BLADE WITH TURBULENT EDDIES OF DIFFERENT LENGTH SCALES

A description of the turbulent inflow noise is critical to the inflow noise model. We consider a horizontal gust of wind, described by

$w = \overline{w}\ e^{i\omega_x(t-x/V_x)}$,

where w is the turbulent velocity in the x direction, which is the downstream direction of the turbine, $\overline{w}$ is the turbulent velocity amplitude, ω_x is the longitudinal frequency of the gust, t is time, and V_z is the mean free stream wind velocity in the downstream direction. The variation of the mean wind speed with height can be described as

$V_z = V_{ref}\left(\frac{z}{z_{ref}}\right)^{\gamma}$, where z is altitude, V_{ref} and z_{ref} are a reference velocity and height, and γ is a power law factor, typically given as (Counihan 1975),

$\gamma = 0.24 + 0.096log_{10}z_0 + 0.016(log_{10}z_0)^2$,

where z_0 is the surface roughness level.

Figure 30 shows a typical graph for the mean wind speed as a function of height. The reference velocity and height were set at 9.8 m/s and 24 m. The surface roughness level was set at 0.35 m. These values are typical for the Rutland site on a very windy day.

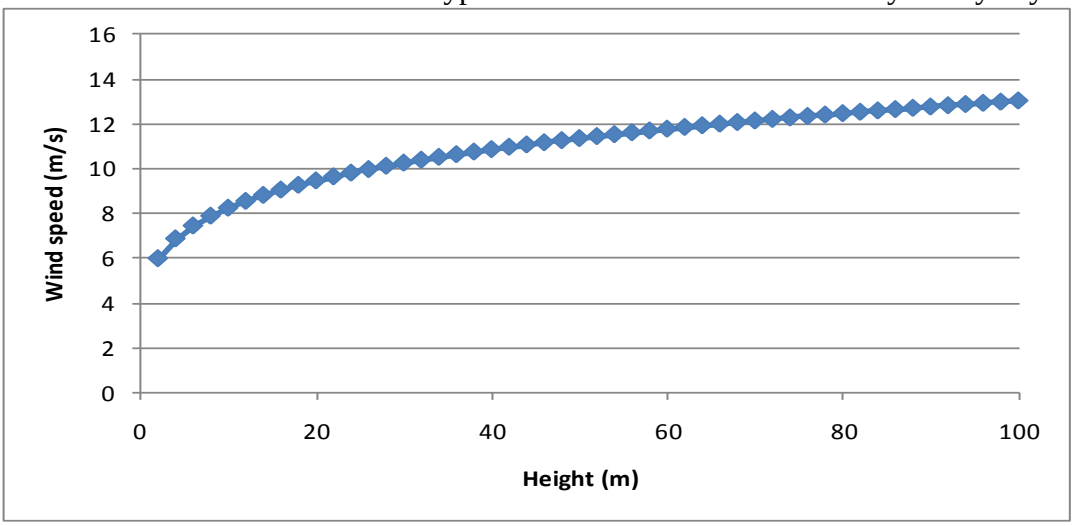

FIGURE 30: VARIATION OF MEAN WIND SPEED WITH ALTITUDE

Next we calculate the turbulence intensity. Three models have been incorporated and their results are compared here. The first model is that of Snyder (1985), where the turbulent velocity in the downstream direction is given by

$$\frac{\bar{w}}{V_z} = \gamma \frac{ln\left(\frac{30}{z_0}\right)}{ln\left(\frac{z}{z_0}\right)}. \qquad (2)$$

A second model is that by Frost which describes the turbulence intensity σ_x, i.e., the ratio of turbulence velocity to mean wind speed in downstream direction, as

$$\frac{\sigma_x}{V_z} = \frac{0.52}{ln\left(\frac{z}{z}\right)}(0.177 + 0.00139z)^{-0.4}. \quad (3)$$

The models by Snyder and Frost directly incorporate the effect of surface roughness level on turbulent intensity. The third model is that of Grosveld, which starts from considering the turbulence spectrum of a neutral atmosphere, given by

$$\varphi_x(\eta, V_z) = \frac{{w_r}^2}{\omega_x}\left[\frac{0.164\eta/\eta_0}{1+0.164(\eta/\eta_0)^{5/3}}\right], \quad (4)$$

Where φ_x is the longitudinal turbulence spectrum (m2/s), w_r^2 is the reference turbulence intensity, η is the reduced frequency, given by $\eta = \omega\, z / V_z$, and η_0 is the reduced normalized frequency (usually at ground level),given by $\eta_0 = 0.0144(z/30)^{0.78}$. The reference turbulence intensity is given by

$${w_r}^2 = [2.18\, V_z z^{-0.353}]^{1/(1.185-0.193log_{10}z)}.$$

Next, integration is performed over frequency to find the turbulence intensity, which is given by

$\bar{w}^2 = {w_r}^2[zw_r/\{V_zR(w_r - 0.014{w_r}^2)\}]^{-2/3}$, where R is the rotor blade radius. Figure 31 represents the turbulent velocity in downstream direction as a function of altitude according to the models by Snyder, Frost, and Grosveld. The models by Snyder and Frost are very similar, and results in a typical turbulence velocity of the order of 2 m/s for altitudes of 10 m and higher. Grosveld's model results in higher turbulent velocities near ground level, and smaller velocities at higher altitudes, typically between 1.25 and 0.5m for altitudes between 10 and 100m.

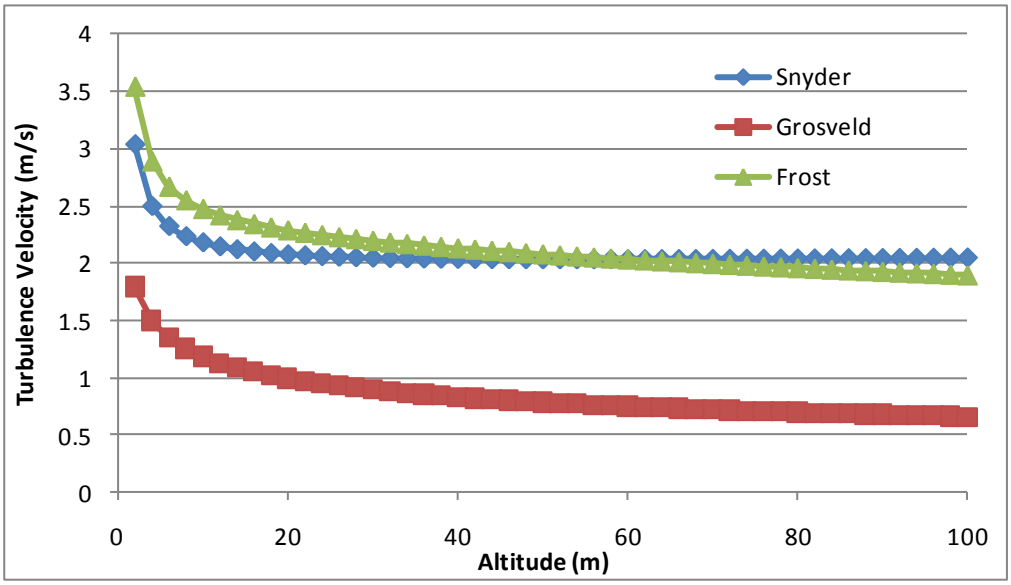

FIGURE 31: TURBULENCE VELOCITY IN DOWNSTREAM DIRECTION AS A FUNCTION OF ALTITUDE FOR THE MODELS OF SNYDER, FROST, AND GROSVELD

Next we discuss the far field noise prediction as a result of the turbulent inflow. The first model is that of Grosveld. Grosveld used the theory of Lighthill to come up with a far field noise prediction. The wind gust results in an induced fluctuating force, which is an acoustic dipole. For a compact source and a wavelength smaller than the distance to the far field receiver, an integral formula can be used to calculate the far field noise. This results in an expression for the mean squared sound pressure in the far field, which can then be integrated over the frequency range for each one third octave band and results in:

$SPL_{1/3}(f) = 10log_{10}\left[B\ \sin^2\theta\rho^2 c_{0.7}R\sigma^2\ {V_{0.7}}^4/(d^2{a_0}^2)\right] + K_a$, where f is the one third octave band center frequency in Hz, B is the number of blades, θ is the angle between the hub-to-receiver line and its vertical projection in the rotor plane in radian, ρ is the air density, $c_{0.7}$ is the blade chord at a radius of 0.7R, where R is the rotor blade radius, σ is the turbulence intensity in m/s, $V_{0.7}$=0.7RΩ, where Ω is the rotor speed in radian/s, d is the distance of the rotor to the listener in m, a_0 is the speed of sound in m/s, K_a is a frequency dependent scaling factor in dB. The frequency f_{peak} is the

frequency where the function K_a is maximum, and is given by $f_{peak}=S_0\ V_{0.7}$ / (H-0.7 R), where S_0 is a constant Strouhal number of 16.6, and H is the hub elevation above ground in m. The frequency dependent function K_a has been determined empirically from measured spectra of rotor noise caused largely by inflow noise (Boeing). Figure 32 shows the function K_a.

Calculations were done for the Briza turbine at the Rutland site. The number of blades is 12, the rotational velocity was set to 330 rpm, reflecting the highest rotational velocities measured, the hub height is 26m, the angle between listener and vertical plane is 45^o, the blade cord is set to 0.1m, the turbulent intensity is 1.4 m/s, the tip radius to 1m, the distance from the listener to the rotor at 37m. The analysis shows that the peak frequency of the function K_a is 16 Hz. Figure 33 shows the 1/3 octave band spectrum for the inflow noise. Since the peak frequency is at 16 Hz, the spectrum levels decrease with increasing frequency.

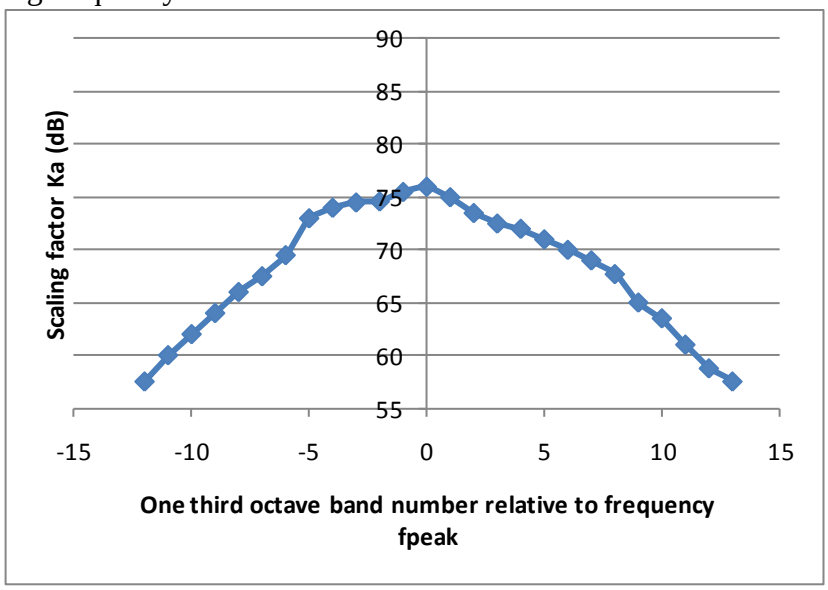

FIGURE 32: FREQUENCY-DEPENDENT SCALING FUNCTION KA USED FOR PREDICTION OF INFLOW NOISE

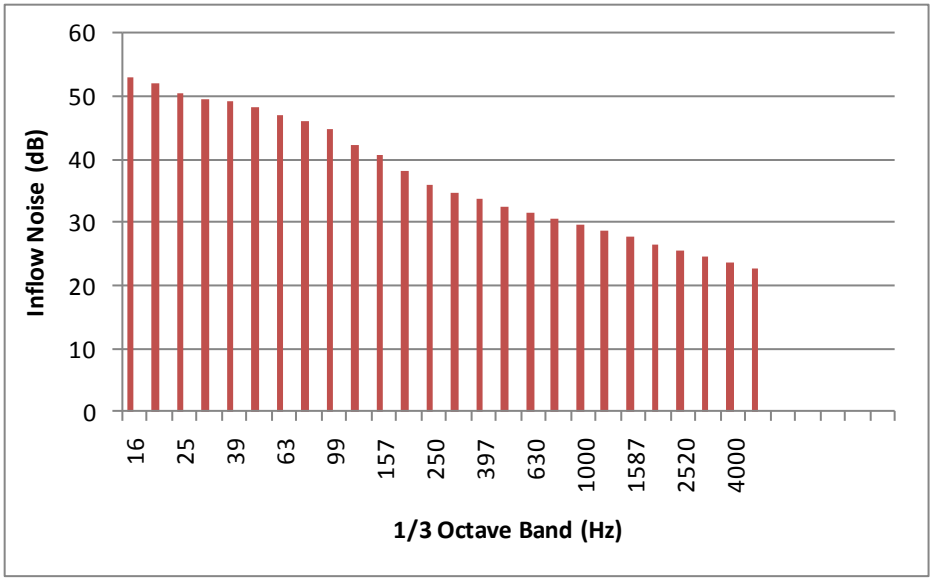

FIGURE 33: PREDICTED 1/3 OCTAVE BAND NOISE LEVELS FOR BRIZA FOR INFLOW NOISE

Next we compare the predicted level to measured spectra at similar rotational speeds. As explained earlier, for a rotational velocity of 330 rpm, significant harmonic noise from the blade passing frequency is observed. Since the measured noise is A weighted, we included an A weighted correction to the predicted noise field. The comparison is shown in Figure 34.

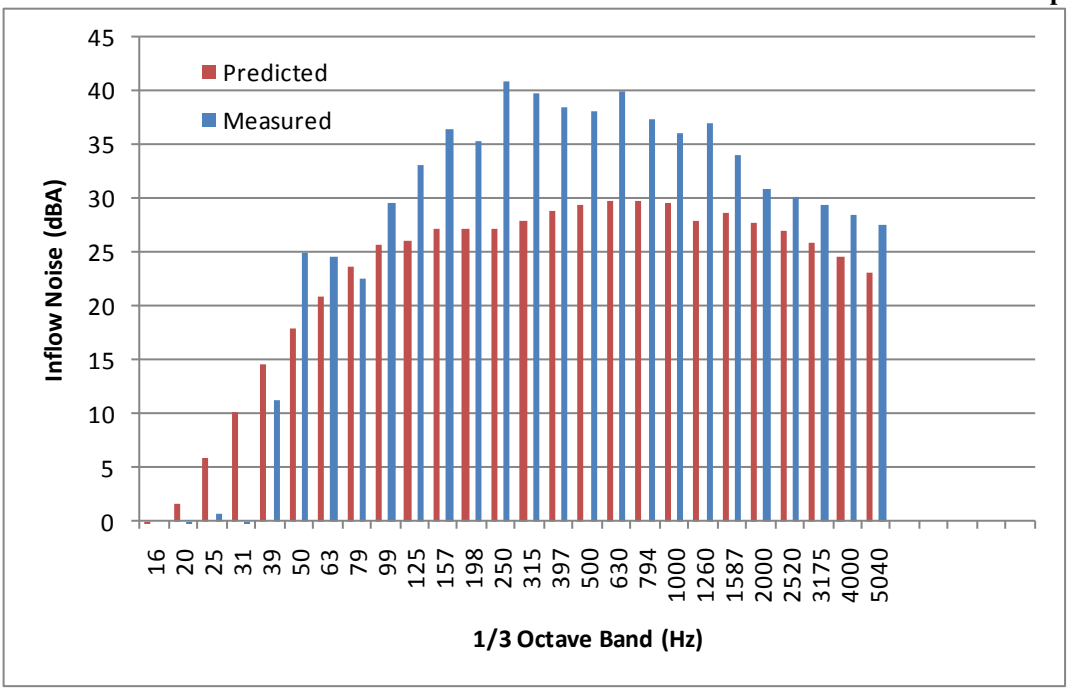

FIGURE 34: COMPARISON OF PREDICTED INFLOW NOISE FOR BRIZA WITH MEASURED NOISE AT 330 RPM

The comparison shows that the prediction of the inflow noise is reasonable and provides a realistic prediction for the broadband noise of the turbine. The other noise sources need to be modeled in order to provide more accuracy but the inflow noise does indeed explain the overall broadband noise contribution observed in the measurement.

iii. Turbulent boundary layer noise

Modeling of turbulent boundary layer noise has not commenced yet.

iv. Trailing edge noise

Modeling of trailing edge noise has not commenced yet.

VI. Future work and recommendations

a. Further testing at Rutland Site

So far we have obtained one quality data set of noise recordings at the Rutland Site. Further testing should include at least a second data set to confirm the measurements obtained so far. Better measurements of the background noise are also needed. Measurements of the noise directionality are needed. Measurements at angles of up to +- 45^{o} from the downstream direction are needed to measure the directionality of the wind turbine noise. So far the testing has been limited to mostly relatively low wind speeds. Testing at sustained higher wind speeds is necessary to accurately measure the noise at elevated wind speeds.

Since the background noise is relatively high at the site, and the Briza is relatively quiet, especially at lower wind speeds, we think that employing a boom to allow for measurements

above ground level may be a better alternative to measure the sound power of the turbine. It may also provide the tools to verify whether the Briza noise source is similar to that of a spherically spreading source.

b. Programming and Processing

More programming and data processing efforts are needed as well. It would be especially helpful to build into the program the capability to select a narrow value of wind speed, and then average the noise characteristics over a pre-determined time period, such as 10 seconds or one minute.

c. Modeling

As explained in the introduction to the noise modeling section, multiple sources of noise need to be considered. A noise model needs to be built for all sources, and then verified against the data to come up with a comprehensive model that takes into account all the sources and the geometry of the turbine. This is a significant effort that will take significant time.

APPENDIX A:

Below is a list of articles related to wind turbine noise measurement and modeling.

Metzger, F. Bruce. "A Review of Propeller Noise Prediction Methodology." (1995). Rpt. in Hampton: National Aeronautics and Space Administration. Print.

Migliore, P., and A. Huskey. "Acoustic Tests of Small Wind Turbines." (2003). Rpt. in By J. Van Dam. Golden: National Renewable Energy Laboratory. Print.

W Z Shen and J N Sørensen 2007 *J. Phys.: Conf. Ser.* **75** 012085
doi: 10.1088/1742-6596/75/1/012085

Vick, Brian D. "AFFECT OF NEW BLADES ON NOISE REDUCTION OF SMALL WIND TURBINE WATER PUMPING SYSTEMS." Print. Rpt. in By R. Nolan. Bushland: USDA-Agricultural Research Service. Print.

Brooks, Thomas, and Michael Marcoloni. "Airfoil Self Noise and Prediction." (1989). Rpt. in By D. Stuart Pope. NASA Reference. Print.

Oerlemans, Stefan. "Detection of Aeroacoustic Sound Sources on Aircraft and Wind Turbines." (2009). Rpt. in Thesis University of Twente, Enschede. Print.

Woodward, Richard P. "Far-Field Acoustic Characteristics of Multiple Blade-Vane Configurations for a High Tip Speed Fan." (2004). Rpt. in By John A. Gazzaniga. National Aeronautics and Space Administration. Print.

Crocker, Raju P. "Eversman Comparison of Radiated Noise from Shrouded and Unshrouded Propellers." (1992). Rpt. in Vol. 1. University of Missouri. Print.

Thomas, Russell H. "Flow and Noise Control: Review and Assessment of Future Directions." (2002). Rpt. in By Meelan M. Choudari. National Aeronautics and Space Administration. Print.

Moccia, Antionio. "INDUSTRIAL CFD SIMULATION OF AERODYNAMIC NOISE." Print. Rpt. in 2007. Print.

Zhu, Wei Jun. "Modeling Of Noise From Wind Turbines." (2004). Rpt. in Mechenical Department,DTU. Print.

Klug, H. "NOISE FROM WIND TURBINES STANDARDS AND NOISE REDUCTION PROCEDURES." (2002). Rpt. in Wilhelmshaven, Germany;: DEWI (German Windenergy Institute). Print.

Fokkerweg, Anthony. "NOISE: Computation of Ducted Fan and Propeller Noise." (2002). Rpt. in National Aerospace Laboratory. Print.

Migliore, P., and A. Huskey. "Acoustic Tests of Small Wind Turbines." (2003). Rpt. in By J. Van Dam. Golden: National Renewable Energy Laboratory. Print.

Schulten, J.B.H.M., and M. Namba. "Numerical Results of Lifting Surface Theory." (2000). Rpt. in National Renewable Energy Laboratory. Print.

Leloudas, Giorgos. "Optimization of Wind Turbines with Respect to Noise." (2006). Rpt. in Master's Thesis Project Supervised by Jens N. Sørensen. Print.

G Leloudas. " Prediction and Reduction of Noise from a 2.3 MW Wind Turbine " *et al* 2007 *J. Phys.: Conf. Ser.* **75** 012083 doi: 10.1088/1742-6596/75/1/012083

Grosveld, Ferdinand W. "Prediction of Broadband Noise from Horizontal Axis Wind Turbines." (1985). Rpt. in 4th ed. Vol. 1. Hampton: Bionetics Corporation. Print.
Oerlemans, S., and J.G. Schepers. "Prediction of Wind Turbine Noise and Validation against Experiment." (2009). Rpt. in National Aerospace Laboratory. Print.
Hodgson, Ernest V. F. "Residential Wind Turbines and Noise Emissions." Web.
Sacks, A. H. "Ducted Propellers- A Critical Review of the State of the Art." (1962). Rpt. in By J. A. Brunell. Vol. 3. Oxford: Pergamon, 1961. Print.
Duane, Oleson R., and Patrick Howard. "SMALL AIRCRAFT PROPELLER NOISE WITH DUCTED PROPELLER." (1998). Rpt. in American Institues of Aeronautics and Astronautics, 1998. Print.
Grosveld, Ferdinand, Brenda Sullivan, and Stephen Rizzi. "TEMPORAL CHARACTERIZATION OF AIRCRAFT NOISE SOURCES." (2004). Rpt. in American Institute of Aeronautics and Astronautics. Print.
G.P.van Den Berg. "The Beat Is Getting Stronger: The Effect of Atmospheric Stability on Low Frequency Modulated Sound of Wind Turbines." Print. Rpt. in 4th ed. Vol. 4. University of Groningen. Print.
Vlterna, Larry. "The NASA-LeRC Wind Turbine Prediction Code." (1981). Rpt. in U.S. Department of Energy. Print.
Migliore, Paul G. *Microsoft Powerpoint*. Computer software. *Wind Turbine Aeroacoustic Issues*. National Renewable Energy Laboratory, Dec. 2002. Web.
Huskeys, A., and M. Meadors. *Wind Turbine Generator Systems Acoustic Noise Test Report*. Tech. National Renewable Energy Lab, 2001. Print.
Rogers, Anthony, and James Manwell. "Wind Turbine Noise Issues." (2002). Rpt. in Huskeys, A., and M. Meadors. Wind Turbine Generator Systems Acoustic Noise Test Report. Tech. National Renewable Energy Laboratory. Web.
Hubbard, Harvey H. "Wind Turbine Acoustics." (1990). Rpt. in By Kevin Sherperd. U.S. Department of Energy. Web.
Rogers, Anthony, and James Manwell. "Wind Turbine Noise Issues." (2002). Rpt. in Huskeys, A., and M. Meadors. Wind Turbine Generator Systems Acoustic Noise Test Report. Tech. National Renewable Energy Laboratory. Web.

APPENDIX B: Labview Programs

The inclusion of the Labview Programs is difficult to do inside a MS Word document. The programs are available for review to anyone from Flodesign or Flodesign Wind Turbine working on the noise of Flodesign wind turbines.

Appendix C: Load Analysis of Horizontal Axis and Mixer-Ejector Wind Turbine Towers

Western New England College

School Of Engineering
October 7, 2010

Load Analysis of Horizontal Axis and Mixer-Ejector Wind Turbine Towers

A Summer Internship
By
Christopher Menino

Project Advisor: Dr. Richard B. Mindek, Jr.

Abstract

This work is follow-on work to a senior project already done, which included developing an MS Excel program to calculate the effects of wind loads on turbines and their towers. Calculations were done to assess the loading conditions on turbine towers exposed to different wind conditions. Towers were modeled in MS Excel using standard Fluids theory and in SolidWorks for use in Abaqus for finite element analysis. It was determined that the mixer ejector wind turbine (MEWT) created 1/3 the load on a typical monopole (tubular) tower while creating the same power output as a horizontal axis wind turbine (HAWT). It was also found that the side load of a HAWT was very large compared to the potential drag force due to a cross wind on the shroud of the MEWT. Through FEA analysis, the steel lattice tower design was found to be much better suited to handle any loads or torques compared to the steel tubular tower. Calculations also showed that the MEWT exerted a much smaller torque from gyroscopic loads than the HAWT due to its much smaller mass moment of inertia and overhang.

Introduction

In order to assess the tower load requirements for the MEWT, it was necessary to analyze how various wind turbine towers react to wind loads. Once a system of analysis was created, comparisons were made between the towers as well as the differences between horizontal axis and mixer-ejector turbines. The numbers from these studies were then to be compared to finite element analysis models for accuracy. The original goal was to use data from actual turbine towers to verify the theoretical calculations.

This project started as a continuation of a project by Alec Bennet[(1)]. Bennet created an MS Excel program to calculate the effect of wind on towers, which interface can be seen in Figure 1.

Wind Turbine Tower Analysis

By Alexander Bennet 5/3/2010
verison 9.0 WNEC

FloDesign

INPUTS

Power Rating	100,000	W
Rated Wind Speed	40	ft/s

HAWT			MEWT		
INPUTS		**Unit**	**INPUTS**		**Unit**
Tower Diameter	6	ft	Tower Diameter	6	ft
Height	100	ft	Height	100	ft
Tower Thickness	1.5	in	Tower Thickness	1.5	in
	0.12500	ft		0.12500	ft

RESULTS

HAWT			MEWT		
Stress/Load Results			**Stress/Load Results**		
		Unit			**Unit**
Rotor Area	1,638	ft^2	Rotor Area	546	ft^2
Rotor Diameter	46	ft	Rotor Diameter	26	ft
Single Rotor Length	23	ft	Single Rotor Length	13	ft
Axial Force on Blades	2,768	lb	Axial Force on Blades	923	lb
Base Axial Moment	276,751	lb-ft	Base Axial Moment	92,250	lb-ft
Base Axial Stress	83,372	lb/ft^2	**Base Axial Stess**	27,791	lb/ft^2
	579	lb/in^2		193	lb/in^2

Figure 1: Alec Bennet's MS Excel Program Output

This program was used to calculate properties of a tower under load from a HAWT, such as axial and tangential forces, base axial (thrust) force, and moments about the base. After initial investigations at the beginning of this project, it was found that Bennet's program was incomplete. Therefore, work was undertaken initially to update the original program. Therefore, a new version of the MS Excel program was created with options included to analyze MEWT's side loading (from a cross wind), HAWT's with blade weight included, drag loads due to wind on the monopole tower, and gyroscopic loads created from sudden changes in wind direction.

Theory

The main Excel program developed is made up of inputs and outputs in which users can input values for power rating, wind speed, tower diameter, tower height, and tower thickness. The program then returns values for rotor area, rotor diameter, rotor length, axial force, axial moment, and axial stress. The HAWT has 3 blades which rotate freely with no shroud. The MEWT is a shrouded turbine with several blades. To calculate the swept area of either wind turbine, the following sets of equations are used,

$$\dot{w}_{ideal\ (HAWT)} = \frac{1}{2}\rho A_R V_1^3 \qquad \dot{w}_{ideal\ (MEWT)} = \frac{3}{2}\rho A_R V_1^3 \qquad \text{(Eq. 1 – a, b)}$$

$$\dot{w}_{\max\ (HAWT)} = \frac{1}{2}\rho A_R V_1^3 C_p \qquad \dot{w}_{\max\ (MEWT)} = \frac{3}{2}\rho A_R V_1^3 C_p \qquad \text{(Eq. 2 – a, b)}$$

$$A_{R-HAWT} = \frac{2\dot{w}_{max}}{\frac{\rho}{32.2}V_1^3 C_p} \qquad A_{R-MEWT} = \frac{2\dot{w}_{max}}{3\frac{\rho}{32.2}V_1^3 C_p} \qquad \text{(Eq. 3 – a, b)}$$

where:

ρ is the density of the fluid.
A_R is the swept rotor area.
V_1 is the initial fluid velocity.
C_p is the maximum betz efficiency.
$\dot{w}$ is the power.

These equations are derived from conservation of energy through a control volume around the turbine. The rotor diameter and rotor length are found using the following equations,

$$A_R = \frac{\pi D^2}{4} \qquad \text{(Eq. 4)}$$

$$D = 2\sqrt{\frac{A_R}{\pi}} \qquad \text{(Eq. 5)}$$

$$L = \frac{D}{2} \qquad \text{(Eq. 6)}$$

where:

D is the diameter of the rotor.
L is the length of the rotor blade.

Next, the axial (thrust) force on the HAWT and MEWT is found by using the next set of equations shown below,

$$F_{ax} = (P_{3-}P_2)A_R \qquad \text{(Eq. 7)}$$

$$(P_{3-}P_2) = \frac{1}{2}\left(\frac{\rho}{32.2}\right)(V_4^2 - V_1^2) \qquad \text{(Eq. 8)}$$

$$F_{ax} = \frac{1}{2}\left(\frac{\rho}{32.2}\right)\left[\left(\frac{1}{3}V_1\right)^2 - V_1^2\right]A_R \qquad \text{(Eq. 9)}$$

The axial force that occurs on the wind turbine creates a moment at the base of the tower. This moment creates a certain amount of stress at the base of the tower which can be described by the following equations,

$$M_{ax} = F_{ax}(h) \qquad \text{(Eq. 10)}$$

$$\sigma_{ax} = \frac{M_{ax}(r_{tower})}{\left(\frac{\pi}{4}\right)[r_{out}^4 - (r_{out} - thickness)^4]} \qquad \text{(Eq. 11)}$$

where:

h is the height of the tower.
r_{tower} is the outer tower radius.
thickness is the tower thickness.

Research was also done in the areas of different types of towers, such as monopole and lattice towers, and how they react to wind as well as cost and feasibility. It was necessary to understand how different towers would affect pricing and the environment.

After research was completed on towers, tangential and centrifugal forces were investigated using the free body diagrams in Figure 2.

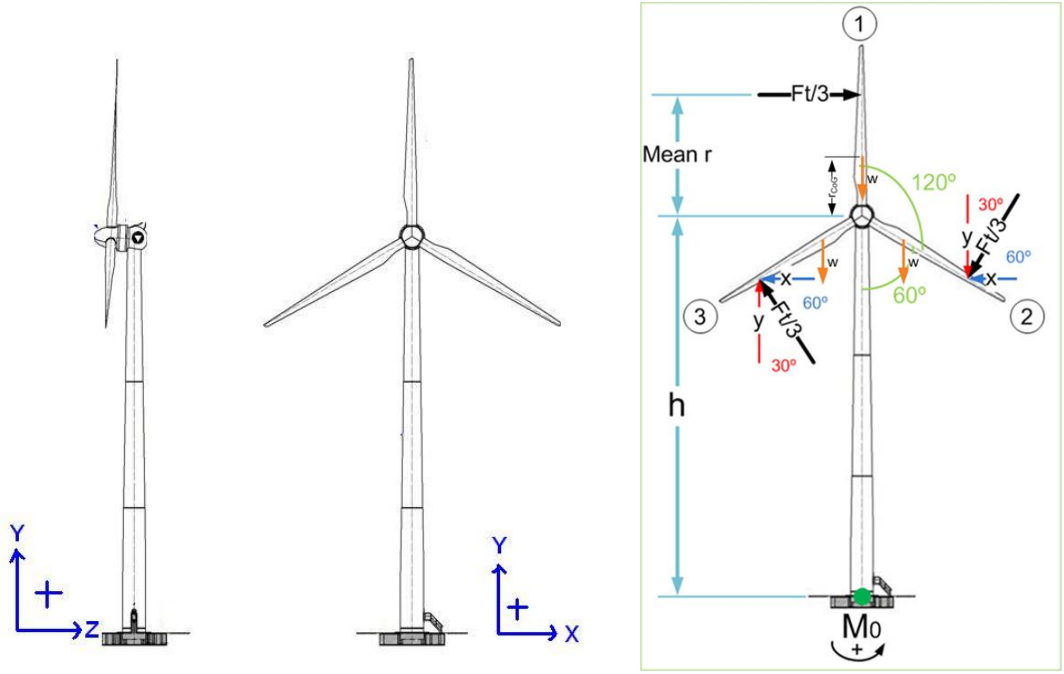

Figure 2: Turbine Free Body Diagram

In order to prove the centrifugal forces of the horizontal axis wind turbine blades cancelled, the forces in each direction were summed.

$$\sum F_x = 0 \qquad \text{(Eq. 11)}$$

$$\sum F_y = 0 \qquad \text{(Eq. 12)}$$

The tangential forces on the blades create a moment on the tower which can be described by the two equations below.

$$M_{ytan} = (-Fcos\theta)([\bar{r}cos\theta] + h) \qquad \text{(Eq. 13)}$$

$$M_{xtan} = (-Fsin\theta)(\bar{r}sin\theta) - W(r_{COG}cos\theta) \qquad \text{(Eq. 14)}$$

where:

$\bar{r}$ is the average radius of the blades.
r_{COG} is the distance to the center of gravity of the blades.

Unlike the HAWT's, the MEWT's have small tangential moments on the blades due to the shroud. Instead, a side load due to cross wind over the shroud can create drag, putting a side load on the tower. In order to calculate this drag, equation 15 and Figure 3 were used, as follows,

$$F_D = \frac{1}{2}\rho V^2 C_D A \qquad \text{(Eq. 15)}$$

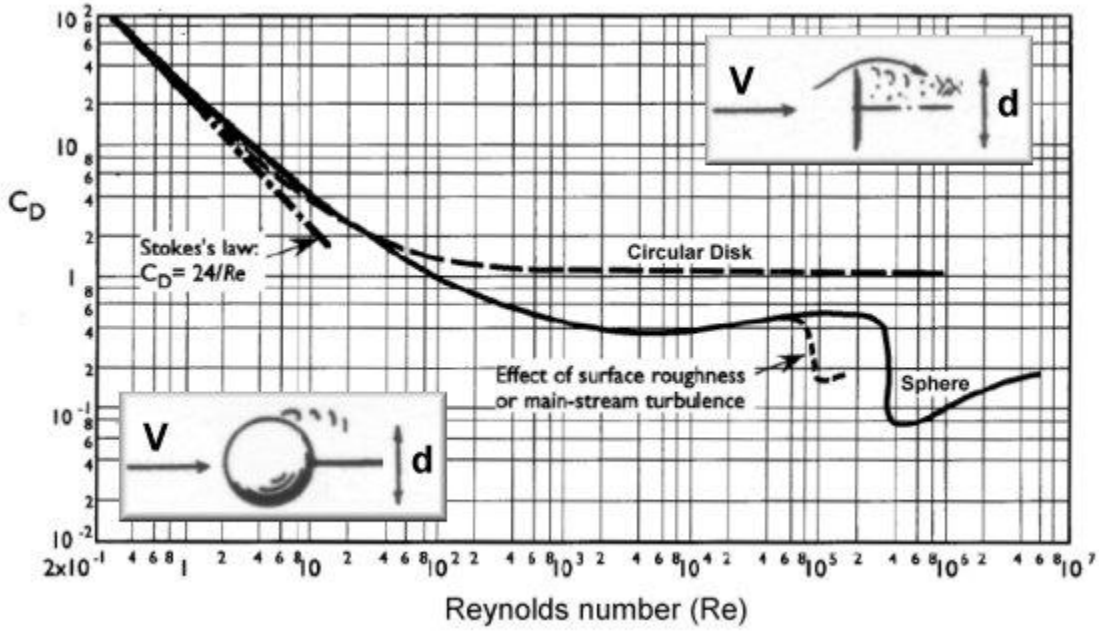

Figure 3: Drag Coefficient vs. Reynolds Number

where:

ρ is the density of the air.
V is the velocity of the air.
A is the cross sectional area.
C_D is the drag coefficient found in the following figure.

In order to find the gyroscopic loads on the tower due to a sudden change in wind direction for either the HAWT or MEWT, the following equations were used from basic Solid Mechanics theory[5],

$$L = \overrightarrow{|L|} = I\overrightarrow{|\omega|} \qquad \text{(Eq. 16)}$$

$$V_p = (\omega_p)(r_p) \qquad \text{(Eq. 17)}$$

$$\tau = (L)(V_p) \qquad \text{(Eq. 18)}$$

where:

L is the angular momentum due to the blade/rotor inertias and their angular velocities.

I is the mass moment of inertia of the spinning blades (HAWT) and/or rotors (MEWT).

ω is the angular velocity of the spinning blades (HAWT) and/or rotors (MEWT).

$V_P$is the velocity of procession of the blades CG (HAWT) or turbine rotors CG (MEWT) about the tower axis due to a sudden change in wind direction (yaw).

$\omega_p$is the angular velocity of procession of the blades CG (HAWT) or turbine rotors CG (MEWT) about the tower due to a sudden change in wind direction (assumed to be 2 degrees / second).

$r_P$is the overhang radius of the blades CG (HAWT) or turbine rotors CG (MEWT) about the tower axis.

τ is the torque created by gyroscopic forces.

Experimental Procedure

The purpose of the new MS Excel program was to allow the user to input known variables such as power, wind speed, and tower dimensions, and receive variable outputs for the horizontal axis and mixer-ejector wind turbines and their towers. The initial page calculates and compares information about the two turbines assuming they are mounted on a 100 ft. steel tubular monopole with a 2 ft. diameter. Equations 1 through 11 were used to determine how the towers will react under load, as shown in Table I. Input values (in green) assume a 100 kW output for both the HAWT and MEWT at a wind speed of 40 ft/s (27 mph) and a monopole tower height of 100 feet. Output values (in blue) predicted by the MS Excel program include swept area, rotor diameter, rotor length, axial force, axial moment (rearward, about x-axis), bending stress at the tower base due to the thrust force, and blade weight for the HAWT only. The specific results shown in Table I will be discussed in the Results and Discussion section of this report.

Table 1: Revised / New MS Excel Program Output

HAWT		
Inputs		
Power Rating	100,000	Watts
	73,756.00	ft-lbs/s
Rated Wind Speed	40	ft/s
Tower Diameter	2	ft
Tower Height	100	ft
Tower Thickness	1.5	in
	0.125	ft
Density		
Default is air at 70°F	0.0765	lb/ft^3
	0.0024	lb_m/ft^3
C_{pBetz}	0.593	
Outputs		
Swept Area	1,636.01	ft^2
Rotor Diameter	45.64	ft
Rotor Length	22.82	ft
Axial Force	2,763.95	lb
Moment (Axial)	268,967.43	ft-lbs
Stress (Axial)	827,561.07	lb/ft^2
Blade Weight	2475.85	lbs
HAWT Blade Offset	3	ft

MEWT		
Inputs		
Power Rating	100,000	Watts
	73,756.00	ft-lbs/s
Rated Wind Speed	40	ft/s
Tower Diameter	2	ft
Tower Height	100	ft
Tower Thickness	1.5	in
	0.125	ft
Density		
Default is air at 70°F	0.0765	lb/ft^3
	0.0024	lb_m/ft^3
C_{pBetz}	0.593	
Outputs		
Swept Area	545.34	ft^2
Rotor Diameter	26.35	ft
Rotor Length	13.18	ft
Axial Force	921.32	lb
Moment (Axial)	92,131.66	lb-ft
Stress (Axial)	283,471.41	lb/ft^2

Next, tower research was conducted with the goal of finding comparisons between various tower types. This comparison gave information about the towers, some pros, some cons, and also a price comparison. This chart can be found in Figure 4 shown below.

The HAWT's blades are spaced equally apart. Spinning objects create centrifugal forces, but due to the spacing of the blades, the centrifugal forces should cancel out. To prove this, equations 11 and 12 were used for each blade.

The tangential forces on the HAWT were found by using equations 13 and 14. These equations determine how forces acting tangential to the spinning blades create side loads and, as a result, moments on the turbine and tower. In order to get a single moment on the tower, the moment created from each blade was summed as all the blades completed a single revolution.

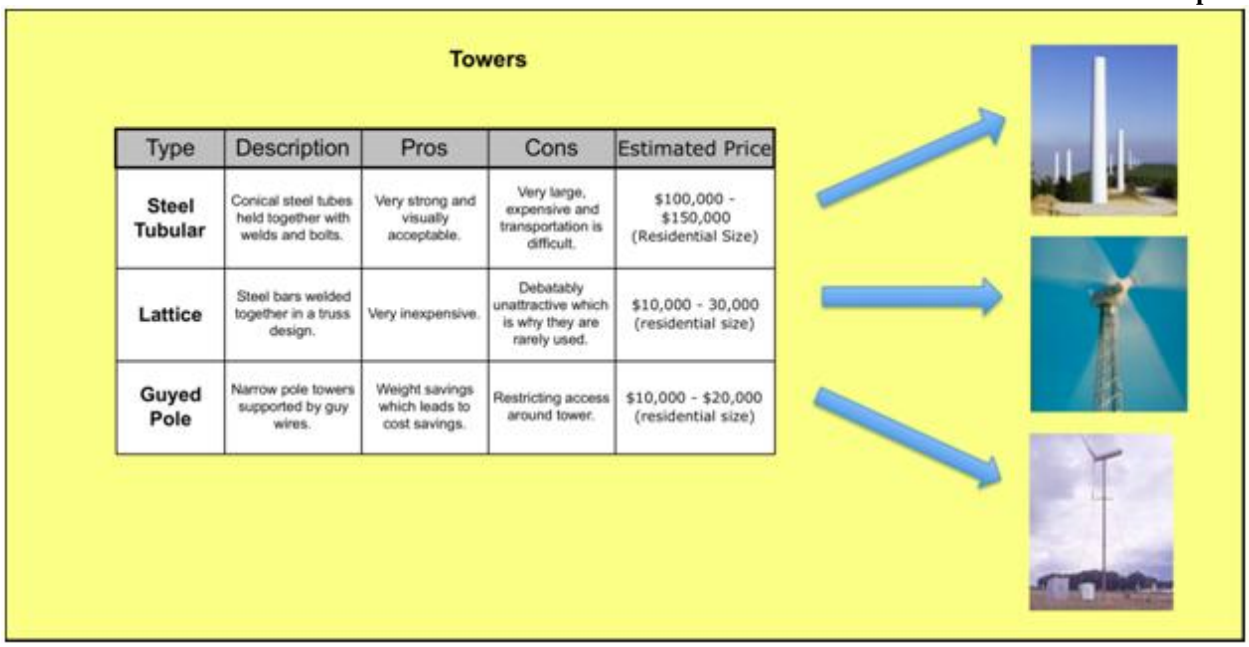

Figure 4: Tower Comparison Research[(1)(2)]

Again, HAWTs require consideration of the tangential forces creating side loads on the blades. The MEWTs, however, require that drag on the side of the shroud body be considered. This drag is calculated using equation 15 along with Figure 3. The drag of the towers themselves must also be taken into account and is calculated using the same drag equation (eqn. 15). The main difference in calculations is the tower is slightly conical so the drag load is calculated in sections and then summed.

In order to start work on the finite element analysis portion of the project, tutorials were completed for the Abaqus program. The tutorials cover the fundamentals of the program and taught how to pre-process, change material properties, partition, seed, mesh, apply boundary conditions, and post-process. Images from the work done can be seen in Figures 5 and 6 below.

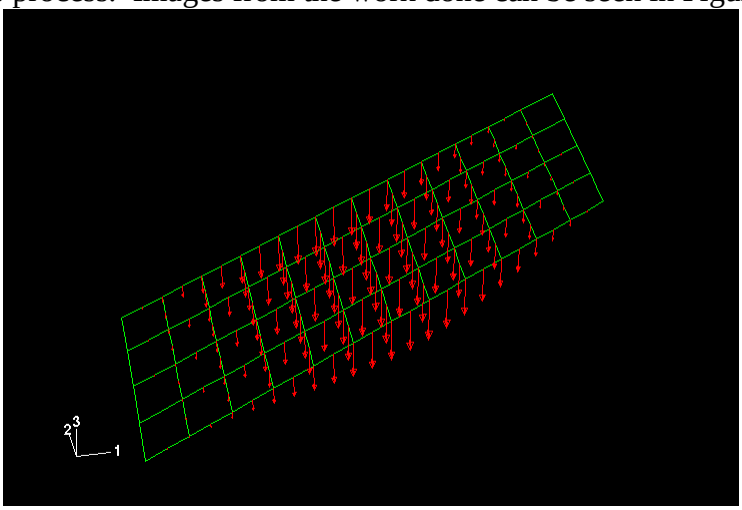

Figure 5: Abaqus Tutorial, distributed load on pinned plate

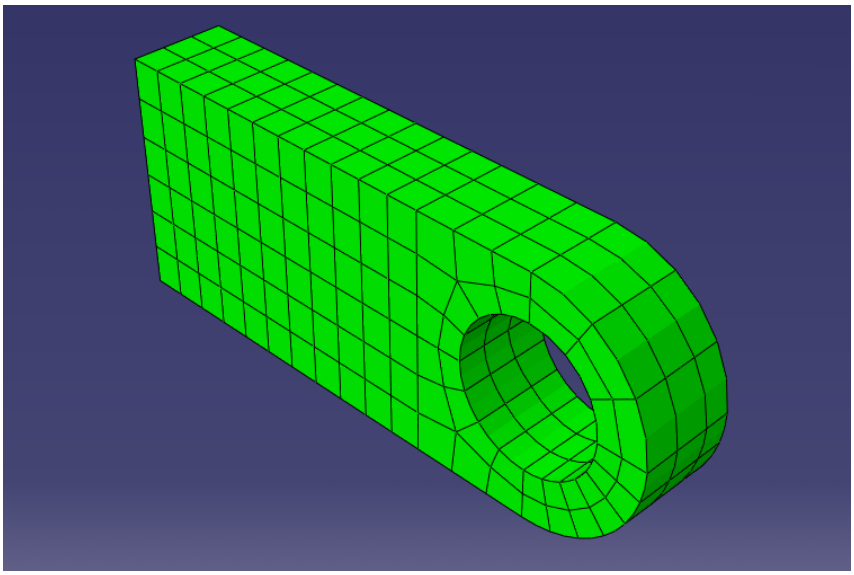

Figure 6: Abaqus Tutorial, lug hole loading model

After completing the Abaqus tutorials, work was started on modeling a steel tubular monopole for the 100 kW HAWT, and lattice tower for the 1 kW MEWT. The models were first created in SolidWorks with the monopole being 100 ft tall and the lattice tower being 75 ft tall.

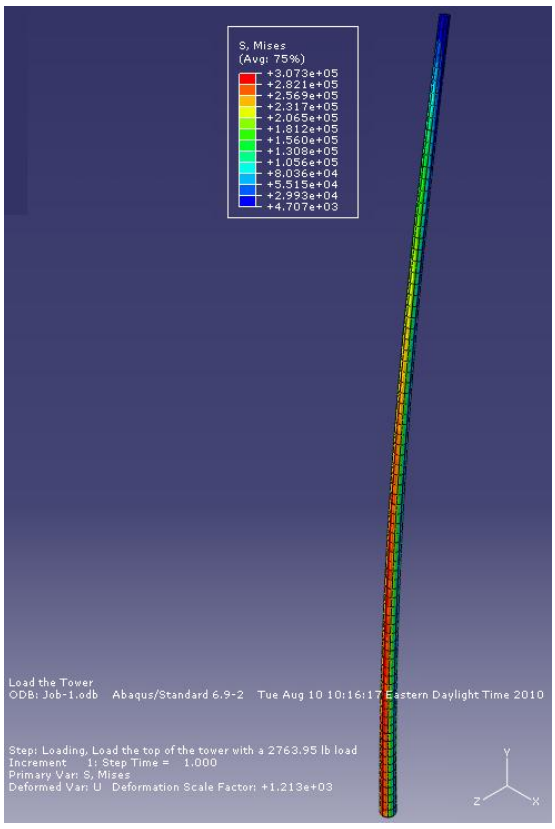

Figure 7: Steel Monopole FEA (100 kW HAWT)

These heights are based on actual towers used for a 100 kW HAWT and the 1 kW MEWT prototype (Briza) currently undergoing field tests by FloDesign Wind Turbines. After solid modeling, the towers were then imported into Abaqus where they were seeded and meshed for a loading simulation. These models can be found in Figures 7 and 8.

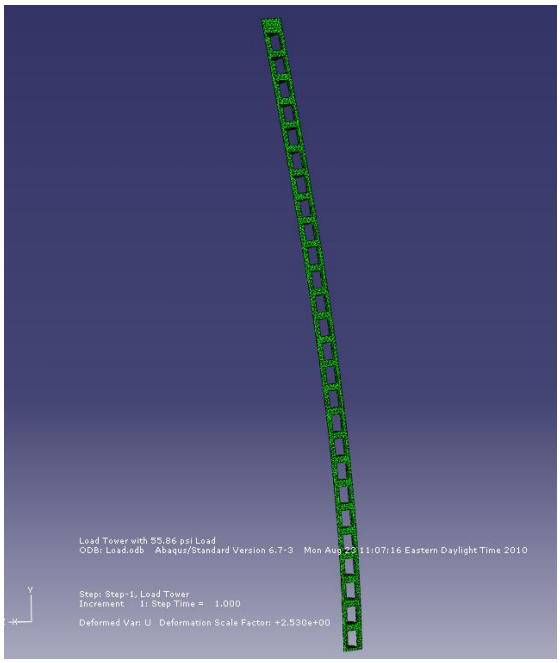

Figure 8: Steel Lattice FEA (1 kW Briza Tower, 100 kW MEWT)

The gyroscopic loads possible on the turbines and towers due to a sudden change in wind direction (yaw) in wind were of interest, so a comparison study was done to compare the torque created on the tower for both the HAWT and MEWT. This was done by first using equation 16 to find the angular momentum of the blades (HAWT) or rotors (MEWT). Next, equation 17 was used to find the linear velocity of the CG of the HAWT and/or MEWT based on an assumed 2 degree per second yaw rate and the respective overhangs of each wind turbine (3 ft. for the HAWT and 3 inches for the MEWT). And finally, equation 18 was used to find the torque about an axis perpendicular to the plane of blade/rotor rotation, in the direction of rotation (i.e., assuming clockwise spinning blades/rotors as viewed from the rear, a CCW yaw would create a backwards rotation of the turbine/tower about the x-axis, and a CW yaw would create a forward rotation of the turbine/tower about the x-axis, as defined in Figure 2). The torque values due to gyroscopic loading were then compared for each turbine.

It is also worth noting that the Excel program was continually updated throughout this project with information and calculations which can be used again to calculate new values for these theoretical calculations. The final program can calculate loads and stresses on HAWT and MEWT turbines, drag on both turbines and towers, side loads, and centrifugal forces created.

Results and Discussion

When comparing a 100 kW HAWT versus 100 kW MEWT, both were considered to be subjected to wind at 40 ft/s (27 mph). The monopole tower diameters were both 2 ft wide with a height of 100 ft and a wall thickness of 1.5 inches. Given this information, the MS Excel program determined, as shown in Table I, that the swept area of the HAWT had to be 3 times larger, from control volume theory, at 1636 ft^2, relative to the MEWT at 545 ft^2. The program also predicts an axial thrust force of 2764 lbf, a rearward (about the x-axis) moment of 268,967 ft-lbf, and bending stress at the tower base of 827,561 lb/ft^2 (5747 lbf/in^2) for the HAWT. For the MEWT, an axial thrust force of 921 lbf, a rearward (about the x-axis) moment of 92,131 ft-lbf, and bending stress at the tower base of 283,471 lb/ft^2 (1968 lbf/in^2) is predicted.

The research done on different tower types yielded mixed results in terms of which tower was the best choice. It was determined that each tower has flaws in terms of price, weight, or harm to the environment. All towers also had benefits such as low price, low weight, or ease of use. A summary of these results can be found in Figure 4 on page 8. In general, which tower is best depends on cost, aesthetics, transportation issues, and space available.

The centrifugal forces created by the horizontal axis wind turbine were calculated using equations 11 and 12 on page 5. These calculations proved that when all the blades centrifugal forces were summed in each direction, they cancel each other out in the horizontal (x-axis) and vertical (y-axis) directions. This creates a stable turbine with no moments due to these forces. If one of the blades were to break while spinning however, this would make a catastrophic, unbalanced turbine. No analysis was done to determine if or how long the towers could endure such an unbalanced situation.

The tangential forces on the 100 kW HAWT due to blade pitch were found to create a side (about z-axis) moment on the turbine hub of 10,137 ft-lbs, corresponding to a moment of 1,013,740 ft-lbs at the base of the tower. The moments created by each blade as well as the total moment on the tower hub are shown in Figure 9 below.

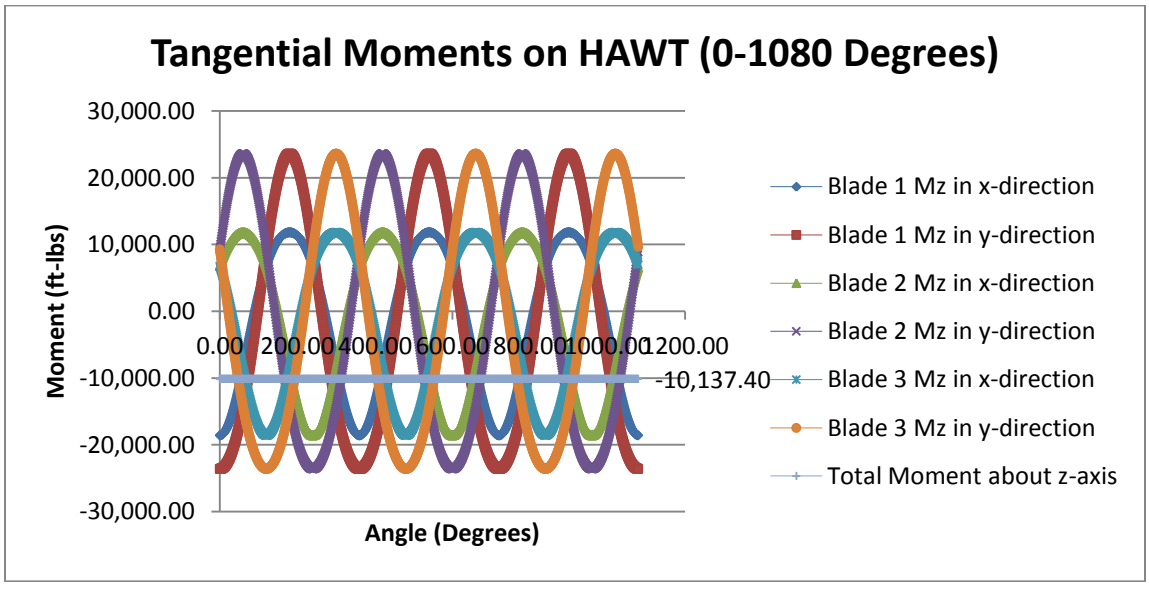

Figure 9: Tangential and Total Moments for HAWT

As a comparison to the tangential forces on the 100 kW HAWT, the 1 kW MEWT was assumed to have a side load (drag due to wind flow around a cylinder), which created a moment

about the tower base. This side moment (about the z-axis) was found to be 79.4 ft-lbs when the wind was hitting the nacelle at 40 ft/s (27 mph) corresponding to a Reynolds number of 10,000. If power is assumed to be directly proportional to diameter, then based on these results a 100 kW MEWT would have a side moment of about 7940 ft-lbs, which is comparable to the HAWT's side moment of 10,137 ft-lbs (see Figure 9), assumed to be due to the tangential force on the blades when the HAWT generates power.

The drag calculated due to wind flow around the 100 ft tall tubular tower itself was not as great. With the same wind conditions used as in the Briza side load (drag) calculation, but now in the thrust direction (z-axis), the tubular tower had a 8709 ft-lb moment (i.e. rearward, about the x-axis). Again, this assumes a tubular tower with a conical type shape, starting with a base of 2 feet in diameter and ending at 1 foot in diameter at the top.

After completing tutorials in Abaqus, the 100 ft tubular tower was created in SolidWorks and imported into Abaqus for a finite element analysis. After running the simulations, the tower had a displacement of 13.4 inches from its original position at the top when 100 kW HAWT conditions were assumed. This displacement was caused by a 55.9 psi shear traction load at the top with the bottom constrained. This shear traction load created a 2764 lb force at the top of the tower, which is what the MS Excel program calculated for an axial load at a wind speed of 40 ft/s for the HAWT (Table I). The FEA output for this model is shown in Figure 10.

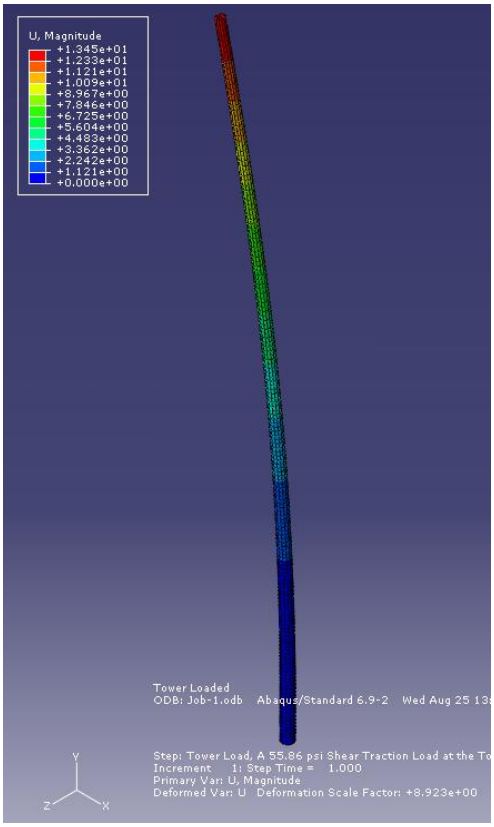

Figure 10: Steel Tubular FEA Displacement (100 kW HAWT)

The tubular tower was then compared against a simulation with a steel lattice tower used currently to support the Briza. This tower was also constrained at the bottom and loaded with a

2.53 psi shear traction force to simulate a 40 ft/s (27 mph) wind load. This shear traction force created a total load of 921 lbs at the top of the tower, which is also what the MS Excel program predicted for that turbine in winds of 27 mph for the 100 kW MEWT. This created a displacement on the tower of 1.82 inches, much less than the 100 kW HAWT mounted on a steel tubular tower. The FEA output from the 100 kW MEWT model is shown in Figure 11.

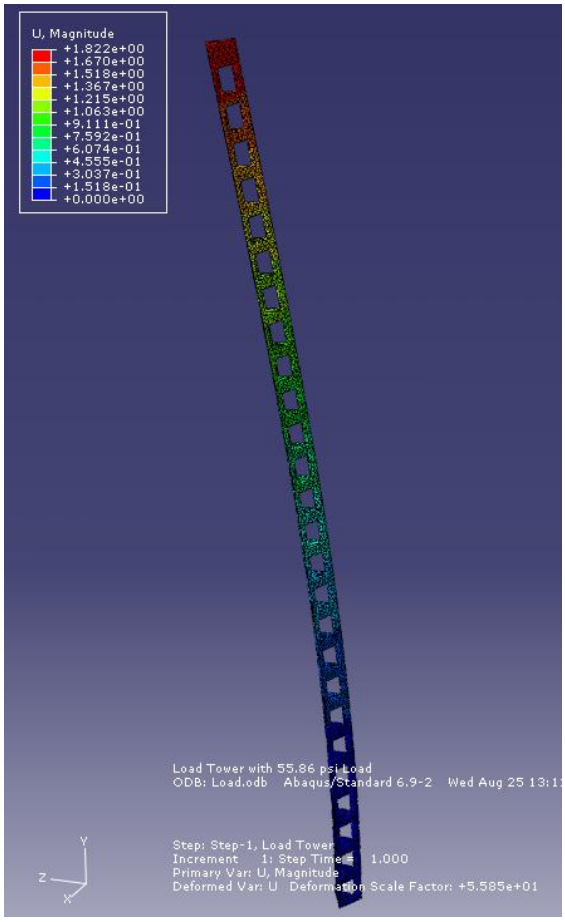

Figure 11: Steel Lattice FEA Displacement (1 KW Briza Tower, 100 kW MEWT)

More can be done with finite element analysis in terms of creating a more realistic and complicated lattice tower model, and analyzing both towers for stress and strain, in addition to the displacement analysis done here.

To compare gyroscopic effects on the turbines, calculations were done to find the resulting torque, using equations 16 through 18 on page 6. These calculations took into account the mass moment of inertia of the spinning blades/rotors of each turbine, as well as their angular and precession velocities. It was found that a 100 kW HAWT at an assumed yaw rate of 2 degrees per second resulted in a gyroscopic torque of 845,967 ft-lbs. A 1 kW MEWT under the same conditions resulted in a gyroscopic torque of 34 ft-lbs. If it is assumed that angular momentum and the resulting gyroscopic torque scales directly with wind turbine power, then a 100 kW MEWT would still result in a much lower gyroscopic torque relative to the three-bladed

HAWT, primarily because of the smaller CG overhang from the supporting tower, rotor mass, and mass moment of inertia of the MEWT relative to the HAWT.

Conclusions

The MS Excel program, which was originally created by Alex Bennet, had some simplifying assumptions in it, such as not including the weight of the turbine blades into the HAWT axial moment calculation, no side load (drag) calculation for the MEWT, and no tower drag or gyroscopic loads considered. These issues were addressed in the revised/new MS Excel program and, using the same loads as used in the Excel model, tower displacements obtained from FEA models of both the monopole and Briza towers give reasonable results. It is clearly seen from the Excel model results that the MEWT is roughly three (3) times smaller than the HAWT, while producing the same amount of power. It also creates 1/3 of the load on whatever tower it happens to be mounted to at an assumed wind velocity of 40 ft/s (27 mph).

The side loads created by the tangential forces on the HAWT seem to be large and could potentially pose the risk of damaging the turbine or the tower. The MEWT does not have tangential loads on the blades due to the shroud. However, the moment created from air flow at 27 mph across the nacelle is comparable to the moment due to tangential forces across the HAWT blades. The drag created on the tower itself from the wind is also a factor, although the moment it produces is measurably less than the side load of either wind turbine.

It was found that the gyroscopic torque of a 100 kW HAWT at an assumed yaw rate of 2 degrees per second is at least an order of magnitude large than a comparable 100 kW MEWT. This is primarily due to the smaller CG overhang from the supporting tower, rotor mass, and mass moment of inertia of the MEWT relative to the HAWT.

Comparing the steel tubular tower with the Briza's steel lattice tower, the lattice tower is the clearly stronger. Aside from having a clear weight advantage, the lattice tower has a much more durable design, which can handle heavy loads while keeping price and weight to a minimum. Of course, the tower design should also be chosen based on the location of the turbine and consider any wild life that might be in the area. This comparison does not take into account a smaller, less costly monopole tower supported by guy wires.

Recommendations

It is recommended that whatever turbine is used is mounted on the appropriate tower for the location. However, the steel lattice tower paired with the mixer-ejector wind turbine make an ideal pairing of energy production with minimal cost, weight, and tower load.

More work should be done in refining the Excel program as well as making it more realistic, such as the load on a tower in a strong storm. Again, more can be done with finite element analysis in terms of creating a more realistic lattice tower model. Eventually, data should be collected from actual turbines to compare with the Excel and model data for accuracy. These comparisons can be used to refine the program and model data which will lead to more accurate results and data which can be used for future turbines. A more detailed study of monopole tower loads (relative to that performed by Alec Bennet) when guy wires are employed is also recommended.

References

1. Bennet, Alec, *Design and Research of Wind Turbine Tower Loads*, ME 440, Senior Design Project, Western New England College, Springfield, MA, Spring 2010.

2. "Wind Turbine Design Cost and Scaling Model." Web. www.nrel.gov/wind/pdfs/40566.pdf, July 2010.

3. FloDesign Wind Turbine Final Report for Briza

4. Mindek, Richard, "Gyroscopic Forces," Lecture, Western New England College, Springfield, MA, August 2010

5. Mikey. "Basic gyroscope equations." Gyroscopes. 2 February 2007

   <http://www.mariner.connectfree.co.uk/html/gyro.htm>.

Appendix D: Dynamic Fatigue Analysis of Turbine Mount Using Dynamic FEA Analysis

By: Christopher Baltazar
Advisor: Dr. Glenn Vallee
Summer 2010

Table of Contents

Abstract 3
Purpose 3
Introduction 3
Theory 7
Experimental Procedure 8
Results and Discussion 16
Conclusion 16
Appendices 17

Abstract

FloDesign Wind Turbine is a company working on improving wind energy, mainly the redesign of the conventional three bladed propeller turbines. Their design is known as the Mixer Ejector Wind Turbine. It is much more efficient and smaller than the existing types of turbines. Currently there is one working prototype known as the Briza and is rated for 1000 watts. The turbine sits upon a mount that couples it to the tower and controls the yaw. This mount is the focus of this report.

To begin analyzing the structural integrity of the mount, Finite Element Analysis (FEA) would be used on a part known as the Load Beam. This piece is equipped with strain gages and is used to determine the loads on the turbine. Using FEA and applying the critical loads caused by an 80 mph wind, the strength of the load beam was determined. It was found that the highest stress at an angle of 225 degrees was 53,020 psi. The yield stress of the material is 40,000 psi. This means that the part needs more attention to determine if it is a potential failure point.

Purpose

The desire of this project is to develop a Finite Element Analysis (FEA) model of the Briza wind turbine tower mount. This is the apparatus that connects the wind turbine to the top of the tower and controls the yaw (Appendix 1). The components of the mount will be analyzed to determine structural integrity, ensuring no potential failures in the design exist.

Introduction

The FloDesign Wind Turbine is a great advancement in the wind energy field. The new mixer ejector design greatly increases the efficiency of the turbine. This is done by increasing the amount of power extracted from the fluid flow, therefore increasing efficiency. It has a significant advantage over the conventional three bladed propeller type turbines. FloDesign currently has a prototype in working order that has been installed in Rutland, Massachusetts. This turbine is known as the Briza and is rated for 1000 watts.

The Briza is mounted on top of an 80 foot collapsible tower with three guide wires for stability seen in Figure 1.

Figure 1: Briza Prototype in Rutland

In between the tower and the Briza is the turbine mount that is the main focus of the project. This mount consists of a small electric motor and appropriate gearing which controls the yaw of the turbine, see appendix 1 for photos. Mounted at its base is the load beam which has been instrumented with strain gages in order to determine the loads that the turbine is subjected to (Figure 2).

Figure 2: Load Beam Instrumented with Strain Gages

The load bearing capabilities of this piece were to be investigated along with the subsequent stresses that are induced. This is a critical component in the tower mount because the yaw assembly and turbine sit atop this piece. To determine the resulting stresses a finite element analysis program called Abaqus was used.

Abaqus is a powerful engineering simulation program that utilizes the finite element method, to solve anything from simple linear analysis to the most complex nonlinear jobs. Finite

element method is a numerical technique for finding approximate solutions to partial differential equations as well as integral equations. This routine is what allows Abaqus to solve very complex problems relatively easily. It has the capability of modeling several different types of materials such as, metals, rubbers, polymers, composites, reinforced concrete, etc. The program includes an extensive library of elements that allows for the modeling of complex components.

The components can be either drawn in Abaqus using the sketch module or imported from a 3D modeling program, such as SolidWorks. The model can then be assigned a material type. This is done by creating a material and specifying if it is elastic or plastic. The final step is to input the applicable material properties such as, Modulus of Elasticity, Poisson Ratio, etc. The part that is being analyzed is divided into elements with nodes at each of its corners. These elements can be assigned different types in order to create an accurate mesh. The accuracy of the part mesh is critical to obtaining accurate results in the analysis. A mesh can range from coarse to fine, referring to the number of elements along each edge of the part. The finer the mesh, generally the more accurate the results will be. Having this type of accuracy causes the job to have to run for a longer time. Therefore the mesh refinement is reduced in areas were the stress is known to not be that significant. It is important to increase it in high stress areas like, bolt holes, fillets, and sharp corners. The types of elements that are utilized in the routine are also an important factor in the certainty of the results. The two most common types of elements are linear and quadratic. Linear elements are 8-node bricks where as quadratic are 20-node bricks. The 20-node type are more accurate than the 8-node because the computation is more extensive with twenty nodes, this causes the job to take longer to complete. Although the time to process is greater the accuracy that is obtained is sometimes required. The next steps would be to apply the appropriate loads and boundary conditions to the model. These need to simulate the actual loading and fixing points of the piece. There are numerous different types of loadings that can be used, for example, concentrated forces, pressures, surface traction, moments, bolt loads, etc. The boundary conditions need to mimic how the part is restrained in its real world application. After all of the necessary steps are taken the job can be submitted and while it is running be monitored for any errors. If the job completes successfully the user can then move on to processing the results. Contour plots showing the resulting stress, strain, reaction forces, and deformation can be viewed. Figure 3 below shows an example of a Von Mises stress contour plot.

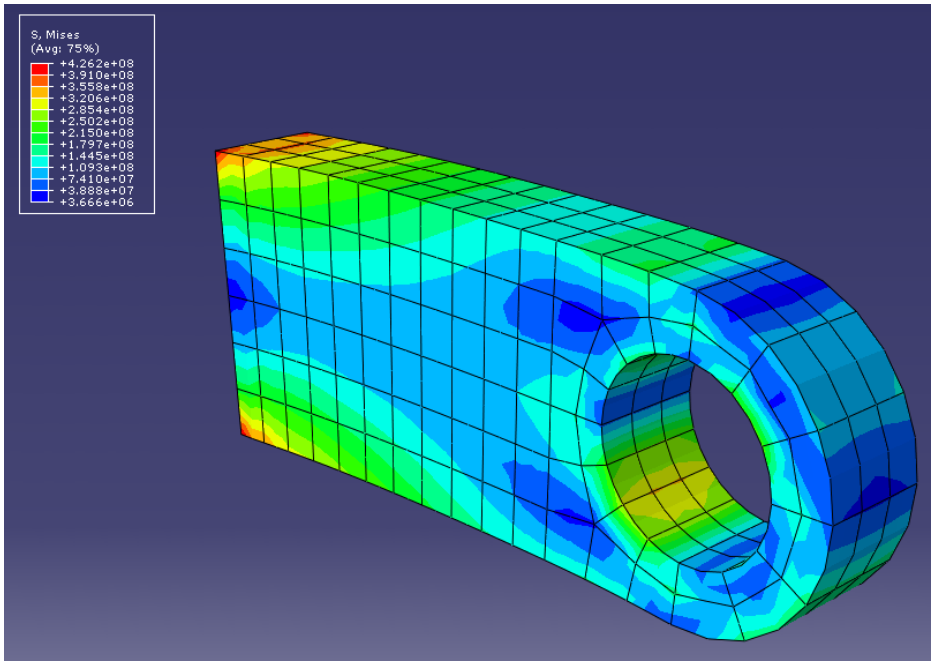

Figure 3: Von Mises Stress Contour Plot

This is a great way of visually interpreting the results that have been obtained, and confirming the highest stress areas. The part can be deemed suitable for the application if the highest stress is below the yield strength of the material. Also knowing these two parameters the factor of safety can be determined. Along with directly viewing the results via contour plots, they can be outputted to data files. These files can then be opened using Notepad or a similar program and evaluated at a later time. The processes described previously are what were used to conduct the analysis on the turbine mount.

Theory

In order to test the strength of the turbine mount, the appropriate loads had to be applied. The loads that were chosen to be applied were the worst case scenario loads. They are the most extreme conditions that the Briza would be expected to be exposed to. The modified free body diagram in appendix 2, shows the forces and moments caused by an 80 mph wind. To simplify the loading these forces and moments were applied as pressures. This made it necessary to convert the forces and moments using the following equation.

$$\boldsymbol{P = \frac{F}{A}}$$

Eq. 1

Where:

P = Pressure (psi)
F = Force (lb)
A = Area (in^2)

The area that was used in the above equation was the projected area of the bolt hole when calculating F_y, F_z, and M_z (Appendix 3). Equation 2 seen below calculates the projected area of a bolt hole.

$$\boldsymbol{PA = L * D} \qquad \textbf{Eq. 2}$$

Where:

PA = Projected Area (in^2)
L = Length of bolt hole (in)
D = Diameter of hole (in)

The magnitudes of the loads mentioned are seen in Table 1.

Table 1: Loads Converted to Pressures

Load	Magnitude (lbs)	Magnitude (psi)
F_y	600.00	266.67
F_z	1200.00	29.70
M_z	590.00 lb-ft	1094.50
M_x	3925.00 lb-ft	767.01

The exact hand calculations made to determine the corresponding pressures of each load can be seen in appendix 3. Having these values now allows for the stress analysis to be executed on the load beam.

Experimental Procedure

The main component of the turbine mount is the load beam (Figure 2). It has been instrumented with strain gages in order to determine the loads on the turbine. The strength of the piece is critical to the turbine not falling to the ground when atop the tower. Therefore extensive FEA must be performed in order to determine that it is suitable. The first step was to construct a 3D model of the load beam. This was done using SolidWorks (Figure 4).

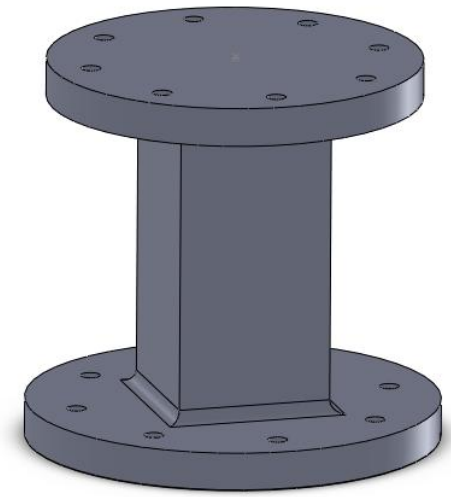

Figure 4: 3D SolidWorks Model of Load Beam

This 3D model can now be imported into Abaqus to be analyzed. The first step in Abaqus was to create the material that the piece is made out of. In this case it is Aluminum 6061-T6 with a Young's Modulus (E) of 9,993,256 psi, and a Poisson Ratio (ν) of 0.33. After assigning the material to the part, and executing the other necessary steps. The mesh could now be created, before meshing, the edges of the model must be seeded. Seeding refers to the number of elements that will be created along each edge. It is increased in high stress areas for more accurate results, in this case around the bolt holes and fillets. Twenty elements were used around the perimeter of the bolt holes and five elements up the fillets. The seeding was reduced in other areas accordingly to cut back on processing time. A tet mesh was utilized for a preliminary evaluation of the strength of the part. The tet mesh uses triangular elements and is automatically created by Abaqus (Figure 5). This is the easiest type of mesh to create but the accuracy obtained is not the kind desired for this analysis.

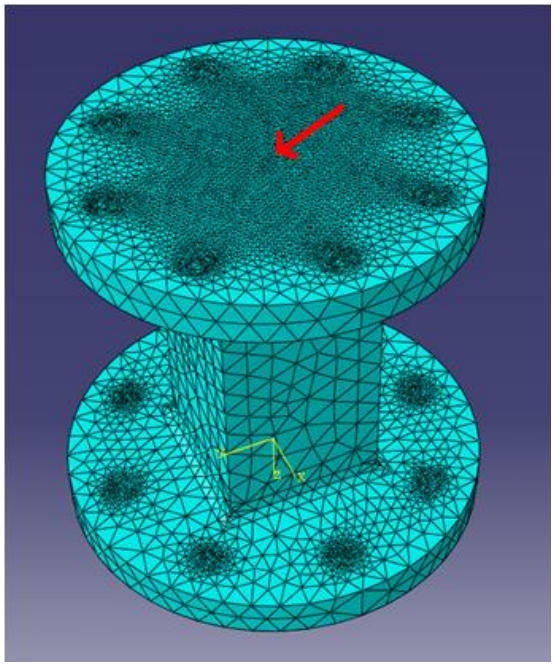

Figure 5: Preliminary Tet Mesh

The red arrow shown above shows the downfall of using the tet mesh. The mesh is overly fine in the center region of the part for no reason. This is not advantageous because it only increases the time for processing the job and does not yield better results. The center of the part is not an area of highest stress therefore this is pointless.

This confirmed the fact that this type of mesh would not be useful for the analysis that was going to be performed. A brick mesh would have to be used, meaning the elements would be rectangular or square in shape. This requires the model to be partitioned into as many rectangular regions as possible, as seen below.

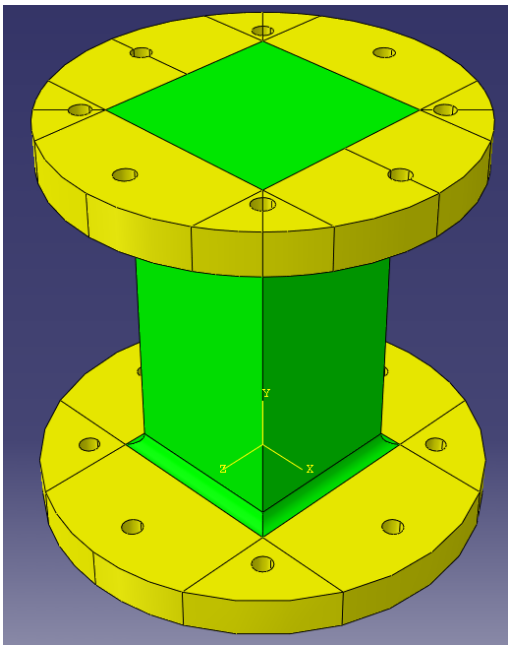

Figure 6: Partitioned Load Beam for Brick Mesh

The mesh controls also need to be changed from tet to hex in order to utilize brick elements, and the technique used needs to be either sweep or structured (Appendix 4). The regions in yellow use a sweep technique and the green areas use structured. A brick type is incredibly more accurate but requires much more effort from the user to execute. In addition to further partitioning the part, the seeding in some regions had to be increased. The seeding in the fillets was set to 7 elements and 20 elements around the bolt holes. The edges of the rectangular region were set to 20 elements. This now allowed for the part to be meshed using a brick element type. The resulting mesh can be seen below in Figure 7.

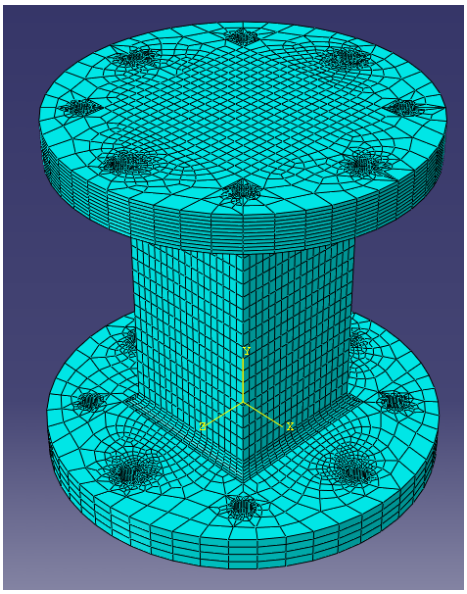

Figure 7: Resulting Brick Mesh

To show that the tet mesh does not produce the same results as a brick mesh a small experiment was performed. The same arbitrary load was applied to both a load beam with a tet mesh (Figure 8) and a brick (Figure 9) to compare results. In this case it was a 100 pound shear traction force, converted to a pressure over the inner surface area of the bolt hole of 113.64 psi. This was applied to opposite holes to simulate a moment (Figure 8, 9).

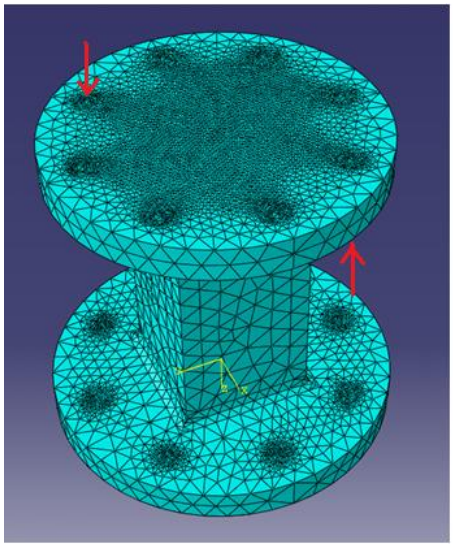

Figure 8: Tet Mesh with Application of Shear Traction Forces

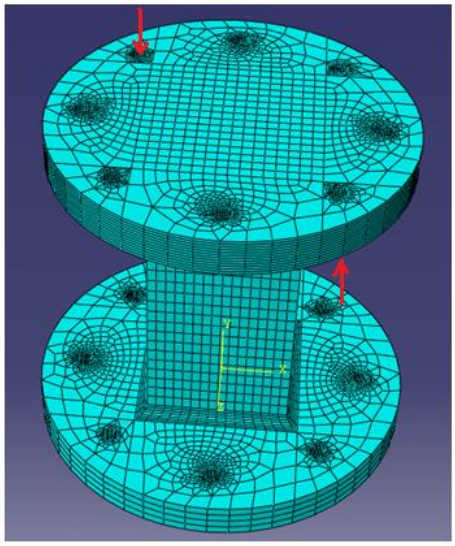

Figure 9: Brick Mesh with Application of Shear Traction Forces

The two different types of jobs were run and the resulting values of stress were compared. Under the loading condition of 113.64 psi described earlier the stresses for the tet and brick model were, 886.2 psi and 656.4 psi respectively. This is a large discrepancy in results considering that it is the same exact model, material, and loading conditions. This further reaffirmed the need for the brick mesh.

Now having the desired type of mesh (Figure 7) and the appropriate loads calculated (Table 1) the analysis could be carried out. As mentioned previously the forces and moments would be applied as pressures. In order to have the pressures mimic the forces and moments they would have to be applied in the correct manner. The wind thrust load (F_y) was applied to half of each bolt hole in a forward direction. To mimic the weight of the turbine (F_z) the equivalent pressure was applied to the entire top area of the load beam. The torsional moment (M_z) was created by applying the pressure to half of the bolt hole area in a clockwise direction. The bending moment (M_x) was applied to two opposite surfaces of the load beam, one bottom surface and one top surface. A diagram depicting the application of the loads can be seen below. The boundary conditions applied were that the bottom piece was "Encastre," meaning it was fixed from any translation or rotation.

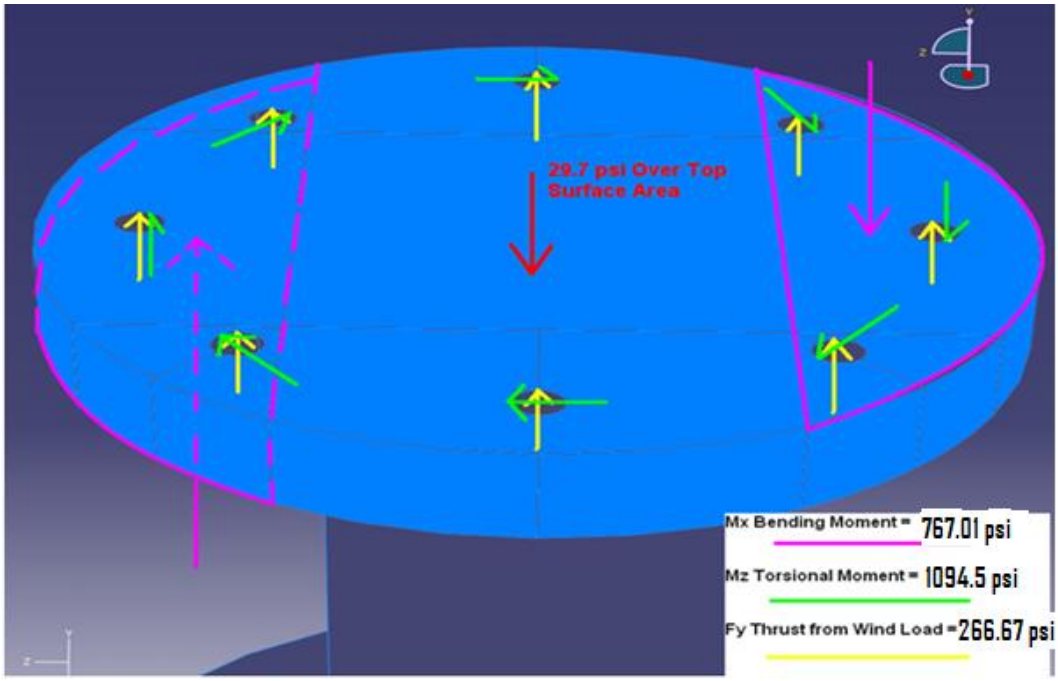

Figure 10: Application of the Forces and Moments

The loading scenario described above is for a loading of zero degrees. This means that the wind is blowing directly at the turbine. To account for the yawing of the turbine the loads would have to be applied at different angles to see how the stress then varies.

It was decided that the loads would be applied in 45 degree increments. This meant that the part would have to be partitioned into 45 degree sections. The partitioning can be seen in Figure 11.

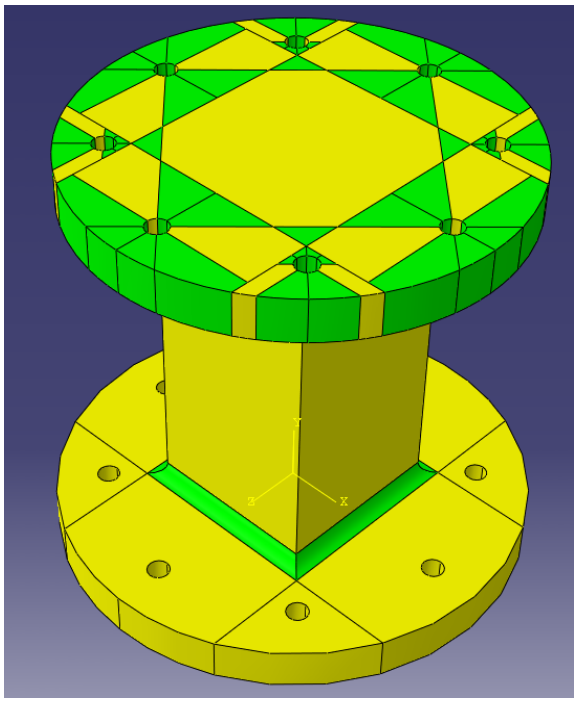

Figure 11: Partitioned in 45 Degree Increments

The part had to be re-meshed because of the partitioning that was done. Before the part was re-meshed the seeding was refined in the important areas. It was changed along the edges of the rectangular region, up the fillet, and around the bolt holes. The number of elements used was switched to 30, 14, and 20 respectively. The appropriate changes can be seen in Figure 12.

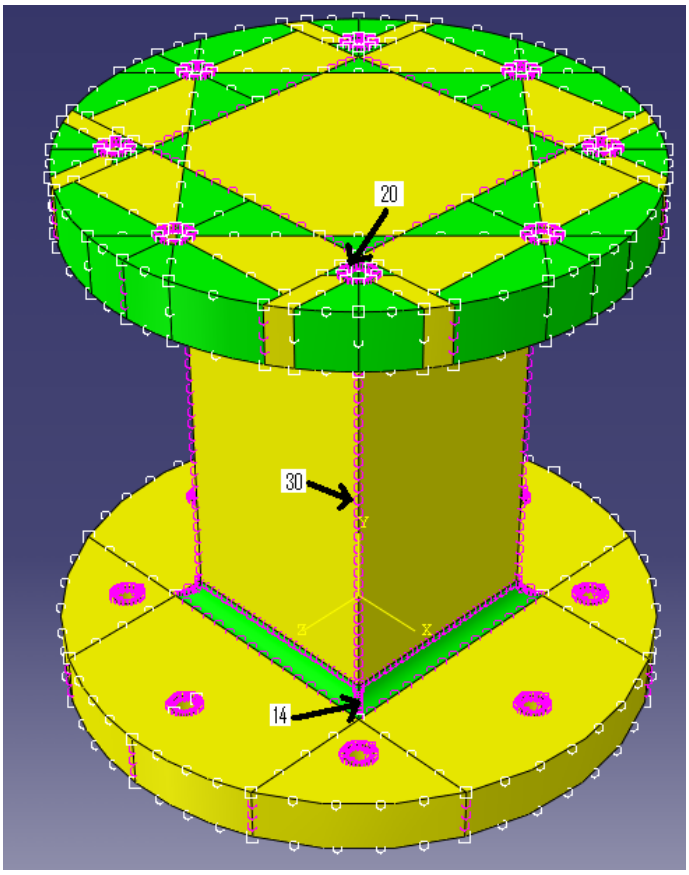

Figure 12: Seeding of the Part

Now that the seeding was re-worked for the final time, the element type to be used was decided upon. There was a choice between choosing the use of 8 node linear brick elements, or 20 node quadratic bricks. The 20 node bricks would produce more accurate results but would take much longer to run the analysis. To decide which would be the best to utilize a test was carried out. The loads seen in Table 1 where applied at zero degrees and the jobs were run using the 8 and 20 node elements and the resulting stresses were compared. The resulting stresses where 42,710 psi and 45,000 psi respectively. These results were very close therefore it was not necessary to use 20 node elements. This was very helpful because the 8 node analysis only took 3 minutes to complete whereas the 20 node took 35 minutes. Using the 8 node method would help to complete the jobs much quicker. Now that the element type had been chosen the final mesh was created (Figure 13).

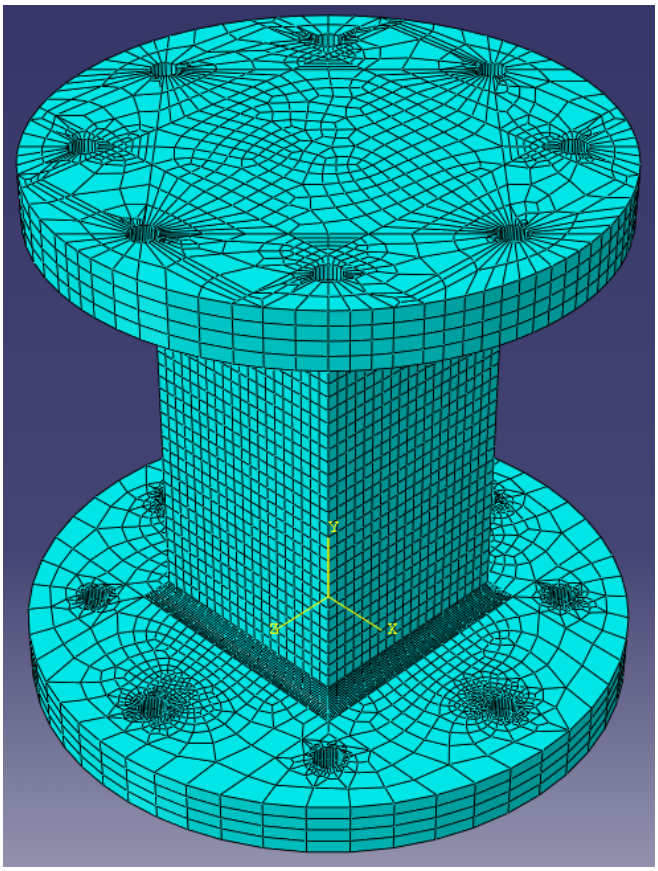

Figure 13: The Final Part Mesh

The final analysis was now carried out by applying the loads in 45 degree increments as discussed earlier. The figure below shows the zero degree orientation. The 45 degree incrimination was carried out in a counterclockwise manner.

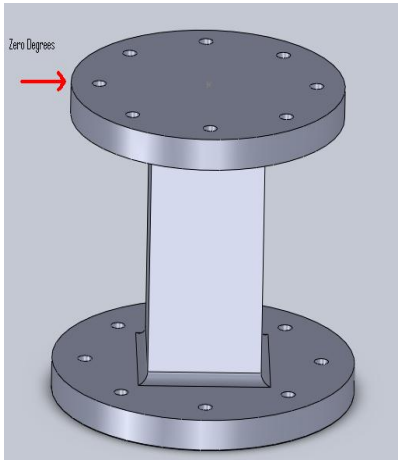

Figure 14: Zero Degree Orientation

The maximum stress for each of the loadings was noted and recorded.

Results and Discussion

The maximum stress was of the most interest in the analysis. Therefore each of the values was recorded for each of the 45 degree increments. These values where plotted in appendix 5, and a table of the values was created. Table 2 shows these values.

Table 2: Maximum Stress at each Wind Direction Angle

Peak Von Mises Stress (psi)	Wind Direction Angle (degrees)
42710	0
52240	45
42530	90
52330	135
42540	180
53020	225
43200	270
52370	315
42710	360

From the table above it is seen that the maximum stress occurs at 225 degrees with a magnitude of 53,020 psi. The area of highest stress is in the fillet region of the part as expected. The yield strength of Aluminum 6061- T6 is 40,000 psi. This high stress value is well above the yield strength, meaning the load beam needs more attention. The resulting stress contour plots for each scenario can be seen in appendix 6- 14.

Conclusion

The severe loads caused by an 80 mph wind that were applied to the load beam suggest that the part needs more attention. The maximum stress induced by these loads at wind directions varying from, 0- 360 degrees in 45 degree increments. Range from 42,530 psi to 53,020 psi. These values are all above the yield stress of Aluminum 6061- T6, which is 40,000 psi. Therefore the need for further analysis is required to be certain that this could be a potential problem.

Appendix 1

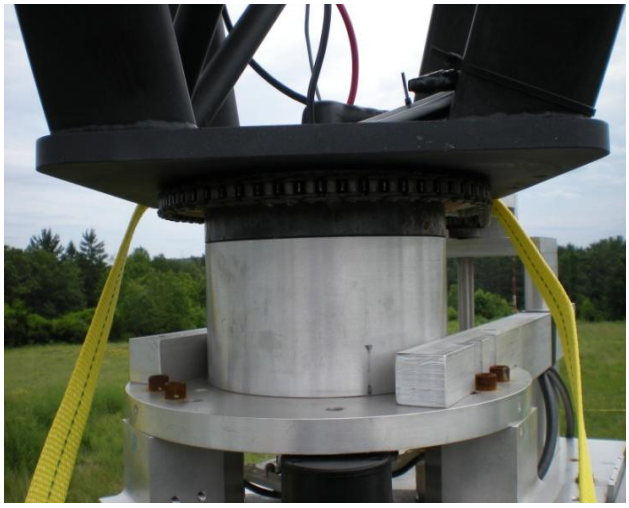

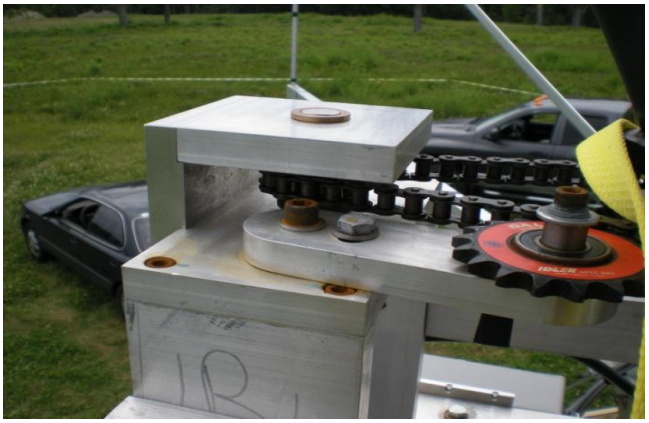

Appendix 2

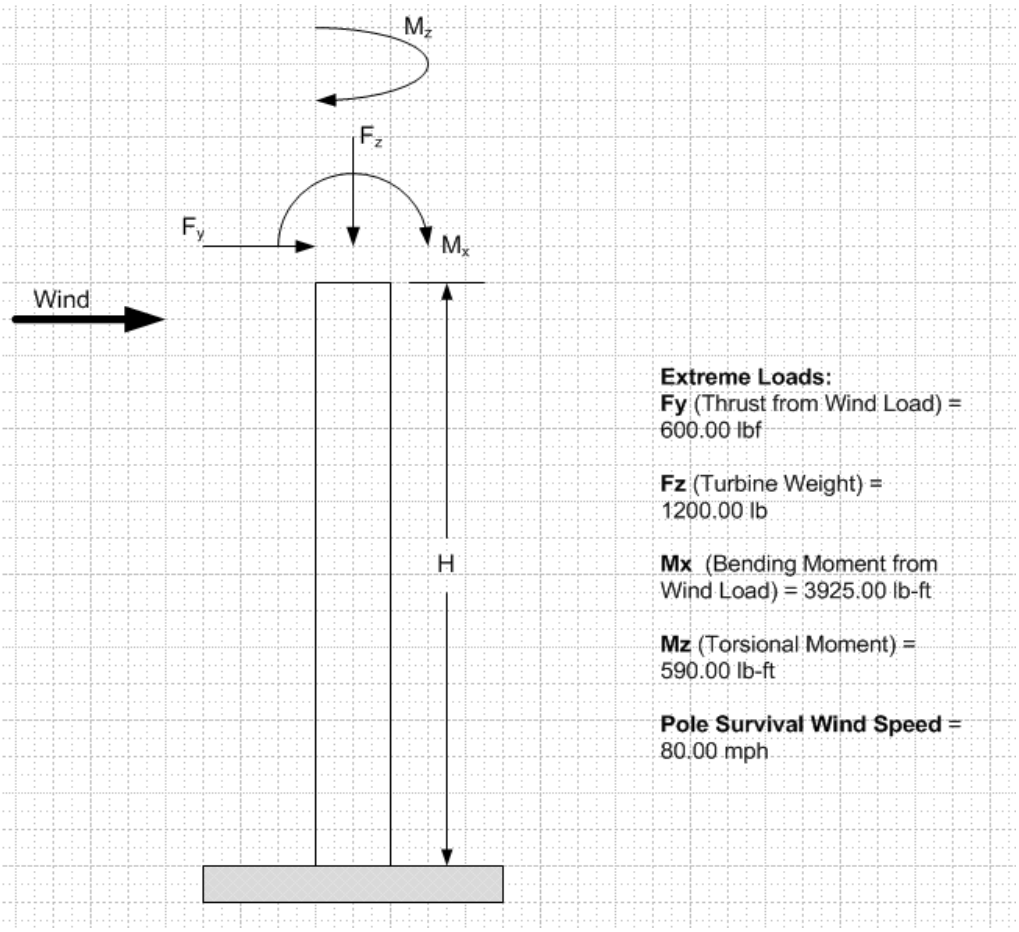

Extreme Loads:
Fy (Thrust from Wind Load) = 600.00 lbf

Fz (Turbine Weight) = 1200.00 lb

Mx (Bending Moment from Wind Load) = 3925.00 lb-ft

Mz (Torsional Moment) = 590.00 lb-ft

Pole Survival Wind Speed = 80.00 mph

Appendix 3

Appendix

Chris Baltazar 8/12/10 Load Beam Calculations

Projected Area of Bolt hole: PA: Projected Area

PA: Length * Diameter of hole PA: (0.75)(0.375 in)

PA: 0.28125 in^2

Fy (Thrust from Wind):

F_y: 600.00 lb $\frac{600\ lb}{8\ holes} = 75\ lb/hole$

$P: F/A = \frac{75\ lb}{0.28125\ in^2} = \boxed{266.67\ psi}$ @ F_y

F_z (Turbine Weight): F_z = 1200.00 lb Area of top piece = 40.4 in^2

$P: F/A = \frac{1200\ lb}{40.4\ in^2} = \boxed{29.70\ psi}$

M_z (Torsional Moment): M_z = 590.00 lb-ft

$(590\ lb\text{-}ft)\left(\frac{12\ in}{1\ ft}\right) = 7080\ lb\text{-}in$

$\frac{7080\ lb\text{-}in}{2.875\ in} = 2462.61\ lbs \left(\frac{1}{0.28125\ in^2}\right) = \frac{8755.95\ psi}{8\ holes} = \boxed{1094.5\ \frac{psi}{hole}}$

2.875 in: Radius from center to center of bolt hole

M_x (Bending Moment): M_x = 3925 lb-ft

$\left(\frac{3925\ lb\text{-}ft}{0.3021\ ft}\right) = 12993.1\ lbs$ $P: F/A = \frac{12993.1\ lbs}{8.47\ in^2} = 1534.01\ psi$

0.3021 ft: Radius of load Beam top circular disk

8.47 in^2: Area seen in fig. below

$\frac{1534.01\ psi}{2\ surfaces} = \boxed{767.01\ psi}$

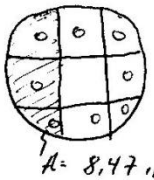

Appendix 4

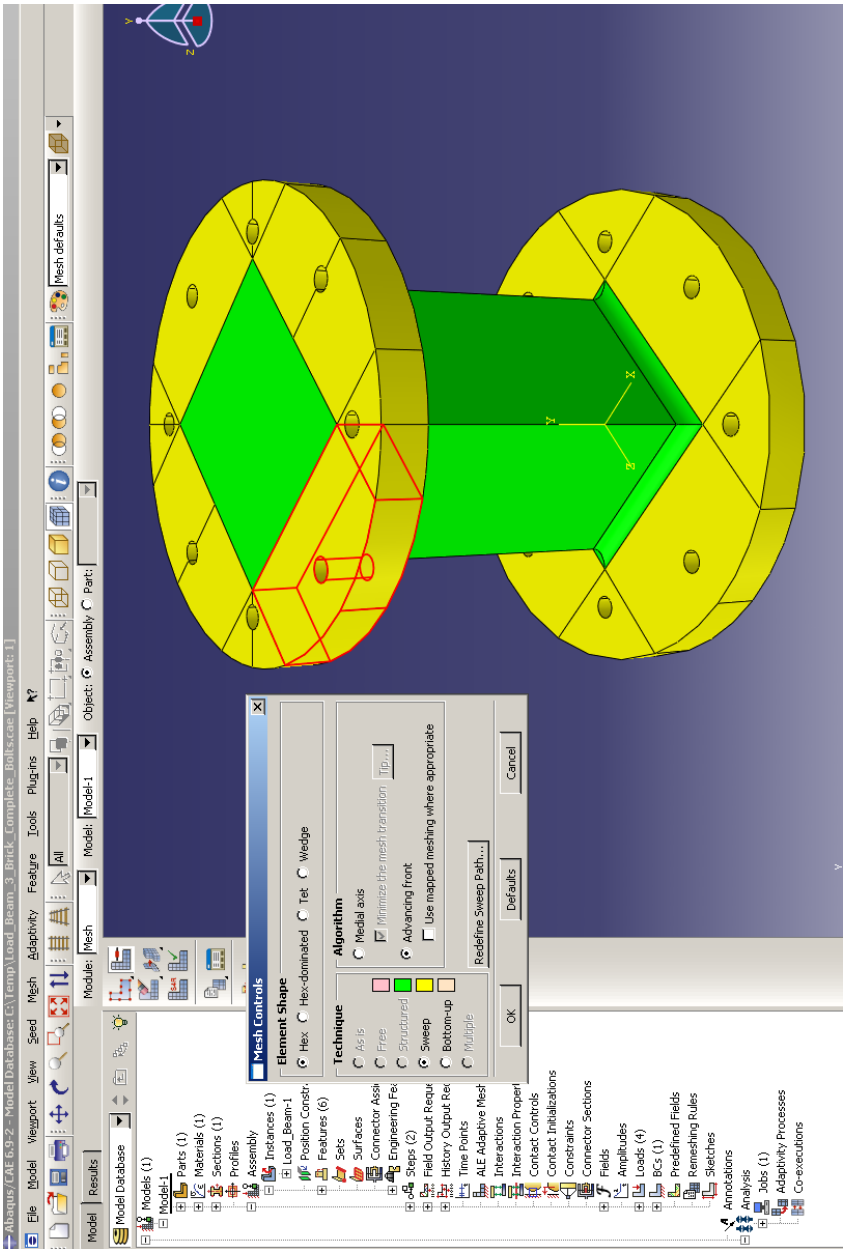
Mesh Controls
Element Shape
Hex
Hex-dominated
Tet
Wedge
Technique
As is
Free
Structured
Sweep
Bottom-up
Multiple
Algorithm
Medial axis
Minimize the mesh transition
Advancing front
Use mapped meshing where appropriate
Redefine Sweep Path...
OK
Defaults
Cancel
Model Database
Models (1)
Model-1
Parts (1)
Materials (1)
Sections (1)
Profiles
Assembly
Instances (1)
Load_Beam-1
Position Constr
Features (6)
Sets
Surfaces
Steps (2)
Field Output Requ
History Output Re
Time Points
Interactions
Interaction Propert
Contact Controls
Contact Initializations
Constraints
Connector Sections
Fields
Amplitudes
Loads (4)
BCs (1)
Predefined Fields
Remeshing Rules
Sketches
Annotations
Analysis
Jobs (1)
Adaptivity Processes
Co-executions

Appendix 5

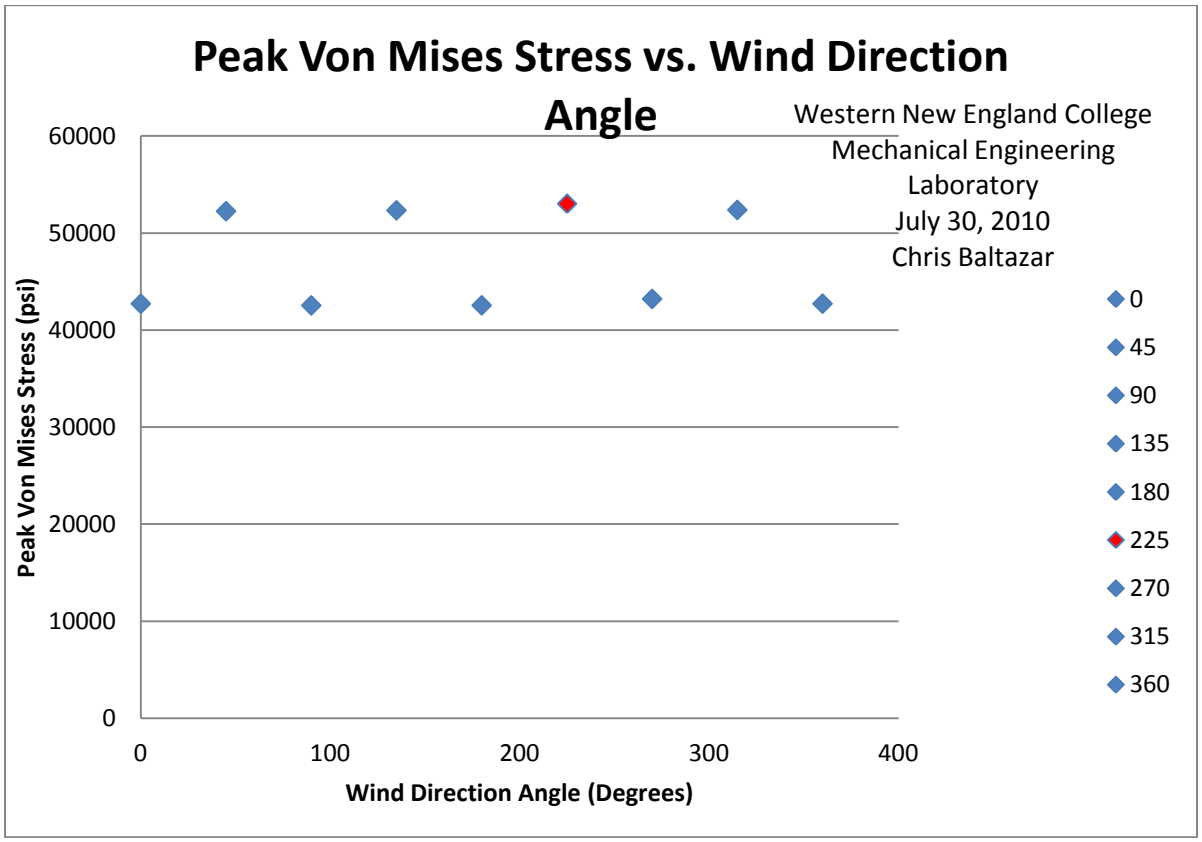
Peak Von Mises Stress vs. Wind Direction Angle
Western New England College
Mechanical Engineering
Laboratory
July 30, 2010
Chris Baltazar
Peak Von Mises Stress (psi)
60000
50000
40000
30000
20000
10000
0
0
100
200
300
400
Wind Direction Angle (Degrees)
0
45
90
135
180
225
270
315
360

Appendix 6
Zero Degrees, Max Stress = 42,710 psi

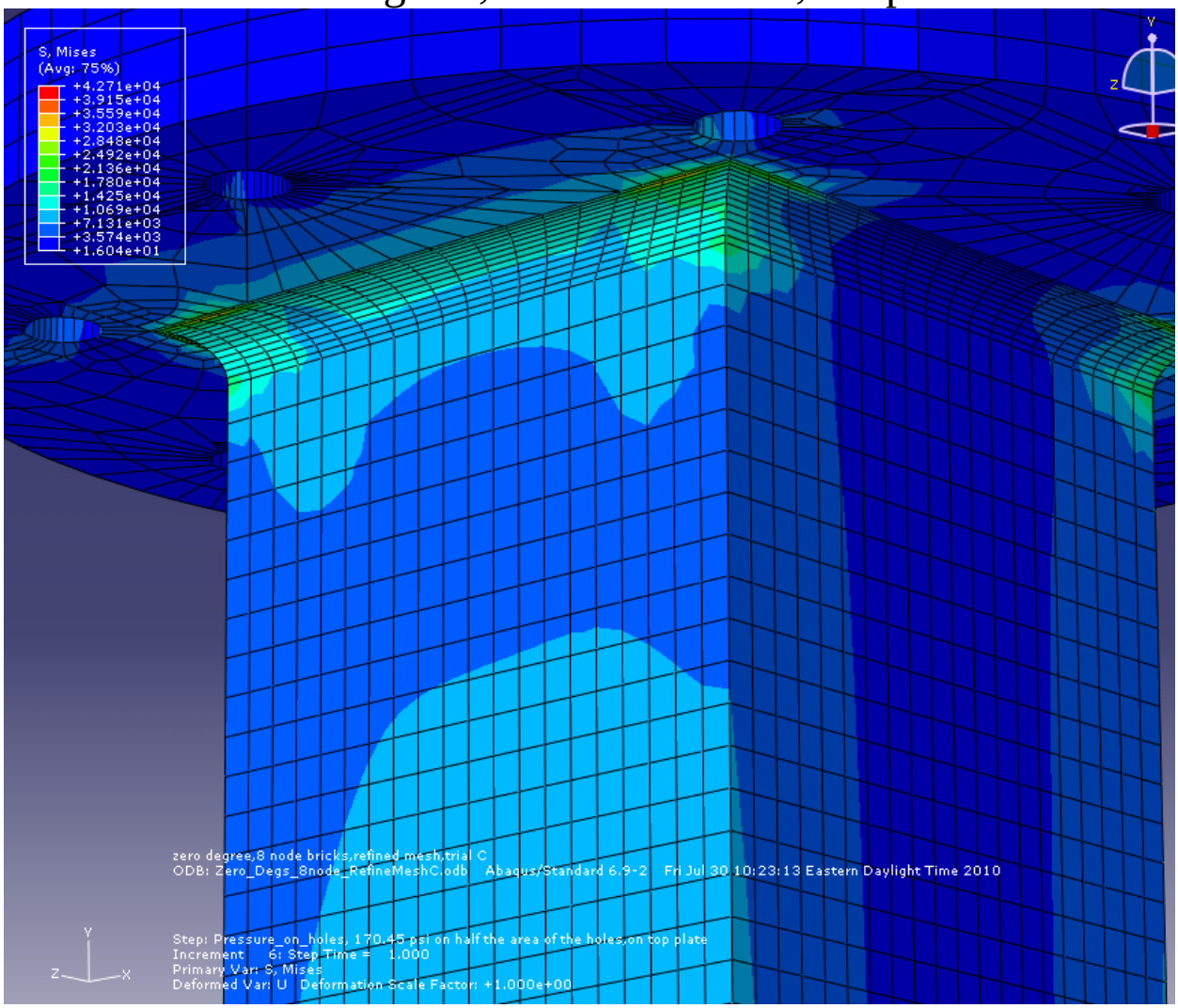

Appendix 7
45 Degrees, Max Stress = 52,240 psi

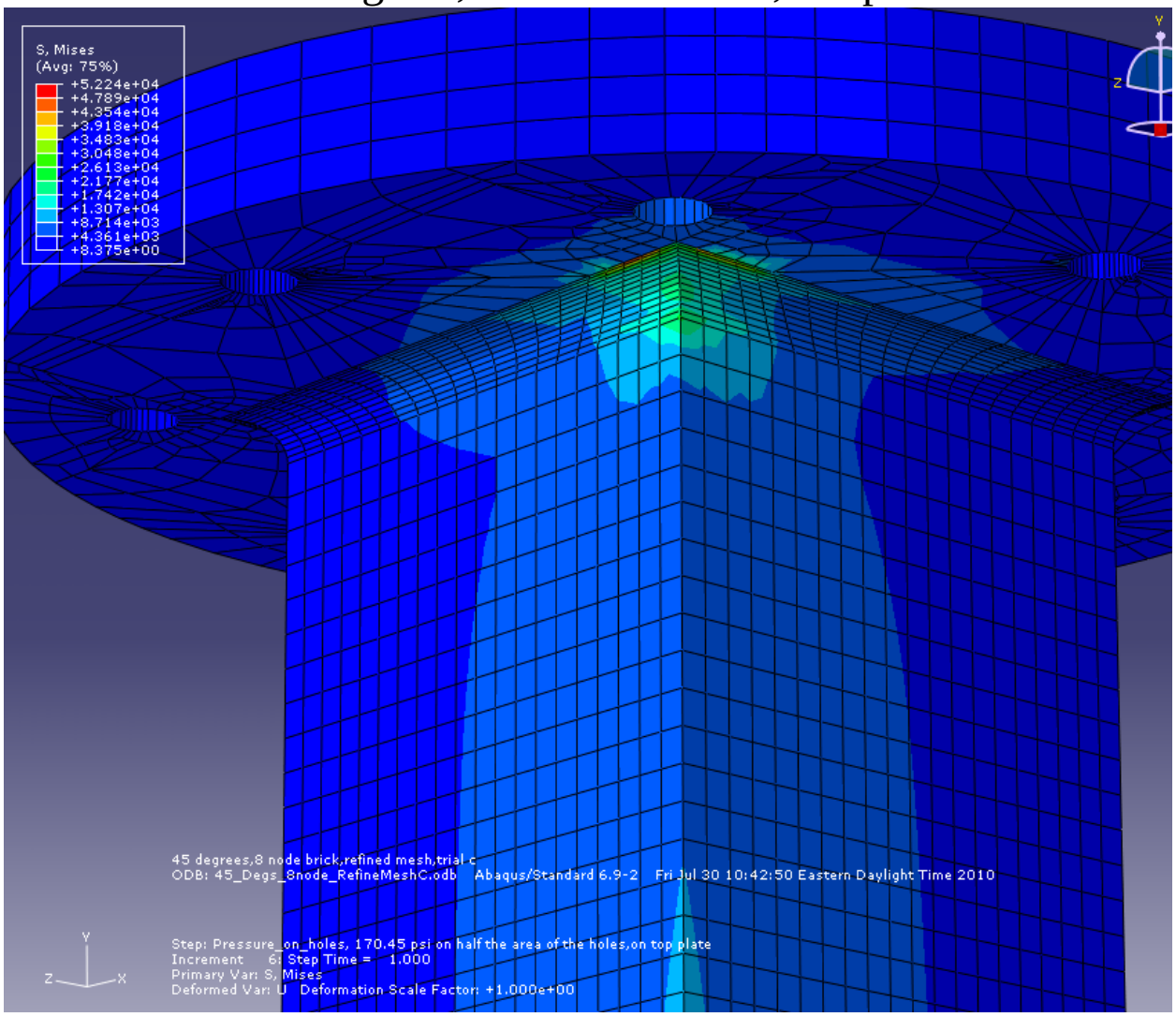

Appendix 8
90 Degrees, Max Stress = 42,530 psi

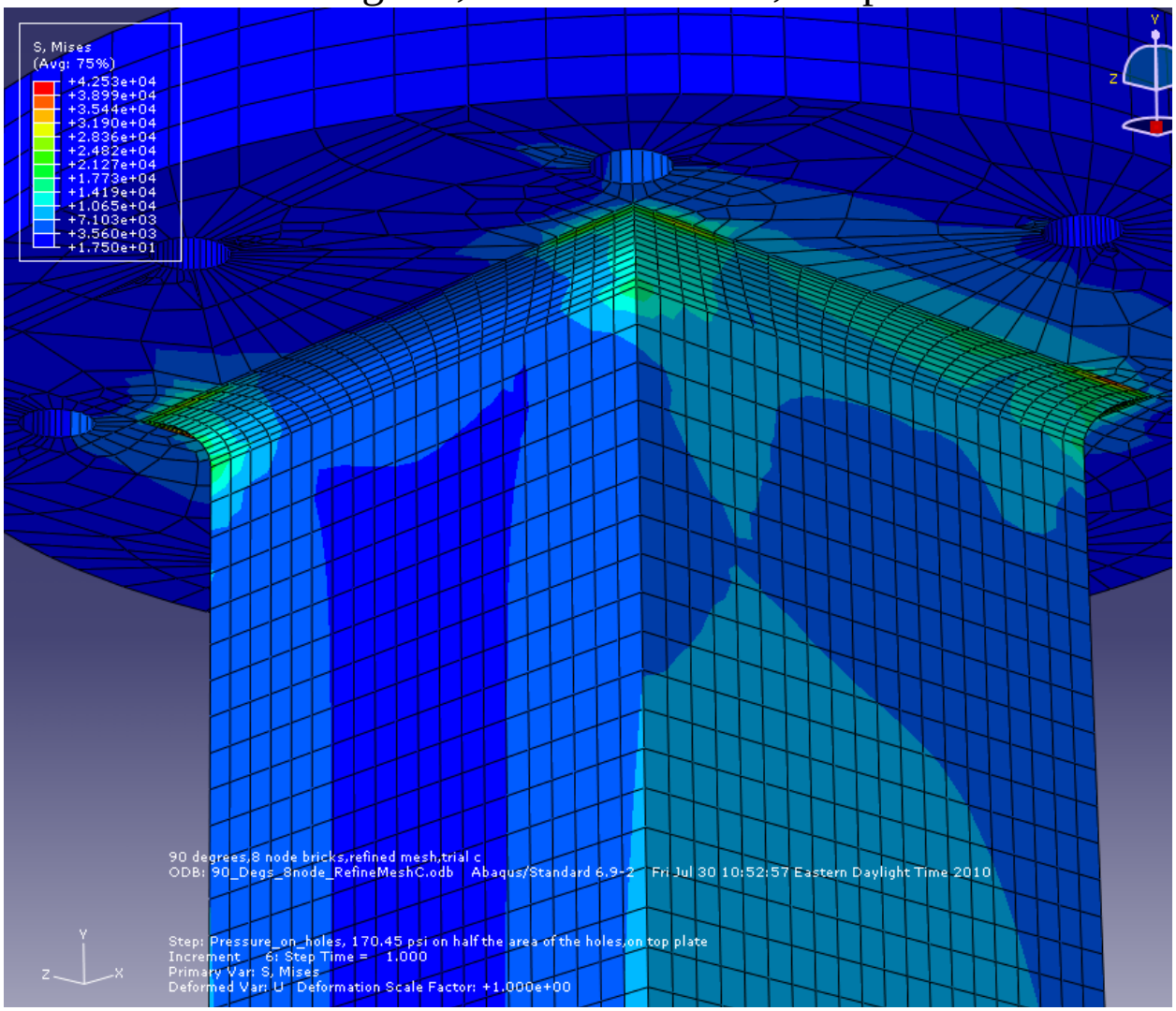

Appendix 9
135 Degrees, Max Stress = 52,330 psi

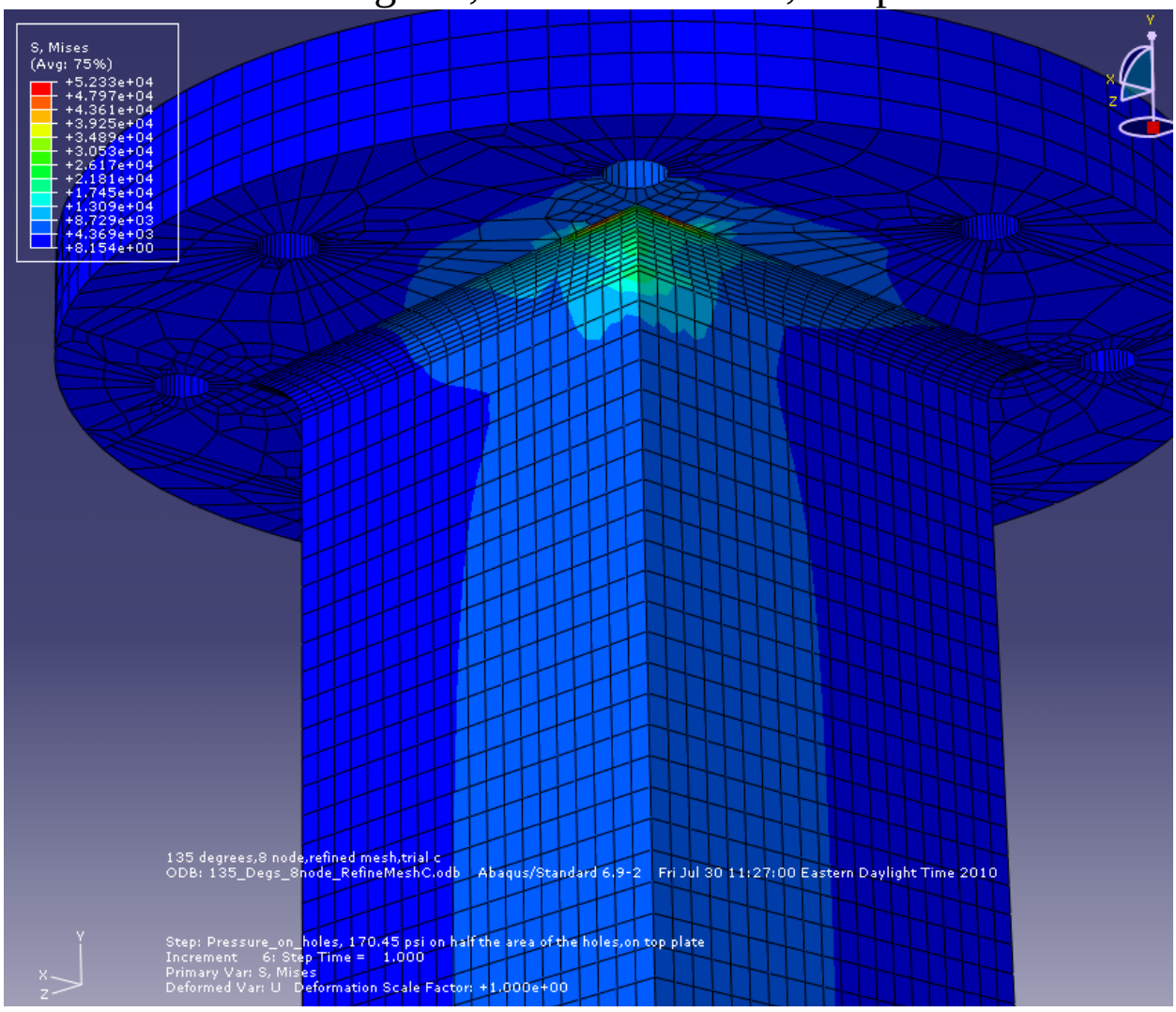

Appendix 10
180 Degrees, Max Stress = 42,540 psi

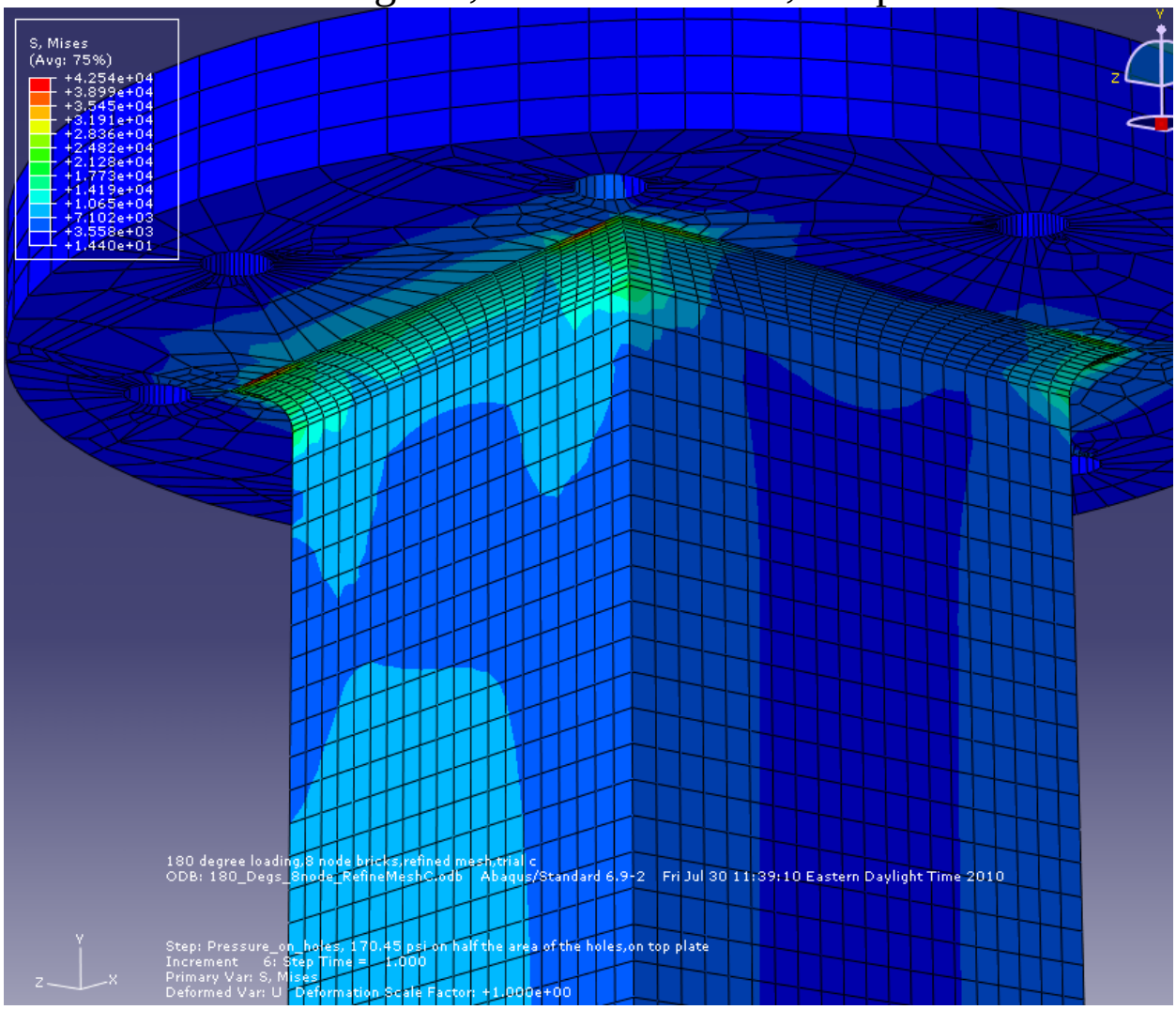

Appendix 11
225 Degrees, Max Stress = 53,020 psi

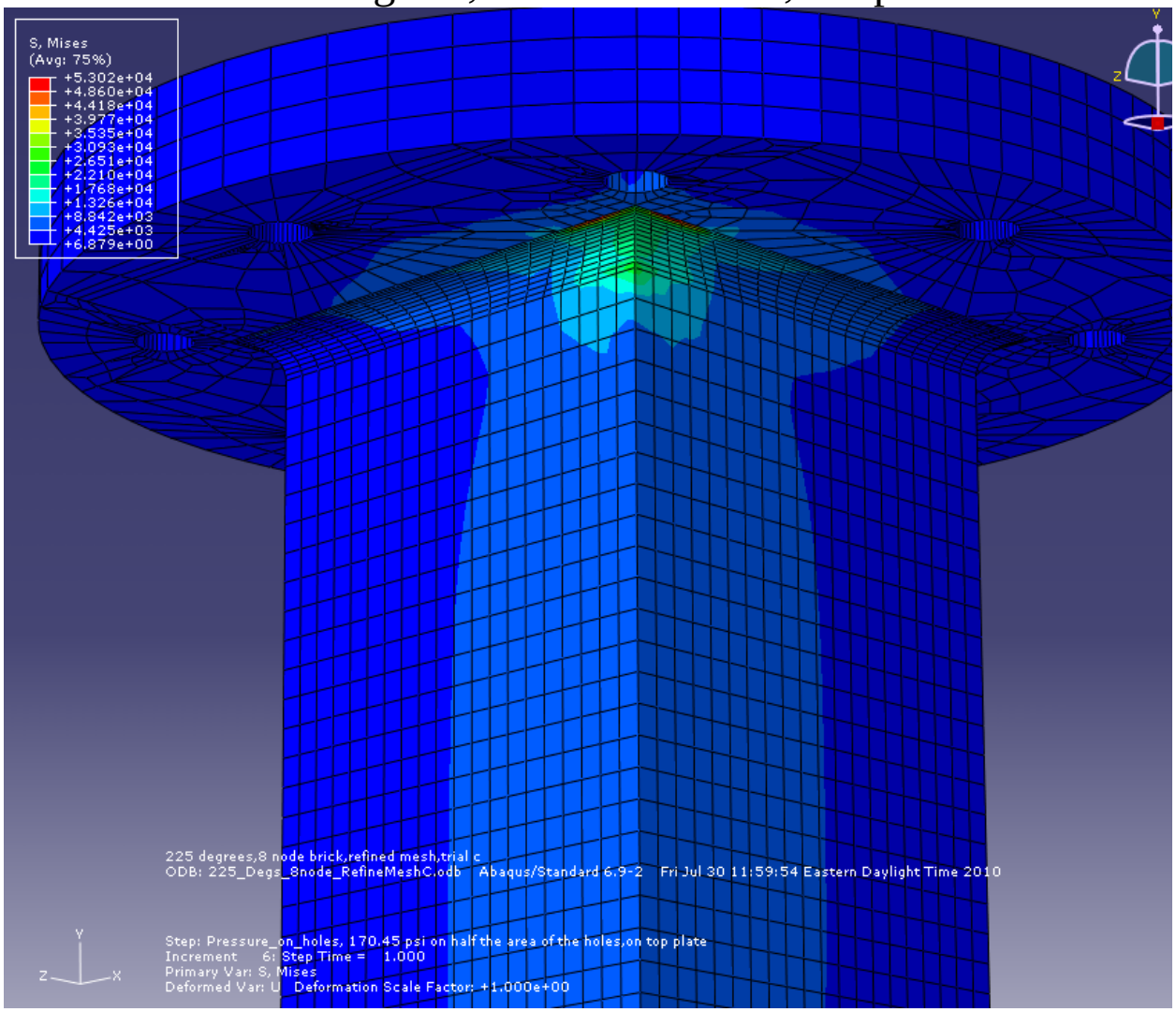

Appendix 12
270 Degrees, Max Stress = 43,200 psi

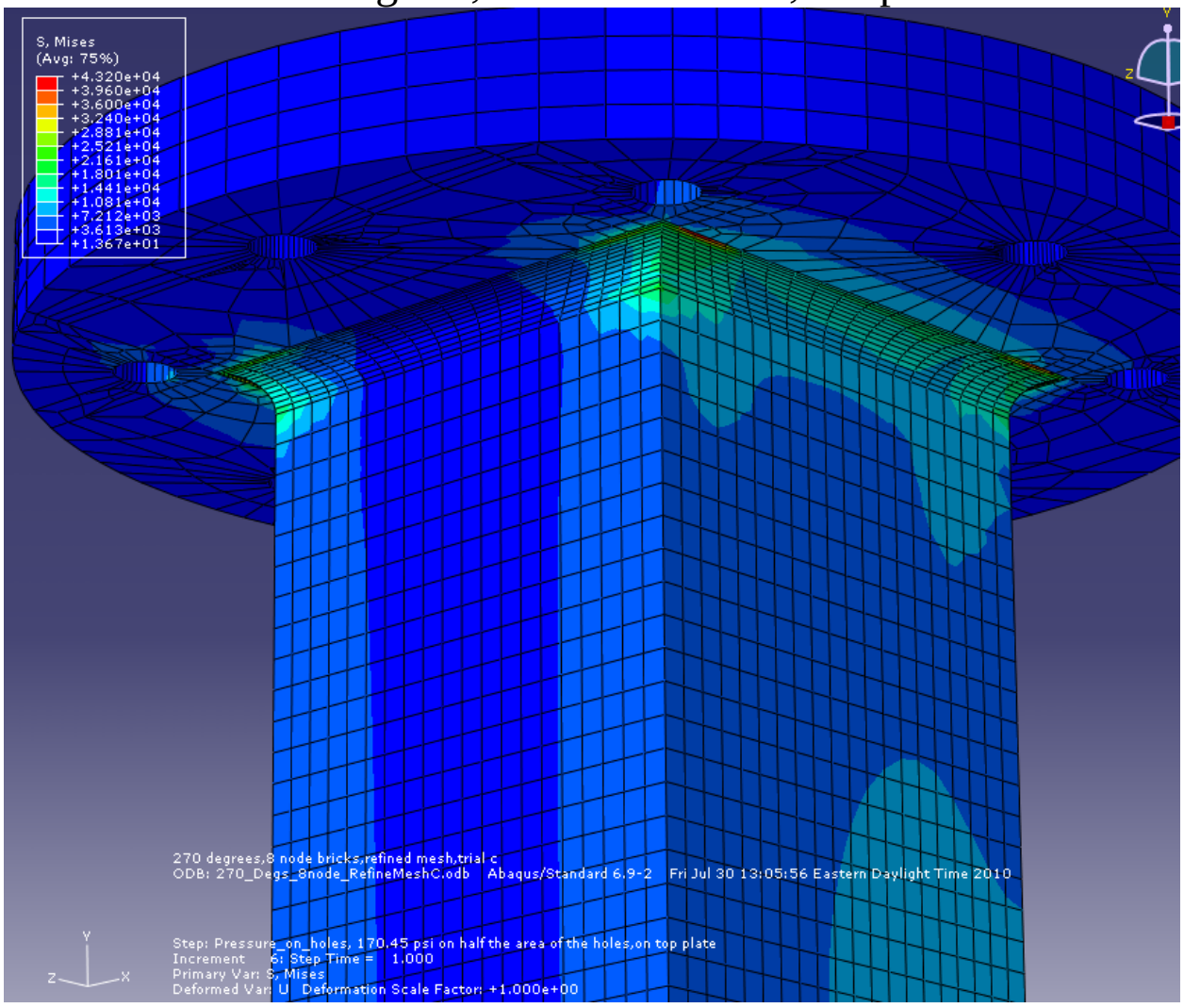

Appendix 13
315 Degrees, Max Stress = 52,370 psi

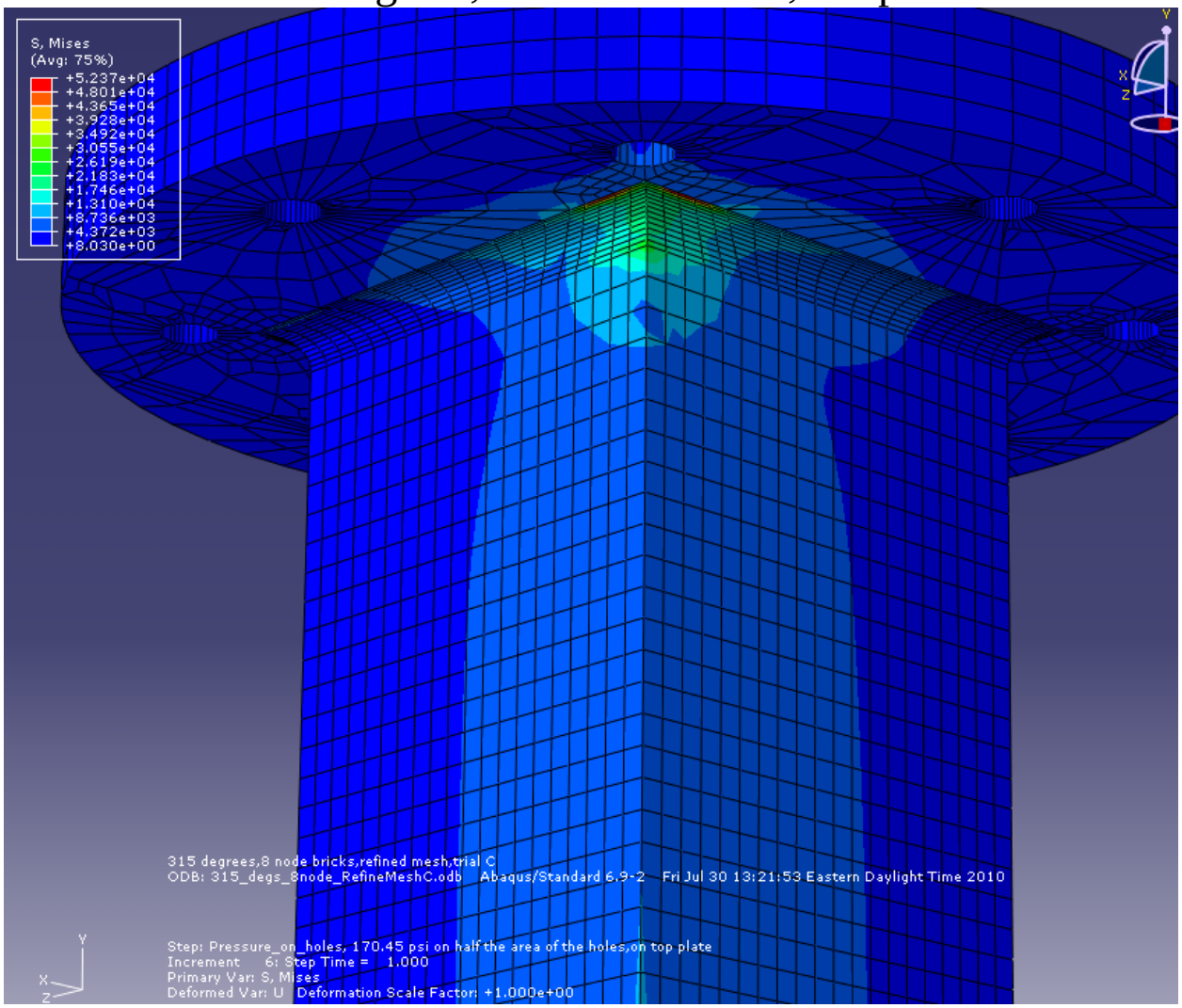

Appendix 14
360 Degrees, Max Stress = 42,710 psi

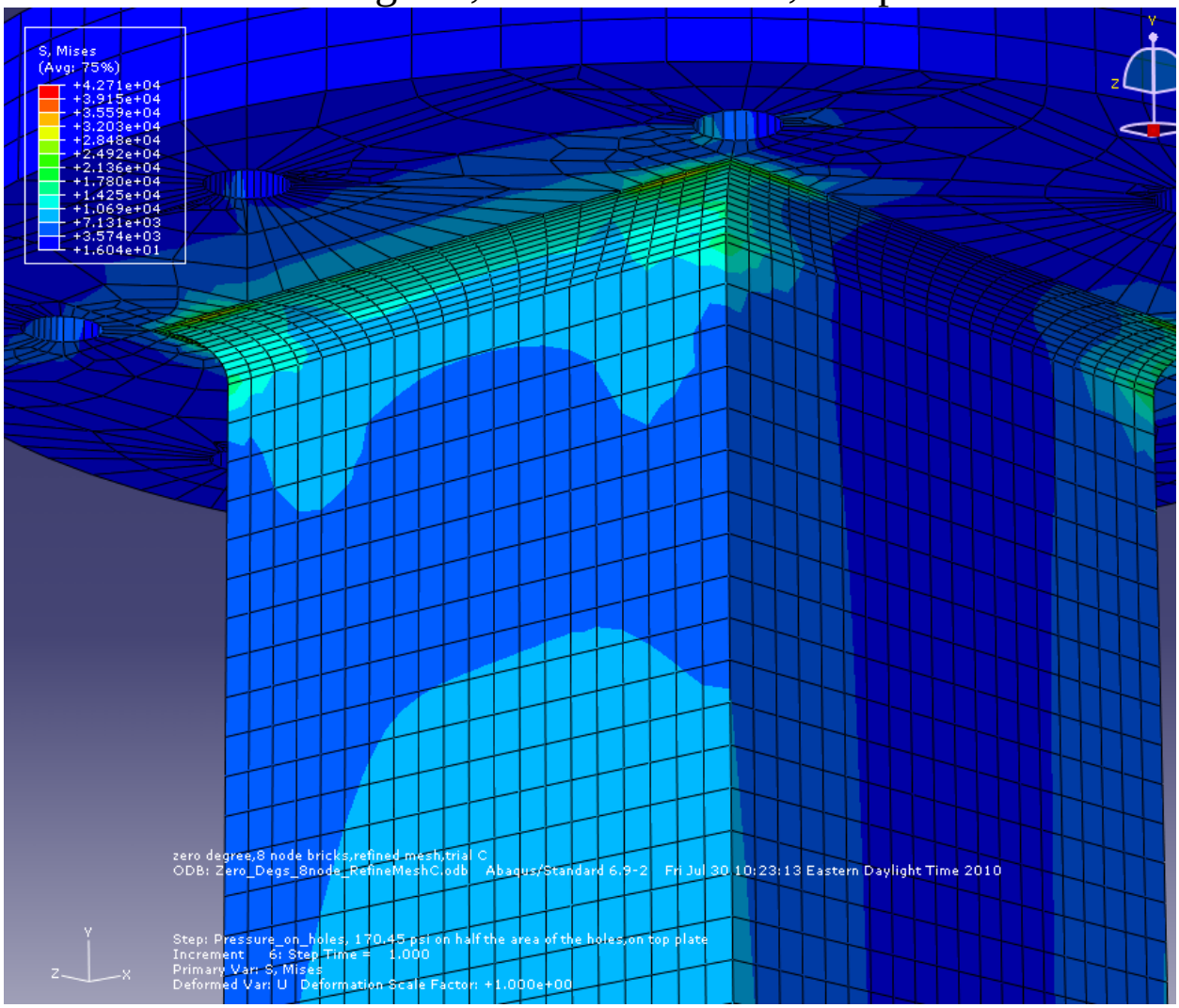

Appendix E: Small Wind Turbine Report

FDWT-Small Wind Turbine

Sample Intern Team Effort

Small Wind Turbine Team
August 26, 2011

Table of Contents

Abstract on Small Wind Turbines *241*
Annual Energy Production *242*
Levelized Cost of Energy *242*
Wind Turbine Classifications *242*
Available Small Wind Turbines *243*
Small Wind Turbine Comparison *84*
Buying a Small Wind Turbine for Comparison *247*
FE 1024 Power Hook-ups *249*
Potential Generators *249*
Copper, Silver, or Gold 252
On/Off Grid Hook-ups *253*
Patent Research *254*
Testing Standards for Certification *255*
Small Wind Certification Council Standards for Certification 256
IEC Standard 61400-2 Design Requirements for Small Wind Turbines 258
Certification ..... Error! Bookmark not defined.
Fabric/Foam Research *274*
Foam Expansion 275
Foam Mold Removal 276
Tower Research *277*
Bergey Tower Research 282
Mobile Towers 283
Mock-up *276*
Prototype Stator Rotor ..... *Error! Bookmark not defined.*
C481 Stator Rotor *287*
Foam Molding and Metal Working Companies *290*
FE 1024 Generator and FF1 Rotor Model *293*
Sectioned Stator *293*
Redesign of Stator and Rotor ..... *Error! Bookmark not defined.*
Modifications to the Model 298

Design Consultation Meetings *300*

Meeting with Paramount and Jeff King 300

Meeting with Mountain Base Mould 301

Aluminum Extrusion Process *301*

Market Study *301*

Manufacturing Study *304*

Conclusion ..... *Error! Bookmark not defined.*

Resources *310*

Table of Figures

Figure 1: Wind Power Classification Key for the Following Maps 243
Figure 2: Wind Map of Massachusetts Showing Annual Average Wind Speeds at 50 m High... 82
Figure 3: Wind Map of Connecticut Showing Annual Average Wind Speeds at 50 m High 82
Figure 4: Wind Map of Maine Showing Annual Average Wind Speeds at 50 m High 246
Figure 5: Comparison of All 1kw Turbines Found Regarding Price, Mass, and Diameter..... 247
Figure 6: Power Hook-up Set-up 249
Figure 7: A Cut-in View of an Induction Generator..... 251
Figure 8: Basic Setup of Turbine Generator with Stator and Rotor Assemblies 252
Figure 9: Opened Permanent Magnet Generator 252
Figure 10: Tying a Wind Turbine into the Grid to Supplement Power Usage (left) and An Off Grid Set-up with Battery Bank for Storage of Excess Produced Power (right)..... 254
Figure 11: Freestanding Monopoles 277
Figure 12: Freestanding Lattice Tower..... 277
Figure 13: Guyed Lattice Tower..... 278
Figure 14: Tilt-up Tower 278
Figure 15: Tilt-down Tower..... 278
Figure 16: Guy-less tilt-Down Tower..... 280
Figure 17: Guyed Tilt-up 281
Figure 18: I-beams 282
Figure 19: A Stress Test at 200 lbs of Force Yielded $3X10^7$ N/m^2 in the Weakest Points..... 283
Figure 20: The TRTMU30MDPL (left) and the RMTU656MDPLGO (right) 284
Figure 21: AllTech 106 foot Tower Being Transported (right) and In Use but Not Fully Extended (left)..... 285
Figure 22: Foam Mockup..... 276
Figure 23: Exploded view of the SLA model 286
Figure 24: Original Stator Blades 287
Figure 25: Adjusted Centerbody..... 287
Figure 26: Angled View of C481 with a Stator Rotor (left) and Close-up of Stator Rotor (right) 288
Figure 27: Stator Rotor Placed in the C481 289
Figure 28: Cutaway of the Leading Edge of the Original and Modified C481 289
Figure 29: Map of Location of Foam and Metal Companies..... 291
Figure 30: Section of Stator 294
Figure 31: Full Assembly..... 294
Figure 32: Inner Stator Section 295
Figure 33: Outer Ring Stator Section..... 295
Figure 34: Full Stator 296
Figure 35: Inner Rotor Hub..... 296
Figure 36: Rotor Blade..... 297
Figure 37: Full Rotor Assembly 297
Figure 38: Stator and Rotor Options 298
Figure 39: Previous Full Model 299
Figure 40: Updated Shroud Configuration 299
Figure 41: Modifications to Stator Connections 300

Figure 42: Small Wind Incentives for Residents 302
Figure 43: Wind Resources in the United States 302
Figure 44: Wind Power Capacity by State 303
Figure 45: U.S. Small Wind Market Trends 303
Figure 46: Materials Used in Wind Turbines by Component 305

Table of Tables

Table 1: Classifications of Wind Turbines 242
Table 2: Specs of the FE 1024 248
Table 3: Purchasing Information 248
Table 4: Sample Generator List 250
Table 5: Sample Inverter List 251
Table 6: Metal Properties 252
Table 7: SWCC Certification Fees 256
Table 8: Basic Parameters for SWT Classes 258
Table 9: Design Load Cases for the Simplified Load Calculation Method 261
Table 10: Force Coefficients, C_f 264
Table 11: Minimum Set of Design Load Cases for Aeroelastic Models 265
Table 12: Equivalent Stresses 266
Table 13: Partial Safety Factors for Materials 266
Table 14: Partial Safety Factors for Materials 267
Table 15: Applications for Certification to the SWCC 273
Table 16: List of Companies and Products for Foam Covering and Coating 275
Table 17: Different Tower Options 279
Table 18: Companies that have been Contacted for Making Custom Parts 291
Table 19: Companies Contacted During Week of 7/18-7/22 293
Table 20: Quotes Received as of 7/29/11 304

Final Report

From: Small Wind Turbine Team
To: Dr. Presz Jr.
Date: August 26, 2011

Abstract on Small Wind Turbines

Horizontal Axis Wind Turbines (HAWTs) are much more efficient than their vertical axis counterparts (VAWTs). HAWTs must face the wind in order to harness its energy. Smaller turbines are pointed in the correct direction through use of a wind vane system, whereas larger turbines use a wind sensor and are turned by a motor. The blades of a turbine are generally stiff because they are placed in front of the supporting tower and turbulence could interfere with the performance of the turbine. In addition, stronger winds could push the blades into the tower. However, a downwind turbine which has its blades behind the tower does not need this precaution and it can also have flexible blades. An advantage to downwind towers is that there is no need for a mechanism to point the tower in the direction of the wind. However, the blades generally fatigue more quickly. Turbines are also placed high above the ground since wind speeds are generally higher 100-300 ft above the ground. The wind turbines, therefore, have a mechanism which shuts the turbine down or does not allow it to rotate above a certain speed.

Research was conducted on the different types of small wind turbines that are currently available in the market. During this research, the parameters which were being addressed were those which seem to be the most important when attempting to design a new small HAWT. One parameter which set the foundation for the project is the allowable power of the turbine. It was initially decided that research was to be focused on 10 kW and smaller HAWTs. Eventually, this was narrowed down further to 1kW, since that was the intended power output for this project. Another important parameter was the cost of the product. Cost is one of the crucial factors in developing a wind turbine; engineers must find a balance between performance and cost as to make the product appealing to a large consumer base.

FloDesign Wind Corp has developed a new shrouded axial flow wind turbine, also known as a mixer-ejector wind turbine (MEWT), which has significant potential benefits over conventional HAWT designs. Many of the benefits are more significant at the smaller size required for distributed wind applications. Typically HAWT designs of a small wind turbine suffer from terrible losses caused by tip losses, low Reynolds flow effects, and frictional effects. The MEWT concept eliminates these problems by shrouding the rotor, allowing the MEWT to have a significant advantage in the small wind market. This paper will present the findings in a study to see how the MEWT system can impact the small wind market.

Annual Energy Production

Annual energy production is the amount of energy a wind turbine can produce in a year. It is a function of the mean power of a turbine and the number of hours in a year. By multiplying the two together, annual energy production is yielded.

Levelized Cost of Energy

The Levelized Cost of Energy is a way of measuring the cost per kWh of electricity a certain system produces. LCOE gives a way to compare the cost of electricity from different energy providing systems such as natural gas and nuclear fuel. It works by averaging the building, maintenance, payroll, fuel, and all other costs with the lifetime of the system. Wind energy has a major upfront cost, but its fuel (the wind) costs nothing, whereas natural gas facilities may be cheaper to build but their fuel costs are more expensive. LCOE gives an easy way to look at and compare the costs per kWh of different energy providing systems to allow somebody to make the most economical decision. This is extremely useful for investors to know what to invest in and also for consumers to pay the lowest amount of money per kWh.

Wind Turbine Classifications

Wind turbines are rated by the International Electrotechnical Commission (IEC) into four classes. These classes are based on the average and maximum wind speed seen by these turbines at hub height. Below, a table can be seen depicting what each class covers.

	Class I	**Class II**	**Class III**	**Class IV**
Annual Average Wind Speed	10 m/s	8.5 m/s	7.5 m/s	6.0 m/s
Extreme 50 Year Gust	70 m/s	60 m/s	52.5 m/s	42.0 m/s
Turbulence Classes	18%	18%	18%	18%

TABLE 1: CLASSIFICATIONS OF WIND TURBINES

Wind speeds are measured every three seconds. The turbulence value is the standard deviation of wind speed measured at 15 m/s wind speed.

Available Small Wind Turbines

A spreadsheet containing all of the information which could be located online was put together. This contained all of the information set forth in the objectives for comparing these small wind turbines. This table can be found in the excel spreadsheet in Appendix 1. The specifications listed in this table were the ones deemed most important when looking at competitors. This data was gathered mostly from www.allsmallwindturbines.com and supplemental information such as the height, weight, and rotor diameter were found through websites and PDF files supplied by the site. The information shows that there is a very large price range which is dependent on many factors such as power output, manufacturer, and the winds which the turbine is able to produce power in.

Another focus included the average wind speeds in different regions which products produced by this company would be marketed to. Figure shows the classification system used by the National Renewable Energy Laboratory (NREL) on the average wind speed maps for the select New England states which follow. Figure 91 shows the average wind speeds for Massachusetts. shows the averages for Connecticut and Figure for Maine.

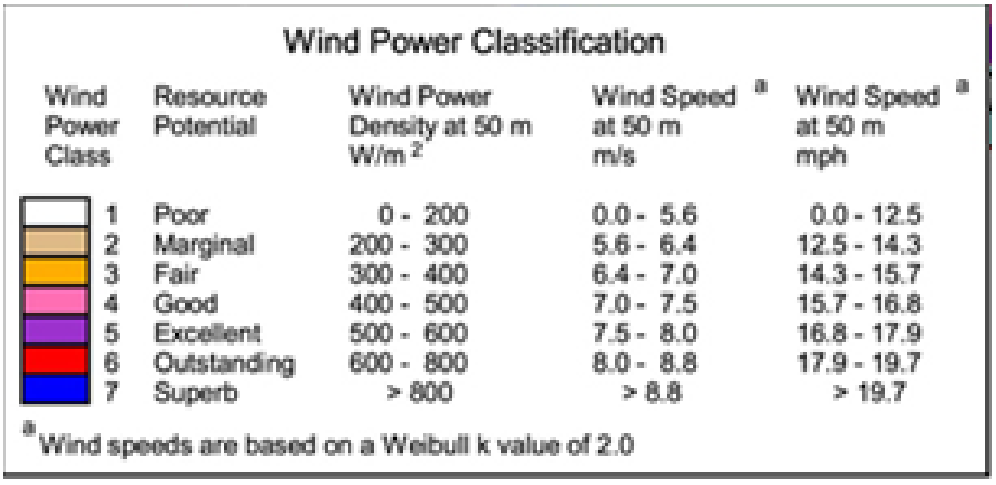

Wind Power Classification

Wind Power Class	Resource Potential	Wind Power Density at 50 m W/m^2	Wind Speed [a] at 50 m m/s	Wind Speed [a] at 50 m mph
1	Poor	0 - 200	0.0 - 5.6	0.0 - 12.5
2	Marginal	200 - 300	5.6 - 6.4	12.5 - 14.3
3	Fair	300 - 400	6.4 - 7.0	14.3 - 15.7
4	Good	400 - 500	7.0 - 7.5	15.7 - 16.8
5	Excellent	500 - 600	7.5 - 8.0	16.8 - 17.9
6	Outstanding	600 - 800	8.0 - 8.8	17.9 - 19.7
7	Superb	> 800	> 8.8	> 19.7

[a] Wind speeds are based on a Weibull k value of 2.0

FIGURE 1: WIND POWER CLASSIFICATION KEY FOR THE FOLLOWING MAPS

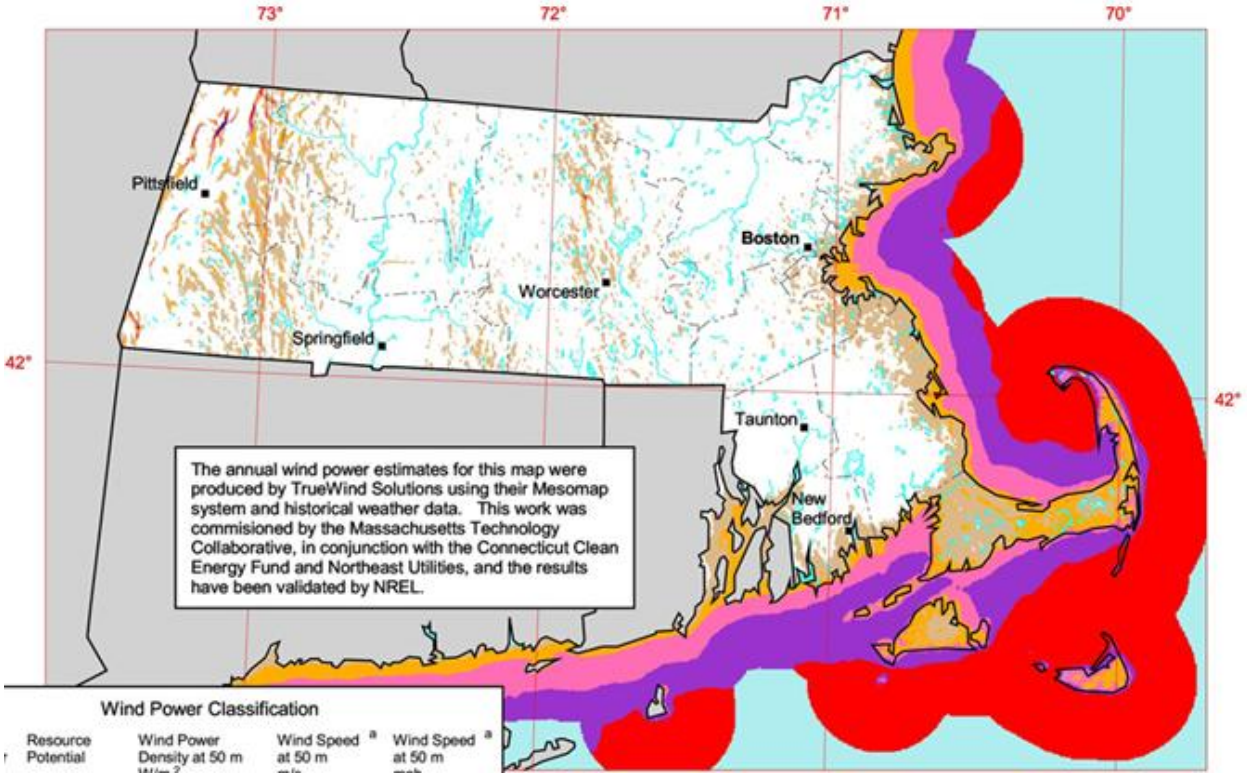

FIGURE 2: WIND MAP OF MASSACHUSETTS SHOWING ANNUAL AVERAGE WIND SPEEDS AT 50 M HIGH

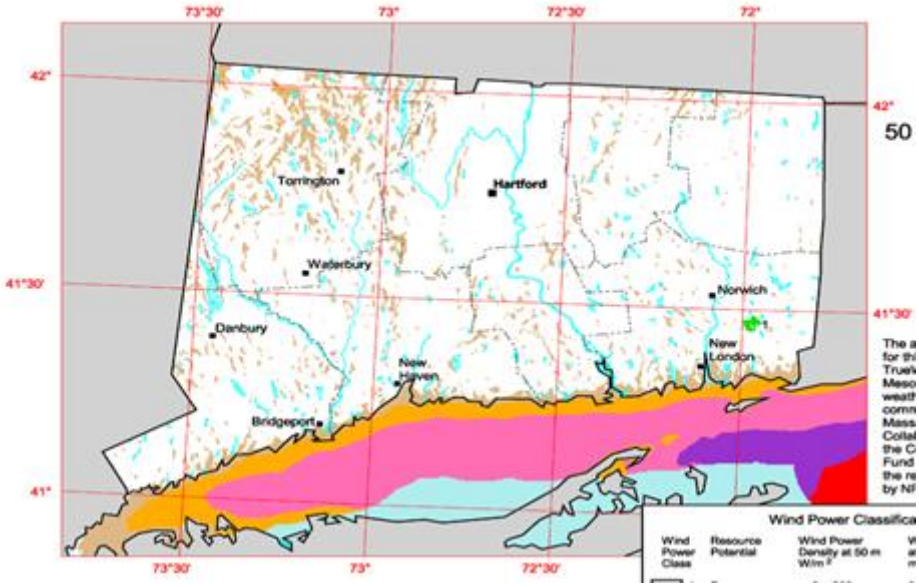

FIGURE 3: WIND MAP OF CONNECTICUT SHOWING ANNUAL AVERAGE WIND SPEEDS AT 50 M HIGH

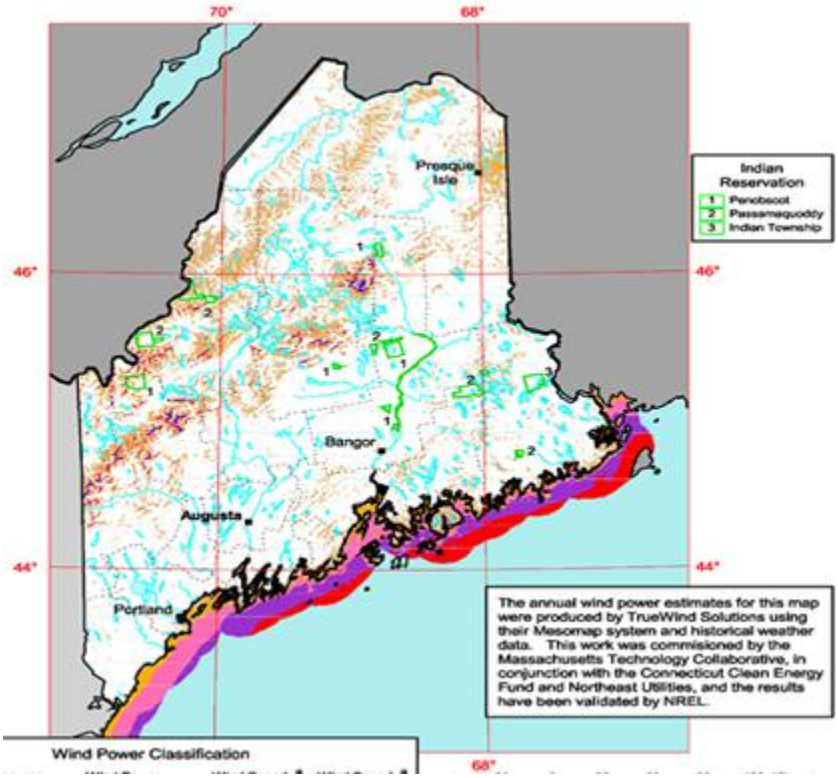

FIGURE 4: WIND MAP OF MAINE SHOWING ANNUAL AVERAGE WIND SPEEDS AT 50 M HIGH

As these figures indicate, New England states do not have the best winds for producing power from a wind turbine since they fall into the "poor" or "marginal" categories listed in Figure . Since these states generally do not have the wind power to drive the current small turbines on the market, there is a need for a turbine which can operate in these smaller average winds.

Small Wind Turbine Comparison

After the list of small wind turbines currently available on the global market was compiled, graphs were made to compare the different turbines. The categories in which they were compared were mass, power in kilowatts, and diametric size. The performance coefficient was compared as well but for this size turbine the accuracy of the calculated C_p values that were found was minimal. Each of these comparisons started as a full comparison of all the turbines. Then the comparison was narrowed down to turbines under three kilowatts because that is closer to the size range being explored for the small wind turbine. Once each category was compared a final comparison was made against all the one kilowatt wind turbines. This graph can be seen below.

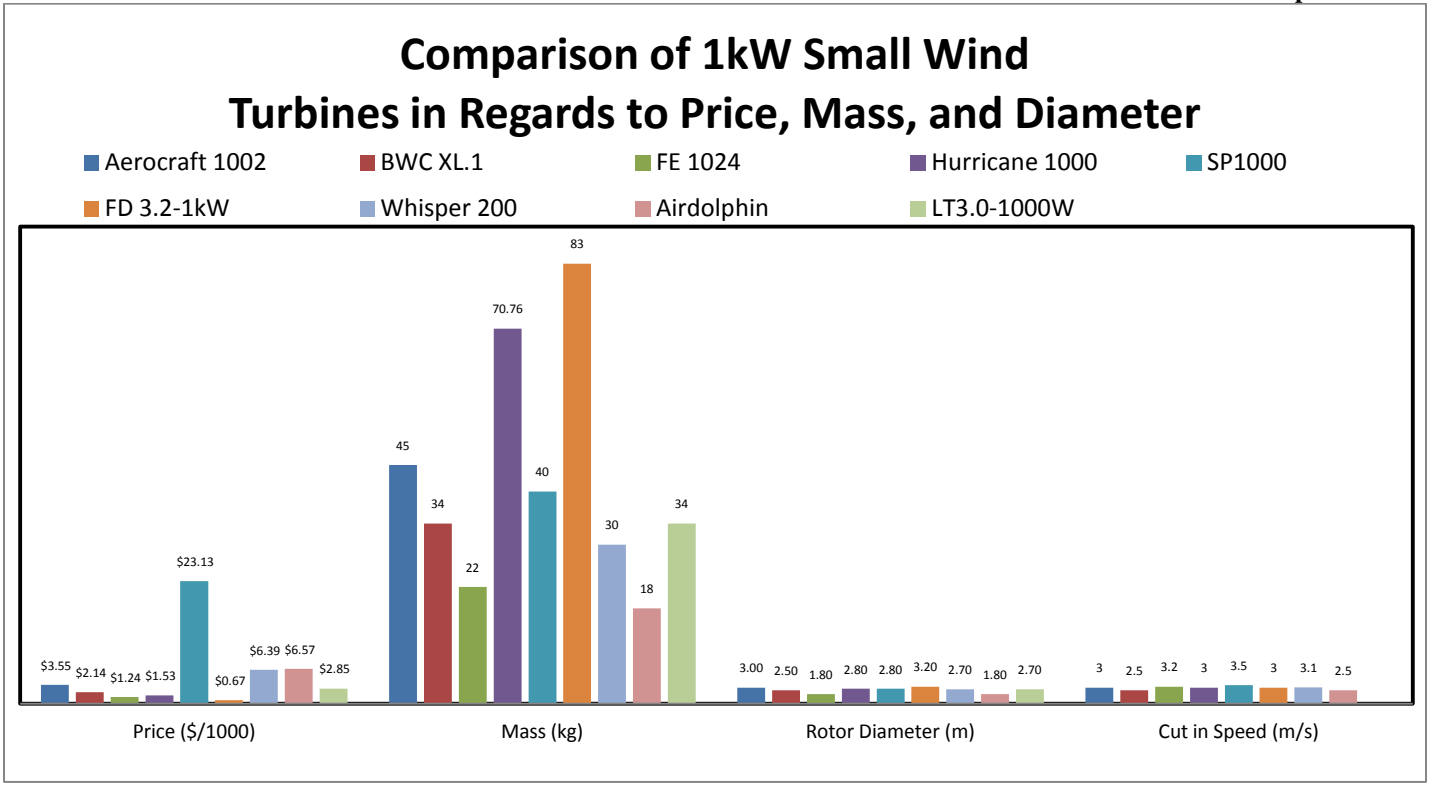

FIGURE 5: COMPARISON OF ALL 1KW TURBINES FOUND REGARDING PRICE, MASS, AND DIAMETER

This graph helped to determine what a good wind turbine would be to purchase in order to re-engineer and compare FloDesign's prototype to. A light wind turbine with a small diameter and low cut in speed is ideal. This would be closest to what the small wind turbine team is trying to construct. With those constraints in mind this chart shows that the best choices would be the Whisper 200, Airdolphin, or the FE-1024. This selection is also due to the price of the wind turbines. Ultimately, the FE 1024 was purchased and partially assembled for testing and comparisons.

Buying a Small Wind Turbine for Comparison

The team has decided to focus on buying a small wind turbine, similar to the model which is being designed in order to have a model for comparison. The turbine which was decided on for purchase was FuturEnergy's FE 1024 1kW; it has a low mass of 22kg compared to similar turbines, and is a reasonable price around $1300. In researching where to purchase this turbine, it was found that the only places which sell it are overseas. The specifications of this turbine can be seen in Table 2: Specs of the FE 1024
below.

FE 1024 Specs	
Rotor Diameter	1.8 m
Tower Diameter	50 mm
Mass	22 kg
Start-up Wnd Speed	2.5 m/s
Cut-in Speed	3.2 m/s
Survival Wind Speed	50 m/s
Rated Wind Speed	11.5-12.5 m/s
Rated Power	1000 W
Max Power	1.2 kW @ 12.5 m/s
Generator	3-Phase Perm Magnet
Noise	35 dB @ 5 m/s & 54 dB @ 7 m/s
	Zinc-plated and stainless steel with powder-coated and anodised aluminum for optimal corrosion and weather resistance

TABLE 2: SPECS OF THE FE 1024

Buying an FE 1024				
Company	**Location**	**Cost (US $)**	**Time to Deliver**	**Warranty**
Energistar.com	UK	1337.78	2-3 days + customs*available immediately (shipped next day)	2 years
FuturEnergy	UK/Europe	1473.25		2 years limited
TA Technology	Sweden	call/email	by agreement	2 years
Renugen-Renewable Generation	UK	email		N/A

TABLE 3: PURCHASING INFORMATION

FE 1024 Power Hook-ups

The plan for testing the FE 1024 was to hook it up to a battery bank to avoid connecting to the grid. The turbine can be sold with a Xantrex C60 Charge Controller. This type of controller is rugged enough to protect against overcharging with this kind of wind turbine. A dump load would also need to be purchased if this system is used. The FE 1024 system would require the C60 charge controller and one dump load.

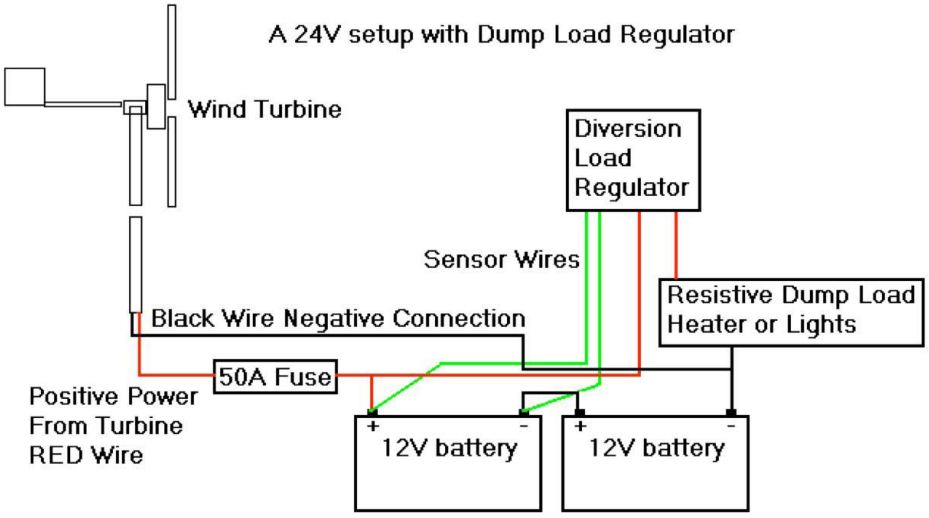

FIGURE 6: POWER HOOK-UP SET-UP

Using an off-grid system is beneficial in this type of testing scenario since the extra hassle of going through the electric company would only add more roadblocks to this project. However, in doing this, the capacity is limited by the size of the wind turbine, available resources and size of the battery bank. Since this turbine is to be used mainly for testing purposes and not as a main energy source for a building, the available resources will only impact what kind of data is produced.

Potential Generators

A generator must always be present in a wind turbine to produce the electrical power that people use every day. Through the research done, it was found that there are a few design options for each generator used.

First is the induction generator which has two coils typically made of copper wire which are used to create a current. This is done by applying an initial electric current to the inner copper wire or rotor coil while the outer wire or stator coil carries the newly produced current out of the turbine. This design has a drawback since it uses some of the produced power to continue to produce power which means the expected output may not be met due to power losses.

Another option is a permanent magnet design which means that magnets replace the inner wire to generate a current. Also, because magnets already have charge, the initial electric pulse

needed to start an induction generator is not needed and some weight may actually be cut out by eliminating the inner copper wire.
Car alternators may also be used but there are some corrections that would need to be made if this path were chosen. For instance, a car alternator is designed to operate at a much higher RPM than a wind turbine will most likely every reach so gears or belts will be needed to increase the RPM of the turbine before reaching the generator. A sample list of generators is shown below.

Name of Generator	Producer	Power (W)	Rated RPM	Starting Torque (Nm)	Price ($)
DC-540	Wind Blue	N/A	12V @ 130 350V @ 2500	N/A	$269.00
DC-500	Wind Blue	N/A	12V @ 1200	N/A	$269.00
GL-PMG-500A	GinLong	500	450	< 0.5	N/A
GL-PMG-1000	GinLong	1000	450	< 0.5	N/A
GL-PMG-1500	GinLong	1500	550	< 0.7	N/A
Brg 198-6	Diamond Industrial Ltd.	950	210	< 1.1	N/A
AG-5250-B-1ES	Moog Inc.	530	650	10 (torque @ rated speed)	N/A
AG-5250-B-2ES	Moog Inc.	1400	1500	10.2 (torque @ rated speed)	N/A
Cat 3	Hurricane Wind Power	Approx. 1200	12V @ 120	N/A	$189.99
Cat 4 Mark 1	Hurricane Wind Power	Approx. 2.3	12V @ 80	N/A	$239.99
WindTura 750	WindyNation	750	12V @ 90	0.75	N/A
30-298	Georater	500	3500	N/A	N/A

TABLE 4: SAMPLE GENERATOR LIST

In addition to the generator, an inverter is needed to take the DC output voltage from the turbine and convert it into a useable AC voltage. While some turbine systems have inverters built in, others do not and a few inverters that function near 1 kW of power were examined and are shown in the table below.

Inverter	Producer	Rated Output Power (W)	Price ($)	Weight (kg)	Input Voltage Range
GCI-2k	GinLong	2000	N/A	12.7	30 - 750 V

Voltec 2000	Voltec	2000	$299	2.73	10.5 - 15.5V
XP 1100	Exeltech	1100	$816	4.55	230 V+/-6%
UWT-I-250	Swea	250	$229.99	N/A	20 – 54V

TABLE 5: SAMPLE INVERTER LIST

Buying these parts separately should only be necessary when building a turbine completely from scratch or altering an existing turbine for improved performance, as most turbine kits will have these parts included and rated for the expected output of that particular turbine model.

Originally, induction generators were common in wind turbines and while they are still easy enough to find, the permanent magnet options have become equally as accessible. Both types of generator typically use copper wires to create and move the electric current through and from the generator. This is usually called the stator coil and it does not spin with the rotor of the turbine.

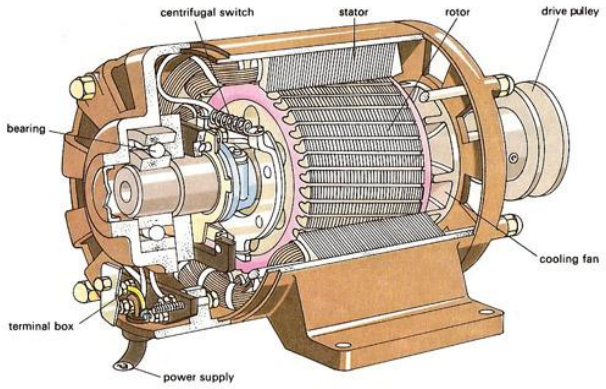

FIGURE 7: A CUT-IN VIEW OF AN INDUCTION GENERATOR

The permanent magnet design has magnets installed with alternating poles that replace the rotor coil to generate a current but the stator coil remains the same for both designs. Also, because magnets have charge already, the initial electric pulse needed to start an induction generator is not needed which cuts down on power losses and some weight may be cut out by eliminating the inner copper wire. Most permanent magnet generators use rare earth magnets which are slightly more expensive and may not tolerate high temperatures as well as inductor coils might. This makes the permanent magnet generator the more expensive option.

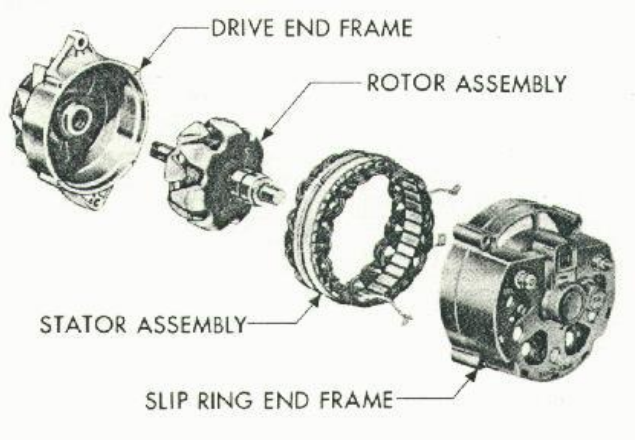

FIGURE 8: BASIC SETUP OF TURBINE GENERATOR WITH STATOR AND ROTOR ASSEMBLIES

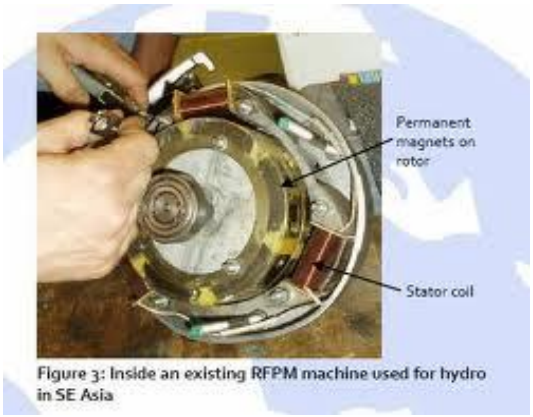

FIGURE 9: OPENED PERMANENT MAGNET GENERATON

Copper, Silver, or Gold

Generators use copper wires for the stator coil (and rotor coil in the case of induction generators) all the time. The possibility of using a different metal for electricity conduction was researched.

Metal	Melting point (Fahrenheit)	Electrical conductivity	Density	Price (per gram)
Copper	1984.3	0.596 10^6/cm Ω	8.96g/cc	$0.13
Silver	1762	0.63 10^6/cm Ω	10.5g/cc	$1.18
Gold	1948.24	0.452 10^6/cm Ω	19.32g/cc	$50.10

TABLE 6: METAL PROPERTIES

Copper is one of the best electrical conductors available and it is resistant to corrosion meaning that it will not rust. It also has a melting point of almost 2000 degrees Fahrenheit and is the cheapest option compared to gold or silver. It has the lowest density of the three options and this makes it the easiest to work into wires or other useful parts for machinery.
Silver is actually the best electrical conductor and is more expensive than copper. Plain silver would not work quite as well for engineering purposes as electrodeposited silver would. Unlike copper, it is not resistant to corrosion which means that it would need some kind of protection to prevent this from occurring. For corrosion protection, an electrodeposited nickel undercoat would work well. Also, silver has a lower melting point than copper so it would need a better cooling system if it were used. Despite being a better conductor, silver would not work quite as well in a generator as copper and therefore is not used.

Gold has the worst conductivity of these three options but its melting point is closer to copper's than silver is. Gold is by far the most corrosion resistant of all the metals. It also has the highest price as it is a precious metal and has the highest density. Due to this, gold may work for electrical systems but it is usually impractical due to its high price tag, making copper the better choice.

On/Off Grid Hook-ups

There are two ways that a wind turbine can be set-up to provide power for a residence or business: tied into the grid to supplement the existing power supply and off grid set-ups which are used to charge batteries which allow the power to be used at a later time. A third option does exist but it is merely a combination of these two with both batteries for storage and a grid tie-in to supplement produced power.

The Public Utility Regulatory Policy Act, a federal law passed in 1978, requires utilities to buy power from independent companies that could produce power for less than what it would have cost the utility. This law helped to create and advance the market for renewable energy by creating feasible energy options that were not based on fossil fuels. The Green Communities Act, a Massachusetts state law passed in 2008, made it possible for home owners to sell extra power from renewable energy sources back to electric companies for further distribution. These two laws enable people today to have wind turbines and solar panels produce power that is not just for use by a single household but capable of being sold to electric companies to help offset the costs of purchasing and installing these types of generators.

Setting up a wind turbine without connecting to the electric grid requires less parts, money, and assistance than tying into the grid to help offset monthly energy bills. By not tying into the grid, batteries become required to store any extra power produce by the generator for later use when the generator is not capable of producing more power, for example, a wind turbine with no wind blowing. The batteries are connected directly to the turbine and while power is used in the home or business, it flows through an inverter which takes the DC current produced by the turbine and converts it into useable AC power before actually being used by the electronic devices that are drawing that power. This kind of set-up can be done without a licensed electrician, though it may be recommended to hire one anyway.

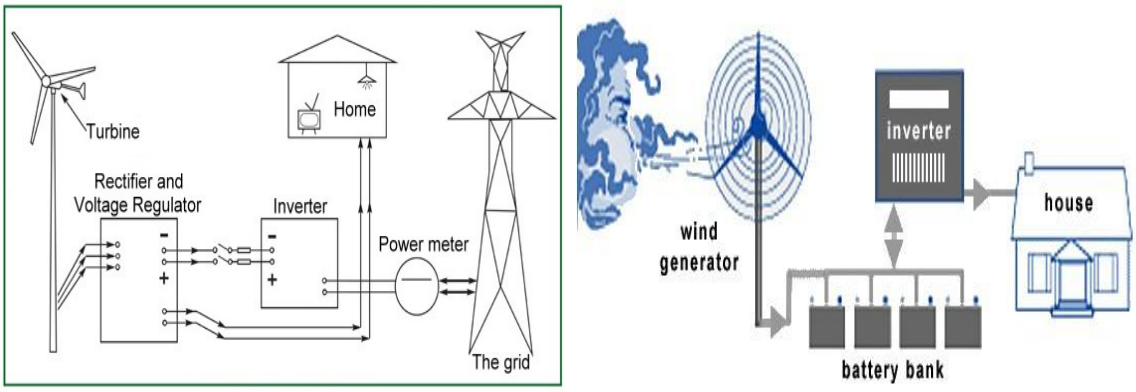

FIGURE 10: TYING A WIND TURBINE INTO THE GRID TO SUPPLEMENT POWER USAGE (LEFT) AND AN OFF GRID SET-UP WITH BATTERY BANK FOR STORAGE OF EXCESS PRODUCED POWER (RIGHT)

To tie into the grid, an agreement must first be signed with the chosen electric company to ensure that the company restrictions are applied to the wind turbine and the power that will be sold back so that accidents are avoided and any safety concerns are met. Instead of batteries, this set-up has the turbine connected to a voltage rectifier and regulator which is connected to both the residence and the inverter. Any power used in the home will flow directly there in AC form while the remaining power will flow through the inverter and into the electric grid. Due to the fact that this set-up now directly involves the electric company, a licensed electrician likely will be required to ensure that the set-up will not interfere with the grid performance or cause accidents if repairs need to be made. This makes tying into the grid the more expensive choice. However, by selling the additional power and making money back, the expenses should be paid off much quicker.

Patent Research

Many patents have been filed for small wind turbines. First, the types of patents which are available were researched. Utility patents are issued for the discovery of a new and useful process, machine, or any new useful improvement. Design patents are granted for the invention of a new, original, and ornamental design of an article to be manufactured. Next, some of the existing patents surrounding small wind turbines were looked into.

Mariah Power Inc. currently has a patent on a vertical small wind turbine system. This system produces less than 10 kW of power at peak operating conditions using a permanent magnet generator. This turbine has a power converter which switches the windings of the generator in order to limit the maximum amount of voltage output in high winds. The power converter also disconnects from the generator in high winds and provides no power to the system grid. In addition, the power converter has an inverter which controls switch firing in apply controlled loads to the generator power according to the wind speed. Genedics Clean Energy has a patent out for making small wind energy devices as well. Using three-dimensional lithography,

parts are manufactured and are handled and assembled with micro-tweezers, micro-scissors, and holographic lasers. Kari and Suri Appa have created a device for turbines which is a passive pitchable device. The device is a camshaft with camgrooves engraved in it in the shape of a half sine wave. Balls are allowed to roll around within these grooves and convert their axial displacement to a rotation or pitch angle for the blade, causing the blade to always be at the best angle of incidence with the wind. As the winds increase, the device continues its axial move outward while the blades rotate in the opposite direction so that dynamic loads are avoided. John Loth has a patent for vorticity cancellation for drag elimination at the trailing edge. By creating upper and lower surface boundary layers, the two cancel each other's opposing vorticities. This can be done using wind-rotor-propeller or fan blades with a platform which causes uniform bound circulation near the tip. Amick Global has constructed a tethered wind turbine which uses lifting gas and a tether to reap the wind's energy at low or high altitude. This design does not need a tower, nacelle, or gearbox. It is light enough to be turned to be aligned with the wind and fly at an optimum altitude with, optimally, a low drag coefficient. Hermann Cymara designed a wind turbine which is made to optimize power without increasing cost. It consists of vertical vanes and, in one manifestation, a shroud is moveable in order to keep an open side in the upwind direction and direct the wind toward the vanes. Another patent is that of General Electric for a wind turbine ring/shroud drive system. This turbine would be capable of driving multiple generators with a ring or shroud system to reduce blade root bending moments. The shroud would also protect the gearing and prevent gear lubricant contamination. In addition, Wind Solutions has designed a 3kW turbine with a 13 foot rotor diameter. This is a Diffuser Augmented Wind Turbine (DAWT) design and the company claims that the payback period for this model is 7.2 years. Composite Support & Solutions has patent for a similar design using a DAWT. A patent issued to Paul Pugh for a Wind Generator Kite System was also found. The generator is suspended in the air by wind currents and is used with many others which are raised to the desired height by rotary blade power and a gas balloon. The Valvular Sail Power Plant was patented by John Goldwater. This turbine is a windmill design which has radial vanes which rotate about a vertical axis in a horizontal plane. Each of the vanes include framework for supporting a grid which supports pivotally connected, vertically aligned, light-weight sails which automatically rotate according to wind direction and turn the windmill. The Vortex Enhanced Wind Turbine Diffuser belongs to Kinetic Harvest Limited. This diffuser for a wind turbine has slots which allow air to enter the diffuser in a swirl opposite to the swirl occurring within the diffuser due to rotation of turbine blades. The two swirls cross one another and cause vortices between them, energizing the Internsal swirl. Finally, Yangzhou Shenzhou Wind-driven Generator Co. makes small wind turbine generators. Their generators operate with low torque and a start-up wind speed of 2 m/s. The company also produces blades made from nylon, carbon fiber, and glass fiber.

Testing Standards for Certification

The standards to which most companies test their wind turbines against are the IEC 61400-2 Part 2: Design Requirements for a Small Wind Turbine and the American Wind Energy Association 9.1-2009. The IEC 61400-2 had been unavailable to this group since it must be purchased in order to view it in full, but was later retrieved. The AWEA standards were readily available. The purpose of these standards is to provide realistic and comparable performance ratings to consumers. They apply to wind turbines with a rotor swept area of 200 m^2 or less and

the primary units which are to be used in reporting the outcomes of testing turbines shall be metric, but inclusion of English units is recommended. Some of the aspects included in AWEA's Performance and Safety Standard for small wind turbines are that the tower design requirements must be included with the turbine and provided by the manufacturer and that, in labeling a turbine, the label must include the rated annual energy (rounded to no more than 3 significant figures), cut-in wind speed, cut-out wind speed, maximum power, maximum voltage, maximum current, and overspeed control.

Small Wind Certification Council Standards for Certification

Research was continued on the testing standards which small wind turbines must conform to so that, once the prototype of FloDesign's small wind turbine is built, it can be tested to these standards. The standards for certification from the Small Wind Certification Council (SWCC) were found. SWCC Certification is based on the evaluation of structural analysis and field testing of the small wind turbine. Field testing includes a power performance test, acoustic sound test, safety and function test, and duration test. The results of field testing and structural analysis are documented in a final report, which is submitted to SWCC for review. There are many fees associated with getting a small wind turbine certified by any organization. Tables 7 shows the fees associated with SWCC certification.

Fee Description	Fee Amount
Preliminary Review Fee	
Notice of Intent to Submit Application (for One)	US $2,500
Each Additional Model Configuration	US $1,250
Test Site Evaluation Fee	Varies
Certification Application Fee	Varies
Conversion from Conditional to Full Certification	Varies
Annual Certification Renewal Fee (per Turbine Model)	US $1,000
Annual Review Services Related to Annual Certification Report	Varies

TABLE 7: SWCC CERTIFICATION FEES

The SWCC also requires many different materials in order for a small wind turbine to seek certification. The materials which are necessary include: an introduction, all of the reference documents for the turbine, a summary report, power performance test report, an acoustic test report, duration test report, safety and function test report, a structural analysis report, and a log book documenting all testing performed.

The standards which the SWCC conforms to are those set forth in the AWEA standard which includes pieces of both the IEC Standard and the BWEA (British Wind Energy Assocation). The SWCC requires a summary report of the testing done on the small wind turbine for certification. This report must include an introduction, tabulated AEP vs. annual average wind speeds at hub height and sea level air density, AEP curve vs. annual average wind speeds at hub height and sea level air density, wind speed and power data at sea level air density, power curve, measured sound pressure levels, AWEA rated annual energy at 5 m/s, AWEA rated sound level, AWEA rated power at 11 m/s, and a summary of the tower design requirements from the manufacturer.

A power performance test report is also necessary, which includes how the test was set up, site assessment for obstacles and terrain, start and end dates and time of testing, the number of hours valid data was collected, completed bins, average air density during testing, cut-in and cut-out wind speeds, maximum power, voltage, and current, AWEA rated annual energy at 5 m/s, AWEA rated power at 11 m/s, wind speed and power data at sea level air density with the number of data points and the Cp for each bin, graph of power and Cp vs. wind speed, graph of binned power and a scatter plot of power vs. wind speed, tabulated AEP and extrapolated AEP, AEP curve vs. annual average wind speed, any data rejection criteria which differ from that in IEC 61400-12-1, and a summary of data analysis tool(s) used during testing.

The acoustic test required by SWCC must include a description of the equipment used and setup, the acoustic data gathered, AWEA rated sound level, description of obvious changes in sound at high wind speeds (at the point in time which overspeed controls are active), characterization of prominent tones observed during testing, and a summary of data analysis tools used.

The duration test must include many parts as well. A description of the test setup, which includes pictures, must be included along with the start and end dates and times of testing, an operational time fraction (OTF), a monthly summary of the OTF, explanations of OTF classifications not attributable to section 9.4.2.2 of IEC 61400-2 ed.2, verification of reliable operation during test, characterization of tower vibrations observed during the test, SWT class, total months of operation (at least 6), total hours of power production in any wind velocities (at least 2500 h), in $1.2V_{ave}$ and above (at least 25 h), and in winds of $1.8V_{ave}$ and above (at least 25 h), average turbulence intensity at 15 m/s, maximum instant wind speed during test, power production degradation results, results of post-test detailed inspection of turbine, with pictures, and a summary of the data analysis tools used.

The safety and function test report must include a summary of the safety and function test, a summary of an additional safety evaluation, and all of the manuals for the SWT.

The SWCC also requires a structural analysis report on any small turbine seeking certification. A licensed Professional or Charter Engineer must be commissioned to evaluate the structural analysis of the SWT and put the information found into a report whose format allows SWCC to review what was performed. The engineer has to show that the load cases were modeled with acceptable methods and the major components such as blade root or connection point, main shaft, yaw axis, connection to tower, and other components required by SWCC after review of the design, have been designed adequately based on load modeling and AWEA Standard requirements. A dynamic test between the turbine and tower must also be performed and documented to demonstrate avoidance of potentially harmful dynamic interactions. Once certification is granted to a turbine, that certification is valid as long as changes to the design have been reported to SWCC as required, the annual certification renewal fee has been

paid, turbine has not been changed in a way which significantly alters the original approved design, all field failures and malfunctions have been reported to SWCC, SWCC marks and labels have been used properly, and the holder of the certification has not been subject to legal or government complaints regarding their turbine or business practices. The requirements for certification renewal include an annual certification report, reporting of significant changes to the model, and the payment of the annual certification renewal fee. The annual report must contain any abnormal operating experiences, failures or malfunctioning of equipment, and other problems; modifications made, to include hardware and software changes; and complaints which relate to the turbine's compliance with the AWEA Standard.

IEC Standard 61400-2 Design Requirements for Small Wind Turbines

The standard set forth by the International Electrotechnical Commission (IEC) handles safety, philosophy, quality assurance, and engineering integrity for small wind turbines. It includes safety requirements for design, maintenance, installation, and operation. This standard can be applied to turbines of swept rotor area 200 m^2 or less and generating a voltage of less than 1000 V A.C. or 1500 V D.C. If the rotor area is less than 2 m^2, the tower is not considered part of the design.

One area which needs to be examined is the external conditions which the turbine will be subjected to. The lifetime of the turbine must be clearly defined in the documentation of the design. The wind turbine class is important in the design of a small wind turbine and can be determined using the table below.

SWT Class		I	II	III	IV	S
V_{ref}	(m/s)	50	42,5	37,5	30	Values to be
V_{ave}	(m/s)	10	8,5	7,5	6	specified
I_{15}	(-)	0,18	0,18	0,18	0,18	by the
a	(-)	2	2	2	2	designer

where

- the values apply at hub height, and
- I_{15} is the dimensionless characteristic value of the turbulence intensity at 15 m/s,
- a is the dimensionless slope parameter to be used in equation (7).

TABLE 8: BASIC PARAMETERS FOR SWT CLASSES

This helps in finding different wind conditions which will be useful in designing the small wind turbine. The Wind Speed Distribution gives the frequency of the occurrence of the different load conditions which the turbine may be subjected to.

$$P_R(V_{hub}) = 1 - e^{-\pi\left(\frac{V_{hub}}{2V_{ave}}\right)^2} \quad (1)$$

Equation 1 shows the wind speed distribution. The Normal Wind Profile Model (NWP) is used to define the average vertical wind shear on the wind turbine.

$$V(z) = V_{hub}\left(\frac{z}{z_{hub}}\right)^{\alpha} \tag{2}$$

Equation 2 gives the normal wind profile model. In this equation, α, the power law exponent, is assumed to be 0.2. The Normal Turbulence Model (NTM) shows the effects of varying wind speed, direction, and rotational sampling. It is the characteristic value of standard deviation of longitudinal wind velocity.

$$\sigma_1 = I_{15}\frac{(15+aV_{hub})}{(a+1)} \tag{3}$$

$$s_1(f) = 0.05(\sigma_1)^2\left(\frac{\Lambda_1}{V_{hub}}\right)^{-\frac{2}{3}} f^{-\frac{5}{3}}$$
$$\Lambda_1 = \begin{cases} 0.7\mathrm{z_{hub}} & \text{for } \mathrm{z_{hub}} < 30\ m \\ 21\ \mathrm{m} & \text{for } \mathrm{z_{hub}} \geq 30\ \mathrm{m} \end{cases} \text{ (turbulence scale parameter)} \tag{4}$$

Equation 3 gives the normal turbulence model. The power spectral density of the longitudinal component of turbulence approaches Equation 4. The Extreme Wind Speed Models (EWM) are given in Equations 5 and 6.

$$V_{e50}(z) = 1.4V_{ref}\left(\frac{z}{z_{hub}}\right)^{0.11} \tag{5}$$

$$V_{e1} = 0.75V_{e50} \tag{6}$$

Equation 5 gives the 50 year extreme wind speed and Equation 6 gives the 1 year extreme wind speed. These equations only apply to the 4 standard turbine classes (not class S). The Extreme Operating Gust (EOG) is given by Equation 7.

$$V_{gustN} = \beta\left(\frac{\sigma_1}{1+0.1\left(\frac{D}{\Lambda_1}\right)}\right) \quad \begin{matrix} \beta = 4.8\ for\ N = 1 \\ \beta = 6.4\ for\ N = 50 \end{matrix} \tag{7}$$

This is the gust magnitude for a recurrence period of N years. The wind speed defined for a recurrence period of N years is given in Equation 8.

$$V(t) = \begin{cases} V(z) - 0.37V_{gustN}\sin\left(\frac{3\pi t}{T}\right)\left(1-\cos\left(\frac{2\pi t}{T}\right)\right) & for\ \leq t \leq T \\ V(z) \quad for\ t < 0\ and\ t > T \end{cases} \tag{8}$$

In Equation 8, T=10.5 s for N=1 and T=14.0 s for N=50. Equation 9 gives the Extreme Direction Change (EDC).

$$\theta_{eN}(t) = \pm\beta_{arctan}\left(\frac{\sigma_1}{V_{hub}\left(1+0.1\left(\frac{D}{\Lambda_1}\right)\right)}\right) \tag{9}$$

$$\theta_N(t) = \begin{cases} 0 & for\ t < 0 \\ 0.5\theta_{eN}\left(1-\cos\left(\frac{\pi t}{T}\right)\right) & for\ \leq t \leq T \\ \theta_{eN} & for\ t > T \end{cases} \tag{10}$$

For Equation 9, θ_{eN} is limited to ±180°. Equation 10 gives the extreme direction change transient. In this equation, T=6 s is the duration of the extreme direction change transient.

$$V(z,t) = \begin{cases} V(z) & for\ t \le 0 \\ V(z) + 0.5V_{cg}\left(1 - \cos\left(\frac{\pi t}{T}\right)\right) & for\ 0 \le t \le T \\ V(z) + V_{cg} & for\ t \ge T \end{cases} \quad (11)$$

The Extreme Coherent Gust (ECG) is given by Equation 11. In this equation, a magnitude of V_{cg}=15m/s is to be assumed and T=10 s is the rise time.

$$\theta_{cg}(V_{hub}) = \begin{cases} 180° & for\ V_{hub} < 4\ m/s \\ \frac{720°}{V_{hub}} & for\ 4\ m/s \le V_{hub} \le V_{ref} \end{cases} \quad (12)$$

Equation 12 gives the Extreme Coherent Gust with Direction Change (ECD) which is when the two occurrences happen simultaneously. These different equations presented here can be helpful in the design of a new small wind turbine when considering external conditions faced by the turbine. Other conditions which deal with the climate also need to be considered. These may include temperature, humidity, air density, rain, snow, hail, solar radiation, chemically active substances, etc. This standard also discusses some normal conditions for operation. Normal operating conditions include ambient temperatures ranging between -10°C and +40°C, humidity up to 95%, intensity of solar radiation up to 1000 W/m^2, and an air density of 1.225 kg/m^3. The IEC Standard also recommends designing to withstand extreme environmental conditions including a range in temperature from -20°C to +50°C and lightning protection as dictated in IEC 61400-24 which does not need to be extended to the turbine blades. Ice and earthquakes should also be thought about; however this standard does not provide any minimum requirements for these extreme conditions, though it is recommended that the turbine be tested with a 30 mm layer of ice with a density of 900 kg/m^3.

In addition to climatic conditions, electrical external conditions need to be considered as well. The normal electrical conditions as set forth by the IEC Standard are as follows: the voltage shall be the nominal value ±10%, frequency normal conditions will be the nominal value ±2%, for a voltage imbalance, the ratio of negative- to positive-sequence components shall not exceed 2%, auto-reclosing cycles shall occur in periods of 0.2 s to 5.0 s for the first reclosure and 10 s to 90 s for the second reclosure, and it shall be assumed that outages occur 20 times per year for up to 24 hours. Some extreme conditions which could occur electrically and should be considered include deviations in voltage from the nominal value ±20%, variations in frequency ±10% of the nominal value, imbalances in voltage up to 15%, symmetrical and unsymmetrical faults, and outages up to 1 week. A battery-charging turbine must be able to operate from -15% to + 30% of its nominal voltage (12V, 24V, 36V, etc.) or 5% beyond the upper and lower settings of the charge controller. If the turbine is connected to the local grid, it must be expected that the turbine will encounter larger variations in voltage and frequency including ±15% of the nominal voltage value and the nominal frequency ±5 Hz.

In order to follow the standard in terms of structural design, the structural integrity must be verified and the ultimate and fatigue strength must be established. The methods which can be used to determine the design loads for the turbine are simplified load equations, aeroelastic modeling, and mechanical loads testing. The loads which need to be accounted for consist of vibration, inertial, and gravitational which are static or dynamic loads which result from inertia,

gyroscopic motion, rotation, gravity, etc; aerodynamic loads caused by airflow and the contact between it and stationary of moving parts can also be static or dynamic; operational loads result from the turbine itself, i.e. yawing, furling, braking, etc; and other loads which may occur depending on the operating environment, i.e. wave loads, wake loads, ice, transport, etc.

Load cases are set forth in this standard to determine the different conditions which a turbine may withstand. They are determined using a combination of assembly, erection, maintenance, and operational conditions. These cases include turbine operation without fault and with normal environmental conditions; turbine operation without fault and with extreme external conditions; turbine operation with fault and appropriate external conditions; and transportation, installation, maintenance design situations and appropriate external conditions. Several of these load cases should be considered to verify the structural integrity of the turbine. When the control and protection systems do not monitor and limit certain parameters of the turbine, cable twist, vibrations, rotor speed, and flutter must be accounted for. In order to use the simplified equations presented in the standard, the following configurations must be met: horizontal axis, two or more bladed propeller, cantilever blades, and a rigid hub. The parameters necessary for the simplified load equations are the design rotational speed, ndesign; design wind speed, vdesign; design shaft torque, Qdesign; maximum yaw rate, wyaw,max; maximum rotational speed, nmax; and the design tip speed ratio which can be found using $\lambda = \frac{V_{tip}}{V_{hub}} = \frac{\omega R}{V_{hub}} \Rightarrow \lambda_{design} = \frac{R}{V_{design}} * \frac{\pi n_{design}}{30}$.

$$\omega_n = \frac{2\pi n}{60} = \frac{\pi n}{30}$$

Table 9 shows some of the design load cases used for the simplified load calculations.

Design situation	Load cases		Wind inflow	Type of analysis	Remarks
Power production	A	Normal operation		F	
	B	Yawing	$V_{hub} = V_{design}$	U	
	C	Yaw error	$V_{hub} = V_{design}$	U	
	D	Maximum thrust	$V_{hub} = 2{,}5V_{ave}$	U	Rotor spinning but could be furling or fluttering
Power production plus occurrence of fault	E	Maximum rotational speed		U	
	F	Short at load connection	$V_{hub} = V_{design}$	U	Maximum short-circuit generator torque
Shutdown	G	Shutdown (braking)	$V_{hub} = V_{design}$	U	
Parked (idling or standstill)	H	Parked wind loading	$V_{hub} = V_{e50}$	U	
Parked and fault conditions	I	Parked wind loading, maximum exposure	$V_{hub} = V_{ref}$	U	Turbine is loaded with most unfavourable exposure
Transport, assembly, maintenance and repair	J	To be stated by manufacturer		U	

TABLE 9: DESIGN LOAD CASES FOR THE SIMPLIFIED LOAD CALCULATION METHOD

In this table, F is the analysis of fatigue loads and U is the analysis of ultimate loads. Also, if other cases are required by the specific SWT which are relevant for safety, they shall be considered. In Case A, constant range fatigue loading for the blade and shaft is assumed.

$$\begin{aligned} \Delta F_{zB} &= 2m_B R_{cog}\omega_{n,design}^2 \\ \Delta M_{sB} &= \frac{Q_{design}}{B} + 2m_B g R_{cog} \\ \Delta M_{yB} &= \frac{\lambda_{design} Q_{design}}{B} \end{aligned} \tag{13}$$

Equations presented in 13 are the blade loads and are considered to occur at the airfoil or hub junction, whichever has the lowest ultimate strength. The shaft loads are given in Equation 14.

$$\begin{aligned} \Delta F_{x-shaft} &= \frac{3}{2}\frac{\lambda_{design} Q_{design}}{B} \\ \Delta M_{x-shaft} &= Q_{design} + 2m_r g e_r \\ \Delta M_{shaft} &= 2m_r g L_{rb} + \frac{R}{6}\Delta F_{x-shaft} \end{aligned} \tag{14}$$

The value of e_r is 0.005R unless a lower value can be proven to be reasonable and the shaft loads are considered at the rotor shaft at the bearing closest to the rotor.

$$\omega_{yaw,max} = 3 - 0.01(\pi R^2 - 2) \tag{15}$$

Case B uses Equation 15 for a passive yaw system and calculates ultimate loads assuming the maximum yaw speed. If the turbine swept area is 2 m^2 or less, the maximum yaw rate is said to be 3 rad/s. In an active yaw system, the max yaw rate is measured in calm winds. To find the loads due to the bending moment on the blade and shaft, use Equation 16.

$$M_{yB} = m_B \omega_{yaw}^2 L_{rt} R_{cog} + 2\omega_{yaw} I_B \omega_n + \frac{R}{9}\Delta F_{x-shaft} \tag{16}$$

$$M_{shaft} = 4\omega_{yaw}\omega_n I_B + m_r g L_{rb} + \frac{R}{6}\Delta F_{x-shaft} \tag{17}$$

$$M_{shaft} = B\omega_{yaw}\omega_n I_B + m_r g L_{rb} + \frac{R}{6}\Delta F_{x-shaft} \tag{18}$$

Equation 17 is used for a two-bladed rotor and equation 18 is used for three or more blades on the rotor. For Case C, a yaw error of 30° is assumed.

$$M_{yB} = \frac{1}{8}\rho A_{proj,B} C_{l,max} R^3 \omega_{n,design}^2 \left[1 + \frac{4}{3\lambda_{design}} + \left(\frac{1}{\lambda_{design}}\right)^2\right] \tag{19}$$

Equation 19 gives the flapwise bending moment to be used in Case C. If no data is available on the maximum lift coefficient, $C_{l,max}$, use a value of 2.0. For Case D, high thrust loads on the rotor act parallel to the rotor shaft.

$$F_{x-shaft} = C_T 3.125 \rho V_{ave}^2 \pi R^2 \tag{20}$$

Equation 20 gives the maximum value and uses C_T as the thrust coefficient, equivalent to 0.5. Case E discusses the centrifugal load in the blade root and the shaft bending moment caused by the centrifugal load and rotor unbalance.

$$F_{zB} = m_B \omega_{n,max}^2 L_{rb}$$
$$M_{shaft} = m_r g L_{rb} + m_r e_r \omega_{n,max}^2 L_{rb} \quad (21)$$

This equation uses the maximum possible rotor speed, $\omega_{n,max}$, as $(\pi/30)n_{max}$. Case F occurs at a direct electrical short at the output or an Internsal short in the generator with a high moment about the rotor shaft.

$$M_{x-shaft} = GQ_{design}$$
$$M_{xB} = \frac{M_{x-shaft}}{B} \quad (22)$$

In Equation 22, when no other values are proven to be more accurate, use G=2.0. For Case G, the braking moment can be greater than the maximum driving moment in the mechanical or electrical braking system. In Equation 23, M_{brake} is derived from calculations or testing.

$$M_{x-shaft} = M_{brake} + Q_{design} \quad (23)$$

If the turbine is on a high speed shaft, M_{brake} must be multiplied by the gearbox ratio. The load the blade is subjected to during shutdown is determined by the shaft torque and the blade mass.

$$M_{xB} = \frac{M_{x-shaft}}{B} + m_B g R_{cog} \quad (24)$$

In the absence of proven, more accurate values, the shaft torque shall be multiplied by 2. Case H says that the out of plane blade root bending moment is dominated by drag.

$$M_{yB} = C_d \frac{1}{4} \rho V_{e50}^2 A_{proj,B} R \quad (25)$$

$$M_{yB} = C_{l,max} \frac{1}{6} \rho V_{e50}^2 A_{proj,B} R \quad (26)$$

$$F_{x-shaft} = BxC_d \frac{1}{2} \rho V_{e50}^2 A_{proj,B} \quad (27)$$

$$F_{x-shaft} = 0.17 B A_{proj,B} \lambda_{e50}^2 \rho V_{e50}^2 \quad (28)$$

$$\lambda_{e50} = \frac{\eta_{max} \pi R}{30 V_{e50}} \quad (29)$$

In Equation 25, C_d is the drag coefficient, assumed to be 1.5 and $A_{proj,B}$ is the planform area of the blade. Equation 26 is used at the point when $C_{l,max}$ occurs on the blade due to varying wind direction and if no data is available at this point, a value of 2.0 should be used. The shaft thrust load is given by Equation 27 and Equation 28 gives the spinning rotor thrust force. If λ_{e50} is not known, it can be estimated using Equation 29. The maximum bending moment of the tower may be calculated using either F x-shaft. The drag and lift forces on both the tower and the nacelle must also be accounted for. The load for each component can be found using Equation 30.

$$F = C_f \frac{1}{2} \rho V_{ref}^2 A_{proj} \quad (30)$$

				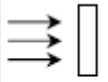	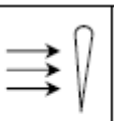	
Characteristic length < 0,1 m	1,3	1,3	1,5	1,5	1,5	2,0
Characteristic length > 0,1 m	0,7	1,2	1,5	1,5	1,5	2,0

TABLE 10: FORCE COEFFICIENTS, C_F

Table gives different force coefficients based on shape. In Equation 30, the force coefficient is C_f and A_{proj} is the component's area in the most unfavorable position. For Case J, loads caused by transportation, assembly, installation, maintenance, and repair are considered. These may include gravity loads during non-upright transportation, special installation tool induced loads, loads from the wind during installation, loads caused by hoisting the turbine onto the foundation, tilt-up tower loads during erection, and support structure loads introduced by climbing the structure. In order to figure out the load on the tower tilt up, use Equation 31.

$$M_{tower} = 2\left(m_{towertop} + \frac{m_{overhang}}{2}\right) g L_{lt} \quad (31)$$

In Equation 31, M_{tower} is the bending moment of the tower at the lifting point attachment in Nm, $m_{towertop}$ is the mass of the nacelle and rotor combined in kg, $m_{overhang}$ is the mass of the tower between the lifting point and the tower top in kg, and L_{lt} is the distance between the lifting point and the top of tower in m. This equation can be used based on the assumptions that the dynamic amplification factor is 2, the center of gravity of the turbine is along the rotor axis, and the maximum bending moment occurs when the tower is horizontal.

Another way to verify the structural design of a wind turbine is through the use of aeroelastic modeling.

Design situation	DLC	Wind condition		Other conditions	Type of analysis
1) Power production	1.1	NTM	$V_{in} < V_{hub} < V_{out}$ or $3V_{ave}$		F, U
	1.2	ECD	$V_{hub} < V_{design}$		U
	1.3	EOG_{50}	$V_{in} < V_{hub} < V_{out}$ or $3V_{ave}$		U
	1.4	EDC_{50}	$V_{in} < V_{hub} < V_{out}$ or $3V_{ave}$		U
	1.5	ECG	$V_{hub} = V_{design}$		U
2) Power production plus occurrence of fault	2.1	NWP	$V_{hub} = V_{design}$ or V_{out} or $2,5V_{ave}$	Control system fault	U
	2.2	NTM	$V_{in} < V_{hub} < V_{out}$ V_{e1}	Control or protection system fault	F, U
	2.3	EOG_1	$V_{in} < V_{out}$ or $2,5V_{ave}$	Loss of electrical connection	U
3) Normal shut down	3.1	NTM	$V_{in} < V_{hub} < V_{out}$		F
	3.2	EOG_1	$V_{hub} = V_{out}$ or $V_{max,shutdown}$		U
4) Emergency or manual shut down	4.1	NTM	To be stated by the manufacturer		U
5) Parked (standing still or idling)	5.1	EWM	$V_{hub} = V_{e50}$	Possible loss of electrical power network	U
	5.2	NTM	$V_{hub} < 0,7V_{ref}$		F
6) Parked and fault condition	6.1	EWM	$V_{hub} = V_{e1}$		U
7) Transport, assembly, maintenance and repair	7.1	To be stated by the manufacturer			U

TABLE 11: MINIMUM SET OF DESIGN LOAD CASES FOR AEROELASTIC MODELS

Situation 1 occurs when the turbine is running and connected to the electrical load and in which deviations from the theoretical optimum situations shall be accounted for. Also, the calculations shall be performed assuming the worst combination of conditions. Situation 2 occurs when a fault in the control or protection systems or an Internsal electrical fault will be assumed to occur during power production. A fatigue case for any single fault must be evaluated for a minimum of 24 hours/year. Situation 3 is all events resulting in loads during normal situations. The number of occurrences shall be estimated based on the control system and if a passive control system does not have automatic shutdown, the fatigue load may be ignored. Loads arising from Situation 4 must be considered and a wind speed limit for performing an emergency or manual shutdown must be prescribed by the manufacturer of the turbine. Situation 5 must be considered with extreme wind speed conditions being either turbulent or quasi-steady with a correction made to account for gusts and dynamic response. If it is possible that significant fatigue damage may occur to some components, the number of hours of non-power production time must be considered. Also, the loss of the electrical power network on a parked wind turbine must be accounted for. Analysis is required in Situation 6 when normal parked behavior has been deviated from due to faults on the electrical network or in the turbine itself. The consequences of any other faults should also be analyzed. Situation 7 is similar to Case J above and has the same examples of loads which should be accounted for. These may include gravity loads during non-

upright transportation, special installation tool induced loads, loads from the wind during installation, loads caused by hoisting the turbine onto the foundation, tilt-up tower loads during erection, and support structure loads introduced by climbing the structure.

Load calculations can be made by accounting for the following, where applicable: wind field perturbations due to the wind turbine itself, influence of three-dimensional flow on blade aerodynamic characteristics, unsteady aerodynamic effects, structural dynamics and coupling of vibration modes, aeroelastic effects, and the behavior of the control and protection system of the wind turbine. Load measurements are taken under conditions as close as possible to the design load case conditions and can be used in place of the design load calculations if they are taken under similar conditions. A stress calculation is calculated on all of the important load carrying components. The individual force and moment stresses may be combined to find equivalent stress. These values must then be compared to design values for material stresses. In addition, stress variations, stress concentrations, the magnitude and direction of resulting loads, component dimensions and material thickness variations, component surface roughness and treatment, the type of loading, and all welding, casting, machining, etc. must be accounted for.

	Circular blade root	Rectangular blade root	Rotor shaft
Axial load	$\sigma_{zB} = \frac{F_{zB}}{A_B}$	$\sigma_{zB} = \frac{F_{zB}}{A_B}$	$\sigma_{x-shaft} = \frac{F_{x-shaft}}{A_{shaft}}$
Bending	$\sigma_{MB} = \frac{\sqrt{M_{xB}^2 + M_{yB}^2}}{W_B}$	$\sigma_{MB} = \frac{M_{xB}}{W_{xB}} + \frac{M_{yB}}{W_{yB}}$	$\sigma_{M-shaft} = \frac{M_{shaft}}{W_{shaft}}$
Shear	Negligible	Negligible	$\tau_{M-shaft} = \frac{M_{x-shaft}}{2W_{shaft}}$
Combined (axial + bending)	$\sigma_{eqB} = \sigma_{zB} + \sigma_{MB}$		$\sigma_{eq} = \sqrt{(\sigma_{x-shaft} + \sigma_{M-shaft})^2 + 3\tau_{M-shaft}^2}$

TABLE 12: EQUIVALENT STRESSES

Condition	Full characterisation	Minimal characterisation
Fatigue strength	1,25[a)]	10,0 [b)]
Ultimate strength	1,1	3,0
[a)] Factor is applied to the stress ranges as shown in equation (48). [b)] Factor is applied to the measured ultimate strength of the material.		

TABLE 13: PARTIAL SAFETY FACTORS FOR MATERIALS

Material factors can be applied to material properties estimated with 95% probability with 95% confidence limits. Strengths occur on either a stress or a strain basis. Factors which should be considered in determining material properties include materials and material configurations representative of the full-scale structure; manufacturing method of the test

samples should be typical of those of the full scale structure; static, fatigue, and spectrum loading testing should be performed; environmental effects accounted for; and geometry effects which affect material properties.

Load determination method	Safety factor for fatigue loads, γ_f	Safety factor for ultimate loads, γ_f
Simple load calculation	1,0	3,0
Aeroelastic modelling with design data (r.p.m., power)	1,0	1,35
Load measurements with extrapolation	1,0	3,0

TABLE 14: PARTIAL SAFETY FACTORS FOR MATERIALS

The Load Partial Safety Factors account for the uncertainty in the load estimation method. Other analyses which can be performed are the limit state analysis and the ultimate strength analysis.

$$\sigma_d \leq \frac{f_k}{\gamma_m \gamma_f} \tag{32}$$

Equation 32 shows the ultimate strength analysis where f_k is the characteristic material strength, γ_m is the partial safety factor for materials, and γ_f is the partial safety factor for loads. Fatigue failure and damage from all loads shall be combined.

$$Damage = \sum_i \frac{n_i}{N(\gamma_f \gamma_m s_i)} \leq 1.0 \tag{33}$$

In Equation 33, n_i is the counted number of fatigue cycles in bin i in the characteristic load spectrum and s_i is the stress or strain level associated with the counted cycles in bin i, including effects of mean and cyclic range. Also, N is the number of cycles to failure as a function of stress or strain and γ_f and γ_m are safety factors for loads and materials, respectively.

$$n = \frac{Bn_{design}T_d}{60} \tag{34}$$

Equation 34 gives the number of fatigue cycles where T_d is the life of the turbine in seconds. If no S-N curve is available, use the ultimate strength as the material strength and the partial safety factor for fatigue and minimal characterization, γ_m=10.0. Critical Deflection Analysis should also be performed to verify that no safety affecting deflections occur during design load cases. In addition, it must be verified that no mechanical interference occurs between the blade and the tower.

The protection and shutdown system of the turbine must be able to keep all parameters within the design limits under all load cases and it may be active or passive. The rotational speed design limit, n_{max}, may not be passed. The protection system must be designed to be fail-safe and be capable of satisfactory operation under manual or automatic control settings. If the turbine swept area is greater than 40 m^2, manual shutdown procedures are required. If the area is less than that, the shutdown procedure still must be specified but a manual shutdown button or switch is not required, although recommended. The manufacturer must also provide a safe method for shutting down the turbine when maintenance, service, or inspections need to be performed. In addition, manufacturer provides a maximum wind speed and other conditions which maintenance

may be performed in. This maximum speed shall not be less than $0.5V_{ave}$. The lowering of a tilt-up tower to bring the turbine to a stop is an acceptable method.

All of the mandatory tests, such as the design load cases previously stated, must be performed used calibrated instruments and appropriate sample rates. The tests must be documented in the final report with a description of test methods, test methods, specifications of the tested turbine and the results of the tests. The tests shall be performed in order to verify the design data by determining the data required for the simplified load analysis or to verify the aeroelastic model. The tests will determine the design power, design rotational speed, design shaft torque, and maximum rotational speed. The design wind speed shall be $1.4V_{ave}$ and the design power and design rotational speed are the power level an rotational speed at that wind speed. These should be determined at the normal electric load. Measured data shall be binned into 0.5 m/s wind speed bins from 1 m/s below V_{in} to $2V_{ave}$ and shall contain at least 30 data points.

$$\begin{matrix} n = 0.6 + 0.000005P_{design} & for\ P_{design} \leq 20000\ W \\ n = 0.7 & for\ P_{design} > 20000W \end{matrix} \quad (35)$$

$$Q_{design} = \frac{30P_{design}}{\eta\pi n_{design}} \quad (36)$$

Equations 35 and 36 can be used to find η, the drive train efficiency. The maximum yaw rate is the maximum speed of the yaw movement of the rotor about the yaw axis. The measured values of the yaw rate cannot be used in the simple load calculations. However, if a manufacturer wishes to validate their design by measuring the maximum yaw rate, it must be considered that yaw rates are highly influenced by the external conditions around it, interpolation or extrapolation may be necessary in finding the maximum yaw rate, and ambiguous results can be a result of deriving the yaw rates from the yaw positions. The maximum rotational speed shall be measured in turbine conditions most likely to yield the highest rotor speed. This shall also be found using interpolation or extrapolation, while accounting for visible slope changes in data. Technical load testing is done to validate design calculations or to determine design loads. Sufficient testing must be done in this category to be able to characterize typical operational behavior. In order to validate a design, the mean, minimum, and maximum values along with their standard deviations are needed. The data which will need to be measured during this type of testing include loads, meteorological parameters (hub height wind speed and direction), and turbine operational data (rotor speed, electrical power, yaw position, and turbine status). Duration testing must also be completed in order to investigate the structural integrity and material degradation of the design, the quality of the environmental protection of the turbine, and the dynamic behavior of the turbine. The turbine passes the duration test only when reliable operation occurs throughout the test period, has at least 6 months of operation time, power production in winds of any velocity for at least 2500 hours, power production in winds of $1.2V_{ave}$ and above for at least 250 hours, and power production in winds of $1.8V_{ave}$ and above for at least 25 hours. The wind speed shall be the 10 minute average of samples of at least 0.5 Hz and the average turbulence intensity at 15 m/s and the highest wind speed occurring during the test shall be stated in the documentation. Throughout duration testing, the turbine behavior shall resemble normal turbine use as much as possible. In addition, the duration test is not required for each tower configuration if it can be demonstrated that the alternate configurations do not exceed the design limits. Reliable operation is said to occur during an operational time fraction of at least

90% and when there is no major failure of the turbine or components in the turbine system. Also, no significant wear, corrosion, or damage to the turbine components may occur and there may be no significant degradation of produced power at comparable wind speeds. The Operational Time Fraction is a measure of performance as a ratio of time a wind turbine shows normal behavior to the test time in any evaluation period expressed as a percentage. Normal turbine behavior is defined by the turbine producing power, automatic start-up and shut-down due to transitioning across low wind cut-in and high winds cut-out, idling or parked states at wind speeds under V_{in} or above V_{out}, and the extended time between normal shutdown (not caused by failure) and a restart of the turbine. This is given by equation 37.

$$O = \frac{T_T - T_N - T_U - T_E}{T_T - T_U - T_E} \times 100\% \quad (37)$$

In Equation 37, T_T is the total time period under consideration, T_N is the time during which the turbine is known to be non-operational, T_U is the time which the turbine status is unknown, and T_E is the time excluded from the analysis. The standard gives some examples of these different values. Power Production Degradation is measured through power levels binned by wind speed and then plotted by bins as a function of time. Then, if a trend is visible in the data, the cause must be determined through investigation. Dynamic behavior must be assessed to verify that the system does not vibrate excessively and observed under all operating conditions from the cut-in wind speed to 20 m/s. Special attention must be paid to tower vibrations and resonances, turbine noise, tail movement and yaw behavior. For a blade test, the applied load shall be the worst combination of the flap-wise bending moment and centrifugal force. No damage may occur up to the maximum operating load to pass, although it is recommended to test the blade to failure. The hub should be tested statically by simulating the centrifugal for and flap-wise bending at all connection points; no damage may occur at the design test load. The nacelle must be tested as it is subjected to the shaft tilt bending moment, axial rotor force, and its own weight. To complete the yaw mechanism test, loads are applied as described under the nacelle frame test and then it must be shown that the yaw mechanism still works properly. A gearbox test is not required; however, it is recommended that one be performed in accordance with the AGMA/AWEA 921-A97 standard. A safety and function test shall verify that the performance of the turbine displays the predicted behavior of the design and shows properly implemented personal safety provisions. Some critical functions to verify the control and protection system are power and speed control, yaw system control (wind alignment), loss of load, overspeed protection at design wind speed or above, and the start-up and shut-down above the design wind speed. Some other entities to observe include excessive vibration protection, battery over- and under-voltage protection, emergency shutdown under normal operation, cable twist, and anti-islanding (for grid-connections). Environmental testing is done to make sure the turbine is designed for the external conditions aside from the normal external conditions and the turbine must be subject to tests simulating those conditions, preferably performed on entire turbine. In terms of electrical testing, the critical electrical subsystems are evaluated and tested to the relevant IEC and national standards.

All electrical system components must comply with the applicable portions of IEC 60204-1 and the national and local codes. All components must be able to withstand all design environmental conditions and mechanical, chemical, and thermal stresses. Protective devices on the electrical equipment must ensure the protection from malfunction of the SWT and the external electrical system. A disconnect device must be provided to allow for complete

disconnection from all sources of electrical energy for maintenance and testing. A semiconductor device cannot be used alone. Earthing systems must include the local authority standards. Lightning protection must be matched by the installation, choice of equipment, and arrangement of the earthing system. The installation documentation must also include the range of soil conditions which may be used. Lightning protection is not required to extend to the blades but the rest of the turbine must comply with IEC 61400-24. Conductors shall be rated with respect to temperature, voltage, current, environmental conditions, and degrader exposure. Mechanical stresses shall also be considered. Armored cables must be used if there is a probability of rodents or other animals chewing on cables; underground cables must be buried at a suitable depth. If the turbine is battery-charging, the battery temperature and expansion as well as the conductor size and rating of insulation must be considered. If the turbine is grid-connected and the turbine is able to be self-excited, the turbine must automatically disconnect in the event of a loss of network power. The harmonic line currents and voltage waveform distortion cannot interfere with the electrical network protective relaying and the overall waveform distortion must not exceed the upper limit for the network.

The support structure shall be included as a part of the system if the swept rotor area is greater than $2m^2$. Local codes and regulations must be met. It is required that continuous operation at resonance frequencies leading to excessive vibrations is avoided. The support structure must be able to withstand all listed external conditions and consideration should be given to operation, installation, and maintenance at extreme environmental conditions. The support structure (along with guy wires, if applicable) must be properly earthed to reduce lightning damage. The rotor area must be specified by the manufacturer if the swept rotor area is greater than $2m^2$ and also, the manufacturer must provide detailed drawing of a sample foundation system and soil conditions. Normal maintenance loads resulting from climbing and raising and lowering the tower must also be considered.

The manuals provided must give a clear description of assembly, installation, operation, and erection requirements. The installation manual must include drawings, procedures, specifications, instructions, and packing lists. It also must have the details of the loads, weights, lifting tools and procedures necessary for a safe installation. If it is required that installation be done by a trained personnel, it must clearly state, “TO BE INSTALLED BY TRAINED PERSONNEL ONLY.” An electrical interconnection wiring diagram with the International markings for electrical machine terminals must be included in the manual. If the swept area is less than 2 m^2, the manufacturer must provide the information necessary to select a support structure. These qualities include details on the mechanical turbine/tower connection, details on the electrical turbine/tower connection, minimum blade/tower clearance, maximum allowable tower top deflection, and the maximum tower top loads. This information is also recommended if the swept rotor area is greater than 2 m^2.

The operation manual must include procedures for stopping and starting the SWT under normal operating conditions. All controller settings must also be included. There must also be a manual procedure written out which includes the wind speed limit and the other safe conditions for procedures. In addition, contact information must be provided.

Maintenance and inspection documents must be provided with space to give the description of the inspection, shutdown procedure performed, and the routine maintenance requirements. If it is required that maintenance and service only be performed by trained personnel, it must state, “MAINTENANCE AND REPAIRS TO BE PERFORMED BY TRAINED PERSONNEL ONLY.” An interval for routine maintenance and repairs must also be

provided. The components which must be inspected, a list of equipment and measurements to ensure proper operation, and a recommendation that a logbook documenting the date, time, inspection, important events, and corrective action be kept must also be included in the documentation. If the turbine must be shut down before maintenance can be performed, state, "CAUTION—PRIOR TO PERFORMING ROUTINE MAINTENANCE, FOLLOW PROCEDURE FOR PROPER SHUTDOWN OF WIDN TURBINE."

Safety procedure documentation must be provided as well. Procedures which must be included are disengaging the load or energy sources, stopping and securing the rotor, stopping and securing the yaw mechanism, stopping and securing the furling system, if appropriate; the procedures to be included are not limited to those previously mentioned. If the turbine is grid-connected, a way to disconnect from the grid must be provided as well. Finally, safety recommendations for climbing the tower, including the equipment needed and the procedure for it, must be included in the safety documentation.

A troubleshooting list should be provided so that it may be checked by a trained operator before calling in service personnel. All manuals must supply personal safety information, such as, for climbing towers, anchor points, etc. A wind speed limit for climbing and/or lowering the tower must also be specified in the documentation.

The IEC Standard requires that certain aspects of the turbine are clearly stated on its packaging. The following must be prominently and legibly displayed on the name plate: turbine manufacturer and country, model and serial number, production date, maximum voltage and current at the turbine system terminals, and the frequency at the turbine system terminals when connected to the grid. In addition, it may be beneficial to add the tower top mass, survival wind speed, SWT class, swept area, design power, and blade length.

An investigation into small wind turbine certification to determine if certification is worth pursuing for FloDesign Wind Turbine's small turbine has been conducted. The aspects which have been looked at in detail include the testing standards which are used on small wind turbines which become certified, the places where certification could be sought, and what it would cost to certify FloDesign's small wind turbine. In the end, a conclusion about whether certification is necessary or worth pursuing is drawn.

The SWCC has many fees associated with its certification of small wind turbines. About half of these fees vary, causing the price of certification to range anywhere above $4,750. Certification through MCS (Microgeneration Certification Scheme) costs between $80,060 and $160,120. Looking at these numbers, it is obvious that it could become very costly to certify a small wind turbine, especially when considering the annual fees associated with certification renewal, around $1,000 per turbine configuration.

Though there are currently no turbines certified by the SWCC, there are several which have been granted a temporary certification and are waiting on a report or two to be completed before full certification is granted. Table shows the status of SWCC applicants for certification.

Applicant	Turbine	Under Contract	Under Test	Certification Granted	Certification Number
American Zephyr Corporation	Airdolphin GTO	5/20/2010	2/12/2010		Application Pending
Bergey Windpower	Bergey 5kW	5/27/2010	4/14/2011		Application Pending

Co.					
Bergey Windpower Co.	Bergey Excel-S	6/15/2010	6/24/2010		Application Pending
BRI Energy Solutions, LTD	Vbine 10-05	1/31/2011			Application Pending
Endurance Wind Power	Endurance S-343	6/7/2010			Application Pending
Enertech, Inc.	Enertech E13	9/27/2010			Application Pending
Evance Wind Turbines Ltd.	Evance R9000	8/13/2010	Certified Under MCS	Conditional Temporary Certification 05/13/2011	SWCC-10-27
Eveready Diversified Products (Pty) Ltd.	Kestrel e400i 3kW 250V	6/18/2010			Application Pending
Eveready Diversified Products (Pty) Ltd.	Kestrel e400i 3kW 48Vdc	6/18/2010			Application Pending
Evoco Energy	Evoco 10kW	2/14/2011	Certified Under MCS	Conditional Temporary Certification 05/05/2011	SWCC-11-01
Gaia Wind Ltd.	GW 133 - 11kW	12/20/2010	Certified Under MCS		Application Pending
Polaris America LLC	P15-50	10/15/2010			Application Pending
Polaris America LLC	P10-20	11/19/2010			Application Pending
Potencia Industrial S.A.	10kW Hummingbird	9/23/2010			Application Pending
Proven Energy Inc.	Proven 11	6/7/2011	Certified Under MCS		Application Pending
Proven Energy Inc.	Proven P35-2	6/7/2011	Certified Under MCS		Application Pending
Renewegy, LLC	Renewegy VP-20	5/25/2010			Application Pending
Seaforth Energy	AOC 15/50	6/16/2010			Application Pending

Southwest Windpower	Skystream 3.7	6/7/2010	Certified Under MCS	Conditional Temporary Certification 05/13/2011	SWCC-10-20
Taisei Techno Co.	TTK-10Kw	10/20/2010			Application Pending
Talk, Inc.	Suelflow 100	2/8/2011			Application Pending
Urban Green Energy	UGE-4K	11/30/2010			Application Pending
Urban Green Energy	UGE-1K	11/30/2010			Application Pending
UrWind Inc.	UrWind O2	6/15/2010	12/13/2010		Application Pending
Ventera Energy Corporation	Ventera VT10	6/11/2010	7/14/2010		Application Pending
Windspire Energy	Windspire - 800040	6/4/2010			Application Pending
Xzeres Wind Corporation	Xzeres-442SR	6/3/2010	Certified Under MCS 07/07/2008		Application Pending

TABLE 15: APPLICATIONS FOR CERTIFICATION TO THE SWCC

Some European wind turbines along with Southwest Windpower's Skystream 3.7 have been able to receive certification through MCS, allowing easier marketing in Europe for those turbines since those will be the turbines which are acceptable to make a homeowner qualify for Feed-in Tariffs and the Clean Energy Cash Back Scheme. Proven Energy has had some turbines certified through the Energy Independence Corporation (EIC) as well. Since many European grants require certification for turbines to qualify and many wind turbine manufacturers are located in Europe, it would be a reasonable conclusion to draw that the United States should follow the same path and most likely will. Some bills proposing required certification and/or a universal testing standard for all small wind turbines are already in the works.

Certification is beneficial to the consumer because it holds all small wind turbines to the same standard, allowing for easy comparisons. The consumer is only able to benefit from certain government and state programs if the turbine which they install is certified through a certain body. For example, Southwest Windpower's certification by MCS allowed their turbine to have homeowners benefit from Feed-in Tariffs in Europe and the Clean Energy Cash Back Scheme. Also, the manufacturers benefit from the increased confidence from funding agencies to back small wind projects. Manufacturers may gain a wider range of market if their turbine is certified and a certain market area requires certification for homeowner grants. The overall industry also benefits from certification since false claims are prevented and credibility of the wind industry is maintained.

Certification benefits greatly outweigh the negatives in these findings. Benefits exist for the consumers, manufacturers, and industry. The need for certification or an International testing

standard cannot be far off, as there are already proposals for both of these. If FloDesign does not wish to seek certification for their small wind turbine and wait until it is required, it is still necessary to perform the tests required by the IEC to verify the design data. In addition, it would be useful to follow the AWEA and SWCC guidelines for certification to ensure that, if certification by any body's standards do become a requirement, problems will not arise with the product already out in use.

Fabric/Foam Research

Coatings and covers were researched for the foam inserts. The urethane foam will need ample protection against denting and also UV radiation to prevent premature deterioration. Composite coatings such as fiberglass will be some of the strongest and longest lasting, but also the most expensive. The foam will have to be sealed before the fiberglass is applied to prevent the epoxy from melting the foam. Fiberglass cloth or mat could be used to coat the inserts depending on which is deemed more economical.

Truck bed liners were another major point of interest since the composition of the spray on liners is made to last for years in the toughest of conditions. It is extremely strong and extremely durable. One concern with this product is the expense, as many of these liners need special equipment to apply them. Also the texture is usually rough to create a nonskid surface which will affect the aerodynamics.

Polyurea/Epoxy foam coatings have been used in foam sculptures for years. They can either be sprayed or painted on and cure into a hard shell on the outside of the foam. Higher grade sprays have UV blocker in them to increase its lifespan. Many people use these coatings, specifically Styrospray 1000, for outdoor applications. It can either be applied to the foam part or it can be sprayed in the mold before the foam is poured. Samples of this material were received by this team.

Fabric and shrink wrap were also looked at, but the life span on these fabrics is at most 2 years, which is well below the expected lifetime of our turbine and replacement of these will be expensive and impractical (climb pole/roof detach the turbine etc.). This fairly routine maintenance will most certainly be a major turn off for potential customers. Research is still being conducted for longer lasting fabrics.

The final option under investigation is to use plastic injection modeling through a company like Quick Parts. The company would be able to use the SolidWorks models developed by the team and create professionally done plastic inserts instead of foam. This will probably not be viable for the prototype due to weight constraints. However it is not being ruled out.

Table shows a list of a few companies and their products. The Styrospray seems to be the most economical for our application with regard to price, set up, application, and ease of use. It is easy to apply and has a reasonable cure time. Styrospray is the product that is used in the foam sculpture industry and has been created for exactly the application the team intends to use it for.

Type	Brand/Site	Product	Material
Composite	Fiberglast	2 oz fabric	Fiberglass cloth
	Fiberglast	Bi-directional	Fiberglass cloth
	Fiberglast	continuous strand	Fiberglass mat
	Fiberglast	chopped strand	Fiberglass mat
Epoxy	Demand Products	Ureshell	Polyurethane Foam Hard Coat
	Demand Products	Liquid Rock	Epoxy Hard Coat

	Industrial Polymers**	StyroSpray**	Polyurethane Foam Hard Coat
Fabric	Marine Shrink Wrap (9 months)	Shrink Wrap	Plastic
	Transhield (lasts 2-4 years)	Fabric	Polyester/Foam
	Transhield (lasts 2-4 years)	Train Shield	Heat Shrink
	Transhield (lasts 2-4 years)	AAD-VCI	Heat Shrink
Truck Bed Liner	Rhino Liner	Bed Liner	Polyurea Spray on Coating
	Line-x	Light Industrial Coating	Polyurea Spray on Coating
Injection Molding	Quick Parts*	Plastic Injection Molding	Urethane

Brand/Site	Application	Cure Time	Unit Size	Cost
Fiberglast	w/ Epoxy	-	3 sq yard	$18.65
Fiberglast	w/ Epoxy	-	3 sq yard	$32.95
Fiberglast	w/ Epoxy	-	3 sq yard	$27.45
Fiberglast	w/ Epoxy	-	3 sq yard	$27.45
Demand Products	Roller/Brush	24 hr	1 gallon	$85.00
Demand Products	Roller/Brush	Dependent on Mass	1 gallon	$69.00
Industrial Polymers**	Roller/Brush/Spray Gun	24hr/Coat every 30 min	1 gallon	$52.38
Marine Shrink Wrap (9 months)	Wrap/Heat	Lasts 9+ months	12'X175'	$177.00
Transhield (lasts 2-4 years)	Wrap Custom Fit Covers	Instant	Any	Quote
Transhield (lasts 2-4 years)	Wrap/Heat	Instant	Any	Quote
Transhield (lasts 2-4 years)	Wrap/Heat	Instant	Any	Quote
Rhino Liner	High Pressure High Heat	24hr		Quote
Line-x	Spray OEM (expensive)	24 hr		Quote
Quick Parts*	Custom			Quote

TABLE 16: LIST OF COMPANIES AND PRODUCTS FOR FOAM COVERING AND COATING

Foam Research

Foam Expansion

The team looked at how the foam actually expands and used that to find out how much would be needed for all 9 lobes. Starting with 5 ml of each chemical and experiencing a 2 ml loss in pouring into the mixing container, the compound was then mixed and poured into a square container, losing 17 ml of expanded foam. The foam was allowed to expand in its container and the next day a water displacement test was done. The foam test measured in with a volume of 110 to 120 ml and with the added foam loss, a total of 127 to 137 ml of foam was created out of the 8 ml of compound. The expansion is around 15.875 to 17.125 times the original compound, rather than the advertised 20 times. After further calculations, it would take from 1,584.196 cubic inches to 1,768.938 cubic inches (or 25 960.3212 **ml** to 28 987.7002 **ml)** of pre mixed compound to create 9 lobes.

Foam Mold Removal

Removal of the foam from its mold casing was explored and it seems that the smoother the surface, the better it works. After testing the ease of removal, it was deemed that a bit of sanding and 2-3 layers of wax, let to dry and harden and then buffed off, would make the removal process the easiest. Other options that have not been tried yet are petroleum jelly or possibly use of a cooking spray along with fine sanding could work as well. But as of now, fine sand paper and 2 to 3 coats of wax will work well. To improve the removal of the foam from the mold, the mold pieces should have a surface finish when ordered from the 3-D printing company. This will aid in the clean removal of the parts.

Mock-up

The foam mockup was constructed to better understand how molding foam works and what the properties of the foam are like. This made it easier when trying to design the full scale foam prototype. The foam mockup was not to scale and did not follow any predetermined lobe configurations. As seen below it was purely a visual and educational mockup.

FIGURE 11: FOAM MOCKUP

Tower

Tower Research

Towers are a vital component of any wind turbine because they control what height the turbine operates at, how easily repairs may be performed, and they are the structural support of the turbine itself. Different towers are available for various needs and situations. The major parameters are tower type, height, foundation and mount type, and efficiency of install and repairs. Different towers have different benefits and disadvantages. The specifications currently being sought include being easy to fix and repair, 7-13 meter height, and inexpensive.

The different types of towers can all be used effectively given the proper situation. Freestanding monopoles seen in Figure are tapered and extremely bulky. They are also hard to install, repair, and maneuver. However, they are also extremely reliable and sturdy as well as aesthetically pleasing.

FIGURE 12: FREESTANDING MONOPOLES

Freestanding lattice towers use a lot of steel and are costly. In addition, they are displeasing to the eye. However, they are quite sturdy and it is much easier to do maintenance work on a large lattice tower than a large monopole.

FIGURE 13: FREESTANDING LATTICE TOWER

Guyed lattice towers take up considerably more space horizontally, but are lighter, take up fewer resources to install and are much cheaper. Its ability to be repaired is still difficult,

since it either must be completely taken down or it must be climbed. These aspects make it very similar to a free standing lattice tower.

FIGURE 14: GUYED LATTICE TOWER

Tilt-up towers require the most land around them to keep them upright, but have the easiest method of repair: simply tilting it downward. They are more expensive then a guyed lattice tower, but cheaper then both of the free standing counterparts.

FIGURE 15: TILT-UP TOWER

Tilt-down towers are usually limited in height up to about 40 feet, but are easy to repair and install. The price of these towers is similar to tilt up towers, and take up less space.

FIGURE 16: TILT-DOWN TOWER

Company	Height (m)	Type	Cost ($)	Mount	Foundation	Climbable

Aerocraft	7 8.75 10.5 12.25	Modular, Guyed	2115.66 - 2954.78	Flange/ bolt	Concrete Blocks	Yes
Windenergy	7 8 8.8 9 10.2 13 13.7 14 15 16.7 18.3 20 21 24	Free, Guyed, Roof, Monopole, Segmented	308 - 11,215	Flange	Cement anchors	No
Ampair	10 12 15 18 24 30 36	Lattice, Monopole	2215.73 - 14666.67	Gantry, Stern, Mizzen, DIY Pole	Bolting	Lattice Only
Wes5	6 12	Monopole	Part of Total Cost	Flange	Concrete Block with Anchor	No
Turby	5 6 7.5 9	Spring Supported or Free Standing	6163.53	Flange	Cross Frame/Tube	No
Quiet Revolution	9 Minimum	Free standing	Part of Total Cost	Flange	Concrete Block, Roof, Tripod	No
Independent Power Systems	12.192	Tilt down	Varies	Custom	Concrete Block	No

TABLE 17: DIFFERENT TOWER OPTIONS

The constraints set forth by the team in terms of tower options have eliminated some of the more complex, expensive types of towers. Most small wind turbines use free standing monopoles or guyed poles, because of their look and lower cost. However, they are hard to repair and install, even if segmented, making it difficult for owners to maintain them. Free standing monopoles also use too much material to be cost effective and lattice towers are obtrusive in the tree line. A lattice tower is simply not something that most would put in their yards and it is still moderately difficult to repair. A tilt-up tower would be fine if the horizontal space is available. Out of all the tower options researched, the best choices would be a tilt-down tower or a telescopic tower, if found. This leaves smaller, less expensive towers with smaller footprints, which include guy less tilt down, a gin pole set up, or possibly creation of a new tower using an I beam.

Since hydraulics make installation of tilt-up towers too expensive, a hand-operated or low power option is needed. This could be a hand crank or winch, which could both operate a telescopic or tilt down tower. Adding a low power or manual winch will cost more but in the end could make the maintenance of the tower much easier.

Although it would be the most expensive option, guy-less tilt down towers create the easiest method of repair and install. It ships in two separate pieces, the top of which can tilt down to achieve the easiest method of repair. It takes up very little room on the ground and one could be ordered from Independent Power Systems.

FIGURE 17: GUY-LESS TILT-DOWN TOWER

The medium cost option is a guyed tilt-up, which take up quite a lot of room. However, it is not too difficult to install or repair, usually just needing a truck or winch to raise it up and down. There are many gin pole kits available and it would be possible to create a tower to fit the specifications set forth, or simply buy a complete set.

FIGURE 18: GUYED TILT-UP

I-beams pose an interesting solution to the cost issue. I-beams are extremely cheap to produce, but there is no current research on using them as towers. The best guess at a drag coefficient of an I-beam would be 2.7, done in a study of fluid movement in mines. If it is possible to design a mount to fit the top, and a foundation to hold it, a very cheap, easy to use solution could be found.

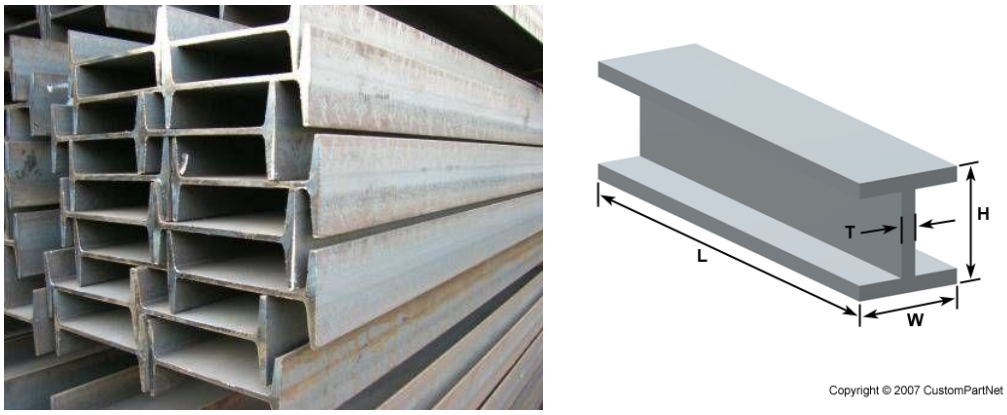

FIGURE 19: I-BEAMS

The draw backs of this method are that they are not aesthetically pleasing, the drag problem mentioned, and the weight. A very sturdy base and mounting method would be needed which may drive the cost up.

Bergey Tower Research

The Bergey tower set up by Curt Freedman at Western New England University stands 50 feet above ground level and has a motorized winch to bring it down for installation and repair. Much is already known about the wind in the area due to prior studies done with the XL1, and therefore makes it a capable tower for use. It currently only supports the 75 lb XL1, but was tested at 200 lbs of force and the highest points of stress were found, shown in Figure .

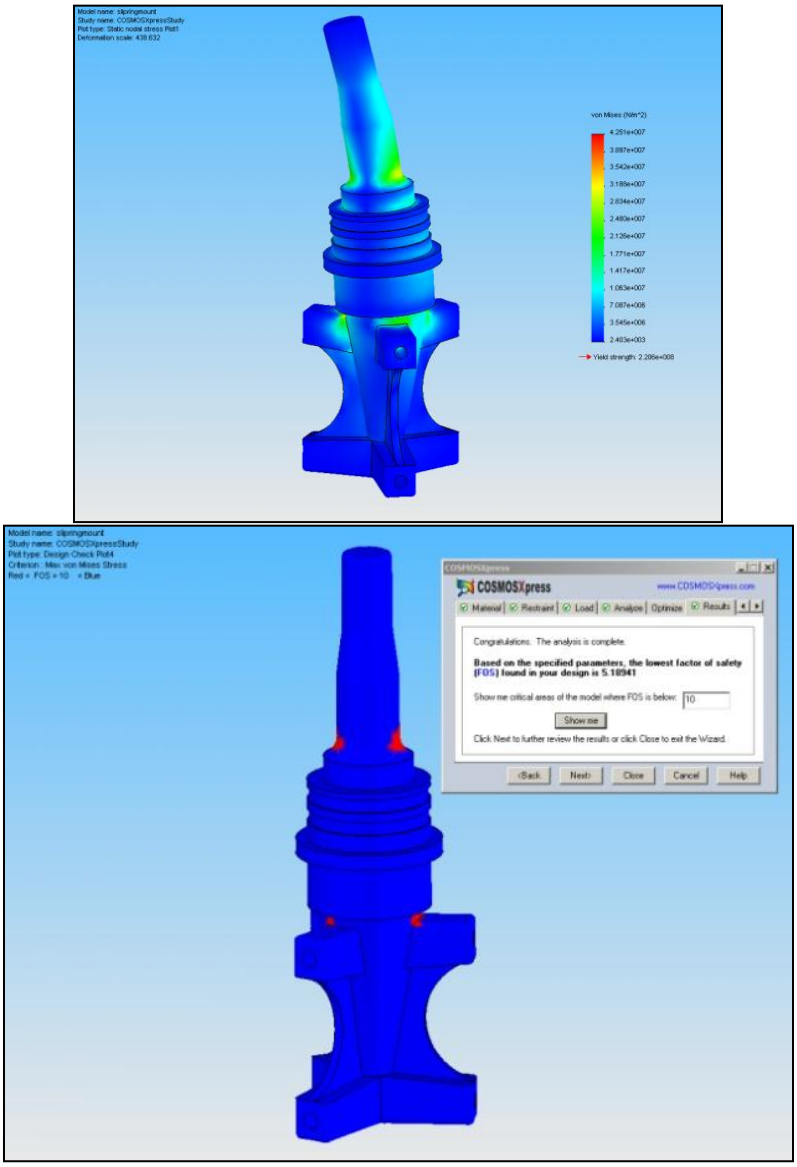

FIGURE 20: A STRESS TEST AT 200 LBS OF FORCE YIELDED 3X10^7 N/M^2 IN THE WEAKEST POINTS

The winch would make it easy to switch the Bergey XL1 out with the FE1024 and the new prototype. There is a monitoring and recording device already hooked up to the Bergey, leaving little extra work to do to before beginning testing. The Bergey tower is 110.1 mm in diameter, so a mount must be designed accordingly for each of the other turbines.

Mobile Towers

For the purpose of testing our prototype and the FE-1024, which will be used for comparison, it was decided that a temporary and mobile tower should be used to avoid any long set-up times and to be able to remove the tower once testing has been completed. Ideally, the

tower chosen should be able to support a minimum of 200 lbs, has a maximum height of 30-50 feet and has a small footprint when set-up.

Only a few companies were contacted for this as most mobile towers were advertised as specialized for communication purposes and had limited or no potential for use with a wind turbine. Of the contacted companies, the Aluma Tower Company showed some promise, though they responded quickly and honestly that their towers probably would not work well with our project. They also recommended the US Tower Corporation which seems to have two mobile towers that would fit our requirements: the TRTMU30MDPL, with a 30 foot max height and 350 lb maximum, and the RMTU656MDPLGO, with a 56 foot max height and 650 lb maximum.

FIGURE 21: THE TRTMU30MDPL (LEFT) AND THE RMTU656MDPLGO (RIGHT)

The team received a quote during the week of 7/18-7/22 from AllTech Communications for leasing a 106 foot mobile tower. AllTech limits leased towers of the 106 foot variety due to the large range of heights this tower can achieve. While a height of 106 feet is a little over the top for the scope of this project, the tower could be set up at any height between 29 feet and 106 feet which should allow for testing at many different heights for the performance of the prototype. The quote was as follows:

ATC-106 Mobile Tower Trailer Rental Rates per Unit / per Month:
1-6 months $3,000
7-12 months $2,500
12+ months Negotiable depending on length of lease

Figure shows a couple of pictures of the 106 foot tower.

FIGURE 22: ALLTECH 106 FOOT TOWER BEING TRANSPORTED (RIGHT) AND IN USE BUT NOT FULLY EXTENDED (LEFT)

Prototyping

The first prototype which was going to be built was an SLA scale model. This prototype would have been built using the C144 lobe and shroud configuration. This was a 9 lobe configuration which has the potential to fit a stator rotor system. The reason the C481 was not used is due the difficultly of putting a stator rotor system into it. The SLA prototype would have been produced to replicate the methods in which the full scale model will be put together. Each lobe and strut will be slid on to the stator rotor support ring. The only part that would not be multiple parts was the ejector. Eventually that will be designed to be disassembled but for now it is being left as is. Certain parts of the prototype would be press fit, like the bearing and nose cone, however other parts will be screwed together. The major components would attach using the t-slot method that this prototype is based on. An exploded view of the SLA model can be seen below.

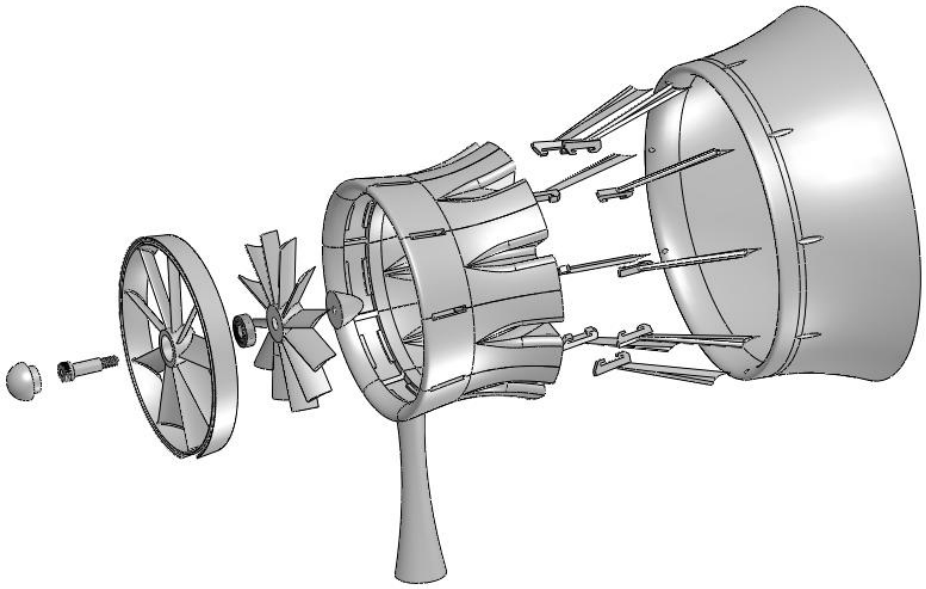

FIGURE 23: EXPLODED VIEW OF THE SLA MODEL

The model had a rotor diameter of about 4 inches while the ejector inlet had a diameter of about 6 inches. That means this model is true to the approximate 1.5 ratio between rotor diameter and ejector inlet diameter. A stand was also designed into the model so it would not fall over. The approximate weight of the model would have been 0.7 lbs when calculated with a SLA material density of 1092 kg/m^3. Due to the sensitive timeline of this project it was decided that a SLA prototype should not be focused on and more effort should be put into the final design.

Stator Rotor Prototype

The stator rotor program from Tim Hickey was used to design the stator and rotor for the 1 kW home turbines. The rotor diameter was originally set to 42 inches with a wind speed of 11 m/s. When the curves were imported to SolidWorks it was realized that the center body was a little too large. After getting in contact with Tim, the program was adjusted to allow for a smaller center body giving the most surface area for the stator and rotor. Another issue was creating a solid body for the curves of the blades. Since the curves were open, a solid loft could not be done, only a surface loft. Then, each curve was manually closed and then a solid loft was performed. The stator blades were originally designed to twist as they extended outwards. After comparing the performance of a twisted stator and a straight blade stator it was determined that there was little difference. For that reason the stator blades were made straight to save on cost.

It was decided to permanently attach the stator to the support ring so that, when the parts are made, the stator and support ring would be cast as one ring. Figure shows the larger center body and Figure shows the corrected center body. The smaller center body gives about a 1 inch difference in diameter to the diameter of the alternator. This has allowed for maximum surface

area for the rotor blades. The stator support ring and also the rotor blade tips would have to be adjusted when the prototype model is completed.

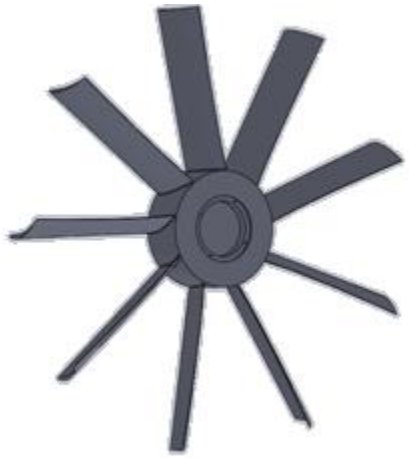

FIGURE 24: ORIGINAL STATOR BLADES

FIGURE 25: ADJUSTED CENTERBODY

C481 Stator Rotor

It was attempted to put a stator rotor in the current C481. This was unsuccessful due to the lack of room for the rotor and stator blades. The leading edge was then extended following the leading edge's original contours as closely as possible until the length was reached for the stator to fit. Figure shows an angled view of the finished product.

FIGURE 26: ANGLED VIEW OF C481 WITH A STATOR ROTOR (LEFT) AND CLOSE-UP OF STATOR ROTOR (RIGHT)

The leading edge was extended 1.525 inches to fit the stator as seen in Figure . This allowed for both the stator and rotor to fit comfortably. It requires that the stator be pushed as far forward as possible. The stator was fit flush against the front face of the leading edge. The original design had a stator rotor support ring with a locking t-slot as seen in figure 22. Because the stator was so far forward the support ring was removed and the stator was turned into its own support ring. In figure 28 it can be seen that the dark grey components in front are the stator components. The t-slot was changed from a male to female and moved from the top to the right side. The model has been greatly reduced in weight due to the reworking of the stator and rotor from 180 lbs to around 70 lbs.

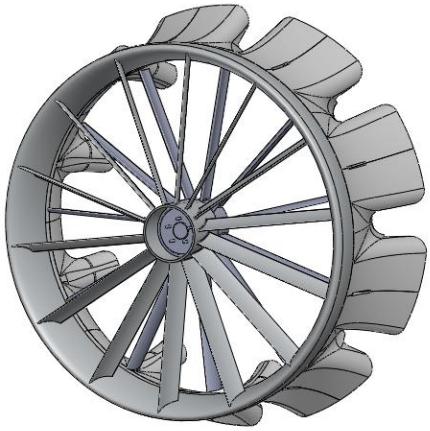

FIGURE 27: STATOR ROTOR PLACED IN THE C481

Figure shows a cut away of the extension to the leading edge. The blue profile is the original and the outside line is the modified version which will be used for the prototype. CFD was planned to run the stator rotor in 3D to determine the lift and drag coefficients. This was then compared to data at FloDesign from previous models.

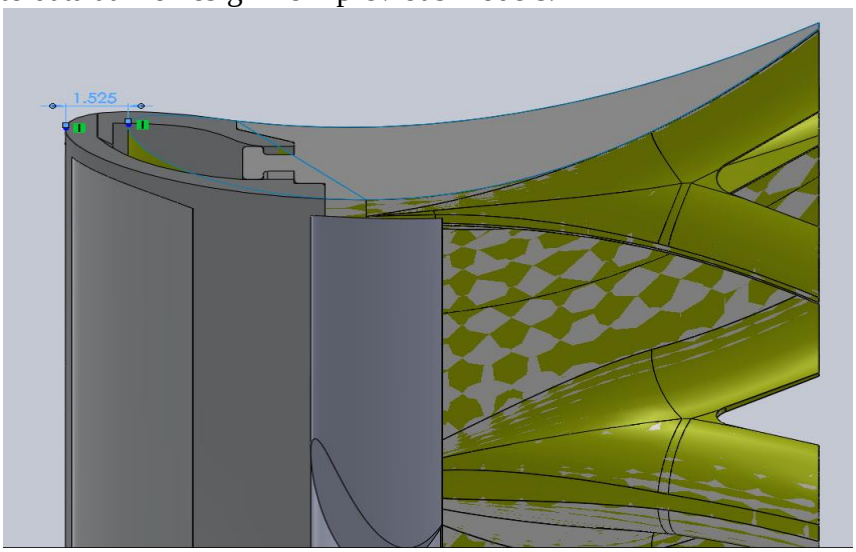

FIGURE 28: CUTAWAY OF THE LEADING EDGE OF THE ORIGINAL AND MODIFIED C481

CFD was run for both the straight profile and curved profile rotor with the straight blade stator. The curved profile rotor had roughly three times greater lift coefficient than the straight blade. Since the rotor is being made as a single piece, it was determined that the curved profile

would be worth the extra effort during fabrication. Also the center body has been increased to an 8.5 inch diameter hub to prevent blockage between the blades at the base.

Finding a company to produce the stator ring turned out to be unsuccessful due to the size and intricate profiles. It was decided to break up the stator ring into three parts, the outside and inside ring and then the stator blades. Since the blades were straight, extruding them through a dye should not be a problem. The blades would then be welded onto both rings. The only problem for extruding the blades is the lead time needed as well as the minimum order size. For a prototype extruded blades is not feasible.

Foam Molding and Metal Working Companies

Several custom foam molding and metal working companies were researched and contacted to see if they would be capable of assisting in the development of the parts for the small wind turbine prototype. These types of companies were located all over America, though to make things easier, a final choice somewhere along the east coast or in New England would probably be best as it would hopefully cut down on delivery time and expenses.

The metal companies were contacted to possibly produce the ejector struts, gurney flap, stator and generator mounting plate. Some of the companies were found in Massachusetts in cities such as Ludlow and South Hadley. While nothing was described in detail with the first contact of these companies, some responses were received saying that assistance would be possible and if there were any questions, send an email along to have them answered.

The custom foam molding companies would be responsible for making the mixer lobes and ejector and hopefully finishing them with a polyurea coating to boost weather resistance and durability. None were found in Massachusetts, though there were some in nearby states, such as Connecticut, New Hampshire and New York. As with the metal companies, nothing was described in detail in the first contact and but most responses said that they would not be able to do it due to part size or some other problem.

The table below shows the complete list of companies originally contacted, what they produce, and if they have sent a response as to whether or not they will be able to help with this project.

Company	Product	Contact Method	Response	Capable
MDI products	foam	email	yes	no
Foam Molders and Specialists	foam	email	no	
Urethane Technology Co.	foam	email	no	
Dayton Rogers	metal	email	no	
Defiance Stamping Company	metal	email	no	
Trident Compinents	metal	email	no	
FM Corporation	foam/metal	email	yes	no
Tech Fab	metal	email	yes	yes
Elite Metal Fab	metal	email	no	
Lomont Molding Inc	foam	email	no	
Harbor Foam	foam	email	no	
GI Plastek	foam	email	yes	yes
EDCO Industries	foam	email	no	
Quick Parts	plastic/metal	online	yes	yes
Alcumet	metal	online	yes	yes

Industrial Polymers	foam	email	yes	no
ProtoCam	foam	email	yes	no
Bergad	foam	email	no	
Armourcoat	foam	email	yes	no
South-Pak	foam	email	yes	no

TABLE 18: COMPANIES THAT HAVE BEEN CONTACTED FOR MAKING CUSTOM PARTS

For the sake of visualization, the map below shows the approximate location of the closest and most capable, three custom foam molders and three metal working shops to FloDesign's location. These companies would be:

- ➔ Foam (green): GI Plastek Wolfeboro (Wolfeboro, NH)

  Edco Industries, Inc (Bridgeport, CT)

  Urethane Technology Company, Inc (Newburgh, NY)

- ➔ Metal (red):Tech Fab, Inc (South Hadley, MA)

  Elite Metal Fabricators, Inc (Ludlow, MA)

  Dayton Rogers Manufacturing Company (Rochester, NY)

FIGURE 29: MAP OF LOCATION OF FOAM AND METAL COMPANIES

Contact with these companies was continued in order to make a reliable and realistic choice of companies to produce the pieces needed to complete this project. Also, as seen above, several companies had not yet responded, so many more options could still be explored.

More companies were contacted in order to find companies which would be able to make the foam and metal parts for the prototype. Many of the companies that the group contacted said that they were not able to create the necessary parts. Some companies did not have machinery to make the parts and others would not take on such a small project because they did not feel it would be worth it for them. Another company said that the design would have to be changed in order to make it feasible. It appeared that the team would need to find some flexibility in the design and must discuss where the flexible areas are. This caused a proposal for a design change in the stator so that the ring and the stator blades would be made separately and then assembled afterward.

Contact was continued with several companies, a few quotes were received and more companies were taken off of the list of possibilities. The quotes that were received are as follows:

- Spectrum Plastics Group had a quote on the nose cone, tail cone and rotor for a total value of $6,762
- Paramount had a quote on the nose cone, tail cone, and rotor for a total of $12,720
- Dayton Rogers had a quote on the ejector strut for a total of $576

Also, none of the estimated lead times offered by these companies have gone past a two week period.

After the redesign of the turbine to its smaller size, many companies had to be contacted again. However, to save on time and hassles, the companies contacted were limited to those who FloDesign already has non-disclosure agreements with. Table below shows the companies contacted and whether or not they would be able to manufacture the stator and rotor.

Company	Phone	Capable?	Email
A.G. Miller Co., Inc	413-732-9297	Yes	wolfgang@agmiller.com
AA Precision Machine Co.	508-673-1698	Center Hub	bill@AAprecisionmachine.com
AdChem Mfg Tech Inc	860-645-0592		Call back 8/2-Carl Buckowiecz
Ameron International Corp	626-683-4000	No	-
Arcor Laser Services LLC	860-370-9780		albert@arcorlaser.com
Ariston Technologies, LLC	1-401-575-8144	No	-
B E Peterson Inc.	508-436-7900		daniel.szczurko@bepeterson.com
C&C Fiberglass Components, Inc.	401-254-4342		cesar_duponte@northcoastboats.com
Camm Metals	860-292-6260		matt@cammmetals.com
Dayton Rogers	1-800-677-8881	No	-
DLBA Robotics, Ltd	757-925-1010	No	designfile@dlbarobotics.com
Essex Engineering	781-595-2114		
Framingham Welding	508-875-3563		

Gilchrist Metal Fab	603.889.2600		
HUB Technologies, Inc	508-947-3513	No	sthomas@vertexfd.com
Klinger Engineering, LLC	413-563-1480		
Mack Prototyping	978-632-3700		
McCauley Propeller Systems	800-621-7767		
McClarin Plastics, Inc	1-800-233-3189		
Mountain Based Mold & Manufacturing	413-527-9590		
Paramount	215-757-9611 (X225)		Garys@paramountind.com
Plainville Machine Works	1-508-699-7575		
Quantum Composites	989-922-3863		
Rotating Composite Technologies	860-829-6809		
Saint-Gobain Performance Plastics Corp	1-800-243-6322		
Scaled Composites, LLC	661-824-4541	No	-
Spincraft	978-667-2771 (MA) 262-784-8440 (WI)		
Windings, Inc	507-359-2034		
Wingard & Co	410-358-2210	No	sales@hydroblanking.com
Yankee Casting Company, Inc.	1-860-749-6171	Yes	mark@yankeecasting.com

TABLE 19: COMPANIES CONTACTED DURING WEEK OF 7/18-7/22

Future Energy 1024 Generator

The Future Energy 1024 generator was received during the week of July 14th. This turbine was opened and inventory was taken to make sure that everything was accounted for. Once all the components were located the turbine was assembled. The blades were attached to the hub and balanced while the generator was assembled on the hub. This gave a better idea of how the FE1024 fits together. The spare permanent magnet generator that was order was taken and fully modeled. A model was already made of the dimensions given online but certain discrepancies were found when modeling the PMG with calipers. It was the model made of the dimensions gathered that was used in the final Solidworks model.

Sectioned Stator

The second stator design was done to make it easier for manufacturing. A solid ring stator is difficult and expensive to manufacture for a prototype. For that reason the stator was broken into seven different pieces. The blades and center body are included in each piece as seen in Figure and Figure .

FIGURE 30: SECTION OF STATOR

FIGURE 31: FULL ASSEMBLY

The entire stator is formed by bolting the seven pieces together. The alternator bracket will slide in before the pieces are fully assembled and lock in place via a key slot. The sectional stator will provide a higher chance of finding a company to produce the parts in a timely fashion.

After making those changes it was decided that each section was still too costly to make so the stator was redesigned again. The stator was redesigned by Christian to have nine blades and about a 38 inch diameter after values were recalculated and 42 inches for the diameter was determined to be too big. He also redesigned the rotor to have 7 blades and a 34 inch diameter. Figure shows the newly designed stator section. Figure is the outer stator ring section and Figure is the full stator.

FIGURE 32: INNER STATOR SECTION

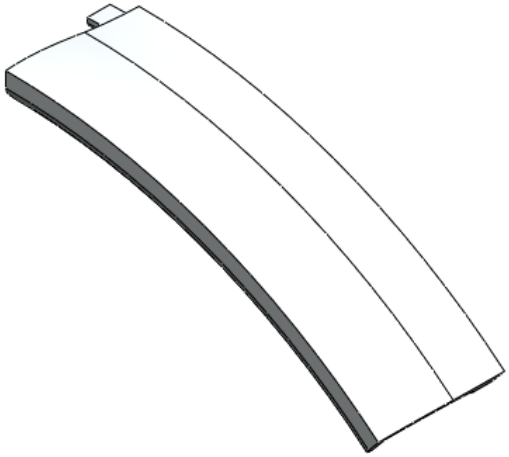

FIGURE 33: OUTER RING STATOR SECTION

FIGURE 34: FULL STATOR

Figure through Figure show the different aspects of the rotor.

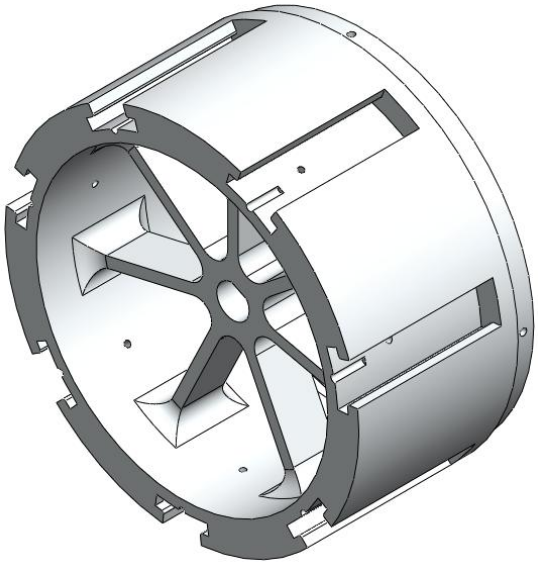

FIGURE 35: INNER ROTOR HUB

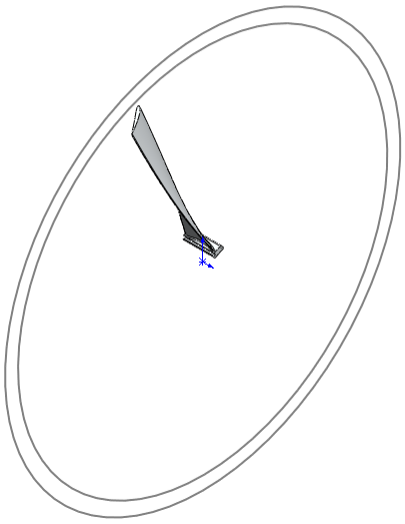

FIGURE 36: ROTOR BLADE

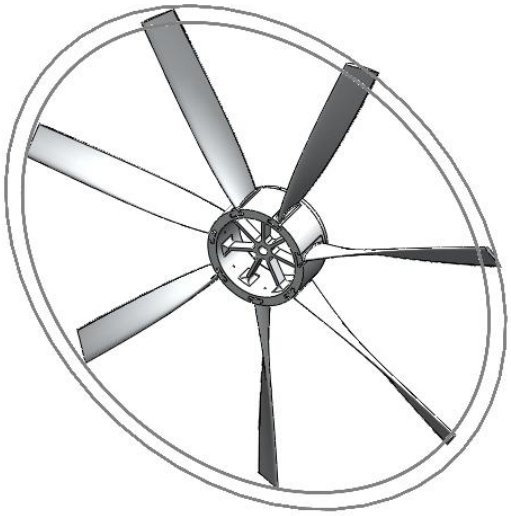

FIGURE 37: FULL ROTOR ASSEMBLY

The stator and rotor sizes were adjusted during the week of 7/25-7/29 to a diameter of about 34 inches. The team met with Tim Hickey to discuss the stator and rotor setup and which parameters to use in the equation. The stator blades have remained straight because the curvature of the profile is very minimal and straight blades makes production much easier. The 60% profile was extruded to create the stator blade. The rotor blades have remained curved because the performance increase is substantial.

A few different options have been created for the stator and rotor. Both the stator and rotor have a design of a single piece and also a design that has the blades separate so that they may either locked in or get welded into place. The most recent designs are shown in Figure .

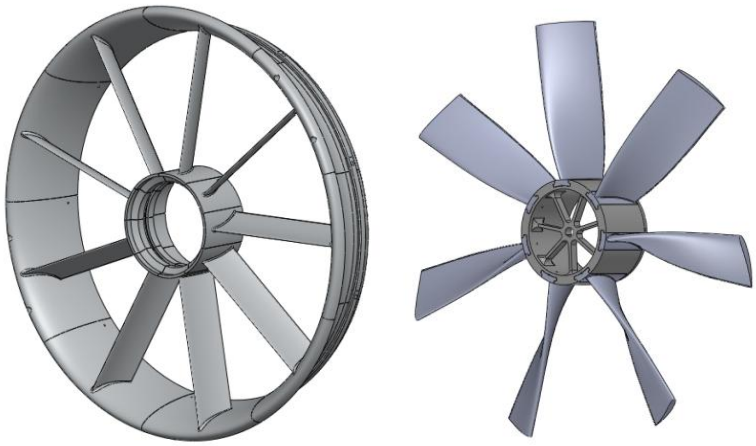

FIGURE 38: STATOR AND ROTOR OPTIONS

After the meeting at Boulevard Machining, it was realized that a solid stator would have to either be casted, which will be difficult, or 5 axis machined which will cost hundreds of thousands of dollars, which is not a viable option. It was also discussed to cut the blades out and make a center body piece and the outer ring. The blades could be extruded through a die and welded using dowel pins to ensure the correct alignment. The outer ring could be lathed out. This option is also expensive because extrusion companies usually require at least 1000 ft before they will consider setting up a die.

A quote was received from Yankee Casting Company for the stator and rotor for both aluminum and magnesium. The cost for setting up the mold for both the stator and rotor is around $20,000 each and then each part costs between $1,000 and $2,000 to pour. This seems to be our best option so far. SLS would cost $25,000 and would result with a plastic stator. This option is not only cheaper than SLS, but also gives the team a strong metal part. However the setup time for the die is 10 to 14 weeks.

Modifications to the Model

Jeff King pointed out that the shroud diameter of the design needed to be increased. Using the program he provided, it was determined that the shroud diameter needed to be increased approximately eight inches. This can be seen in Figure and Figure .

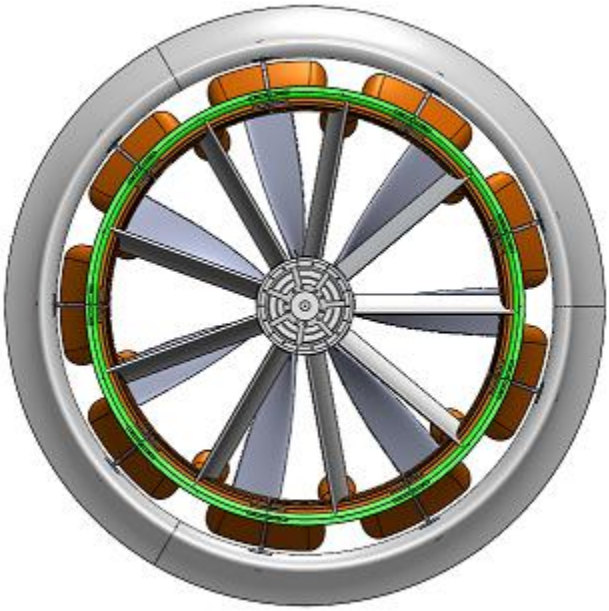

FIGURE 39: PREVIOUS FULL MODEL

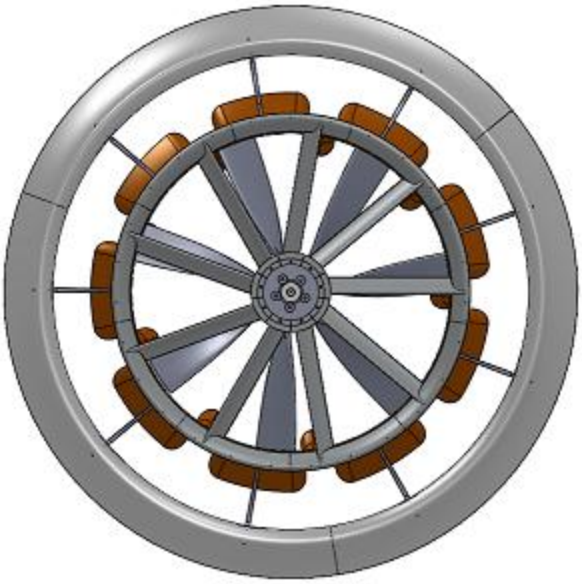

FIGURE 40: UPDATED SHROUD CONFIGURATION

In addition, Jeff expressed concerns about the rotor size and its capabilities to be able to produce 1 kW of power. Also, some changes to the way the stator pieces connect to one another were made.

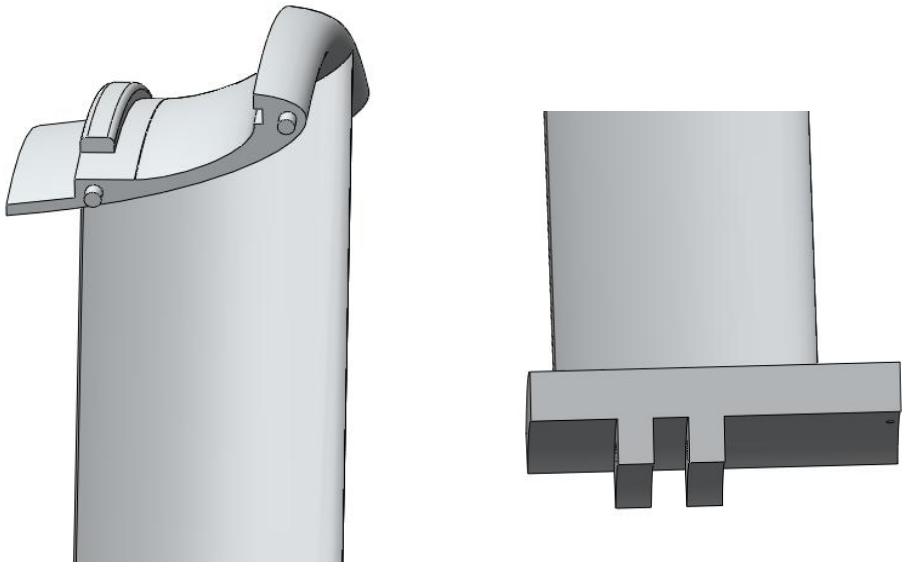

FIGURE 41: MODIFICATIONS TO STATOR CONNECTIONS

The team was informed at the meeting with Boulevard Machine and Gear that the slight modifications, such as making square corners rounded, would make a large difference in price.

Design Consultation Meetings

Meeting with Paramount and Jeff King

The team met with Mark Dupuis from Paramount Industries on August 2, 2011. The updated stator and rotor designs were presented to him to see if he could make any suggestions in terms of production. He explained the process of a QuickCast, in which aluminum is cast inside an SLA coating. This is a more expensive option than the SLS, but would most likely be a sturdier, long term option. However, SLS should be sufficient for a prototype. The quotes for producing the stator in each of these forms are still being drawn up. The team had previously discussed the option of producing the rotor in SLS and received a quote from Paramount Industries for $3,480 for the rotor alone, which covers a dry fit of the assemble-able rotor made in 8 different pieces; 7 blades and the center hub. This showed that the previous quote of $25,000 for both the stator and rotor was mostly driven up by the stator. Now that the stator is in smaller sectioned pieces, the cost to produce the stator will hopefully decrease substantially.

In addition to meeting with a Paramount representative, the team also met with Jeff King at FloDesign on August 2. He explained the manufacturing process in some more detail than was previously within the knowledge of the team, design aspects which showed some problems in the design presented at this meeting, and coating options for the foam pieces which are planned to be used in the shroud and mixer ejector lobes. During this meeting, it was discovered that the start of the shroud was too close to the ends of the mixer lobes, causing he shroud to need to be increased in diameter and the ejector struts to be extended. He also questioned the size of the rotor and its ability to produce the goal power of 1 kW. Jeff also spoke a little about the future production of this turbine and where the best options to spend more or less on during fabrication

now lie. For example, creating a $20,000 mold for casting drives the individual part cost down significantly, but since the design is likely to be changed again before mass production begins, the casting mold would not be a wise use of funds. Also, he mentioned that the team should look into the use of Monokote as a foam covering. It is a type of plastic which can be stretched over the foam pieces and then, once heat is applied to it, it shrinks to the necessary size and shape of the foam.

Meeting with Mountain Base Mould

The team met with the owner of Mountain Base Mould and Manufacturing on August 5 to discuss the construction of the prototype and possible places for improvement in the design. Previously, the team had been told that the stator could not be machined in the pieces which it had been broken up into without use of a five-axis machine. However, Mountain Base Mould has made full stators for FloDesign using a three-axis machine. In addition though, it would be in the best financial interest to break the stator up further to decrease the amount of waste produced in machining these parts. The larger the piece of aluminum which needs to be started with, the more costly it will be. If the inner portion of the stator is further broken up into its ring, the blade, and the inner hub, this will decrease the amount of waste and also the overall cost to machine this part. The budget of getting the stator and rotor made for $10,000 is still tight at this time.

Aluminum Extrusion Process

One process which has been looked into for producing the stator blades was aluminum extrusion. This process consists of creating a die to push a large piece of aluminum through, causing it to take on the shape of the die. This would be a good option, except that many companies require a minimum of 500-2000 lbs of material to be extruded which is far beyond the capacity of this project, at least for now. In addition to the large amount of minimum material, the tooling for this process is between $5,000 and $8,000 in some cases and the only company which provided a lead time said that the process would take about five weeks.

Market Study

This week the market for small wind turbines was examined to get an idea of where the market was and is growing as well as how fast it was expanding. There are a few contributing factors to the expansion of the small wind market, these include government incentives, zoning laws and average wind speeds at the turbine location.

Several states now have government incentives in place to promote green energy. These incentives may be net metering, tax rebates or buy back policies for the produced power. With incentives like these in place, people are encouraged to purchase alternative energy sources and in return, they tend to purchase less power from companies and are compensated for the extra power that they produce. The map below shows which states have government incentives in place and some states even have several different incentive programs.

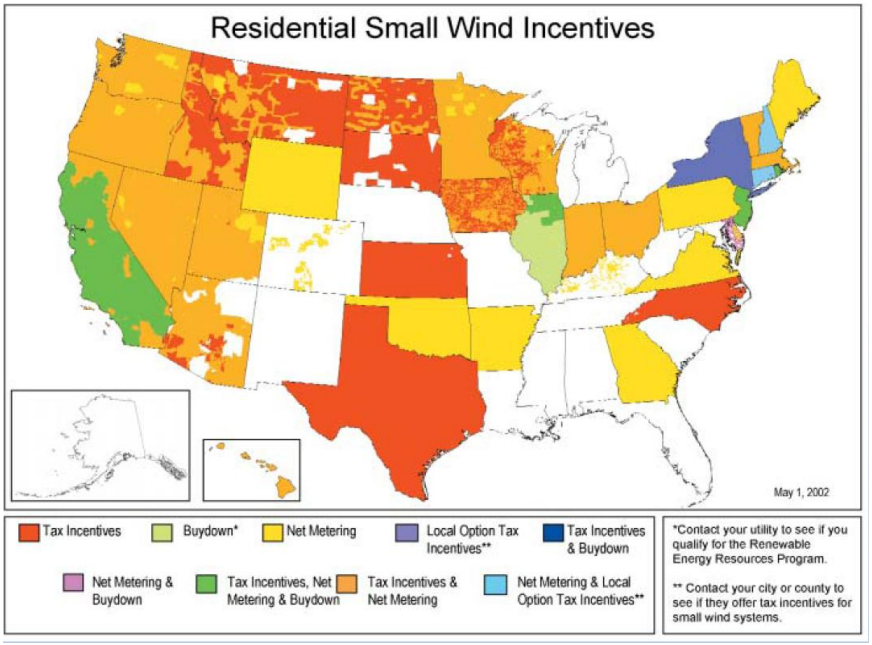

FIGURE 42: SMALL WIND INCENTIVES FOR RESIDENTS

Zoning laws are different everywhere you go which means that it would be up to the individual buyer to determine if and where they could install a wind turbine or other energy source. Average wind speeds however are probably the largest factor in purchasing a small wind turbine because if there is not enough wind to spin the turbine, then your turbine will not be able to produce power. The following map shows wind energy production based on average wind speed.

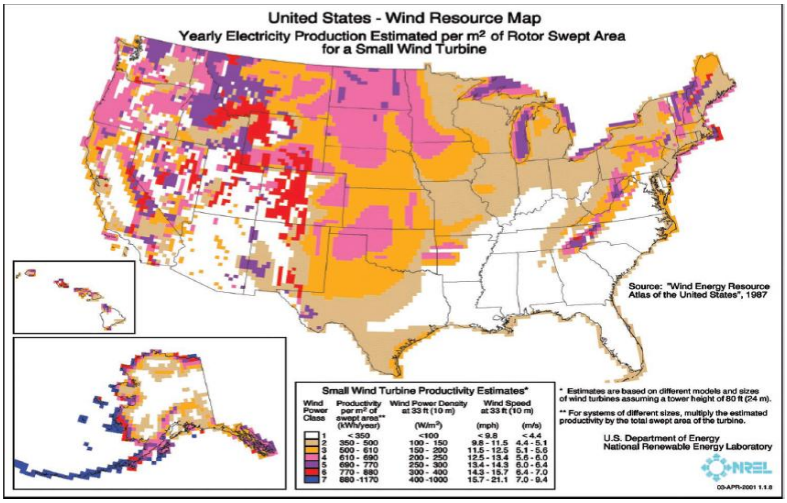

FIGURE 43: WIND RESOURCES IN THE UNITED STATES

Now looking at the expansion of the wind turbine industry, we can see that from 2000 to 2009 most states in America have come to utilize wind energy to some extent.

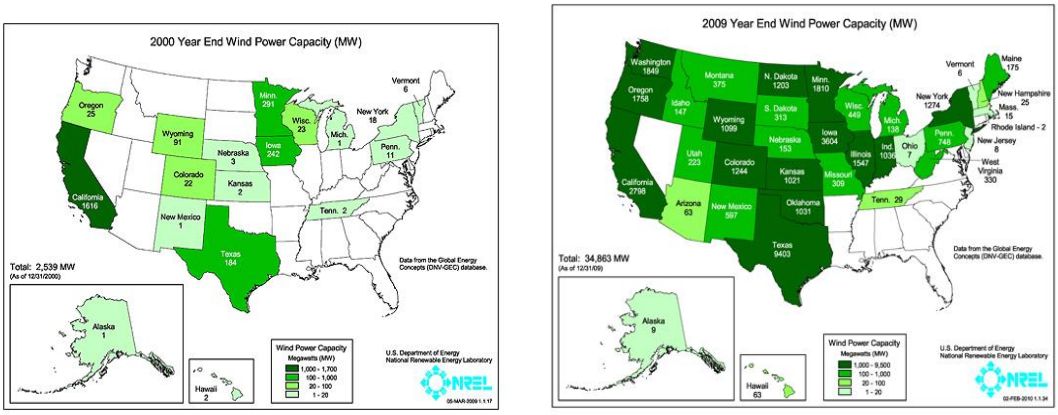

FIGURE 44: WIND POWER CAPACITY BY STATE

As would be expected with this much expansion, sales of wind turbines have risen drastically in recent years.

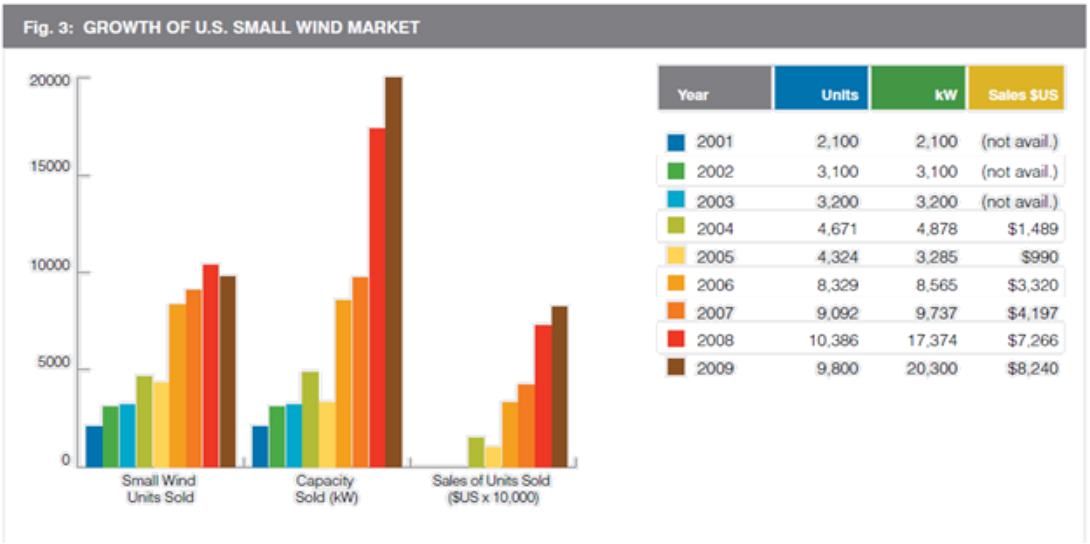

FIGURE 45: U.S. SMALL WIND MARKET TRENDS

Seeing the growth of the wind turbine industry is great, but that does not say what will happen in the future. According to the American Wind Energy Association's 2009 market study, there is an average annual growth rate of roughly 14% - 25%. While nothing is certain about the future, using this estimation and based off of the approximately 10,000 small wind turbines sold in 2009, a rough estimation of about 13,000–16,000 small wind turbines may be sold in 2011 and 15,000–19,500 in 2012.

There is still plenty of room for improvement and growth in the small wind industry but there will always be restrictions and barriers to overcome. A turbine that can overcome these restrictions, such as being able to perform in very low wind speeds, could change the entire industry and become hugely successful.

Manufacturing Study

The costs of mass manufacturing this small wind turbine were explored this week. This was done by obtaining quotes from different companies on how much having a single part made would cost, and how that cost would change based on the number of pieces which needed to be produced. It was requested that the prices for number of parts be given in increments of 50 all the way up to production of 5000 parts. The companies who have returned correspondence have provided the information that they could. Many companies have not responded yet with the information needed to complete this study, so work will be continued in upcoming weeks. Table shows the quotes received so far.

Number Produced		Cost to Produce Rotor				Cost to Produce Stator			
		Investment Cast		Carbon Fiber	SLS	Investment Cast		Carbon Fiber	SLS
		Aluminum	Magnesium			Aluminum	Magnesium		
	Name of Company	Yankee Casting		Goetz Boats	Paramount	Yankee Casting		Goetz Boats	Paramount
Pattern		$19,125.00		N/A	N/A	$20,900.00		N/A	N/A
1		$1,250.00	$1,485.00	$58,850 (both)	$25,000.00	$1,435.00	$1,635.00	$58,850 (both)	$25,000.00
5		$1,102.00	$1,310.00			$1,251.00	$1,540.00		
25		$955.00	$1,142.00			$1,072.00	$1,449.00		
50		$948.00	$1,135.00			$1,064.00	$1,441.00		

TABLE 20: QUOTES RECEIVED AS OF 7/29/11

So far, the best option for a single model appears to be using SLS for the stator rotor system. At $25,000 dollars, it is the cheapest option. However, this would not be a practical material for mass production due to the high production costs long term. A better long term option would be to cast the stator rotor system. The initial cost for each piece to set up the mold is around $20,000. However, once the mold is created, the part prices drop down significantly based on the number ordered. That makes casting a good, long-term solution.

When contacting companies for this study, the quotes were to be based on the material and process which the companies normally used. However, it was found that steel is the dominating material overall used in wind turbines. In addition, a rising interest in aluminum as a lower-weight option seems to be taking place, provided that it can meet the same fatigue requirements. Also, the need for gearboxes is shown to be eliminated through using a variable-speed generator in addition to new electronics with higher power. Wood epoxy is generally no longer used in blade design, as well.

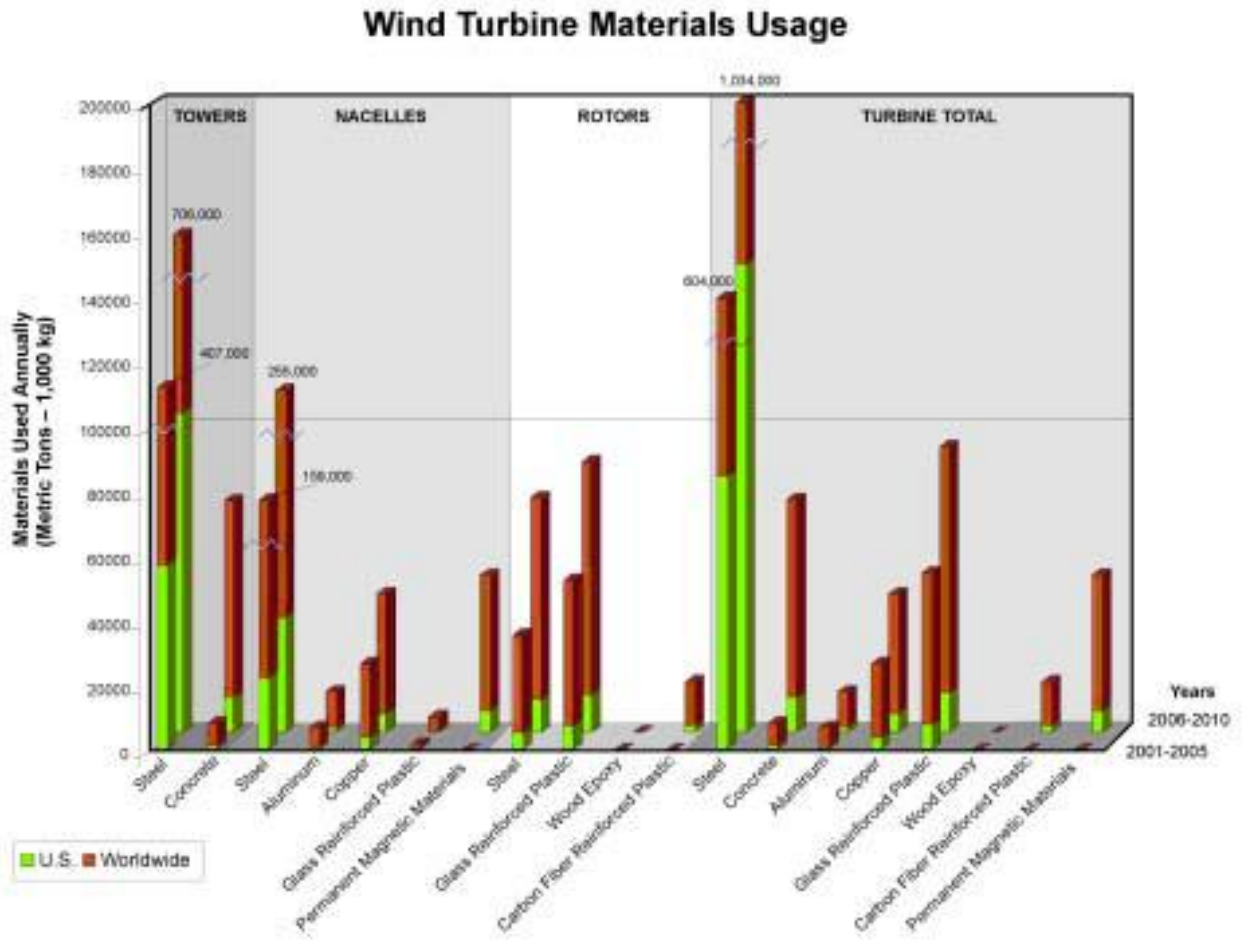

FIGURE 46: MATERIALS USED IN WIND TURBINES BY COMPONENT

This study will be helpful in the long run to determine what type of material should be used in mass production of this turbine. The final decision shall be based on cost, weight, durability, and ease of use and manufacturing processes.

Final Model

Stator

At the end of the Internship and after meeting with countless vendors and FDWT employees, a design was reached that allowed for a small wind turbine to be built for around $25,000 with the stator and rotor assembly hitting the $10,000 dollar goal.

The stator was broken into 36 major pieces. These pieces are all seen below in figure 47.

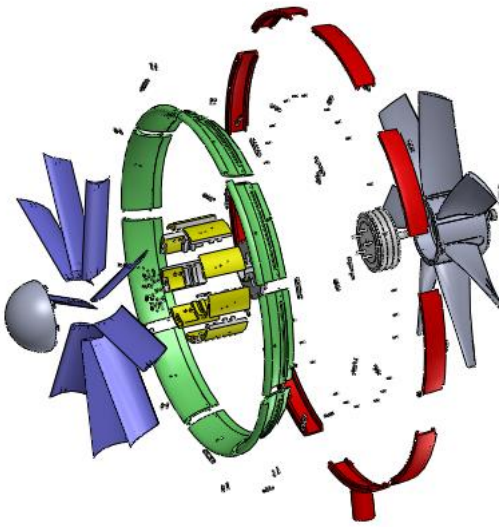

FIGURE 47: FINAL STATOR ROTOR ASSEMBLY

The red pieces are the nine different outer stator sections. The green pieces are the 9 inner stator sections. The yellow pieces are the nine center hub pieces and the blue blades are the nine straight stator blades. Having the stator split up into this many pieces reduced cost significantly and brought the stator part costs to $7,000 roughly when order from Paramount Industries. Before Paramount would ship this part out they would dry fit it to make sure that all the parts fit together correctly. Once it was in house, bolts and aluminum tabs would hold this entire assembly together. The final cost for the stator including all dry fitting surface coating is $9,360.

Rotor

The rotor assembly is broken into eight total parts. The center hub is made as one part and each of the seven blades is slid into a t-slot. Once assemble set screws will hold each blade in place. This set up allowed for the lowest cost to be seen. This part is also from Paramount and would cost a total of $3,480. The rotor assembly is the gray components in figure 47.

Ejector and Lobes

The ejector and lobe components, nine of each, will be made out of 2 lb density foam and then coated with a polymer coating to protect the parts from weather and physical conditions. The foam used is liquid two part expanding urethane foam. It has been proven to create a strong and light weight part when mixed and used properly. The lobe will be molded around a t-slot connection as seen below.

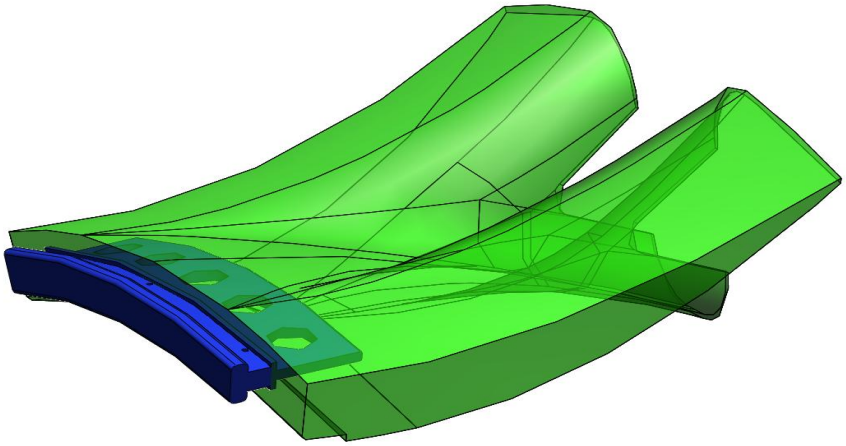

FIGURE 48: MIXER LOBE WITH T-SLOT CONNECTOR

The mold will be ordered from Paramount while each part will be formed in house. The ejectors will be molded a similar way just without the polymer inserts. The full model can be seen below.

FIGURE 49: RENDERED FINAL MODEL

The final dimensions are shown in the drawing below.

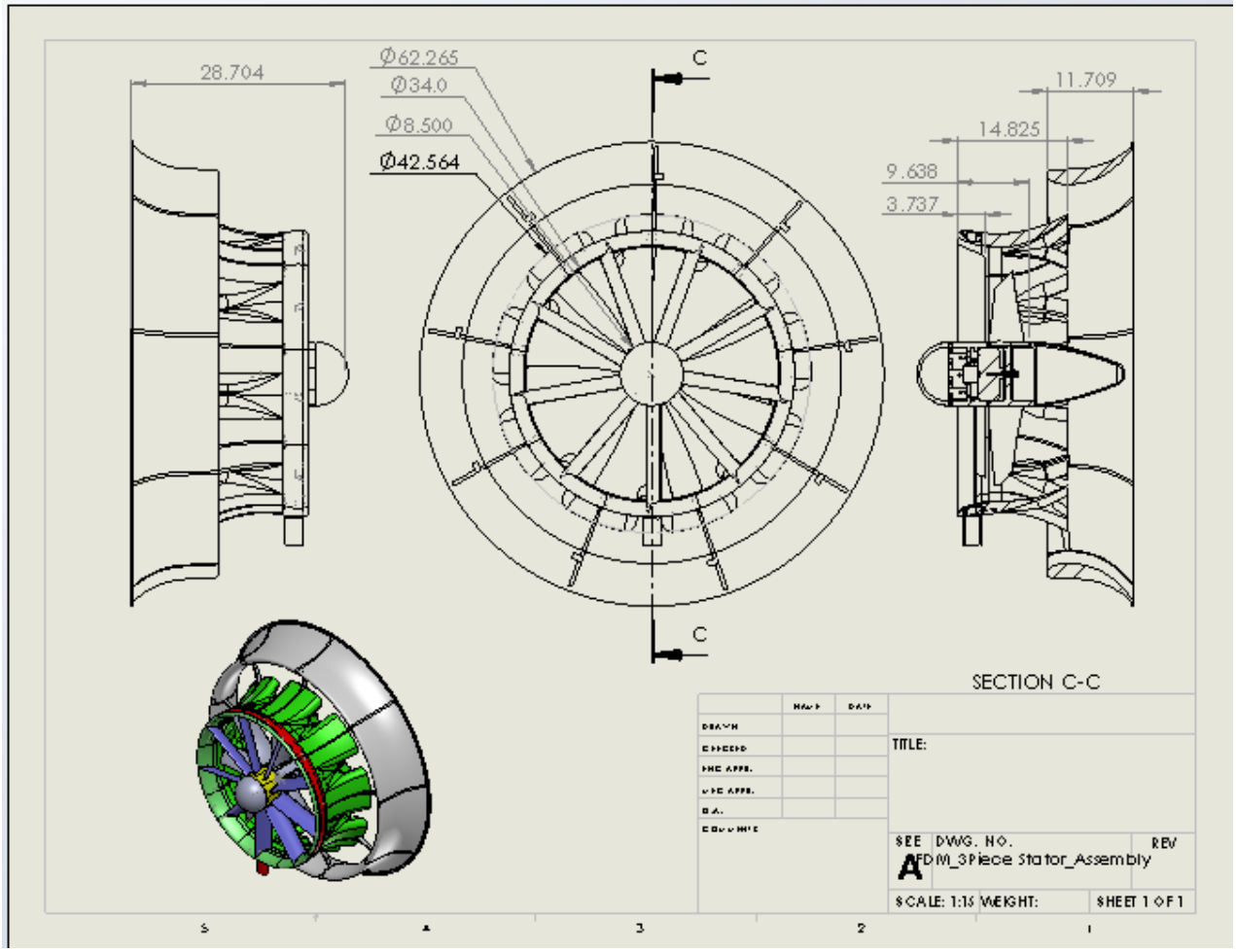

FIGURE 50: DRAWING OF TURBINE

The final estimated prototype budget can be seen below. This includes all the components and hardware needed.

TABLE 21: BILL OF MATERIALS FOR FINAL MODEL

Bill of Materials for FloDesign Wind Turbine "Mustang 1kW Turbine"									
Total Cost:	$23,590.65	Total Weight (lbs):	60.679	Total Volume (in^3):	1626.34	Final Lead Time:			
Company	**Part**	**Material**	**Qty**	**Volume (in^3)**	**Density (lbs/in^3)**	**Weight (lb)**	**Total Weight**	**Cost**	**Total Cost**
In House	FDM_Mixer Lobe	Foam	9	318.9	0.00174	0.55	4.98	$100.00	$900.00
Paramount	FDM_MixerMold_Mod	SLS	8					$530.00	$4,240.00
Paramount	FDM_Stator Outer	SLS	8	11.65	0.03443	0.40	3.21	$260.00	$2,080.00
Paramount	FDM_Stator Inner	SLS	8	22.03	0.03443	0.76	6.07	$260.00	$2,080.00
Paramount	FDM_Stator Outer Slot	SLS	1	9.9	0.03443	0.34	0.34	$260.00	$260.00
Paramount	FDM_Stator Inner Slot	SLS	1	20.93	0.03443	0.72	0.72	$260.00	$260.00
Paramount	FDM_Stator Blade	SLS	9	11.51	0.03443	0.40	3.57	$260.00	$2,340.00
Paramount	FDM_Stator Hub	SLS	9	10.26	0.03443	0.35	3.18	$260.00	$2,340.00
MBM	FDM_Leading Edge Key	Aluminum	9	0.15	0.09838	0.01	0.13	$33.33	$300.00
MBM	FDM_T-Slot Key	Aluminum	9	0.15	0.09838	0.01	0.13	$33.33	$300.00
MBM	FDM_Stator Outer Key	Aluminum	9	0.28	0.09838	0.03	0.25	$33.33	$300.00
Paramount	FDM_Rotor Hub	SLS	1	104.25	0.03443	3.59	3.59	$435.00	$435.00
Paramount	FDM_Rotor Blade	SLS	7	27.57	0.03443	0.95	6.65	$435.00	$3,045.00
MBM	FDM_PMG Plate	Aluminum	1	29.67	0.09838	2.92	2.92	$400.00	$400.00
Paramount	FDM_Nose Cone	SLS	1	55.1	0.03443	1.90	1.90	$600.00	$600.00
Paramount	FDM_Tail Cone	SLS	1		0.03443	0.00	0.00	$600.00	$600.00
MBM	FDM_Strut	Aluminum	9	8.46	0.09838	0.83	7.49	$110.00	$990.00
In House	FDM_Ejector	Foam	9	995.53	0.00174	1.73	15.56	$222.22	$2,000.00
Company	**Part**	**Description**	**Head**	**Qty**	**Size**	**Per Pack**	**Cost**	**Packs**	**Total**
McMaster	Rim Bolts	Bolt outer and Inner Rim	Low Profile Socke	27	8-32 x 3/4"	25	$13.79	2.00	$27.58
McMaster	Key Bolts	Bolts thru key bar to inner rim an	Low Profile Socke	36	6-32 x 3/8"	25	$9.20	2.00	$18.40
McMaster	Top Blade Bolts	Bolts rim to blade	Socket	18	10-32 x 9/16"	50	$6.10	1.00	$6.10
McMaster	Bot. Blade Bolts	Bolts hub to blade	Flat	18	10-32 x 5/8"	100	$12.90	1.00	$12.90
McMaster	Hub Bolts	Bolts hub to PMG Plate	Socket	9	1/4-20 x 1.5"	50	$7.92	1.00	$7.92
McMaster	Ejector Bolt	Bolts Ejector to struts	Flat	9	1/4-20 x 2"	25	$8.37	1.00	$8.37
McMaster	Thrust Bearing	Between PMG and Rotor	-	1	20 mm	1	$4.21	1.00	$4.21
McMaster	Washers	For thrust bearing	-	2	20 x 2.75 mm	1	$9.32	2.00	$18.64
McMaster	Shaft Collar	To hold on rotor	-	1	20 mm	1	$2.61	1.00	$2.61
McMaster	Set Screws	Hold on rotor Blades	-	7	10-32 x 1/2"	$25.00	$13.92	1.00	$13.92

Conclusion

These studies were performed by WNU student Interns, The focus was to determine the feasibility of the Mustang, a state of the art conceptual MEWT system that is directed towards residential and distributed wind applications. There were design studies, cost breakdowns, and AEP comparisons with other common small wind turbines, as well as a market study on the future of distributed wind. With the advantages of the MEWT system, the Mustang can revolutionize the small wind market; the small wind turbine market is growing steadily, with more and more wind turbine companies putting products into this market, it will be very competitive, but with the advantages leaning towards the MEWT system. The main factors which consumers are looking for include an affordable unit which can operate in low wind speeds and help cut down on home energy costs. If this company is able to produce a small wind turbine which meets these needs, there is no reason the market would not be responsive to such an item.

Resources

"Diffuser-augmented Wind Turbine - Composite Support & Solutions, Inc." *Patent Searching and Invention Patenting Information*. Free Patents Online. Web. 14 June 2011. <http://www.freepatentsonline.com/7218011.html>.

Gabrys, Christopher W. (Reno, NV, US) 2008 Small wind turbine system United States Mariah Power Inc. (Reno, NV, US) 7352076 http://www.freepatentsonline.com/7352076.html

Goldwater, John M. "U.S. Patent 4,684,817." *Patents - NASA Wind Energy Airborne Harvesting System Study*. NASA Wind Energy Airborne Harvesting System Study, 11 Mar. 1985. Web. 14 June 2011. <http://awtdata.webs.com/patents.htm>.

"Home of the Small Wind Turbines." *All Small Wind Turbines - Portal to the World of Small Wind Turbines*. Web. 8 June 2011. <http://allsmallwindturbines.com>.

"Horizontal Axis Wind Turbine." *Top Alternative Energy Sources. Alternate Energy For Our Future*. Web. 07 June 2011. <http://www.top-alternative-energy-sources.com/horizontal-axis-wind-turbine.html>.

"Kinetic Harvest." *Kinetic Harvest*. Web. 14 June 2011. <http://kineticharvest.com/?page_id=2>.

"Panemone Wind Turbine - Patent 4260325." *Docstoc – Documents, Templates, Forms, Ebooks, Papers & Presentations*. 7 Apr. 1981. Web. 14 June 2011. <http://www.docstoc.com/docs/ 31510253/Panemone-Wind-Turbine---Patent-4260325>.

"Patent, How to Get a." *United States Patent and Trademark Office*. 26 Mar. 2008. Web. 10 June 2011. <http://www.uspto.gov/web/patents/howtopat.htm>.

Pugh, Paul F. "U.S. Patent 4,486,669." *Patents - NASA Wind Energy Airborne Harvesting System Study*. NASA Wind Energy Airborne Harvesting System Study, 4 Dec. 1984. Web. 14 June 2011. <http://awtdata.webs.com/patents.htm>.

"Tethered Wind Turbine - Provisional Patent Application." *Amick Global - Energy Design Innovations*.Web.14 june 2011. <http://amickglobal.com/wind_turbines/twt/twt_ppa.htm>.United States. United States Patent and Trademark Office. *United States Patent: 7134631*. US Patent & Trademark Office, Patent Full Text and Image Database, 14 Nov. 2006. Web. 14 June 2011. <http://patft.uspto.gov/netacgi/nph-Parser?Sect1=PTO2&Sect2=HITOFF&p=1&u=%2Fnetahtml %2FPTO%2Fsearch-bool.html&r=1&f=G&l=50&co1=AND&d=PTXT&s1=%22smal l+wind+turbines %22&s2=shrouds&OS=>.

United States. United States Patent and Trademark Office. *United States Patent: 7789624*. [US Patent & Trademark Office, Patent Full Text and Image Database], 7 Sept. 2010. Web. 10 June 2011. <http://patft.uspto.gov/netacgi/nph-Parser?Sect1=PTO2&Sect2=HITOFF&p=1&u=%2Fnetahtml %2FPTO%2Fsearch-bool.html&r=5&f=G&l=50&co1=AND&d=PTXT&s1=%22small +wind+turbines %22&OS=%22small+wind+turbines%22&RS=%22small+wind+turbines%22>.

United States. United States Patent and Trademark Office. *United States Patent: 7950143*. US Patent & Trademark Office, Patent Full Text and Image Database, 31 May 2011. Web. 10 June 2011. <http://patft.uspto.gov/netacgi/nph-Parser?Sect1=PTO2&Sect2=HITOFF&p=1&u=%2Fnetahtml %2FPTO%2Fsearch-

bool.html&r=1&f=G&l=50&co1=AND&d=PTXT&s1=%22small+wind+turbines%22&OS=%22small+wind+turbines%22&RS=%22small+wind+turbines%22>.

"Vortex Enhanced Wind Turbine Diffuser - Patent WO/2010/131052." *SumoBrain - Big, Powerful, Smart Searching*. Web. 14 June 2011. <http://www.sumobrain.com/patents/wipo/Vortex-enhanced-wind-turbine-diffuser/WO2010131052.html>.

"Wind Powering America: 80-Meter Wind Maps and Wind Resource Potential." *Wind and Water Power Program: Wind Powering America*. U.S. Department of Energy. Web. 10 June 2011. <http://www.windpoweringamerica.gov/wind_maps.asp>.

"Wind Turbines, Geothermal Energy, Solar Power Energy in Rochester, NY." *NRG Solutions | Wind Turbines, Geothermal Energy, Solar Power Energy*. Web. 14 June 2011. <http://www.mynrgsolutions.com/wind-solutions>.

"Wind Turbine Ring/Shroud Drive System." *OSDir.com :: Open Source, Linux News & Software*. Web. 14 June 2011. <http://osdir.com/patents/Fluid-pumps/Wind-turbine-ring-shroud-drive-system-06951443.html>.

Yangzhou Shenzhou Wind-driven Generator Co., Ltd. Web. 14 June 2011. <http://shenzhouwindturbine.en.nobodybuy.com/about-us.htm>.